Defining the role of cross-protective antibodies in protection against emerging viruses at the species and sub-species level

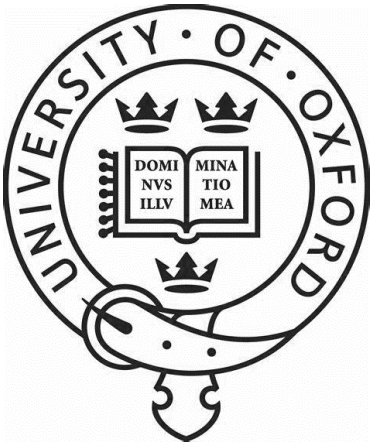

Nazia Thakur

St. Cross College

Nuffield Department of Medicine

University of Oxford

A thesis submitted for the degree of

Doctor of Philosophy

Hilary term, January 2025

Table of Contents

Acknowledgements

First and foremost, I give thanks to the Almighty Allah for showering His endless blessings and mercy upon me, for "w*hatever of blessings and good things you have, it is from Allah." (Quran 16:53)*. May I continue to remain under His watchful eye to attain more success and good fortune in this life and in the hereafter. Next, most wholeheartedly, I would like to thank my dad Yasin Thakur, my mum Jarina Thakur, and my brother Nabil Thakur, for their eternal support and unwavering belief in me. They have been my rock through every stage in life and I am infinitely grateful for you all. All that I am is because of you, and everything I do is for you. I hope I have made you all proud.

To my supervisor, Dr Dalan Bailey whose mentorship, advice and guidance over the 10 years that I've known him have truly shaped me into the scientist I am today. He has seen potential in me when I've doubted myself, and always pushed me to be the best version of myself. Dalan, thank you for not only challenging me, but for showing me what great mentorship looks like with your humble approach to research. I could not have asked for a better supervisor. I would also like to thank my co-supervisor, Professor Teresa Lambe, who has always reminded me to not to dim the light on my achievements. You truly embody what it is to be a strong, female scientist and I am filled with nothing but admiration for you. I would also like to thank Professor Simon Graham, Professor Elma Tchilian, Dr Edward Wright, Professor Nigel Temperton, Professor Miles Carroll and Dr Daniel Gonçavles for their guidance and training. I am grateful to the past and present members of the Viral Glycoproteins Group for your help, stimulating discussions and friendship: Dr Giulia Gallo, Dr Fatoumatta Jobe, Dr Joseph Newman, Dr Igor Santos, Dr Carina Conceição, Dr James Kelly, Ahmed Mohammed, Jim Chadwick, Alex Norman and Elizabeth Martin-Drew.

I would also like to extend my appreciation to the rest of my family – to all the Thakurs (especially my "Crazy Cuzzies"), Surves and Sawants for their endless support and prayers. To my grandparents, who although are no longer with us to see what I have achieved, I hope are smiling down on me with pride. Thank you also to all my friends who have supported me: to my roots, Husna, Furah and Habib for always keeping me grounded and imparting the best words of encouragement; to my sisters, Pooja and Monica, for forever being my biggest cheerleaders; and to my "day one homie", Dr Rebecca McLean, for your continuous support and for being ones of my greatest inspirations. Finally, I offer endless gratitude to my best friend Mariea, my "Taani partner", you have been my pillar of strength throughout this journey. You believed in me when I didn't believe in myself, listened to all my woes and have given me the greatest advice. Thank you for always clapping so loud for me that I could never hear who wasn't. As you once said: *"The best views always come after the hardest climbs."*

Declaration

This thesis is submitted to the University of Oxford in support of my application to the degree of Doctor of Philosophy. It has been composed by me and has not been submitted in any previous application for any degree. The work presented was carried out by me, including experimental design, data acquisition, data analysis, image or text. Where data has been carried out in studies led by others, this has been explicitly stated and attributed to the originator in the text and referenced where appropriate. Parts of this thesis have been published, or published work formed the basis for this study, where I am listed as first author, co-first author (*) or co-author:

- Newman J*, **Thakur N*** et al. Neutralising antibody activity against 21 SARS-CoV-2 variants in older adults vaccinated with BNT162b2. ***Nat Microbiol*** 2022 Aug 7(*):1180-1188.
- van Doremalen N, Schulz JE, Adney DR, Saturday TA, Fischer RJ, Yinda CK, **Thakur N** et al., Efficacy of ChAdOx1 vaccines against SARS-CoV-2 Variants of Concern Beta, Delta and Omicron in the Syrian hamster model. ***Nat Commun*** 2022 Aug 13(1):4610.
- **Thakur N** et al. SARS-CoV-2 variants of concern Alpha, Beta, Gamma and Delta have extended ACE2 receptor host-ranges. ***J Gen Virol*****.** 2022 Apr; 104(4).
- Spencer AJ, Morris S, Ulaszewska M, Powers C, Kailath R, Bissett C, Truby A, **Thakur N** *et al*. The ChAdOx1 vectored vaccine, AZD2816, induces strong immunogenicity against SARS-CoV-2 B.1.351 and other variants of concern in preclinical studies. ***EbioMedicine*** 2022 Mar; 77:103902.
- **Thakur N,** Gallo G, Elreafey AME, Bailey D. Production of Recombinant Replication-defective Lentiviruses Bearing the SARS-CoV or SARS-CoV-2 Attachment Spike Glycoprotein and Their Application in Receptor Tropism and Neutralisation Assays. ***Bio Protoc***. 2021 Nov 5;11(21):e4249.
- Lambe T, Spencer AJ, Thomas KM, Gooch KE, Thomas S, White AD, Humphries HE, Wright D, Belij-Rammerstorfer S, **Thakur N** *et al.* ChAdOx1 nCoV-19 protection against SARS-CoV-2 in rhesus macaque and ferret challenge models**.** ***Commun Biol****.* 2021 Jul 26;4(1):915.
- **Thakur N** *et al.* Micro-fusion inhibition tests: quantifying antibody neutralization of virus-mediated cell-cell fusion. ***J Gen Virol*****.** 2021 Jan;102(1):jgv001506.
- Conceicao C*, **Thakur N*** *et al.* The SARS-CoV-2 Spike protein has a broad tropism for mammalian ACE2 proteins*.* ***PLoS Biol***. 2020 Dec 21;18(12):e3001016. doi: 10.1371/journal.pbio.3001016.
- Graham SP, McLean RK, Spencer AJ, Belij-Rammerstorfer S, Wright D, Ulaszewska M, Edwards JC, Hayes JWP, Martini V, **Thakur N** *et al.* Evaluation of the immunogenicity of prime-boost vaccination with the replication-deficient viral vectored COVID-19 vaccine candidate ChAdOx1 nCoV-19*.* ***NPJ Vaccines***. 2020 Jul 27;5(1):69.

Nazia Thakur

List of Figures and Tables

Abbreviations

ACE2	Angiotensin converting enzyme 2
ADE	Antibody dependent enhancement
AGM	African green monkey
ALP	Alkaline phosphatase polymer
ALVAC	Canarypox vaccine vector
AngV	Angavokely henipavirus
APC	Antigen presenting cell
APN	Aminopeptidase N
AU	Antigenic units
AWERB	Animal Welfare and Ethical Review Bodies
BCoV	Bovine coronavirus
BHK-21	Baby hamster kidney-21 cells
BoHV4	Bovine herpesvirus 4
BSL4	Biosafety level 4
CCoV	Canine coronavirus
CedV	Cedar virus
CEPI	Coalition for Epidemic Preparedness
CFR	Case fatality ratio
ChAdOx1/ ChAdOx2	Chimpanzee adenovirus vector vaccine
CHV	Camp Hill virus
CL2	Containment level 2
COVID-19	Coronavirus disease 2019
CRCoV	Canine respiratory coronavirus
DARV	Daeryong virus
DC	Dendritic cell
DewV	Denwin virus
DMEM	Dulbecco's modified Eagle's medium
dpc	Days post challenge
DPP4	Dipeptidyl peptidase IV
E	Envelope
EC_{50}	Effective concentration, 50%
EDTA	Ethylenediaminetetraacetic acid
ELISA	Enzyme linked immunosorbent assay
EPT	End-point titre
F	Fusion glycoprotein
FBS	Foetal bovine serum

FCoV	Feline coronavirus
G	Attachment glycoprotein
G2P	Genotype to Phenotype
GAKV	Gamak virus
GHNV	Ghanaian bat henipavirus
H&E	Haematoxylin and eosin
HA	Haemagglutinin
hACE2	Human ACE2
HCE	Humane clinical endpoint
HCoV	Human coronaviruses
HEK293T	Human embryonic kidney 293T cells
HeV	Hendra virus
HRP	Horseradish peroxidase
i.m.	Intramuscular
i.n.	Intranasal
i.p.	Intraperitoneal
i.u.	Infectious units
IBV	Infection bronchitis virus
IC	Inhibitory concentration
IFN	Interferon
Ig	Immunoglobulin
IL	Interleukin
ISG	Interferon stimulated gene
ISH	*in situ* hybridisation
L	Large polymerase protein
LayV	Langya virus
LMICs	Lower-and middle-income countries
M	Matrix/membrane protein
M2e	Matrix protein 2 ectodomain
mAb	Monoclonal antibodies
MeliV	Melian virus
MERS-CoV	Middle Eastern respiratory syndrome coronavirus
MeV	Measles virus
mFIT	Micro fusion inhibition test
MHC	Major histocompatibility complex
MHRA	Medicines and Healthcare products Regulatory Agency
MHV	Murine hepatitis virus

MojV	Mojiang virus
mpox	Monkeypox
MPXV	Monkeypox virus
MuV	Mumps virus
mVNT	Micro neutralisation test
N/NP	Nucleoprotein/nucleocapsid
NA	Neuraminidase
nAb	Neutralising antibodies
NaCl	Sodium chloride
NBF	Neutral-buffered formalin
ND	Neutralising dose
NE	Non-enveloped
NiV	Nipah virus
NiVB	Nipah virus, Bangladeshi strain
NiVM	Nipah virus, Malaysian strain
NK	Natural killer cell
NSP	Non-structural protein
NTD	N-terminal domain
OD	Optical density
ORF	Open reading frame
P	Phosphoprotein
PAMP	Pathogen associated molecular patterns
PBS	Phosphate-buffered saline
PDCoV	Porcine deltacoronavirus
PEDV	Porcine epidemic diarrhoea virus
PEI	Polyethyleneimine
PHEV	Porcine haemagglutinating encephalomyelitis virus
PPRV	Peste des petits ruminants
PRCV	Porcine respiratory coronavirus
PRR	Pattern recognition receptors
RBD	Receptor binding domain
RdRp	RNA dependent RNA polymerase
rLuc	Renilla luciferase
RPV	Rinderpest virus
S	Spike
SADS-CoV	Swine acute diarrhoea syndrome coronavirus
SARS-CoV-1	Severe acute respiratory syndrome coronavirus 1

SARS-CoV-2	Severe acute respiratory syndrome coronavirus 2
sG	Subunit vaccine expressing henipavirus G protein
$TCID_{50}$	Tissue culture infection dose, 50%
Tfh	T follicular helper cell
TGEV	Transmissible gastroenteritis virus
TMB	3,3',5,5'-tetrametehylylbezidine
TMPRSS2	Transmembrane protease, serine 2
TNFα	Tumour necrosis factor alpha
UKHSA	UK Health and Security Agency
VAR	Variola virus
VLP	Virus-like particles
VOC	Variants of concern
vp	Virus particles
VSV	Vesicular stomatitis virus
VUI	Variants under investigation
VUM	Variants under monitoring
WHO	World Health Organisation
WT	Wild-type

Abstract

Emerging viruses often pose a threat to human populations due to the lack of pre-existing immunity. The WHO has prioritised groups of viruses for vaccine research and development, particularly viruses with pandemic potential. We have been investigating the effectiveness of vaccines against two of these priority groups of viruses, betacoronaviruses and henipaviruses, at an intraspecies and genus-wide level. In this study, the effectiveness of COVID-19 vaccines were examined in an older adult cohort to understand the antigenicity of SARS-CoV-2 variants. This analysis was further expanded to understand whether pre-existing immunity against SARS-CoV-2 can provide cross-protection against other betacoronaviruses, particularly sarbecoviruses, which are phylogenetically similar to SARS-CoV-2. For the henipaviruses, bio-banked sera from a pig immunisation study were analysed, whereby animals received homologous prime-boosts of Nipah virus and Hendra virus-based vaccines. Cross-reactive antibodies were detected against all the henipaviruses tested, but cross-neutralising antibodies only against Nipah and Hendra virus. Immunisation of mice with Nipah virus and the more distantly related Ghanaian bat henipavirus immunogens showed a degree of cross-neutralisation using homologous and heterologous vaccination regimes, but did not confer protection in a hamster challenge model. However, hamsters did exhibit evidence of reduced pathology and virus infiltrates in tissue sections of the brain, lungs and spleen with homologous prime-boost vaccination with a Ghanaian bat henipavirus subunit vaccine. This data suggests that pre-existing immunity against one virus may provide cross-protection against related viruses, but the utility of these vaccines may become limited with more distantly related viruses. This highlights the requirement for broad and novel vaccine development strategies against emerging viruses in any outbreak scenario.

Chapter 1: Introduction

1.1 The immune response to viral infection

1.1.1 Innate immune response to viral infection

The immune system employs many mechanisms in response to recognising foreign antigens following viral infection. The first-line defence against infection is the innate immune system, which is non-specific, short-lived and generally destructive, with the aim of rapid viral clearance [1]. These processes can be mediated by physical barriers, such as ciliated epithelial cells which secrete mucins to capture and expel inhaled virus particles, or can include the use of soluble proteins such as pro-inflammatory chemokines and cytokines (e.g., tumour necrosis factor alpha (TNFα), interleukin (IL)-1), IL-6) that attract inflammatory leukocytes (**Figure 1.1A**) [1, 2]. The release of these cytokines also stimulates the recruitment of natural killer (NK) cells, involved in the degranulation and apoptosis of infected cells [1]. In addition, some cells of the innate immune response also express pattern recognition receptors (PRRs) such as toll-like receptors, that bind to pathogen associated molecular patterns (PAMPs) on invading pathogens within hours of viral exposure (**Figure 1.1A**) [1, 2]. These processes cumulatively result in the recruitment of cellular elements in the form of mature myeloid hematopoietic stem cell-derived leukocytes. This includes granulocytes such as neutrophils and macrophages that possess phagocytic properties to internalise and degrade pathogens, or in the case of macrophages, engulf pathogens to mark them for clearance by complement [1]. The innate antiviral response is further amplified by induction of type I interferon (IFN) and interferon stimulated gene (ISG) expression, some of which are directly acting including restriction factors such as IFITs, tetherin and IFITMs (**Figure 1.1A**) [2]. Maturation of leukocytes (e.g., dendritic cells (DCs), macrophages and monocytes) via type I IFNs induces formation of antigen presenting cells (APCs) [1, 2]. These APCs play a role in the adaptive immune response by processing viral fragments and presenting them for recognition by T cells through expression of class I and II major histocompatibility complex (MHC) molecules [1].

1.1.2 Adaptive immune response to viral infection

The adaptive immune response generates antigen-specific, long-lasting immunity against a viral pathogen. APCs presenting viral antigens via MHC class II results in activation of naïve $CD4^+$ T helper cells and the proliferation and differentiation of B cells (**Figure 1.1B**) [1, 3]. T helper cell activation leads to the differentiation of various helper cells, for example, migration of naïve T cells in the germinal centre results in their differentiation into T follicular helper (Tfh) cells (**Figure 1.1B**) [3]. These cells interact with follicular B cells, which subsequently proliferate and undergo somatic hypermutation of the immunoglobulin (Ig) V-

region gene, resulting in affinity maturation of antibodies with increased binding for viral antigens [2].

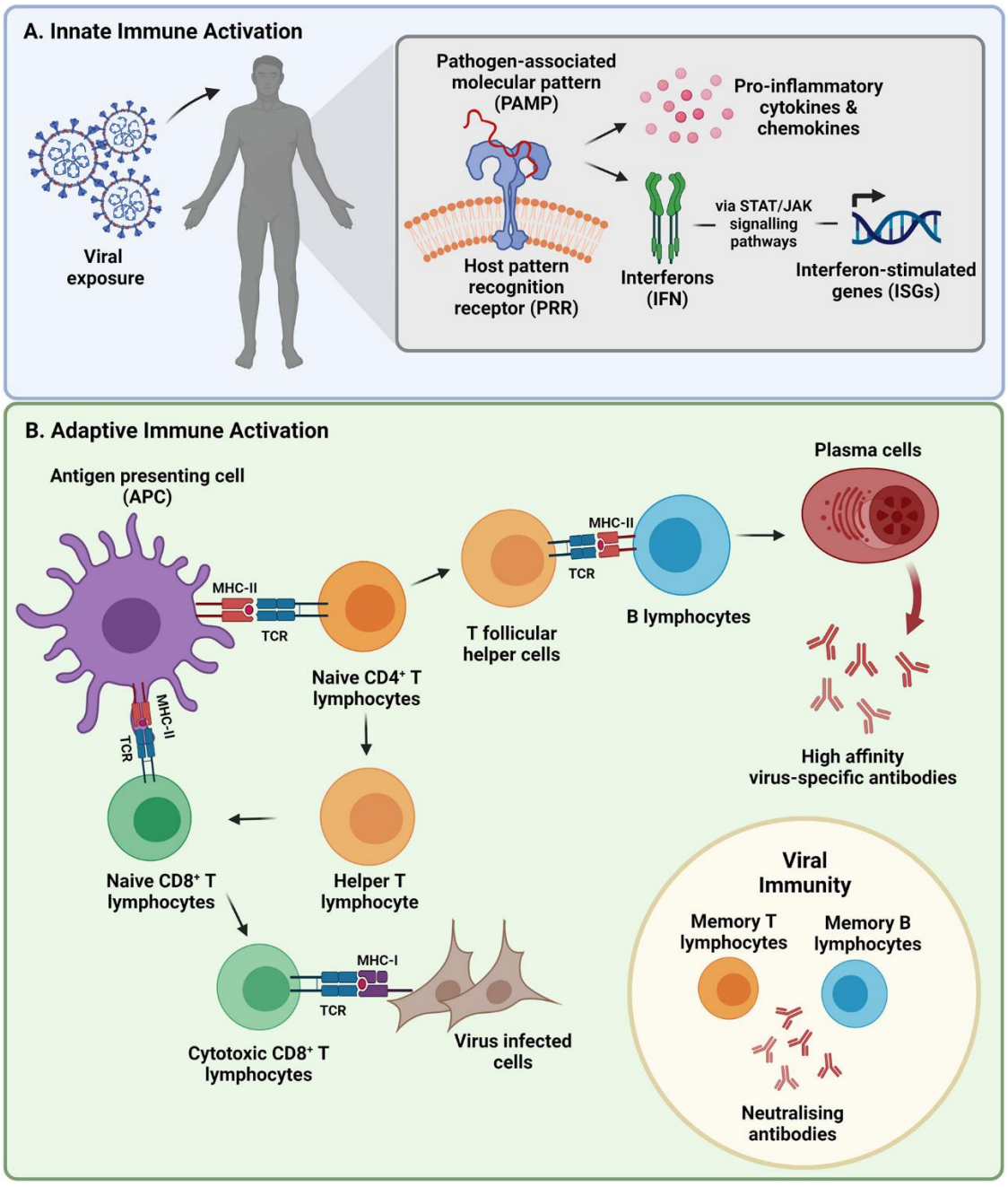

Figure 1.1: Innate and adaptive immune response following viral infection.
(A) Upon first encounter, viral antigens activate the innate immune response, which occurs within the first few hours of infection, but is short-lived and non-specific. Viral antigens have pathogen associated molecular patterns (PAMPs) which are recognised by pathogen pattern receptors (PRRs) on leukocytes. This leads to the secretion of pro-inflammatory cytokines and chemokines, and the stimulation of the interferon response and subsequent interferon stimulated genes (ISGs). **(B)** Leukocytes involved viral uptake process viral antigens into fragmented, smaller peptides and present them on the surface (antigen presenting cells, APCs), mediated by major histocompatibility complex (MHC) class I and II molecules. Antigens are then recognised by cells part of the adaptive immune response, including $CD8^+$ cytotoxic cells and $CD4^+$ helper T cells. The activation of naïve T-cells causes differentiation into different subtypes, of which T follicular helper cells (Tfh) initiate the maturation of memory B cells and long-lived, high affinity plasma cells through interactions in the germinal centre. The Th1 helper cells mediate cellular immune responses, activating cytotoxic $CD8^+$ T cells to carry out apoptosis of the infected host cell. These processes allow for a quicker and stronger immune response upon subsequent encounter of the viral antigen. Image taken from Mistry P et al., *Front Immunol* (2022) [2].

Mature B cells in their naïve form produce IgM and IgD, but activation of mature B cells modulated by $CD4^+$ T cells, results in isotype class switching and the production of IgG (most abundant), IgA (mucosal immunity) and IgE (allergy response) [2]. During class switching, the variable region (antigen binding site) of the IgG heavy chain remains the same, but the constant region (determines isotypes) changes, meaning antigenic specificity remains the same. B cells then differentiate into long-lived, high affinity antibody-producing plasma cells or into memory B cells that are rapidly reactivated following reinfection with the same viral antigen, resulting in virus neutralisation [2]. Presentation of processed viral antigen via MHC class I is recognised by cytotoxic $CD8^+$ T cells with the help of Th1 cells, which signals the infected cell for apoptosis (**Figure 1.1B**) [3, 4]. Subsequently, $CD8^+$ T cells can differentiate into T memory cells for rapid reactivation of the cytotoxic response upon rencounter of the same antigen [4]. Another way to simulate this first wave of infection is through vaccination, which means that upon encountering the same viral antigen, the adaptive immune system is primed to activate and respond more quickly and specifically to infection.

1.2 Understanding the utility of vaccines

1.2.1 Cross-protective human and animal vaccines

Vaccination has long been used as an effective tool to protect against infection and mortality caused by viruses or other pathogens. The development of safe, low-cost, and effective vaccines for use in humans and animals is of great importance for the prevention of epidemics, epizootics and pandemics. More recently, emphasis has been placed on developing vaccines that can cross-neutralise and provide cross-protection against multiple viruses within the same virus family, particularly as multiple viruses can theoretically emerge from high-risk viral families.

The first human disease for which a vaccine was developed was smallpox, caused by the variola virus (VAR), taxonomically classified within the *Orthopoxvirus* genus. The disease is typified by high fever, vomiting, mouth sores and fluid-filled lesions across the whole body [5]. Prior to the discovery of vaccination, the most effective method of combating smallpox was through inoculation of nonimmune individuals with matter lanced from smallpox pustules [5]. However, in 1796, Edward Jenner discovered that inoculation with matter from cowpox pustules resulted in protection from variola virus infection and smallpox disease [6]. The use of cowpox virus pustules as a vaccine was adopted by other countries and by the 1950s, the vaccine formulation was updated with advances in technology to produce freeze-dried vaccines. This allowed distribution of the vaccine globally, which eventually led to the eradication of smallpox in 1980 (**Figure 1.2**) [6, 7]. More recently, there has been emergence of monkeypox (mpox) virus (MPXV), also classified within the *Orthopoxvirus*

genus. This is endemic in Central and West Africa, but in 2017 caused outbreaks in Nigeria, the United Kingdom and Singapore, and from 2022 – 2024 mpox became a global epidemic, with cases noted in 117 countries [7]. MPXV has high antigenic similarity with VAR, sharing 84.6% nucleotide identity with the India-1967 VAR strain and 84.5% with the Garcia-1966 VAR strain [8]. Therefore, it was suggested that the smallpox vaccine may also be effective in eliciting cross-protective immunity against mpox. Indeed, vaccination with a smallpox vaccine was effective in reducing mpox infection rates, effectively reduced the risk of severe mpox infection and, induced neutralising antibodies (nAb) against MPXV (**Figure 1.2**) [7].

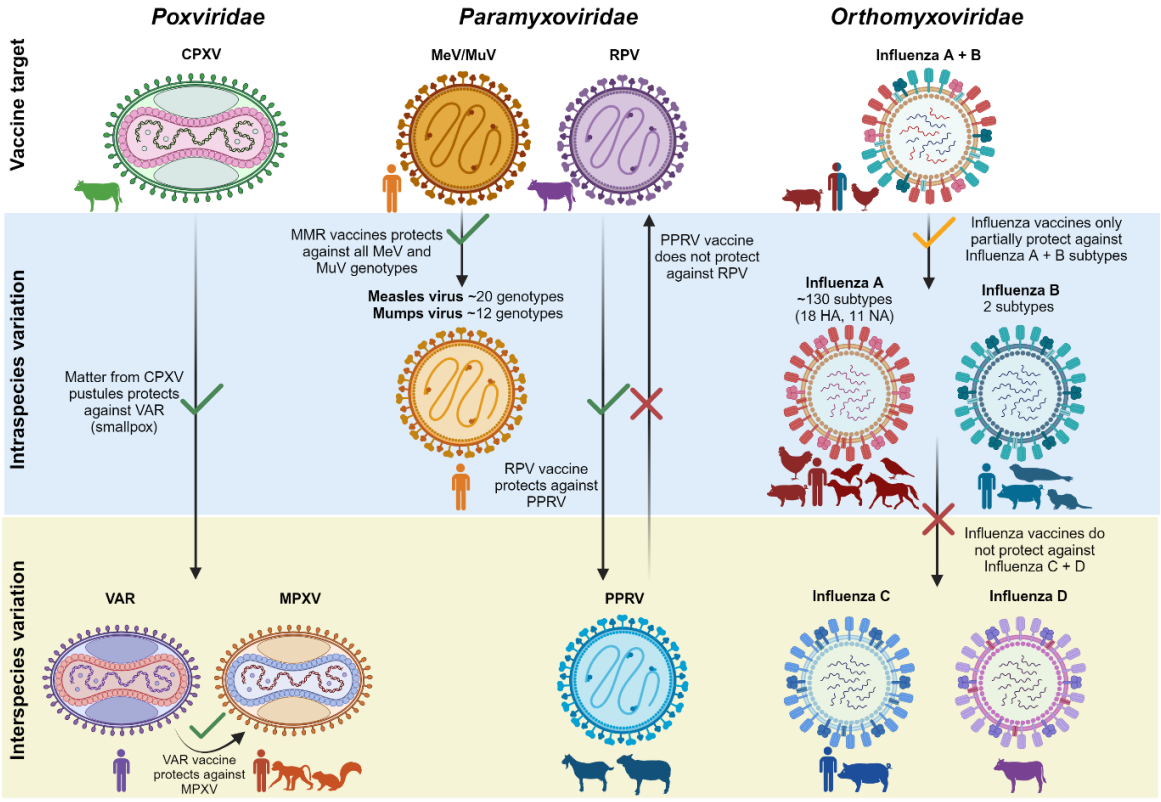

Figure 1.2: Utility of approved vaccines for use against poxviruses, paramyxoviruses and influenza viruses.
Poxviruses such as cowpox virus (CPXV) result in pustules in cows. Matter from cowpox pustules has been shown to be effective at protecting against smallpox, caused by variola virus (VAR), which has since been eradicated. Subsequently, updated VAR vaccines have been shown to confer protection against infection from monkeypox virus (MPXV). Paramyxoviruses such as measles virus (MeV) and mumps virus (MuV) cause disease in humans, and although there are several genotypes of these viruses, there is only one serotype, meaning the MMR vaccine is efficacious against all genotypes of these viruses (intraspecies variation). A vaccine against another paramyxovirus, rinderpest virus (RPV), which has also been eradicated, was shown to cross-protect against peste des petits ruminants virus (PPRV), however PPRV vaccines do not protect against RPV infection (interspecies variation). Orthomyxovirus vaccines are directed against Influenza A and B subtypes, but only provide partial protection due to antigenic drift and shift. These vaccines do not confer cross-protection against Influenza C and D. The animal reservoirs of each virus or the animal target for the corresponding vaccine is shown. Image was generated using Biorender.

Another example of vaccine success is vaccines developed against measles virus (MeV). MeV is a negative-sense RNA virus, taxonomically classified within the *Morbillivirus* genus, part of the *Paramyxoviridae* family. MeV is the causative agent of measles, which is a highly contagious disease that remains a significant cause of childhood morbidity and mortality,

despite the availability of safe and efficacious vaccines [9, 10]. In developed countries, an attenuated MeV vaccine is delivered in combination with live virus vaccines against mumps, rubella (MMR) and sometimes varicella (MMRV), but in lower-and middle-income countries (LMICs), the MeV vaccine is often given by itself [10]. Despite the presence of several genotypes of MeV and mumps virus (MuV), there is only one serotype for each of these viruses. This means that at the intraspecies level, a vaccine against a single serotype can be effective against all genotypes of this virus (**Figure 1.2**) [10-12]. Furthermore, humans are the only susceptible host for MeV and MuV [11, 12], limiting the possibility of virus spillover from animal reservoirs. A wider host range could result in mutation of the virus and antigenic drift, generating variants that might not be neutralised by the current vaccine.

MeV vaccination programmes generally result in the development of protective antibody titres in ~85% of vaccinated children at 9 months old, which increases to 90-95% after 12 months of age [11]. However, the immunity derived from MeV vaccination is more variable than that acquired through infection, with waning antibody responses noted 10-15 years after vaccination [11]. A similar issue is observed with vaccination against MuV, where the effectiveness of the mumps vaccines can range from 49-92% after one dose, and from 66-95% after 2 doses, dependent on the vaccine strain. Indeed outbreaks of MuV infection have been seen in fully vaccinated populations in Europe [12]. Furthermore, vaccine hesitancy, historical concerns about adverse side effects and religious/philosophical objections to vaccination have resulted in decreased uptake of vaccines, leading to the resurgence of measles in many developed countries [12]. As a result, new strategies are being explored to reduce the incidence of MeV and MuV infections, including administering a third MMR vaccination, or the formulation of new vaccines with updated technology. An example of this has been explored with subunit vaccines against another paramyxovirus, human respirovirus (types 1 and 3), using structure-based design to stabilise the fusion protein in a pre-fusion state as the vaccine antigen [13]. This approach has been shown to induce strong nAb responses in mouse and rat immunogenicity and efficacy studies [13]. A similar vaccine strategy has also successfully been employed for the development and approval of the first vaccine against respiratory syncytial virus, which causes annual severe acute lower respiratory tract illness in infants and older adults [14, 15].

Rinderpest virus (RPV) is another morbillivirus, along with MeV and peste des petits ruminants virus (PPRV), that has caused devastating epidemics in the past, this time in cattle. RPV virus was eradicated in the wild following a mass vaccination programme with a live attenuated RPV vaccine. It was also shown that administration of an attenuated RPV vaccine to sheep and goats protected them from PPRV infection and associated disease (**Figure 1.2**) [16]. A further study in goats and cattle aimed to investigate whether the

opposite situation was true and immunised animals with wildtype PPRV or two established vaccine strains of PPRV, Nigeria/75/1 or Sungri/96, followed by challenge with RPV. Animals immunised with wildtype PPRV were fully protected from RPV challenge, whereas animals vaccinated with PPRV/Sungri/96 showed only partial protection and animals receiving PPRV/Nigeria/75/1 were not protected (**Figure 1.2**) [17]. Furthermore, although sera from RPV-vaccinated animals have been shown to cross-neutralise PPRV, only sera from wildtype inoculated PPRV animals was able to neutralise pseudotyped RPV, unlike sera from animals inoculated with vaccine strains of PPRV [17]. The inverse correlation between protection and nAb production in this study points to the potential significance of non-neutralising antibodies in mediating immune protection. This study also highlights the lack of bidirectionality in cross-protection with morbillivirus vaccines to closely related viruses and suggests the need to further elucidate and characterise the mechanisms of vaccine-induced cross-protection.

1.2.2 Advances towards broad-spectrum vaccines

Although some vaccines do confer protection against multiple serotypes or other members of the same genus, there are also examples of where vaccines are ineffective at providing protection, even at the intraspecies level. Influenza viruses for example, are characterised into four subtypes (A, B, C and D) based on differences in the nucleoprotein and matrix 1 protein and can variably infect and cause disease in humans and/or various animals [18, 19]. Unlike the viruses and vaccines described in *1.2.1*, influenza viruses have rapid mutation rates, undergo genetic reassortment, infect several susceptible hosts and cause waves of infection in the winter and spring, all of which contributes to the evolution and emergence of different influenza strains. The viral envelope of Influenza A, for example, has 18 recognised haemagglutinin (HA) subtypes (H1 – H18) and 11 neuraminidase (NA) subtypes (N1 – N11) [19], meaning a possible ~200 different combinations of Influenza A subtypes could arise during reassortment events (antigenic shift), of which 130 have been identified in nature [20]. Furthermore, each subtype branches into separate clades and subclades of viruses brought about by gradual mutations in HA and NA (antigenic drift). Influenza A viruses have frequently been associated with large outbreaks, including the H3N2 subtype responsible for seasonal flu, the H1N1 subtype known for its role in the 2009 swine flu pandemic and “Spanish flu”, the highly pathogenic H5 viruses, and H5N1 avian influenza, responsible for the current epizootic in poultry and wild birds [18, 21, 22]. Influenza B viruses cause less extensive outbreaks than influenza A viruses and primarily infect humans. However, exceptions to this pattern have been observed for example, following outbreaks of the influenza B Victoria lineage in 2019-2020, which accounted for 50% of all documented influenza virus cases [21]. Influenza C only has a single serotype and typically causes sporadic and mild disease in humans, whereas Influenza D possesses

a unique HA-like protein that has limited antigenic similarity or cross-reactivity with the other influenza viruses. They are however, of veterinary significance owing to the respiratory disease they cause in cattle [21].

Antigenic drift, antigenic shift and a range of ecological (e.g., migration of and interactions between different host species) and genomic factors (e.g., epistatic mutations in the viral genome) make vaccine formulation challenging for the influenza viruses (**Figure 1.2**). Several influenza vaccines have been developed and utilised over the years, e.g. recombinant virus (produced in insect cells), live attenuated vaccines (produced in chicken embryos) and subunit vaccines (produced in chicken embryos and cells lines) [22, 23]. The World Health Organisation (WHO) Global Influenza Surveillance and Response System continually monitors circulating influenza viruses and uses this information to predict and recommend prevalent strains to be included in annual influenza vaccines, usually a trivalent or quadrivalent vaccine comprising the influenza A H1N1 and H3N2 and either one or two influenza B viruses [18]. However, even when there is a perfect match with the outbreak strain of influenza virus, vaccine effectiveness is ~60% and immunity is short-lived and wanes by 6-8 months post-vaccination, which can be even more varied when there is mismatch between the vaccine and circulating strains. These influenza vaccines do not confer any cross-reactivity or protection against influenza C or D (**Figure 1.2**) [23]. These factors present a barrier to vaccine development against influenza viruses, which is compounded by the insufficient scale of vaccine production available through the use of chicken embryos. This can limit the speed at which vaccines are produced, which could be detrimental in potential pandemic situations.

Novel technology platforms and universal vaccine design strategies are being employed in an attempt to circumvent the issues currently facing influenza vaccine researchers and developers. To address the time limitations of current vaccine production, some subunit and all recombinant vaccines can be produced using cell-based technology, which shortens production to 3-4 months, however this is a more costly method [23]. The use of alternative novel adjuvants [23, 24] or next-generation platforms are also being utilised to try to enhance the immune response mediated by influenza vaccines. This includes the use of a quadrivalent mRNA-based vaccine, which has shown to induce greater HA inhibition titres compared to conventional influenza vaccines [25]. In addition, universal influenza vaccines are being explored that target more conserved regions of the HA stalk domain, which have been shown to be cross-reactive with other phylogenetically similar HAs and induce high T-cell responses, but exhibit lower nAb responses than those generated against the HA head domain [18, 26].

Other approaches being explored include targeting other influenza viral structural proteins as vaccine antigen targets, including the nucleoprotein, the matrix protein 2 ectodomain (M2e) or NA. The high conservation of M2e and the nucleoprotein makes them attractive vaccines, which has been demonstrated through use of a monoclonal antibody against this protein resulting in inhibition of viral replication [24]. However, antibodies against M2e are generally poorly neutralising, instead working by mediating FcγR-dependent non-neutralising antibody responses, such as antibody-dependent cell cytotoxicity [24]. A study in pigs receiving aerosol immunisation with a ChAdOx2-based matrix 1 and nucleoprotein vaccine exhibited both T-cell and antibody responses and showed reduced lung pathology and eliminated viral shedding following challenge with H3N2 [27]. The NA glycoprotein functions as a sialic acid cleaving enzyme, playing a role in viral replication. NA also has slower antigenic evolution compared to HA, and antibodies against NA are thought to reduce disease severity and reduce virus transmission by an alternative method of protection [18]. In summary, the poor utility of established vaccines against influenza has prompted the requirement for improved or universal vaccines. This knowledge is vital when considering the design of vaccines for emerging viruses, and was readily applied during vaccination and surveillance of severe acute respiratory syndrome coronavirus 2 (SARS-CoV-2) variants during the coronavirus disease 2019 (COVID-19) pandemic, which is examined in this study.

1.2.3 Cross-protective vaccines for zoonotic viruses with pandemic potential

The ability of some vaccines such as the poxvirus and rinderpest vaccines to induce cross-protection against genetically similar viruses suggests broader utility for these vaccines at an interspecies genus-wide level. More generally, these data and approaches can help shape the development of future broad-spectrum vaccines. The investigation of vaccine utility is particularly pertinent for zoonotic viruses with pandemic potential. This study explores the effectiveness of vaccines against two such groups of viruses, betacoronaviruses and henipaviruses, at an intraspecies and genus-wide level. This will aid our understanding of whether vaccines developed against these viruses can induce cross-protection like the smallpox or rinderpest vaccines, or induce immune-escape like the influenza vaccines, and will inform future vaccine design against these viruses.

1.3 Coronaviruses as emerging and pandemic-causing viruses

1.3.1 Animal and human coronaviruses

The emergence of SARS-CoV-2 in late 2019, denoted the third occurrence of zoonotic spillover of a highly pathogenic coronavirus into the human population in the 21st century. The first of these outbreaks was severe acute respiratory syndrome coronavirus 1 (SARS-

CoV-1), emerging in 2002 in China and infecting ~8,000 individuals, resulting in 10% mortality across 29 countries [28]. Disease presentation following infection with SARS-CoV-1 included fever, cough, dyspnoea and in some cases, watery diarrhoea [29]. There was evidence of human-to-human transmission of the virus, notably within healthcare workers, and a higher fatality rate in older adults [29]. Subsequently in 2012, an outbreak of Middle Eastern respiratory syndrome coronavirus (MERS-CoV) was reported following isolation of the virus from the sputum of a male who died from respiratory and renal failure [30]. Similar to SARS-CoV-1, viral replication of MERS-CoV was preferentially in the lower respiratory tract, resulting in prominent gastrointestinal symptoms and often caused acute kidney failure, and in most cases also leading to the development of hospital-acquired infections [29, 30]. Unlike SARS-CoV-1 which although spread rapidly worldwide, was contained and eliminated within a relatively short space of time using public health measures, MERS-CoV subsequently caused outbreaks in South Korea in 2015 and again in Saudi Arabia in 2018, with ongoing sporadic outbreaks still being reported [28, 29]. Since 2012, there have been 2,260 confirmed cases of MERS-CoV across 27 countries, of which 803 have been fatal (~35% mortality) [28, 31].

In addition, the seasonal human coronaviruses (HCoV) HCoV-OC43, HCoV-229E, HCoV-HKU1 and HCoV-NL63 also result in phenotypically mild upper respiratory illness, and are collectively associated with 10-30% of common cold cases [32, 33]. The coronaviruses are single-stranded, positive-sense RNA viruses, within the family *Coronaviridae* which is specified further into the *Orthocoronavirinae* subfamily consisting of four genera: *alphacoronavirus*, *betacoronavirus*, *gammacoronavirus* and *deltacoronavirus* [31]. Of the coronaviruses that cause disease in humans, SARS-CoV-1, SARS-CoV-2, MERS-CoV, HCoV-HKU1 and HCoV-OC43 are classified as betacoronaviruses, whereas HCoV-2293E and HCoV-NL63 are classified as alphacoronaviruses [32, 34]. The use of an alternative receptor and receptor distribution of the α-coronaviruses, or because HCoVs are endemic and encountered early in life, may explain in part the less severe pathogenicity and self-limiting infection [34] these human viruses exhibit compared to human β-coronaviruses. Several of these viruses are thought to have originated from bats, transmitted to humans via intermediate hosts. For example, HCoV-229E is thought to have been transmitted to humans from bats via alpaca, SARS-CoV-1 via masked palm civets and MERS-CoV via camels. For HCoV-HKU1 and HCoV-OC43 however, the natural host of these viruses is thought to be rodents, with zoonotic spillover to humans for HCoV-OC43 via a bovine intermediate host [32].

Coronaviruses are also of agricultural significance, showing evidence of infection and disease in animals, and prior to the emergence of SARS-CoV-2, the coronavirus research

field predominantly focused on coronaviruses with veterinary significance. The first coronavirus identified in 1937 was the avian gammacoronavirus, infectious bronchitis virus (IBV), causing acute respiratory disease in domestic fowl [35]. There is also evidence of alphacoronavirus infection resulting in respiratory disease in cats (feline coronavirus, FCoV), dogs (canine coronavirus, CCoV) and pigs (porcine respiratory coronavirus, PRCV; swine acute diarrhoea syndrome coronavirus, SADS-CoV) [31, 35]. Interestingly, the emergence of PRCV occurred as a result of a mutation causing a deletion in the N-terminal domain in the Spike attachment protein of another alphacoronavirus, transmissible gastroenteritis virus (TGEV) [36]. This Spike mutation results in altered *in vivo* tissue tropism of these viruses, with PRCV exhibiting mild respiratory disease, whereas TGEV causes diarrhoea in pigs [35, 36]. Other coronaviruses are also enteropathogenic in pigs, including the alphacoronavirus, porcine epidemic diarrhoea virus (PEDV), first isolated in 1977, and the porcine deltacoronavirus (PDCoV), initially detected in 2009 [32, 35, 37]. Betacoronaviruses also cause infection in mice (murine hepatitis virus, MHV), cattle (bovine coronavirus, BCoV), pigs (porcine haemagglutinating encephalomyelitis virus, PHEV), and in dogs (canine respiratory coronavirus, CRCoV) [35]. In this study, the utility of vaccines has been assessed for a single genus within the *Orthocoronavirinae* family, the betacoronaviruses, with a focus particularly on the *Sarbecovirus* subgenus to assess the antigenicity of the pandemic-causing SARS-CoV-2 and related sarbecoviruses with spillover potential.

1.3.2 SARS-CoV-2 and the COVID-19 pandemic

The COVID-19 pandemic emerged in late 2019 caused by infection with SARS-CoV-2 [38]. Infection with SARS-CoV-2 varies from asymptomatic and mild flu-like symptoms to more severe respiratory disease, long-term pulmonary, cardiological and neurological complications, and death [28]. Mutations in the SARS-CoV-2 genome have continued to emerge during the pandemic, resulting in the emergence of SARS-CoV-2 variants that showed increased transmissibility, disease severity and immune escape from vaccination or naturally acquired immunity [39]. In particular mutations have arisen within the surface Spike glycoprotein, which is the main target for nAb responses and the target antigen for the majority of approved COVID-19 vaccines [40]. The first documented mutation that emerged in Spike was an amino acid change at position 614 – a glycine (G) to an aspartic acid (D) change, giving rise to Pango Lineage B.1, which replaced the original Wuhan variant, with 75% of all cases being attributed to this variant by the end of November 2020 [41-43]. Since then, other variants have continued to emerge in various parts of the world, with the majority acquiring the D614G mutation from B.1, along with additional mutations in the Spike protein [44]. Viral genome sequencing efforts, such as the COVID-19 Genomics UK Consortium and CoVariants were subsequently established to monitor the evolution of

the virus worldwide and to collect epidemiological data [44]. These variants were assigned Pango Lineage nomenclature, and variants which were assigned high priority due to their ability or suspected ability to cause more severe disease, or variants which conferred immune evasion were assigned Greek letter identifiers by the WHO (**Figure 1.3**) [45].

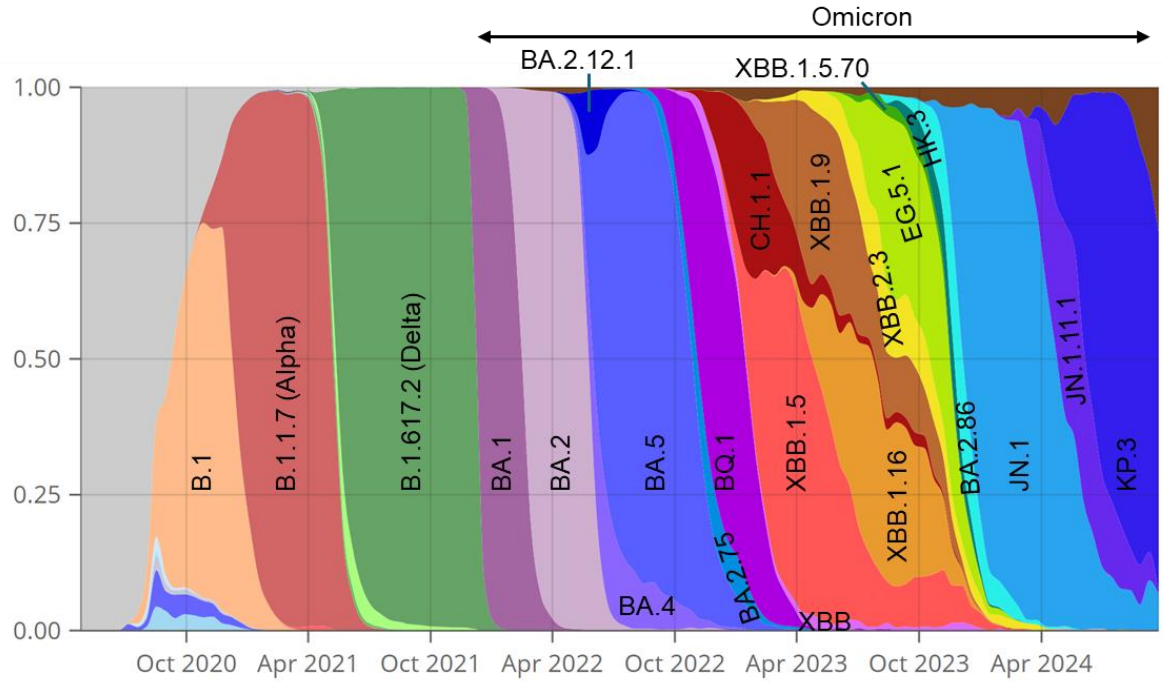

Figure 1.3: Emergence of SARS-CoV-2 variants in the UK.
A number of SARS-CoV-2 variants have continued to emerge over the course of the COVID-19 pandemic, some of which have been designated Greek alphabet identifiers based on their priority for monitoring based on increased transmissibility, disease severity and immune escape profile (Alpha, Delta and Omicron in the UK). The Omicron variant emerged in December 2021, with subsequent variants all sub-lineages of Omicron. Data is accurate as of October 2024 from https://covariants.org.

Moving forward, in the UK the Alpha variant (Pango Lineage B.1.1.7) emerged in late September 2020, quickly replacing B.1 as the dominant circulating strain (**Figure 1.3**) [46]. The Alpha variant harbours 3 deletions and 7 mutations in the Spike protein, in addition to the already established D614G mutation [46]. Transmission of this variant was 43-90% greater compared to Wuhan, attributed to the presence of an N501Y mutation in the Spike receptor binding domain (RBD), which has been shown to result in higher viral loads and prolonged persistence of the virus in the respiratory tract [46, 47]. Despite the increased transmission of the Alpha variant, it was still neutralised well by convalescent plasma and vaccine sera [48]. In other parts of the world, the Beta (Pango Lineage B.1.351, South Africa) and Gamma (Pango Lineage P.1, Brazil) variants also emerged, possessing the same N501Y mutations as Alpha, with additional RBD mutations E484K and K417N/T which resulted in ~10-fold reduction in neutralisation from vaccinee sera [49-51].

The Delta variant (Pango Lineage, B.1.617.2) was first detected in India in October 2020, and subsequently emerged in the UK in December 2020, superseding the Alpha variant to become the dominant circulating strain (**Figure 1.3**). This variant showed evidence of reduced nAb titres in convalescent sera and in vaccine sera [49, 52]. This was likely due to the presence of an L452R mutation in the Spike RBD, which was shown to have increased affinity for ACE2 and induce higher pathogenicity in hamster models compared to B.1 [53, 54]. Later, the emergence of Omicron (Pango Lineage B.1.529) BA.1 and BA.2 in November 2021 in Botswana, resulted in an almost complete loss of nAb titres from pre-existing vaccine-induced immunity in individuals who had received two vaccine doses [49, 55-57]. Despite this, the BNT162b2 and Ad26.COV.2 vaccines were still able to provide robust protection against severe disease (70-72%) despite the obvious reduction in nAb response, suggesting the involvement of non-neutralising antibodies and cell-mediated immune responses in mediating protection [34]. This finding suggests although nAbs are an important measure of immunity, they may not be the definite marker of protection, and leans to more significant involvement of other arms of the immune response in mitigating serious risk from disease. To mitigate against the threat of variants, booster vaccinations particularly to clinically vulnerable individuals (e.g. older adults, immunosuppressed individuals [58]) have continued to be administered which have shown to be able to induce sufficient nAb responses against Omicron subvariants as they have continued to emerge [49, 59, 60].

Later in the pandemic, vaccines with updated Spikes harbouring more recent Omicron subvariants have also been developed and administered to vulnerable cohorts, including monovalent or bivalent mRNA-based vaccines (e.g., Spikevax Wuhan/BA.1 [61], Comirnaty Wuhan/BA.5 [62], Comirnaty XBB.1.5 [63]), which have induced broad nAb responses and cellular responses against more recent Omicron subvariants, including E.G.5.1, XBB.1.5, XBB.1.16 and JN.1 [60, 61, 64, 65]. However, boosting with the Comirnaty XBB.1.5 vaccine yields neutralisation titres against the antigenically distinct JN.1, ~2.5-fold lower than against the homologous XBB.1.5 antigen [63]. Therefore, the current recommendation from WHO advises the use of a vaccine encompassing the JN.1 variants in future vaccine formulations to mitigate disease against evolving SARS-CoV-2 variants [58]. These data highlight that although COVID-19 vaccines were successful in reducing infection and disease from SARS-CoV-2 infection, particularly earlier on in the COVID-19 pandemic, the emergence of antigenically distinct variants has reduced the efficacy of established vaccines, requiring booster vaccinations or the development of updated vaccines to increase immunity. In this study, this is explored using sera from a clinically vulnerable cohort of older adults to assess vaccine efficacy and antigenicity at the intraspecies level.

1.3.3 Other sarbecoviruses

Several other sarbecoviruses have been identified in bat and pangolin reservoirs that as of yet, do not appear to show evidence of spill-over into other animal or human populations [66-71]. Some of the bat sarbecoviruses that have been discovered cluster phylogenetically with SARS-CoV-1 or SARS-CoV-2 and show evidence of binding to ACE2 [66, 72]. Many of the ACE2s of the respective host bat species these bat sarbecoviruses were isolated from, also exhibit the ability to bind and allow entry of SARS-CoV-1 and/or SARS-CoV-2 [73]. For example, RaTG13 which arose in China, and bat sarbecoviruses found in Laos (e.g., BANAL-20-52) have exhibited high nucleotide sequence similarity with SARS-CoV-2 throughout the length of the genome (96.1% for RaTG13, 96.8% for BANAL-20-52) [66]. Additionally, pangolin-derived sarbecoviruses have shown high sequence similarity to the SARS-CoV-2 RBD, such as GX_P2V, GD/1/2019 and GC_P1E [71]. Furthermore, there have also been viruses isolated that cluster with the clade Ia virus, SARS-CoV-1, including WIV-1, which also exhibits the ability to use ACE2 as a receptor for entry [72]. Subsequently, bat coronaviruses have been isolated in other parts of the world that fall into other sarbecovirus phylogenetic clades, including Rc-o319 (clade V) [68], RhGB07 (clade III) [74], and RaTG15 (clade IV) [75]. In addition, several clade 2 sarbecoviruses (e.g., Rp3, Rf1) have been identified, mainly in China, but these viruses appear to have large deletions within the receptor binding motif, which results in these viruses being unable to use ACE2 as their functional receptor, and the receptor for these viruses is yet unknown [71, 72]. Given the history of the emergence of SARS-CoV-1 and SARS-CoV-2 in animals and humans, there could be the possibility that other sarbecoviruses are also zoonotic. Therefore, in this study the zoonotic potential of bat sarbecoviruses has been explored through assessment of mammalian ACE2 usage. This analysis has been expanded further to examine the cross-neutralisation profile of bat sarbecoviruses to understand the likelihood of SARS-CoV-2-derived immunity in eliciting cross-protection against related viruses at the subgenus level.

1.4 Sarbecovirus molecular biology and entry

1.4.1 Sarbecovirus molecular biology

Sarbecoviruses comprise a subgenus within the *Betacoronavirus* genus of the *Orthocoronavirinae* family of viruses. The sarbecovirus virus particle consists of an enveloped positive-stranded RNA genome of ~30kB in size that contains 14 open reading frames (ORFs) and encodes 29 viral proteins (**Figure 1.4A**) [76]. The genome is flanked by two short untranslated regions at the 5' and 3' end, with two overlapping polyproteins, pp1a and pp1ab located at the 5' end. These polyproteins account for two-thirds of the sarbecovirus genome and are digested into 16 non-structural proteins (NSPs) by viral

proteases (**Figure 1.4B**) [76]. These NSPs are involved in numerous functions in viral replication and assembly, and participate in viral pathogenesis through immunomodulation, antagonising the antiviral response and regulation of early transcription [77]. The genome also consists of structural proteins encoded by four 3' ORFs, including a nucleocapsid protein (N) enclosed in a lipid bilayer expressing three membrane proteins involved in viral entry: the Spike (S) attachment protein, membrane protein (M) and envelope protein (E) (**Figure 1.4A**) [30, 77]. Several accessory proteins (ORF3a, ORF3b, ORF6, ORF7a, ORF7b, ORF8b, ORF9b, ORF10) lie between the structural genes and are responsible for regulating viral infection (**Figure 1.4B**) [76]. The N protein also plays a role in modulation of the host cellular response to infection in addition to its primary role in packaging and stabilisation of the viral genome [77].

The Spike protein is a homotrimeric type I membrane protein, mediating fusion of the viral and host cell membranes. It comprises two functional subunits, S1 and S2, responsible for attachment and membrane fusion, respectively (**Figure 1.4B**). For the sarbecoviruses, the S1/S2 interface is cleaved by furin-like proteases, including transmembrane protease serine 2 (TMPRSS2), trypsin, cathepsin B or cathepsin L to mediate a conformational change that allows the S2 to perform its role in fusion, whilst remaining associated to S1 through non-covalent interactions [30, 33, 76]. The S1 domain consists of the NTD and RBD (**Figure 1.4B**). The RBD adopts two conformations, starting in a pre-fusion closed "down" state, which shields the receptor-binding regions, which then adopts an open "up" state that is receptor-accessible [78]. The exact function of the NTD is not well characterised, but it is suggested that part of the sequence contains a highly conserved N-glycosylation site that can mediate binding to host-cell sugars, which has been observed with other coronaviruses such as TGEV and BCoV [35]. Additionally, sites in the NTD could allow binding to alternative receptors to mediate entry, which has been described for the betacoronavirus MHV, which binds to CEACAM1 [35]. The S2 domain contains fusion peptide regions which are inserted into the host cell membrane during fusion, and heptad repeats important during pre-fusion rearrangements that aid bringing the viral and host cell membrane in close apposition to allow for fusion to occur (**Figure 1.4B**).

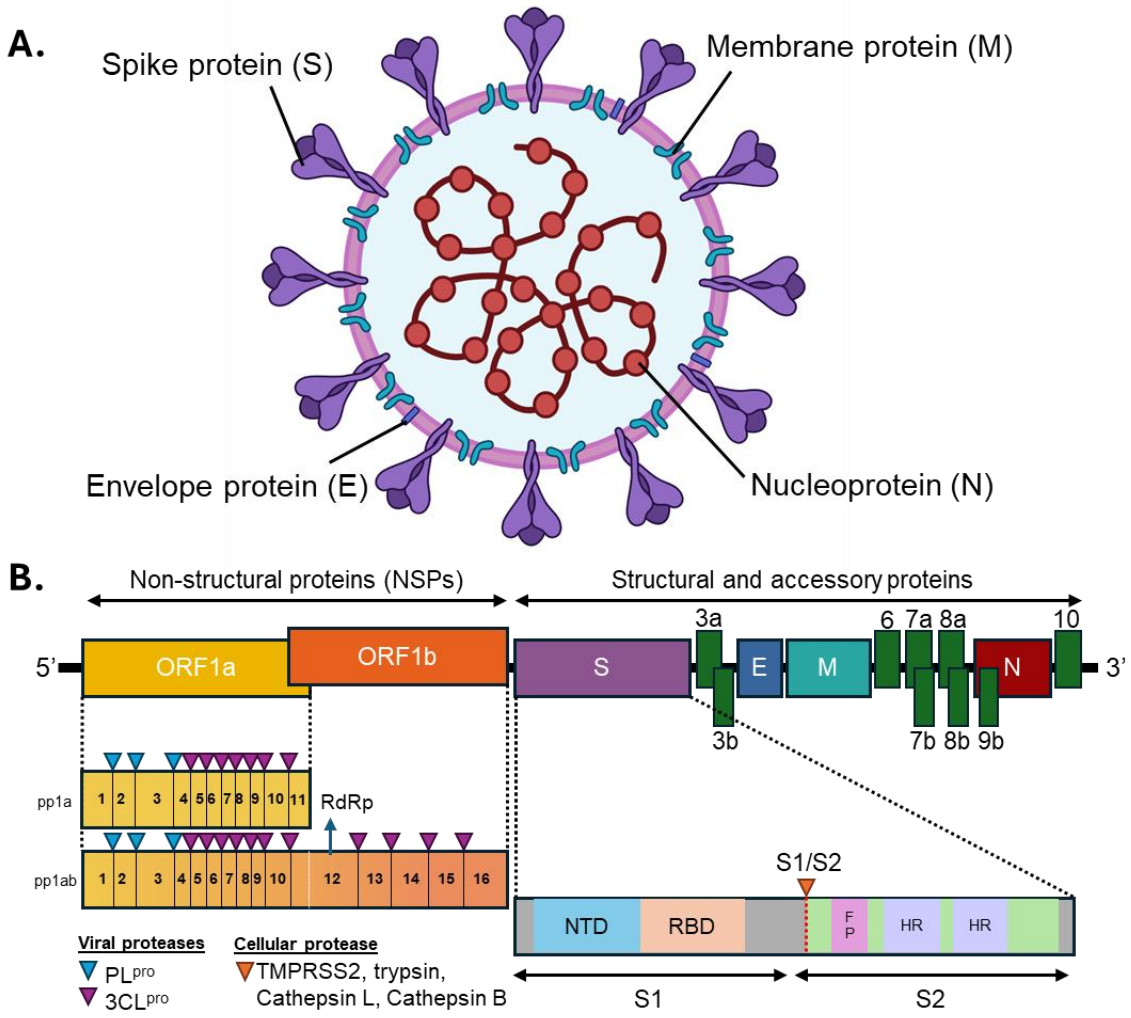

Figure 1.4: Sarbecovirus virion and genome arrangement.
(A) Sarbecovirus virion comprising a lipid bilayer embedded with the attachment Spike (S) protein, membrane protein (M) and envelope protein (E), enclosing the nucleoprotein (N) associated with positive-stranded viral RNA. Image was generated in BioRender. **(B)** Sarbecovirus genome, flanked by 5' and 3' UTRs. At the 5' there are two overlapping open reading frames (ORFs) that encode 2 polyproteins (pp1a, pp1ab) that are cleaved by the viral proteases, papain-like protease (PL^{pro}) or 3C-like protease ($3CL^{pro}$) generating 16 non-structural proteins (NSPs). NSP12 contains the RNA dependent RNA polymerase (RdRp). The rest of the viral genome encodes the structural proteins (S, E, M, N), along with several accessory proteins (ORF10 is in SARS-CoV-2 only). The Spike protein facilitates entry into the host cell, and comprises: (i) the S1 domain, which contains the N-terminal domain (NTD) and receptor binding domain (RBD) required for receptor attachment and, (ii) the S2 domain which contains a fusion peptide (FP) and heptad repeats (HR) which facilitate fusion of the cell and viral membranes. The red dotted line depicts the S1/S2 cleavage site to mediate a conformational change in the Spike protein to allow the S1 and S2 proteins to carry out their functions. The S1/S2 site is cleaved by host proteases such as TMPRSS2, trypsin, Cathepsin L or Cathepsin B.

1.4.2 Sarbecovirus entry and replication

Virus entry is initiated by binding of the Spike protein to the host receptor for attachment to the cell membrane and subsequent fusion of the viral and host membranes to allow release of viral RNA into the cell. For the sarbecoviruses the functional receptor for entry is angiotensin converting enzyme 2 (ACE2) [32, 69]. The alphacoronvirus, HCoV-NL63 also uses ACE2 as its entry receptor, whilst other alphcoronaviruses use aminopeptidase N (APN) [32]. Alternative receptors are also used by other coronaviruses that cause human disease, with HCoV-OC43 using sialic acids to mediate entry, and MERS-CoV utilises

dipeptidyl peptidase IV (DPP4) [32]. Upon receptor binding and fusion of Spike with the host membrane, a fusion pore is formed via insertion of the fusion peptide, which enables release of the viral RNA into the cell [76, 77]. Subsequently, processing of the polyproteins via 3C-like protease and papain-like protease gives rise to mature 16 NSPs, consisting of the RNA-dependent RNA polymerase (RdRp, NSP12) that assemble to initiate viral RNA replication and transcription [76, 79]. Following capping, subgenomic viral mRNAs are able to act as templates for protein translation. Mature progeny virions are assembled in the endoplasmic reticulum and Golgi body (mediated by M and N for SARS-CoV-1, or M and E for SARS-CoV-2 [33]), and are subsequently transported in vesicles to the plasma membrane, and released via exocytosis [76, 79].

1.5 Vaccine development and the use of monoclonal antibodies against betacoronaviruses

1.5.1 Monoclonal antibodies against SARS-CoV-2

At the beginning of the pandemic potent monoclonal antibodies (mAbs) that had been generated against SARS-CoV-1 were investigated for repurposing against SARS-CoV-2 [80]. These mAbs target the Spike protein, however mAbs such as M396, 80R and 4A8 exhibited lower affinity for their respective epitopes in SARS-CoV-2 Spike, although CR3022 showed some capacity to bind [80]. CR3022 in particular showed great promise as a potential broad-spectrum monoclonal because it binds to a conserved region distal to the ACE2 receptor binding site on the RBD of both SARS-CoV-1 and SARS-CoV-2 [80]. However, CR3022 was unable to neutralise SARS-CoV-2 pseudovirus, including the Alpha and Beta variants [81].

Later, regulatory bodies such as the US Food and Drug Administration and the European Medicines Agency, granted emergency use for authorisation of several mAbs specific for the treatment of mild-moderate SARS-CoV-2 infection in individuals who did not require hospitalisation, but were considered at risk of more severe disease progression [82]. Different classes of mAbs were selected that target different regions and conformations of the Spike protein: (i) imdevimab (REGN10933) and etesevimab (LY-CoV016), which bind to epitopes on the ACE2 receptor binding site when the RBD is in the “up” conformation, (ii) bamlanivimab (LY-CoV555), which also binds the receptor binding site, but is able to do so when the RBD is in both the “up” and “down” conformation, and (iii) casirivimab (REGN10987) and sotrovimab (VIR-7831), which bind to a highly conserved epitope away from the receptor binding site, that is only accessible in the RBD “up” conformation [82].

Bamlanivimab was able to confer protection against SARS-CoV-2 infection in non-human primates [83]. This mAb also showed evidence of prophylaxis in randomised phase 2/3, placebo-controlled studies with reduced viral loads either administered on its own, or in combination with etesivimab, and was generally well-tolerated even at high doses (7000mg) [84, 85]. However, emergency use of bamlanivimab was revoked in April 2021 due to resistance against emerging circulating SARS-CoV-2 variants at the time, such as Beta and Gamma [82]. Two non-competing mAbs known as REGN-COV2 (casirivimab and imdevimab) target different regions in SARS-CoV-2 Spike, with imdevimab directly binding the receptor binding site, and casirivimab binding a distal site [82]. This antibody cocktail was delivered as a prophylactic in pre-clinical rodent and non-human primate studies, which showed evidence of reduced viral load in the upper and lower respiratory tracts, and subsequently, reduced pathology [86]. REGN-COV2 mAbs also resulted in significant reduction in viral titre in phase 1-3 clinical trials in individuals receiving 2400mg or 8000mg doses [87].

The most promising mAb that has been approved for use is sotrovimab, which was isolated from an individual who had been infected with SARS-CoV-1 in 2003 [82]. A randomised phase 3 study resulted in reduced requirement of hospitalisation of emergency department visits in 85% of individuals who were administered sotrovimab, and adverse effects were noted in 17% of treated patients [88]. Sotrovimab has also exhibited neutralisation of other SARS-CoV-2 variants, including Alpha, Beta, Delta and Gamma, and is also effective against the Omicron BA.1 variant [82]. However, there have been concerns of mutations arising in both BA.1 and BA.2 lineages following treatment with sotrovimab in immunosuppressed individuals [89]. This poses a risk of breakthrough infections with more antigenically distant SARS-CoV-2 variants that could invalidate current mAbs approved for emergency use. These studies do however highlight the success of antibody cocktails that target different epitopes in Spike, particularly to conserved regions. This approach could be explored further for the development of more broad-acting antibody therapies against not only SARS-CoV-2 variants, but also other related sarbecoviruses.

1.5.2 Vaccine development for SARS-CoV-2

Prior to the COVID-19 pandemic, there were no licensed vaccines for use against human coronaviruses. Vaccine development for COVID-19 occurred at an unprecedented speed, with the first two vaccines, the BioNTech/Pfizer (Comirnaty®, BNT162b2) and the Oxford-AstraZeneca (Vaxzervria™, AZD1222) vaccines, being given emergency approval for use. Both vaccines were highly efficacious, resulting in reduced hospitalisation and mortality [90, 91]. However, the rapid evolution of SARS-CoV-2 revealed concerns that strain-specific vaccinations might be insufficient in inducing long-term immunity against antigenically

variable variants. To date, there have been nine COVID-19 vaccines authorised for use in multiple countries that have been designed to target the original WT SARS-CoV-2 sequence. These have all been shown to be effective at inducing nAbs and cell-mediated responses to varying levels [34, 92]. The initial vaccines were all based on the ancestral Wuhan virus, including inactivated virus vaccines (CoronaVac, Civilo, Covaxin), mRNA-based vaccines (Spikevax mRNA-1273, Comirnaty-BNT162b), viral-vectored vaccines (Vaxzevria and Covishield ChAdOx1, Ad26.COV2) and subunit proteins (Nuvaxovid and Covovax NVX-CoV2373) (**Table 1.1**) [34, 93]. Two doses of the BNT162b2 [91], mRNA-1274 [94] or the Ad26.COV.2 [95] vaccines showed 94-95% efficacy in randomised, placebo-controlled phase 3 clinical trials [34]. Although all the vaccines did not necessarily prevent symptomatic infection (52.4% - 93%), there were effective at reducing severe disease, which was vital to reduce the burden on hospital staff and in reducing mortality rates (**Table 1.1**).

Table 1.1: COVID-19 vaccines authorised for use globally using different vaccine platforms.

				Efficacy		
Platform	**Vaccine**	**Manufacturer**	**Authorisation status**	**Phase 3 clinical trial**	**Preventing symptomatic infection**	**Preventing severe disease**
mRNA	BNT162b2 [96]	Pfizer/ BioNTech	**Approved** in several countries. Emergency use in USA, EU and other countries	95%	91.3%	96.7%
	mRNA-1273 [94]	Moderna	**Approved** in Switzerland. Emergency use in USA, UK, EU, and other countries	94%	93.2%	98.2%
Viral vector	AZD1222 [97]	Oxford/ AstraZeneca	Emergency use in the UK, EU and other countries	62%	74%	100%
	Ad26. COV2.S [95]	Janssen	Not approved	94%	52.4%	74.6%
	Ad5-nCoV [98]	CanSino Biologics	Limited use in China. Emergency use in Mexico, Pakistan	65.7%	57.5%	91.7%
Inactivated virus	BBV152, Covaxin [99]	Bharat Biotech	Emergency use in India	-	77.8%	93.4%
	BBIBP-CorV [100]	Sinopharm	**Approved** in China, UAE, Bahrain, Emergency use in Egypt and other countries	79%	78.1%	100%
	CoronaVac [101]	Sinovac	**Approved** in China. Emergency use in Brazil and other countries	50-91%	50.7%	100%
Subunit protein	NXV-CoV2372 [102]	Novavax	Not approved	-	89.7%	100%

Adapted from Rando H et al., *mSystems* (2023) and Tan CW et al., *Cell Host Microbe* (2023)

1.5.3 Broad-spectrum vaccines against other coronaviruses.

Vaccines have been developed against several animal coronaviruses, including CCoV, FCoV, PEDV, TGEV, BCoV, MHV, IBV and PDCoV. These vaccines have generally been designed using live-attenuated or DNA vaccines platforms, but recombinant virus platforms (TGEV, PEDV, BCoV) and mRNA-based (PEDV) platforms have also been developed [32]. Many of these vaccines have been approved for use in agriculture, with varying effectiveness. For example, live-attenuated vaccines against PEDV have yielded high

protection rates in piglets, but a bivalent TGEV/PEDV attenuated vaccine induces inadequate protection against different virus strains [32].

Moreover, various vaccines targeting SARS-CoV-1 and MERS-CoV have been developed and tested in pre-clinical models, using various vaccine platforms (e.g., whole virus, Spike/Nucleocapsid subunit vaccines, viral vectors), but approval for these vaccines was halted when evidence of human infection ceased. Examples of SARS-CoV-1 vaccines include inactivated virus and DNA vaccines which reached phase 1 clinical trials [30]. For MERS-CoV, several vaccines have been developed that have reached various stages of clinical trial, including DNA vaccines (Phase 1/2a completed) and viral vectored vaccines, including the ChAdOx1 platform (Phase 1) that the latterly-approved COVID-19 ADZ1222 vaccine was based on [28, 34]. These vaccines induced strong antibody-dependent and CD4+ T cell-dependent protection in humans and animals, however some adverse effects were also noted, including antibody-dependent enhancement (ADE) of disease, indicating the requirement for further optimisation of these vaccines [28, 103].

Theoretically some of these vaccines, had development continued, may have been suitable candidates for testing and administration early in the COVID-19 pandemic, which may have saved many lives. Studies in mice have shown that immunisation with a SARS-CoV-1 vaccine conferred protection against SARS-CoV-2 while infection of mice with HCoV-OC43 elicited cross-reactive antibodies against SARS-CoV-1 and SARS-CoV-2 (**Figure 1.5**) [104]. Another study examined the pan-sarbecovirus nAb responses in survivors of SARS-CoV-1 infection immunised with BNT162b2 and noted the presence of potent nAbs against both viruses, SARS-CoV-2 variants (Alpha, Beta, Delta) and against bat and pangolin sarbecoviruses (GD-1, RaTG13, GX-PSL, RsSHC014, WIV-1) [105]. This highlights the importance of understanding the degree of cross-protection across virus families conferred by vaccines.

Taking into consideration the desire for universal viral vaccines, elucidating whether the currently approved COVID-19 vaccines could provide any degree of cross-protection against SARS-CoV-1, MERS-CoV or other sarbecoviruses would provide information on their use as proactive vaccines to protect against future zoonosis. A study analysing sera from COVID-19 convalescent and vaccinee sera noted the presence of modest nAb responses against WIV16, the absence of nAbs against SARS-CoV-1, but interestingly, greater nAb titres against RaTG13 than that observed against SARS-CoV-2 (**Figure 1.5**) [106]. Similarly, analysis of sera from individuals vaccinated with BNT162b2 or mRNA-1273 revealed little to no nAb response against SARS-CoV-1 pseudoviruses after 2 vaccines doses, however this was increased slightly in individuals who showed evidence of prior

infection in addition to vaccination [107]. Recently, more pan-sarbecovirus vaccine candidates have been developed, with one such candidate utilising a mosaic nanoparticle platform to express the RBDs of SARS-CoV-2 and seven bat or pangolin sarbecoviruses (RaTG13, RsSHC014, Rs4081, RmYN02, Pang17, Rf1 and WIV1). This vaccine induced broad nAb responses in mouse and non-human primate models, and protected from infection against SARS-CoV-2 Delta and SARS-CoV-1 [108].

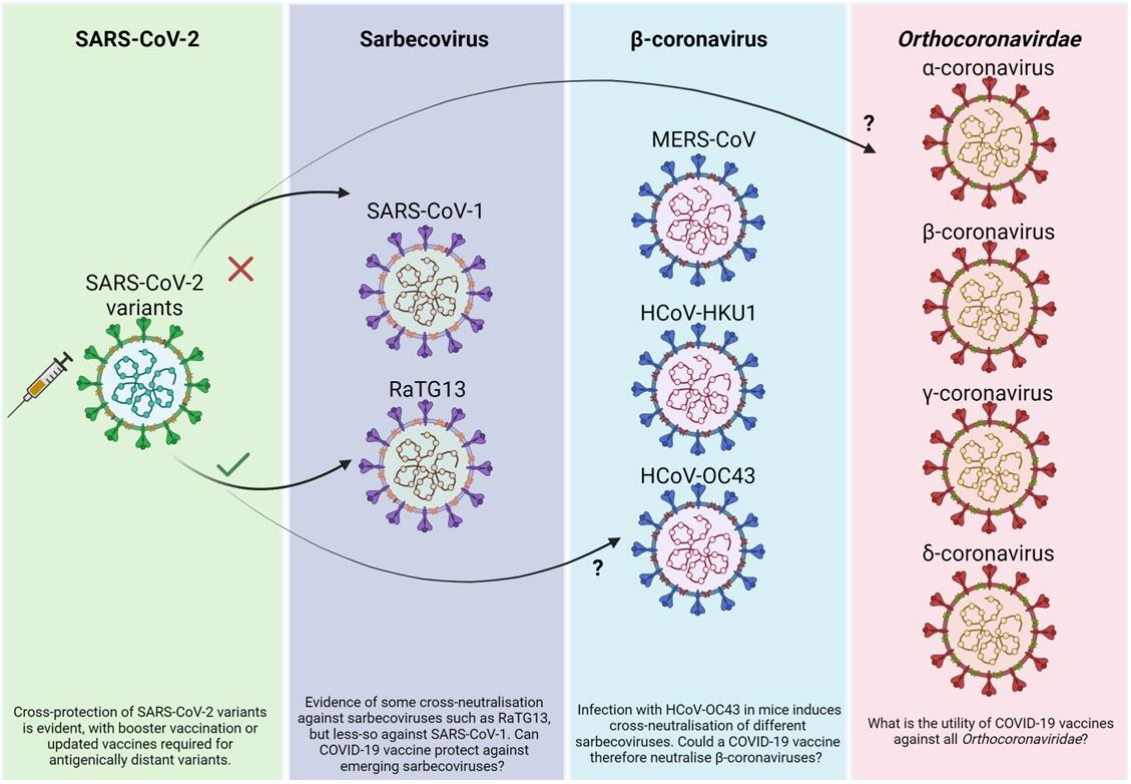

Figure 1.5: Understanding the utility of COVID-19 vaccines at the genus-wide and family-wide level. COVID-19 vaccines have shown robust neutralisation of SARS-CoV-2 variants, with escape from neutralisation noted against more antigenically distant variants (e.g., Omicron). Neutralisation of these more distant variants can be achieved with booster vaccinations and the use of updated vaccines expressing Omicron Spikes. There is evidence of cross-neutralisation of the bat sarbecovirus RaTG13 with SARS-CoV-2 convalescent or vaccinee sera, but this does not extend to SARS-CoV-1, but points to the possibility of a pan-sarbecovirus vaccine. Further studies are yet to be conducted to understand the utility of COVID-19 vaccines to act as pan-β-coronavirus or pan-coronavirus vaccines, with the aim of developing universal vaccines. Image was created using BioRender.

The presence of cross-neutralising antibodies against SARS-CoV-2 variants (at the intraspecies variation level) and other sarbecoviruses (interspecies variation) following COVID-19 induced infection or immunisation suggests the possibility of repurposing these vaccines as pan-sarbecovirus vaccines. However, more research is required to understand the breadth of immunity provided by these vaccines against more distantly related viruses, focusing on those that have the greatest potential to spillover into animal or human populations. Also, understanding the utility of these vaccines at the whole coronavirus genus or family level would also be of interest, given the propensity of seasonal coronaviruses to cause mild disease in humans (**Figure 1.5**). These studies would allow us

to utilise the knowledge gained through vaccine development for COVID-19 and apply it to other virus groups with pandemic potential, e.g. the henipaviruses.

1.6 Henipaviruses and parahenipaviruses as emerging pathogens

1.6.1 Hendra virus emergence and transmission

The WHO have identified several priority viral pathogens for research and development based on those that pose the greatest risk to public health, i.e. due to their epidemic potential and/or the availability of countermeasures. Nipah virus (NiV) and other henipaviral diseases are listed amongst those priority pathogens due to the high mortality rate and the lack of licensed vaccines or therapeutics [109]. The henipaviruses are negative sense, single-stranded RNA viruses, taxonomically classified within the *Paramyxoviridae* family. NiV and Hendra virus (HeV) cause severe and often fatal encephalitis and respiratory disease in human populations and in animals, both naturally and experimentally [110-112]. HeV was the first henipavirus discovered, isolated in 1994 after an outbreak of disease in 21 horses that presented with high fever and acute respiratory symptoms, following spillover via *Pteropus* flying foxes (*P. conspicillatus, P. scapulatus, P. alecto, P. poliocephalus*) through exposure to infected urine and faecal matter [113]. The virus was subsequently transmitted to 2 people who had close contact with the infected horses, one of whom died [113]. There have since been sporadic outbreaks of equine HeV infection in horses in Australia, with 67 total outbreaks noted and the most recent occurring in 2013 [113]. In 2021, a novel, phylogenetically distinct HeV genotype was characterised following surveillance and positive genome sequencing of spleen and kidney samples from 11/98 Australian flying foxes, demonstrating 83% nucleotide similarity to previously published HeV genomes [114, 115].

Although not yet confirmed experimentally, horse-to-horse transmission of HeV was noted during the 1994 and 2008 outbreaks, but there is little evidence of spillover of HeV to other species, either via bats or through the equine intermediate reservoir, apart from to humans (7 cases, 57% fatality) (**Figure 1.6, green**) [113]. However, antibodies to HeV were detected in a dog in 2013, but no virus was detected, and the dog was euthanised as a precautionary measure [113]. Despite the apparent lack of natural infection of other species by HeV, several mammalian species develop clinical disease following experimental infection with HeV, such as guinea pigs, hamsters, ferret, pigs, African green monkeys, and particularly cats, which develop similar disease to that seen in horses [113, 116, 117]. Clinical presentation of HeV in humans presents as non-specific influenza-like symptoms lasting from 5 to 21 days. In four patients this progressed to more severe disease, including acute encephalitis, meningitis and lung infiltrates [113]. The pathological hallmarks of HeV

infection in humans include vasculitis, ischaemia, tissue necrosis and presence of viral antigens or RNA in CNS tissues [113].

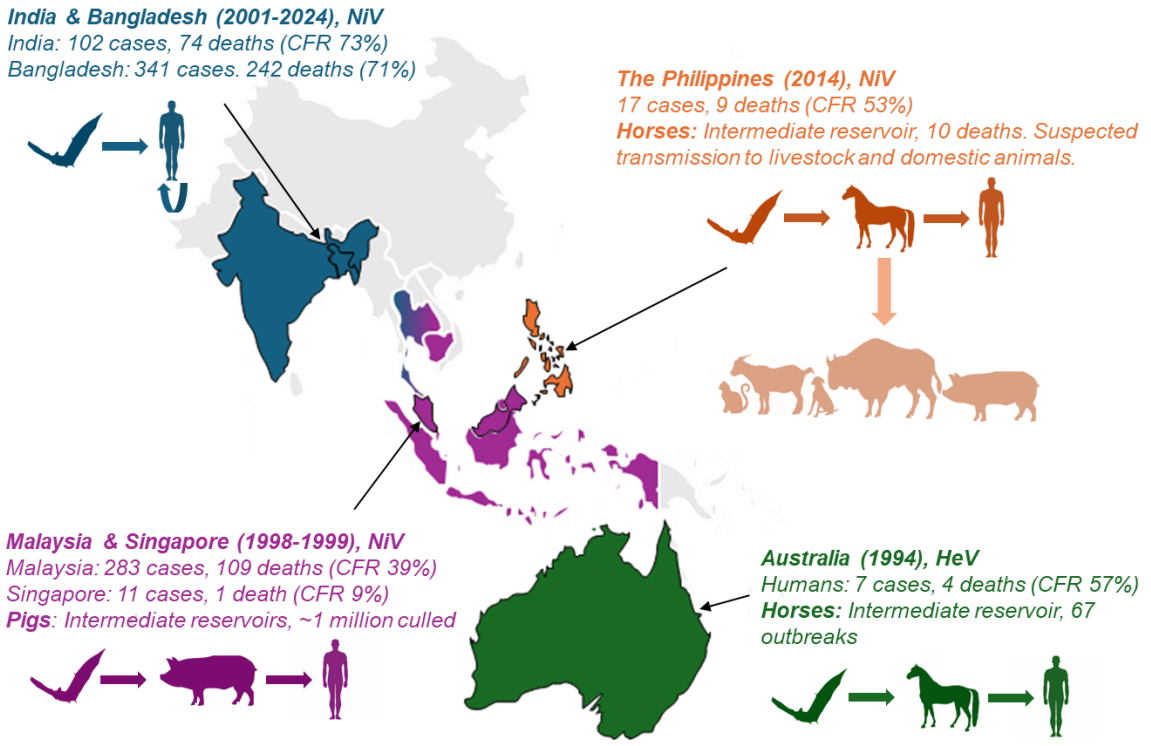

Figure 1.6: Henipavirus transmission, cases, deaths and case fatality ratios (CFR).
Map showing Nipah virus (NiV) and Hendra virus (HeV) outbreaks, with affected countries outlined in black and the animal transmission chain also described. The number of reported cases and deaths, and the case fatality ratio (CFR, %) for each outbreak is also included. **Green**: outbreak of HeV in Australia, with virus spillover from bats to humans via an equine intermediate host. **Purple**: outbreak of NiV in Malaysia and Singapore, transmitted from bats to pigs to humans. **Blue**: NiV outbreak in India and Bangladesh from bats directly to humans, and between humans. **Orange**: NiV outbreak in The Philippines from bats to horses to humans, with suspected transmission to pets and livestock. Isolates of the Malaysian (NiVM) and Bangladeshi (NiVB) strains of NiV have also been identified in bats in Indonesia (NiVM), Cambodia (NiVM) and Thailand (NiVM and NiVB), as indicated by the coloured map.

1.6.2 Nipah virus outbreaks

Paramyxoviruses generally have limited host range, as is the case for HeV, however NiV exhibits broad tropism, with the ability to naturally infect bats, pigs, horses, dogs, cats, goats, buffalo and humans [110, 118]. Furthermore, unlike HeV, NiV is able to infect humans directly from its natural host, *Pteropus* bats (*P. hypomelanus, P. lylei, P. vampyrus, P. giganteus*), from animal reservoirs, and can also transmit between humans [119, 120]. NiV infection in bats is asymptomatic and leads to seroconversion; experimentally confirmed through subcutaneous inoculation of bats with high doses of NiV, wherein there were no signs of clinical disease [121]. NiV was first identified in Malaysia (NiVM) and Singapore in 1998 following an outbreak of neurological and respiratory disease in pigs. These infected pigs acted as an amplification reservoir for onward transmission to humans where many individuals exhibited encephalitis [122]. The initial spillover of NiV to pigs likely occurred through consumption of fruit contaminated with infectious bat (*P. hypomelanus*) secretions,

including saliva and urine [123]. Infected pigs presented with acute febrile disease and respiratory disease, which was more severe in suckling piglets who presented with a “barking cough” [110]. Experimental infection of pigs with a high dose of NiV resulted in clinical disease like that seen in naturally infected pigs [124]. Onward transmission of NiVM from pigs to humans, particularly pig farmers, occurred through close contact with bodily excretions from infected pigs, resulting in the death of 105 individuals from the total 265 confirmed cases in Malaysia (39% mortality rate) and a single death from 11 confirmed cases in Singapore (9% mortality rate) (**Figure 1.6, purple**) [125]. This outbreak led to the culling of over 1 million pigs to control the outbreak, and an international ban on the export and import of pigs and pig products was issued in Malaysia by the Malaysian government in conjunction with international bodies like the Food and Agriculture Organisation and the World Organisation for Animal Health, which is still in effect to this day [126]. A epidemiological study was subsequently carried out in *Pteropus* bats in Southeast Asia, Australia and neighbouring countries, which revealed the seroprevalence of anti-NiV antibodies in *P. lylei* in Cambodia [127] and in *P. vampyrus* in Indonesia [128]. Additionally, a small outbreak of encephalitis in The Philippines was reported in 2014, most likely caused by a NiVM strain. This was attributed to consumption of horses infected with NiV, transmission from slaughtered horses, or through direct contact infected horses or their bodily fluids (**Figure 1.6, Orange**) [129].

Separately, a distinct genetic lineage of NiV was isolated in Bangladesh (NiVB) in 2001, and sporadic and isolated outbreaks of NiVB have been reported in Bangladesh and India annually since, with the most recent outbreak being reported in February 2024 in Dhaka, Bangladesh in which two individuals subsequently died (**Figure 1.7**) [130]. The intraspecies (NiVM vs NiVB) sequence similarity between the two NiV clades is ~93.6-94.6% based on recorded N gene sequences [131]. Unlike the NiVM outbreak, pigs were not identified as the amplification host for NiVB, likely attributed to the little to no pig farming occurring in these countries [132]. Instead, direct transmission of NiV from *P. giganteus* bats to humans was reported, attributed to the consumption of contaminated raw date palm sap, as well as direct human-to-human spread following contact with infected individuals (**Figure 1.6, blue**) [132]. There has also been evidence of long-term NiV persistence in bats in Thailand, with the presence of NiV RNA in secretions from circulating bats, and IgG antibodies in bat serum [133]. NiV isolates from Thailand appear to cluster with both the NiVM and NiVB clades of viruses, based on N-gene sequences (**Figure 1.6**) [131].

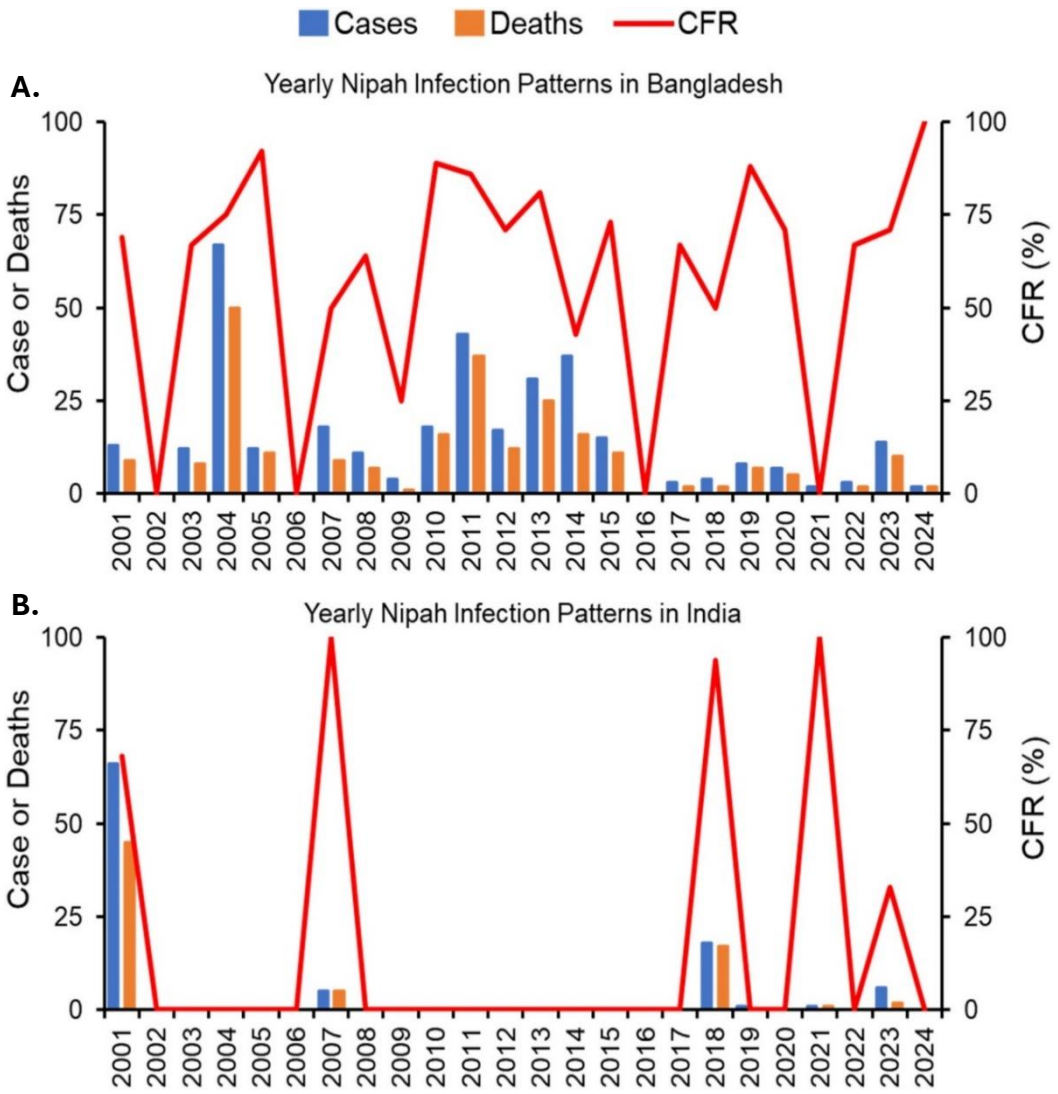

Figure 1.7: Epidemiological data of Nipah virus infections.
The number of cases, deaths and case fatality ratios (CFR,%) resulting from Nipah virus infection in **(A)** Bangladesh and **(B)** India during 2001 – 2024. Data is accurate as of May 31st 2024. Data taken from Khan S et al., *IJID Regions* (2024) [134].

NiV pathogenesis is widespread and targets multiple organs including the brain, lung, heart, kidney and spleen. The ubiquitous expression of the cellular receptors for NiV, EphrinB2 and EphrinB3, in endothelial vasculature and in the central nervous system, likely contributes to the broad tissue tropism and pathophysiology of the pathogenic henipaviruses [135]. The clinical presentation following NiV infection is similar to that observed with HeV, including fever, headache, dizziness and vomiting, resulting in the onset of severe encephalitis and meningitis [131, 136]. Many individuals who develop encephalitis show reduced level of consciousness, seizures, myoclonic jerks, gaze palsy, and areflexia [110, 131]. Unlike HeV however, the incubation period of NiV can be much longer from 4 days to 2 months, which in some cases has resulted in a clinically quiescent period, followed by relapse and late-onset encephalitis, the longest of which was after 11 years [136]. There are also differences in clinical disease between NiVM and NiVB, where NiVB presents with more severe respiratory disease (50-69% of cases, compared to 14-29% of NiVM cases)

and a higher case fatality rate (~75%), albeit in these smaller scale outbreaks [111]. In contrast, NiVM disease presents with more neurological disease and cognitive dysfunction, which is not common in NiVB cases [137]. The differences in disease presentation also translate into animal models, where compared to NiVM, NiVB has been shown to be more pathogenic in African green monkeys with a narrower window for antibody therapy [138], increased oral shedding and high levels of virus replication in the respiratory tract of ferrets [139].

1.6.3 Other henipaviruses and henipa-like viruses

NiV and HeV are the only two henipaviruses known to cause disease in humans and because of their high pathogenicity and the lack of approved therapeutics are classified as biosafety level 4 (BSL4) pathogens. Aside from NiV and HeV, the only other henipavirus that has been isolated is Cedar virus (CedV) which was discovered in 2009 in Australia circulating in *P. alecto* bats, with little evidence for natural human or livestock infection and disease. Experimental infection of ferrets, guinea pigs and hamsters are able to support CedV replication and results in the production of nAb, yet do not cause clinical disease [140, 141], suggesting there is zoonotic potential of this virus. Recombinant CedVs have been generated using reverse genetics approaches, expressing reporter proteins, or the surface glycoproteins of NiV or HeV [142, 143]. These tools provide a powerful tool to study highly pathogenic henipaviruses and to test candidate antivirals and vaccines through use of a modified non-pathogenic henipavirus.

Other viruses such as Ghanaian bat henipavirus (GHNV) and Angovkely henipavirus (AngV) have also been identified and taxonomically classified within the *Henipavirus* genus [144]. These are the only henipaviruses that have been isolated outside of southeast Asia (in Ghana and Madagascar, respectively) after detection in fruit bats – GHNV in *Eidolon helvum* and AngV in *Eidolon deprenum* [145]. The geographic distribution of these fruit bats overlaps with the spread of henipavirus spillover events, but evidence for pathogenesis and cross-neutralisation is limited for these viruses, despite the presence of cross-reactive antibodies against henipavirus sequences found in *E. helvum* from Ghana. Separately, there has been identification of henipa-like RNA sequences in faecal droppings from Ghana and the Republic of Congo [146], highlighting the likelihood of more diversity in this genus.

Other “henipa-like” viruses, recently reclassified within the *Parahenipavirus* genus, have been isolated from shrew and rodents, rather than bats. Viruses within this genus include Mojiang virus (MojV), identified by PCR from *Rattus flavipectus* rat rectal swabs in China [147]. Langya virus (LayV, China) [148], Gamak virus (GAKV, Korea), Daerong virus (DARV,

Korea) [149], Melian virus (MeliV, Guinea) and Denwin virus (DewV, Belgium) [150] have also been identified in novel RNA sequences from *Crocidura* shrew. Most recently, a novel parahenipavirus was detected following RNA metagenomic analysis of tissues from short-tailed shrew in the USA and subsequently named Camp Hill virus (CHV) [151]. Of the parahenipaviruses, MojV and LayV have both been associated with human pathogenesis, with fatal disease in Chinese mine workers who contracted severe pneumonia, an infection that was retrospectively associated with MojV, and non-fatal febrile illness in 35 individuals who were infected with LayV [147, 148]. Although none of the other parahenipaviruses have shown evidence for spillover, GAKV has been isolated from kidney tissue and been demonstrated to infect human lung epithelial cells *in vitro*, suggesting the potential for zoonotic transmission and that human infection could be possible [149, 152]. More recently, the complete genomes of five other Henipa-like viruses have been identified in Chinese shrew and striped field mice [152]. Partial sequences of Peixe-Boi virus (PBV) have also been found in Brazilian opossums [153] along with viruses isolated from wild rodents and shrew in Zambia [154], suggesting the possible existence of additional henipa-like clades and an even broader geographic distribution for the parahenipaviruses.

1.7 Henipavirus molecular biology and entry

1.7.1 Henipavirus molecular biology

The *Henipavirus* and *Parahenipavirus* genera are taxonomically classified within the *Paramyxoviridae* family. The classified viruses are generally larger in terms of genome size, when compared to other paramyxoviruses (~18.2kB) [135]. These viruses harbour a non-segmented, negative sense, single-stranded RNA genome, encoding six structural proteins flanked by 3' leader and 5' trailer regions: nucleoprotein (N), phosphoprotein (P), matrix protein (M), fusion glycoprotein (F), attachment glycoprotein (G), and a large RNA-dependent RNA polymerase protein (L) – *3'-N, P, M, F, G, L-5'* (**Figure 1.8**) [112]. Gene transcription is more abundant at the 3' end and decreases in a gradient manner towards the 5' end because of the inability of the RNA polymerase to access the genome for transcription at any point other than the 3' end [155]. The N, M and L genes are highly conserved between the more closely related NiV and HeV viruses, with nucleotide homologies of 79%, 77% and 89%, respectively [156]. The N protein tightly encapsidates the viral genome and complexes with P and L to form the ribonucleoprotein, which is contained within a lipid bilayer (envelope) lined with M proteins. The exterior surface of the virion is embedded with the surface F and G glycoproteins (**Figure 1.8A**) [135].

The P gene further encodes accessory proteins, which are translated by an alternative open reading frame within P (C protein) or by co-transcriptional mRNA editing during P

transcription (V and W proteins). These proteins antagonise double-stranded RNA and IFN signalling, and are thought to be important in influencing the pathogenic potential of NiV and HeV [135, 155]. Interestingly, the CedV P does not undergo RNA editing and thus lacks the coding capacity for the V protein, which may explain the lack of pathogenicity of this virus (**Figure 1.8B**) [155]. Immune modulation is mediated through interaction with several innate signalling pathways, including binding of P, V and W with STAT1 to block type I IFN signalling as well as inhibition of RIG-I signalling. The C protein can modulate viral replication to suppress inflammatory cytokines [135, 157]. The henipavirus M protein is responsible for virion assembly and budding, but can also inhibit IFN through interactions with the E3-ubiquitin ligase, TRIM6 [157].

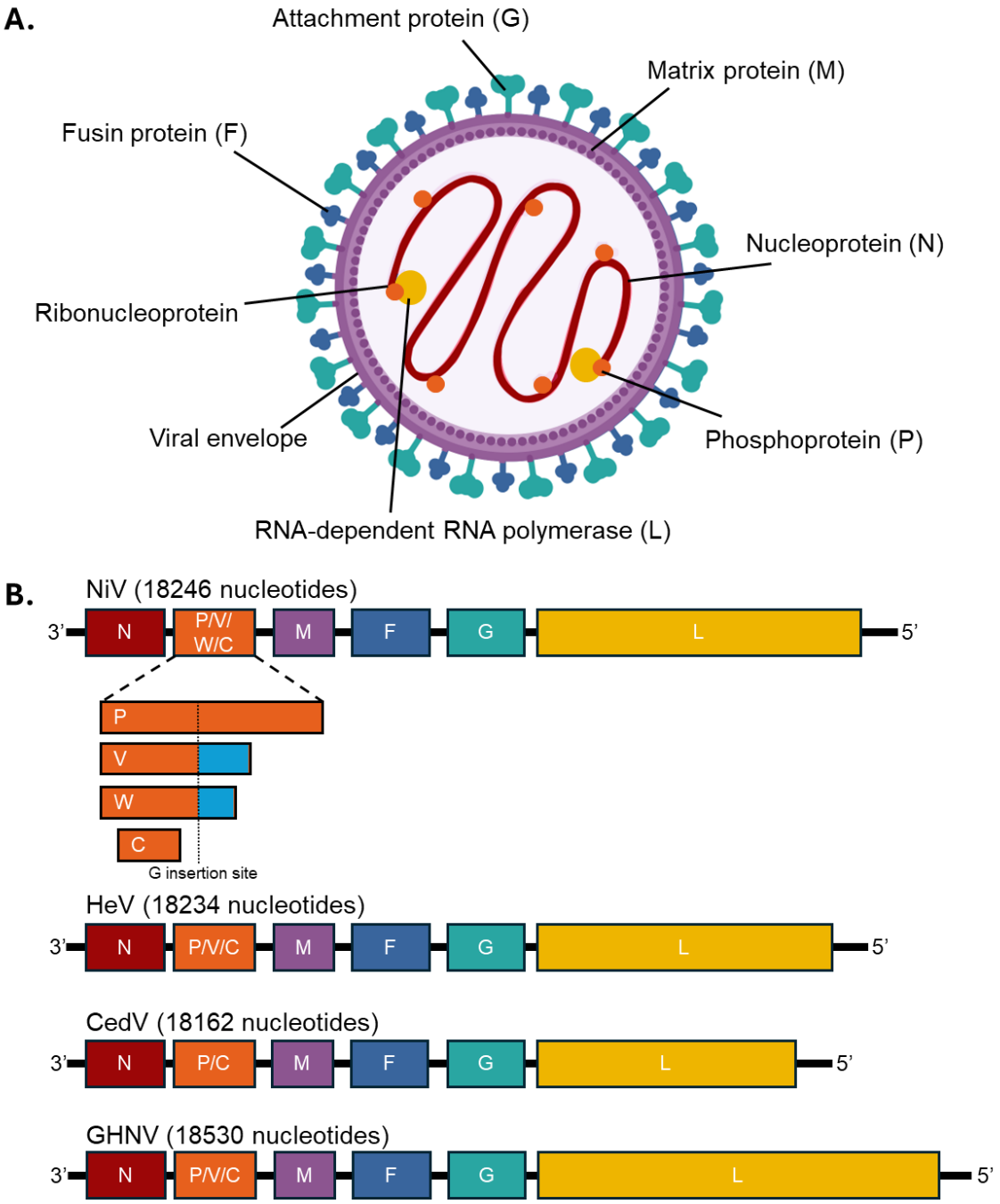

Figure 1.8: Henipavirus virion and genome arrangement.
(A) Schematic outlining the henipavirus virion, consisting of a viral lipid envelope, with multiple copies of the fusion (F) and attachment (G) glycoproteins embedded and the matrix protein (M) inside the lipid bilayer. The envelope surrounds a negative-sense single-stranded RNA genome, comprising the ribonucleoprotein, which consists of the nucleoprotein (N) and associated phosphoprotein (P) and large RNA-dependent RNA polymerase (L). Henipavirus genome schematic was created in BioRender. **(B)** Schematic of henipavirus genomes of NiV, HeV, CedV and GHNV with their respective genome lengths. The genome is flanked by a 3' leader sequence and a 5' trailer sequence, separated by short intergenic regions – *3'-N-P-M-F-G-L-5'*. The P gene additional consists of the V and C genes (and W for NiV), involved in immune modulation, except for CedV, which lacks the V gene. The V protein contains a single G nucleotide insertion, and the W protein 2 G insertions, shifting translations to a +1 and +2 reading frame, respectively. The C protein is translated from a P gene open reading frame. Data adapted from: Mbu'u CM et al., *Vector-borne and Zoonotic disease* (2019) [156].

1.7.2 Henipavirus entry and replication

The F and G glycoproteins mediate pH-independent virus entry into host cells. The homotetrameric G protein interacts with the homotrimeric F protein, keeping the F protein

in an inactive pre-fusion state (F_0) prior to receptor binding. The globular head of each G monomer binds to the host cell surface receptor, which for the henipaviruses, has been shown to be EphrinB2. NiV and HeV can additionally use EphrinB3, and CedV has been shown to use EphrinA2, EphrinA5 and EphrinB1 in addition to EphrinB2 *in vitro.* NiV appears to use EphrinB3 more efficiently than HeV with 30-fold high affinity [158, 159]. The receptor for the parahenipaviruses is yet to be elucidated, but these viruses do not possess the ephrin receptor binding motif and also contain an extra open reading frame in the F gene [152].

Upon receptor engagement, the G protein undergoes conformational changes which allows dissociation from F, allowing F to undergo conformational changes of its own which results in fusion of the viral and host membranes and subsequent viral entry. The link between the G protein and F activation is less well understood, with two models being proposed: (i) the “clamp” model, whereby the F protein is activated after removal of an inhibition brought about by the clamping of the G protein, or (ii) a “provocateur” model, where F activation is reliant upon positive signalling by the G protein [160]. Similar to many paramyxoviruses, proteolytic cleavage of F_0 by the host protease cathepsin L results in formation of the active disulfide-linked F_1 and F_2 subunits, which for the henipaviruses, occurs after internalisation of the F protein by endocytosis [157, 161]. After fusion of the viral and cellular membrane, the viral genome is released into the host cell cytoplasm where transcription and translation occurs, after which viral proteins are trafficked to the plasma membrane and virion assembly and budding is initiated, mediated by the M protein [155]. Following egress, the hydrophobic fusion peptide of F_1 is able to penetrate the host cell membrane of uninfected neighbouring cells, which results in cell-cell fusion and in syncytia formation, a feature that is characteristic of other paramyxoviruses [161].

The viral glycoproteins are embedded into the surface of the enveloped henipavirus virion, with the majority of the protein being present on the exterior of the virion. Thus, F and G are also, unsurprisingly, major targets for nAbs, the development of which are considered pivotal for long-lasting immunity and the prevention of viral transmission following natural infection, or immunisation [1]. The development of antibodies against the G protein or the pre-fusion F protein would likely be favourable, as this would more likely inhibit particle entry. Neutralisation of the virus particle usually occurs by inhibiting attachment, receptor engagement or virus uptake into the host, but can also be mediated through inhibition of cell-cell fusion [162]. Several assays have been developed to measure nAb responses, including neutralisation assays using live virus or pseudotyped viruses, plaque reduction assays or cell-cell fusion inhibition tests [110, 162]. Indeed, the majority of vaccines and therapeutics against henipaviruses are designed with the surface glycoproteins as targets.

1.8 Current vaccines and therapeutics for henipaviruses

1.8.1 Antivirals used in henipavirus outbreaks

There are currently no approved antiviral drugs for use in humans or animals infected with NiV or HeV. Several broad-spectrum drugs have been administered previously, including ribavirin which is an approved treatment against viruses including respiratory syncytial virus, and remdesivir, which has antiviral activity against paramyxoviruses and coronaviruses. However, ribavirin failed to prevent HeV-induced deaths, had no effect on experimental HeV infection in hamsters, and did not affect disease progression in African green monkeys (AGMs) experimentally infected with HeV, despite delaying onset of disease by 1-2 days [163]. However, ribavirin did show benefit following the 1998 NiV outbreak in Malaysia, where it appeared to reduce mortality by 36% [110, 164]. On the other hand, a challenge model in AGMs with a lethal dose of NiVB resulted in 100% survival following intravenous administration of remdesivir, but this drug has not been used in humans against henipaviruses [164]. Additionally, the malaria drug chloroquine was shown to inhibit the replication of both NiV and HeV *in vitro* but had no benefit, either alone or in combination with ribavirin in challenged ferret or hamster models, nor had any clinical benefit in a HeV-infected individual [110, 161]. Of note, in monkeys challenged with HeV, treatment with ribavirin resulted in increased neurological symptoms [161].

Various forms of poly(I:C) have been explored as antivirals due to their ability to induce strong IFN production, and were shown to block NiV replication, and prevent disease in 5/6 hamsters challenged with a lethal dose of NiV [161, 164]. Other antivirals, such as a cholesterol-tagged peptide-based fusion inhibitor have also been shown to inhibit *in vitro* NiV membrane fusion and infection [110, 161]. Furthermore, the small nucleoside inhibitor, 4'azidocytidine (R1479), which has shown to be effective against other paramyxoviruses, has also been exhibited strong antiviral effects against henipaviruses *in vitro* [164]. Nonetheless, clinical trials with a prodrug of R1479, balapiravir resulted in poor efficacy and negative side effects against flavivirus infections, so was discontinued [110, 164]. 2-monofluoro- and 2'difluoro-derivatives of R1479 have shown more promising results, increasing the antiviral effects on NiV up-to 20-fold *in vitro,* showing more promise that previously [164].

1.8.2 Henipavirus monoclonal antibodies

The most promising postexposure prophylaxis is the recombinant monoclonal antibody (mAb) m102.4 directed against the HeV-G glycoprotein, isolated from a phage-display antibody library [165]. This mAb targets a specific epitope in the receptor binding site for EphrinB2 and EphinB3 and is cross-reactive against both NiV and HeV and potently

neutralises both viruses *in vitro* and *in vivo* [165]. m102.4 likely works better as a prophylactic, as evidenced by ferret studies infected with NiV and treated with m102.4 before and after infection [166]. However, a separate study showed that m102.4 was able to prevent disease in non-human primates against lethal doses of NiVM and NiVB post-exposure [167]. A small number of individuals at high-risk exposure of HeV or with severe NiV infection have been administered m102.4 on compassionate grounds, but there is likely a short therapeutic window for use of this mAb, which is shorter for NiVB (3 days) compared to NiVM [138, 168]. This mAb is now being tested in phase 2a clinical trials for use in humans, after promising results in a phase 1 safety trial, where single and repeated doses of m102.4 have been documented to be well-tolerated, with no evidence of adverse side-effects [169].

Other mAbs have also been developed that instead target the F-protein of NiV including h5B3, hu1F5 and hu12B2, all of which work by inhibiting the conformational change of F, locking it in a pre-fusion state, albeit by binding different epitopes on F [170, 171]. Ferrets receiving two doses of 20mg/kg of h5B3 were protected against NiVM or HeV infection, administered 3-days following challenge, but animals still exhibited clinical signs [172]. Both hu1F5 and hu12B2 were assessed in hamster infection models with NiVB, where hu1F5 conferred complete protection against challenge, whereas hu12B2 only partial protection [173]. hu1F5 also appears more potent that m102.4, which exhibited complete protection following NiVB infection in AGMs with a longer therapeutic window (5 days), whereas a comparable dose of m102.4 resulted in the survival of only 1/6 AGMs infected [173]. Hu1F5 appears to be a promising candidate for prophylactic treatment against NiV, and potentially HeV infection, and has been enrolled in CEPI-funded phase 1 clinical trials [174].

1.8.3 Henipavirus vaccine candidates

Due to the severity of disease, the high mortality rate observed with infectious HeV and NiV, and the containment level of these viruses, live or inactivated virus vaccines are not favoured for the henipaviruses. However, several other vaccine platforms have been developed for HeV and NiV including live-recombinant viral vectors, virus-like particles (VLP), protein subunit and mRNA platforms (**Table 1.2**). Many of these vaccines have been examined in immunogenicity and/or efficacy studies in various animal models including mice, hamsters, ferrets, cats, horses, pigs and AGMs. Adjuvanted subunit vaccines based on soluble recombinant proteins are the most extensively examined vaccine approach developed against both the HeV and NiV G protein (HeVsG and NiVsG, respectively), and the HeVsG subunit vaccine have been approved for use in horses in Australia (Equivac®) [163]. Cats, ferrets and AGMs immunised with HeVsG exhibited high levels of cross-reactive and cross-neutralising antibodies against NiV, but low antibody responses to NiV

in pigs vaccinated with HeVsG post-challenge and highlighted the importance of cellular immunity [175-178]. Similarly, a NiVsG vaccine has shown complete protection against NiV infection in cat and hamster models (**Table 1.2**) [179, 180].

Viral-vectors are favourable vaccine platforms due to their ability to induce strong antibody and T-cell responses in immunised animals. A number of virus vectors have been developed against NiV, with one of the first described using an attenuated recombinant vaccinia virus expressing NiV-F or -G, individually or in combination. Immunised hamsters were able to confer complete challenge following NiV challenge (**Table 1.2**) [181]. A recombinant canarypox vaccine vector (ALVAC) using a similar approach has also been examined in pigs, with the bivalent ALVAC NiV-F and -G vaccine producing the highest nAb response, and all vaccine regimens conferred protection against NiV infection, despite lower nAb responses in the ALVAC NiV-F vaccinated group (**Table 1.2**) [182]. Paramyxovirus vectored platforms have also been employed to develop NiV vaccines including recombinant measles virus based on either the HL or Edmonston strains expressing NiV-G or -F, which was shown to confer complete protection in hamsters following challenge, but only partial protection in AGMs following two vaccine doses, with evidence of neurological disease [183]. Another platform utilised a recombinant Newcastle disease virus, again expressing NiV-G or -F proteins. This was used in mouse and pig immunogenicity studies and vaccinated animals developed both humoral and cellular immune responses (**Table 1.2**) [184].

Table 1.2: Candidate henipavirus monoclonal antibodies and vaccines tested in immunogenicity and efficacy studies in several animal models.

	Platform/viral vector	Target antigen	Animal model	Study design – Treatment (T)/ Immunisation (I)/ Challenge (C)	Ref
Monoclonal antibodies	**m102.4** [a]	HeV-G	Ferret	**C: ON** $5x10^3$ $TCID_{50}$ NiVM **T: IV** 50 mg/kg, pre challenge (24 hrs before) or post challenge (10hrs after)	[166]
			AGM	**C: IT** $5x10^5$ PFU NiVM or $4x10^5$ $TCID_{50}$ HeV **T: IV** 15 mg/kg, 1, 3 or 5 days post challenge, then again after 2 days	[167] [185]
	h5B3.1	NiV-F	Ferret	**C: IN** 5.10^3 PFU NiVM or HeV **T: IP** 20mg/kg 1 or 3 days post challenge.	[172]
	hu1F5 [a]	NiV-F	Hamster, AGM	**C: IN** $5x10^6$ PFU NiVB for hamster, or $4x10^4$ PFU NiVB for AGM **T: IP** 5mg/kg 1 day post challenge for hamsters, **IV** 25mg/kg or 10mg/kg 5 days post challenge for AGM	[173]
	hu12B2	NiV-F	Hamster	**C: IN** $5x10^6$ PFU NiVB **T: IP** 5mg/kg 1 day post challenge	[173]
Vaccine Candidates	**Vaccinia virus**	NiV-F and/or -G	Hamster	**I: SC** 10^7 NiV-F or -G OR $5x10^6$ NiV F and G combined. Boost after 1 month **C: IP** $1X10^3$ PFU NiVM	[181]
	Canarypox virus (ALVAC)	NiV-F and/or -G	Pig	**I: IM** 10^8 PFU NiV-F, -G or F and G. Boost after 14 days **C: ON** $2.5x10^5$ PFU NiVM	[182]
	Vesicular stomatitis virus (VSV)	NiV -F and/or -G [c], or -N	Ferret	**I: IM** 10^7 PFU NiVB -F, -G or F and G **C: ON** $5x10^3$ PFU NiVM	[186]
			Hamster	**I: IM** $1x10^6$ ip NiVM-F or -G **C: IP** 10^5 $TCID_{50}$ NiVM	[187]
			Hamster	**I: IP** 10^5 PFU NiV-F, -G or -N **C: IP** $6.8x10^4$ $TCID_{50}$ NiVM	[188]
			AGM	**I: IM** 10^7 PFU NiV G **C: IT** 10^5 TCID50 NiVM	[189]
	Adeno-associated virus	NiV-G	BALB/c mice, Hamster	**I: IM** (2.10^{10} infectious particles) or **ID** (1.10^{10}) for mice; **IM** (6.10^{11}) for hamster **C**: IP 10^4 PFU NiVM	[190]
	Chimpanzee adenovirus (ChAdOx1)	NiV-G [c]	Hamsters	**I: IM** 1x108 ip NiVB-G **C: IP** $5.3x10^5$ $TCID_{50}$ NiVB or $6.8x10^4$ $TCID_{50}$ NiVM or $6.0x10^3$ $TCID_{50}$ HeV	[191]
			AGM	**I: IM** $2.5x10^{10}$ ip NiVB-G prime only or prime-boost 4 weeks apart **C: IT** $2.5x10^4$ $TCID_{50}$ and IN $1x10^5$ TCI_{50} NiVB	[192]
	Measles virus	NiV-G	Hamster	**I: IP** $2x10^4$ $TCID_{50}$ NiVM-G for hamster. Boost after 3 weeks **C: IP** 10^3 $TCID_{50}$ NiVM	[183]
			AGM	**I: SC** $1x10^5$ $TCID_{50}$ for NiV-G for AGM. Boost after 4 weeks **C: IP** 10^5 $TCID_{50}$ NiVM	[183]
	Recombinant subunit	HeV soluble G (sG)	Ferret	**I: SC** 4, 20 or 100 μg HeVsG. Boost after 20 days **C: ON** $5x10^3$ $TCID_{50}$ NIVB or HeV	[193] [177]

Vaccine Candidates		[b,c] or NiVsG	Cat	**I: SC** 100 μg NiVsG or HeVsG. Boost after 2 and 4 weeks **C: SC** $5x10^2$/ **ON** $5x10^4$ $TCID_{50}$ NiVM	[179] [175]
			AGM	**I: IM** 10, 50 or 100 μg HeVsG. Boost after 3 weeks **C: IT** 10^5 $TCID_{50}$ NiVM or $5x10^5$ PFU HeV	[116] [176]
			Horses	**I: IM** 50 or 100 μg HeVsG. Boost after 3 weeks. **C:** ON $2x10^6$ $TCID_{50}$ HeV	[194]
			Hamster	**I: IM** 5 μg NiVM-G or HeV-G/ Boost after 3 weeks. **C: IP** $1x10^2$ $TCID_{50}$ NiVM	[180]
	Newcastle disease virus	NiV-F and/ or -G	BALB/c mice	**I: IM** 10^8 EID_{50}. Boost after 4 weeks	[184]
			Pig	**I: IM** $2x10^9$ EID_{50} of NiV-F, -G or F and G. Boost after 4 weeks	[184]
	Bovine Herpes virus 4 (BoHV4)	NiV-F and/ or -G	Pig	**I: IM** 10^6 TCI_{50} NiVM-F, -G or F and G. Boost after 3 weeks	[195]
	Venezuelan equine encephalitis virus replicon particles	NiV-F or -G	C3H/He mice	**I: Footpad inoculation** $3.1x10^5$ infectious units. Boost after 5 and 18 weeks	[196]
	Virus-like particles (VLPs)	NiV -F, -G and -M	Hamster	**I: IM** 30 μg VLP. Boost after 21 and 42 days OR IM 30 μg VLP **C: IP** $1.6x10^4$ PFU NiVM OR IP $3.3x10^4$ NiV-M	[197]
	mRNA	NiV-G [c]	Pig	**I: IM** mRNA NiVM-G 100 μg. Boost after 3 weeks.	[198]

[a] m102.4 is currently in phase 2a and hu1F5 in phase 1 clinical safety trials in humans, [b] HeVsG licenced for use in horses (Equivac®), [c] vaccines in phase 1 clinical safety trials in humans. TCID50 = 50% tissue culture infectious dose, PFU = plaque forming units, EID50 = 50% embryo infectious dose, ip = infectious particles, AGM = African green monkey **IV** = intravenous, **ON** = oronasal, **IT** = intratracheal, **IP** = intraperitoneal, **IM** = intramuscular, **ID** = intradermal, **SC** = subcutaneous. Adapted from Thakur N et al., *Microbes and Infection* (2019) [110], Broder C et al., *Vaccine* (2016) [199]

Furthermore, several vesicular stomatitis virus (VSV) vector-based platforms have been developed by pseudotyping a replication defective VSV lacking its envelope protein with NiV -F or -G, or using live attenuated recombinant VSV expressing NiV-F, -G or -N against both the NiVM and NiVB strains. Single doses of these vaccine candidates expressing F or G were able to fully protect Syrian hamsters, ferrets and AGMs following challenge with lethal doses of NiV, with the development of high nAb titres and an absence of pathology noted in vaccinated animals [186-189]. Interestingly, vaccines expressing NiV-N only developed primarily cell-mediated immunity and conferred partial protection in hamsters infected with NiV, highlighting the importance of the surface glycoproteins in mediating immunity against viral infection (**Table 1.2**) [187]. Other virus vectors have also been explored, including an adeno-associated virus vector expressing the NiV-G protein. This induced strong antibody responses in a mouse immunogenicity study; further examination of a single dose of this vaccine demonstrated complete protection in hamsters challenged

with NiV, but only partial protection against HeV challenge [190]. An immunogenicity study with bovine herpesvirus 4 (BoHV4) vectored NiV-F or NiV-G vaccines has also been shown to induce strong nAb and enhanced T-cell responses in immunised pigs which were more pronounced in the NiV-G vaccinated group. Conversely the NiV-F vaccinated group induced significant nAb against cell-cell fusion (**Table 1.2**) [195].

More recently, two candidate vaccine platforms have been explored: the replication-deficient chimpanzee adenovirus vectored vaccine (ChAdOx1) and an mRNA-based vaccine, both of which have successfully been developed and licensed for use against SARS-CoV-2 as COVID-19 vaccines [90, 91]. An mRNA NiV-G vaccine has been examined in a pig immunogenicity study and induced strong nAb response against NiVM and NiVB, but limited neutralisation against HeV following two vaccine doses. Induction of antibodies capable of neutralising NiV mediated cell-cell fusion was also noted, as well as both $CD4^+$ and $CD8^+$ T cell responses (**Table 1.2**) [198]. The ChAdOx1 NiV-G vaccine based on the NiVB strain conferred complete protection in Syrian hamsters following a prime-only or prime-boost regimen following challenge with NiVM and NiVB, but only partial protection against HeV challenge [191]. Similarly, in AGMs with ChAdOx1 NiV-G, prime and prime-boost vaccination provided protection against NiV infection, with no signs of clinical disease or infectious virus detected in infected animals (**Table 1.2**) [192].

Clinical trials for four of the vaccine candidates are currently underway, including 3 CEPI funded vaccines: (i) a subunit HeVsG vaccine (clinical trial number NCT04199169, phase 1 trial completed); (ii) a recombinant VSV-Nipah virus, PHV02 (clinical trial numbers NCT05178901 and NCT06221813, phase 1 trial completed); (iii) a ChAdOx1 NiVB-G vaccine from the Oxford Vaccine Group (Eudract number 2023-503872-25, phase 1 trial underway); and (iv) a NIAID funded mRNA bivalent NiV-G and prefusion-F vaccine (clinical trial number NCT05398796, phase 1 trial underway). The progression of these vaccines to clinical trial provides a promising outlook for licensure of a suitable vaccine for the highly pathogenic NiV. However, NiV vaccines only induce partial protection against the closely related HeV, so further research is required to understand the utility of current candidate henipavirus vaccines against other henipaviruses and parahenipviruses, which is explored in this study. This will broaden our understanding on whether new vaccines would need to be developed should a novel henipavirus, known or unknown, emerge in the human population with severe pathogenicity, high infectivity, broad host range and therefore, pandemic potential.

1.9 Animal reservoirs of zoonotic viruses

1.9.1 Bats as natural reservoirs

Emerging viruses that are of public health importance are frequently of animal origin, with cross-species transmission driven by virus evolution and host ecology. This makes understanding the interplay of animal species and virus families most likely to result in zoonoses of great significance. Bats comprise approximately 22% of all characterised mammalian species, making them the second most diverse mammalian order *(Chiroptera*) and have been identified as the natural host for several emerging viruses (**Figure 1.9**) [200]. This includes viruses that are pathogenic in humans such as NiV and HeV, as well as viruses suspected to have originated in bats like Ebola virus and several coronaviruses including SARS-CoV-1, SARS-CoV-2 and MERS-CoV. Transmission to humans is either directly from bats or via an intermediate host [31, 119, 200]. Furthermore, there are also examples of bat-derived viruses that cause disease in animals of agricultural importance but do not transmit further to humans, as is the case with several coronaviruses which have been suggested to be of bat origin, including avian IBV, porcine TGEV, PEDV and SADS-CoV [31].

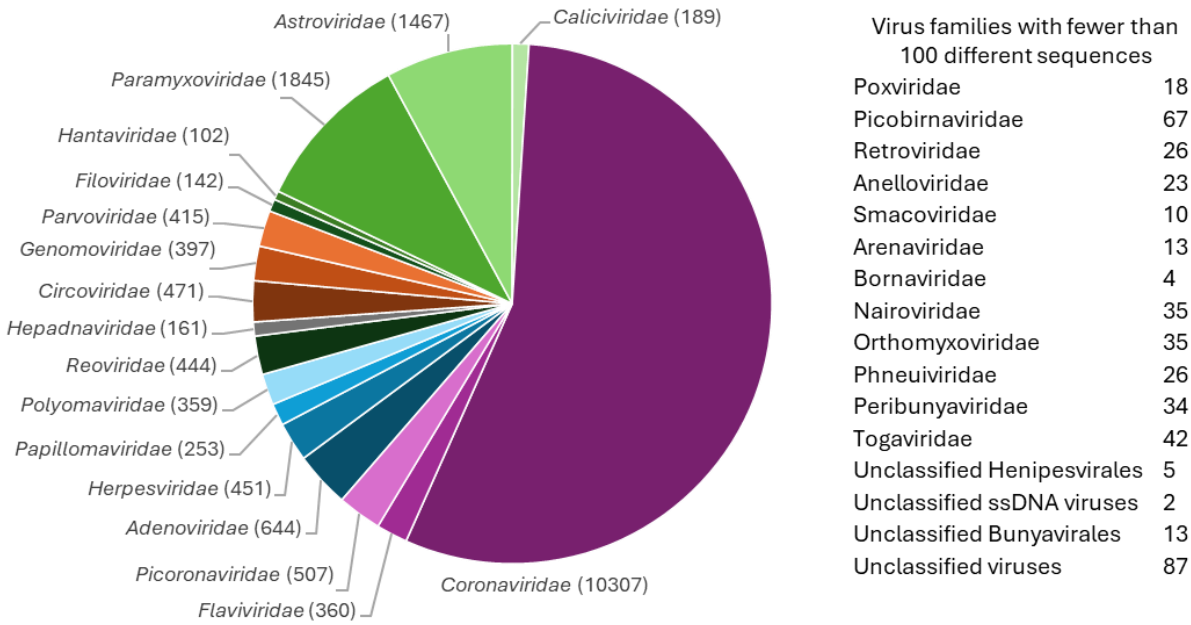

Figure 1.9: Bat-associated viruses and their related viral families.
Genetic sequences for bat-derived viruses (publicly available at: database of bat-associated viruses) were collated and grouped by viral family, excluding virus families with fewer than 100 different sequences, which are instead tabulated adjacent to the graph. Virus families are coloured by double stranded DNA viruses (dsDNA, blue), dsRNA viruses (grey), partially dsDNA viruses (teal), single-stranded DNA viruses (ssDNA, orange) or ssRNA viruses – negative strand (green) or ssRNA viruses – positive strange (pink). A large part of bat virus diversity remains uncharacterized. Adapted from: Letko M et al., *Nature Reviews Microbiology*, (2020) [200].

Although great advances have been made in identifying novel bat-derived viruses to broaden our understanding of possible future emerging viruses, many of these sequences

do not include the genes expressing the virus surface glycoproteins, knowledge of which is vital in predicting and/or determining virus entry into the host [200]. There is also a significant requirement to understand the fluctuations in viral shedding in bat populations over time to predict when and where future spillover events may occur, particularly because peaks in bat viral shedding appear to coincide with spillover events in other species. It was initially thought that zoonotic infections in bats follow a cycle of acute infection, recovery and immunity, but more recent evidence suggests that persistent or recurring infections may also occur, which could be attributed to the relatively long lifespans of bats, their body size and perhaps unique metabolism [201, 202].

Despite evidence of virus shedding and replication in bats following natural infection of experimental models of NiV, Marbug virus, Ebola virus and MERS-CoV, bats present with apparent asymptomatic infection [200, 203]. It has been hypothesised that the naturally increased body temperature in bats during flight mimics that seen in other animals during an immune response, potentially reducing viral pathogenesis in bats [204]. Furthermore, the immune response in bats also differs to other animals, particularly IFN pathways. For example in *Pteropus* bats which appear to constantly express IFNα and have a strong type III IFN response, or in *Rousettus* bats which have an expanded IFNα locus so can strongly induce type I IFN in response to viral infection, which may contribute to the ability of bats to better handle viral infections [200]. This stronger innate immune response in bats may result in the reduced need for affinity matured B cells and high affinity antibodies, evidenced by experimental infection of bats with Marburg virus [205], which showed waning antibody titres below detectable levels within 3 months. However, rechallenging bats resulted in reduced viral spread, indicating some level of immune memory [205]. Conversely, infection of both human and bat cell lines resulted in antagonism of type I and type III IFNs following henipavirus infection, suggesting a non-IFN-mediated mechanism to control henipavirus replication in bats [206].

Interestingly, while bats infected with Ebola, Marburg and Sosuga virus produced antibodies to these viruses, the antibodies were unable to neutralise live virus [207], suggesting the importance of non-neutralising cell-mediated responses in viral clearance. In contrast, nAbs are produced against NiV following infection, but virus can still be detected in bat saliva or urine up to 18 days post infection [121]. Furthermore, recent research has identified mechanisms which naturally reduce inflammation in response to infection through upregulation of key inflammasome sensors, caspases and cytokines [203]. This helps bats manage inflammation without triggering excessive immune responses. Overall, it is possible an enhanced host innate immune responses coupled with immune modulation likely contributes to bat-specific responses to viral infections. Further studies of bat diversity,

their ecology, geographic distribution, immunology and proximity to other species is important to better understand these animals as hosts of emerging viruses and how we can use this information to understand future spillover events. This is especially true given the vast diversity of bat-derived viruses that have been discovered in these animals.

1.9.2 Rodents and shrews as natural reservoirs

Rodents are the most diverse mammalian order, and like bats, harbour a large amount of viral diversity. Furthermore, they are evolutionarily diverse and include several species with peridomestic habits. However, rodents are not as geographically widespread as bats so their geographic range is smaller. Nevertheless, rodents are more diverse than bats in terms of the numbers of species (>2,000) and are also greater in number [208]. The total number of zoonotic viruses identified in rodents is 68 (111 non-zoonotic), compared to 61 (76 non-zoonotic) in bats is likely due to the greater number of rodent species, although statistically speaking bats host more zoonotic viruses per species than rodents [208]. Examples of rodent derived zoonotic viruses include hantaviruses [209] and arenaviruses [210]. Old World hantaviruses (e.g., Hantaan virus) are known to cause haemorrhagic fever with renal syndrome, whereas New World hantaviruses include pathogens (e.g., Andes virus, Sin Nombre virus) responsible for hantavirus pulmonary syndrome, both having relatively low mortality rates ranging from 10-40%, with Old World viruses having less lethality [211]. Similarly, the New (e.g., Junin virus) and Old World (e.g., Lassa virus) arenaviruses are a diverse group of viruses, at least 8 of which cause severe pathology in humans including encephalitis and severe haemorrhagic fever [212]. Tacaribe virus is the only arenavirus that has been isolated from a fruit-eating bat, rather than a rodent [213]. The converse is true for the henipaviruses, which are all derived from bats. However, the more recently described henipa-like viruses (recently classified by ICTV as parahenipaviruses), such as Mojiang virus were detected in rats, associated with disease observed in Chinese miners [147].

Other parahenipaviruses are continually being discovered following a study that identified shrews as the potential reservoir of multiple paramyxoviruses, detecting viruses by RT-PCR [154]. Spillover of parahenipaviruses from shrews into humans and possibly livestock has also been suggested, with Langya virus (LayV) causing febrile disease in humans [148]. Shrews are thought to share a common ancestor with bats, diverging from the last Chiropteran ancestor almost 100 million years ago, giving rise to the *Eulipotyphia* order. This splitting event may have also given rise to the same lineage as rodents (order *Rodentia*) [152]. Shrews comprise over 370 different species, making it one of the most species-abundant mammalian families. Shrews have been identified as natural hosts for other zoonotic viruses, including flaviviruses, hantaviruses and bornaviruses, and the close

proximity of shrews to humans in some ecological areas suggests a high probability of future zoonotic spillover events [152]. In fact, recent surveillance of shrews in Singapore identified a novel orthonairovirus called Cencurut virus. Elsewhere hepatitis B homologs (crowned shrew hepatitis B virus and musk shrew hepatitis B virus) were also detected in African shrews [214]. The close proximity of shrews to humans and livestock highlights the importance of studying their potential role as virus reservoirs. Investigating shrew-mediated transmission mechanisms and their zoonotic risk is crucial, particularly given their capacity to harbour and shed several viruses.

Furthermore, surveillance of domestic animal, wildlife and livestock whose habitats overlap with these natural hosts could provide insight into potential susceptible hosts for the zoonotic spillover of emerging viruses. Several methods have been implemented to monitor susceptible hosts to virus infection, and also to predict virus spillover. For example, ecological niche modelling is a computational approach that has been used to study zoonotic risk by predicting the distribution of a potential host species [215]. However, such models tend to overestimate the geographic range of spillover and lack the specificity required to take other factors into considerations, such as interactions between other species or sociocultural factors (e.g., hunting, consumption of wild meat). HeV infection is an example of this, where the geographic range of the natural host of HeV is wide, but the virus itself causes disease only in Australia [113, 215]. Furthermore, increased sampling from suspected animal reservoirs and genomic analysis may also provide evidence of zoonotic spillover potential. Since the emergence of SARS-CoV-2, genomic analyses carried out in viruses isolated from bats identified other coronaviruses closely related to SARS-CoV-2, including RaTG13, BANAL-20-52 and RMYN02 [216, 217]. In this study, the host-range of sarbecoviruses with mammalian species has been assessed using functional pseudovirus assays to infect cells expressing the suspected target mammalian receptor. This method provides a high-throughput method of predicted susceptible hosts to virus spillover, and has been described previously for example, for SARS-CoV-2 [218, 219] and alphacoronaviruses [220].

Aims of the Study

Vaccines have been a pivotal discovery in managing morbidity and mortality against viruses with significant risk to agriculture and public health. Over the decades, several vaccine platforms have been developed with new technologies continually being explored to further improve the cost, efficacy, availability and production time of vaccines. This has been particularly important with the emergence of SARS-CoV-2, which resulted in a global pandemic and saw novel vaccine platforms vaccines being tested and approved for use in humans at unprecedented speed. These vaccines have continued to be updated as new SARS-CoV-2 variants emerged. The WHO listed several viral pathogens as a priority for research and development for broad spectrum, safe and efficacious vaccines against virus families. In this study, the utility of vaccines at the intraspecies and interspecies level has been explored, using the betacoronaviruses as a model of vaccine utility during the COVID-19 pandemic, and using that information to understand the utility of candidate vaccines against emerging viruses in the *Henipavirus* genus. Animals susceptible to virus infection are also of concern as they provide a reservoir for zoonosis or sustained transmission for emerging viruses, so the host range of sarbecoviruses across multiple mammalian species was also investigated.

Aims:

1. Understand the utility of COVID-19 vaccines against SARS-CoV-2 variants (intraspecies variation) and whether these vaccines could provide any degree of cross-protection against related bat sarbecoviruses (interspecies variation), should they emerge in the human population.
2. Examine the host range of SARS-CoV-2 variants and bat sarbecoviruses for mammalian ACE2 and investigate the genetic determinants that underpin differences in species tropism.
3. Establish surrogate binding and entry assays for henipaviruses and utilise them to assess the immune response induced by candidate henipavirus vaccines in pig and mouse immunogenicity studies, and a hamster efficacy study against different henipaviruses and parahenipaviruses.
4. Assess the extent of cross-protective immunity generated against different henipaviruses in immunogenicity and efficacy studies using henipavirus candidate vaccines.

Chapter 2: Materials and Methods

2.1 Cells and cell culture

Human embryonic kidney (HEK) 293T were used as producer cells to generate lentiviral-based pseudotyped viruses and baby hamster kidney (BHK)-21 cells (ATCC; HEK293T: CRL-3216™, BHK-21: CCL-10™) were used for receptor usage screens and neutralisation assays for henipaviruses and sarbecoviruses. HEK293T cells stably expressing human angiotensin converting enzyme 2 (hACE2) were using for sarbecovirus-related neutralisation assays (shared by Dr Thomas Peacock and Dr Wendy Barclay, Imperial College London, UK). HEK293T cells stably expressing Lenti- *Renilla* Luciferase (rLuc)-green fluorescent protein (GFP) 1-7 or BHK-21 cells stably expressing Lenti-rLuc-GFP 8-11 were used for fusion assays and micro fusion inhibition tests (mFITs), as described previously using a lentiviral transduction system under 1 µg/mL puromycin (Gibco, Cat# A1113803) selection [8]. All cell lines were maintained using DMEM-10%: Dulbecco's modified Eagle's medium – high glucose (DMEM, Merck, Cat#D5796) supplemented with 10% foetal bovine serum (FBS; Life Science Production, Cat# S-001A-BR), 1% 100mM sodium pyruvate solution (ThermoFisher Scientific, Gibco™, Cat# 11360070) and 1% penicillin/streptomycin, 10000 U/mL (ThermoFisher Scientific, Gibco™, cat# 15140122) at 37°C with 5% CO_2.

For the parahenipavirus entry and cell-cell fusion assays A549 (DMEM-10%), DEDE (McCoy's 5a medium (ThermoFisher Scientific, Gibco™, Cat#16600082) supplemented with 20% FBS (Life Science Production, Cat# S-001A-BR), 1% penicillin/streptomycin, 10000 U/mL (ThermoFisher Scientific, Gibco™, Cat# 15140122), 1% 100mM sodium pyruvate solution (ThermoFisher Scientific, Gibco™, Cat# 11360070), CHO (DMEM-10%), McCoy (DMEM-10%), RAW264.7 (DMEM-10%) or PC12 (RPMI-1640 (ThermoFisher Scientific, Gibco™, Cat# A1049101) supplemented with 10% FBS (Life Science Production, Cat# S-001A-BR, 1% penicillin/streptomycin, 10000 U/mL (ThermoFisher Scientific, Gibco™, cat# 15140122)) cells (The Pirbright Institute, Cell Servicing Unit) were used as target cells in addition to the HEK293T and BHK-21 cells already described and were maintained at 37°C with 5% CO_2 in the cell culture medium indicated.

2.2 Plasmids

2.2.1 Sarbecovirus plasmids

For SARS-CoV-2, pcDNA3.1 plasmids expressing SARS-CoV-2 Spike based on a codon optimised SARS-CoV-2 Pango Lineage B reference sequence (GenBank ID NC_045512.2) bearing a Δ19 mutation to improve fusogenicity were used (shared by Dr Thomas Peacock

(The Pirbright Institute) and Dr Wendy Barclay (Imperial College London), or synthesised by Dr Joseph Newman (The Pirbright Institute) as part of the SARS-CoV-2 Genotype-to-Phenotype, Genotype-to-Phenotype 2 and Genotype-to-Phenotype Global consortia) for functional assays. For the SARS-CoV-2 NTD analysis conducted in **Chapter 3**, Spike (B.1, Beta, Delta, BA.1, BA.2) and mutant plasmids were synthesised and subcloned into a pcDNA3.1 vector backbone with a Δ19 mutation between HindIII-NotI restriction sites, expressing a c-terminal FLAG tag (BioBasic, Canada). Mutants of B.1 and BA.1 were generated by site-directed mutagenesis, using the QuikChange Lightning Single- and Multi Site-Directed Mutagenesis kit (Agilent, Cat#200523). The Spikes used included WT Spike (B, D614, Wuhan-01, vaccine variant), B.1 (D614G), various SARS-CoV-2 variants and mutant plasmids (**Table 2.1, Table 2.2**). **Table 2.1** outlines the different SARS-CoV-2 variants and their corresponding mutations in relation to WT Spike and **Table 2.2** contains mutants built in a B.1 background.

Table 2.1: SARS-CoV-2 variants, listed by Pango Lineage and their associated Spike mutations expressed in a pcDNA3.1 vector with a Δ19 truncation.

Pango lineage	Spike mutations (compared to Wuhan-01)
B (WT SARS-CoV-2)	n/a
B.1	D614G
B.1.1.7 (Alpha)	Δ69-70, Δ144, **N501Y**, A570D, D614G, P681H, T716I, S982A, D1118H
B.1.351 (Beta)	L18F, D80A, D215G, Δ242-244, **K417N, E484K, N501Y,** D614G, A701V.
B.1.617.2 (Delta)	T19R, G142D, Δ156-157/R158G, **L452R, T478K**, D614G, P681R, D950N
C.37 (Lambda)	G75V, T76I, Δ246-252/D253N, **L452Q, F490S**, D614G, T859N
B.1.621 (Mu)	T95I, Y144T/144insS/Y145N, **R346K, E484K, N501Y**, D614G, P681H, D950N
BA.1 (Omicron)	A67V, Δ69/70, T95I, G142D, Δ143/145, N211I, Δ212, INS214EPE, **G339D, S371L, S373P, S375F, K417N, N440K, G446S, S477N, T478K, E484A, Q493R, G496S, Q498R, N501Y, Y505H,** T547K, D614G, H655Y, N679K, P681H, N764K, D796Y, N856K, Q954H, N969K, L981F
BA.2 (Omicron)	T19I, L24S/Δ25-27, G142D, V213G, **G339D, S371F, S373P, S375F, T376A, D405N, R408S, K417N, N440K, S477N, T478K, E484A, Q493R, Q498R, N501Y, Y505H,** D614G, H655Y, N679K, P681H, N764K, D796Y, Q954H, N969K
BA.5 (Omicron)	T19I, L24S/Δ25-27, Δ69-70, G142D, V213G, **G339D, S371F, S373P, S375F, T376A, D405N, R408S, K417N, N440K, L452R, S477N, T478K, E484A, F486V, Q498R, N501Y, Y505H**, D614G, H655Y, N679K, P681H, N764K, D796Y, Q954H, N969K
BQ.1.1 (Omicron)	T19I, L24S/Δ25-27, Δ69-70, G142D, V213G, **G339D, S371F, S373P, S375F, T376A, D405N, R408S, K417N, N440K, K444T, L452R, N460K, S477N, T478K, E484A, F486V, Q498R, N501Y, Y505H**, D614G, H655Y, N679K, P681H, N764K, D796Y, Q954H, N969K
XBB [XBB1.5]* (Omicron)	T19I, L24S/Δ25-27, V83A, G142D, Δ145/H146Q, Q183E, G213E, V213G, **G339H, R346T, L368I, S371F, S373P, S375F, T376A, D405N, R408S, K417N, N440K, V445P, G446S, N460K, S477N, T478K, E484A, F486P*, F490S, Q498R, N501Y, Y505H**, D614G, H655Y, N679K, P681H, N764K, D796Y, Q954H, N969K
XBB.1.16 (Omicron)	T19I, L24S/Δ25-27, V83A, G142D, Δ144, H146Q, E180V, Q183E, V213E, G252V, **G339H, R346T, L368I, S371F, S373P, S375F, T376A, D405N, R408S, K417N, N440K, V445P, G446S, N460K, S477N, K478R, E484A,**

	F486P, F490S, Q498R, N501Y, Y505H, D614G, H655Y, N679K, P681H, N764K, D796Y, Q954H, N969K
EG.5.1 (Omicron)	T19I, L24S/Δ25-27, Q52H, V83A, G142D, Δ144, H146Q, Q183E, V213E, G252V, **G339H, R346T, L368I, S371F, S373P, S375F, T376A, D405N, R408S, K417N, N440K, V445P, G446S, F456L, N460K, S477N, T478K, E484A, F486P, F490S, Q498R, N501Y, Y505H**, D614G, H655Y, N679K, P681H, N764K, D796Y, Q954H, N969K
XBB.1.5.70 (Omicron)	T19I, L24S/Δ25-27, V83A, G142D, Δ144, H146Q, Q183E, V213E, G252V, **G339H, R346T, L368I, S371F, S373P, S375F, T376A, D405N, R408S, K417N, N440K, V445P, G446S, L455F, F456L, N460K, S477N, T478K, E484A, F486P, F490S, Q498R, N501Y, Y505H**, D614G, H655Y, N679K, P681H, N764K, D796Y, Q954H, N969K
HK.3 (Omicron)	T19I, L24S/Δ25-27, Q52H, V83A, G142D, Δ144, H146Q, Q183E, V213E, G252V, **G339H, R346T, L368I, S371F, S373P, S375F, T376A, D405N, R408S, K417N, N440K, V445P, G446S, L455F, F456L, N460K, S477N, T478K, E484A, F486P, F490S, Q498R, N501Y, Y505H,** D614G, H655Y, N679K, P681H, N764K, D796Y, Q954H, N969K
BA.2.86 (Omicron)	INS16MPLF, T19I, R21T, L24S/Δ25-27, S50L, V127F, G142D, Δ145, F157S/R158G, L212I/Δ211, V213G, L216F, H245N, A264D, **I332V, G339H, K356T, S371F, S373P, S375F, T376A, R403K, D405N, R408S, K417N, N440K, V445H, G446S, S477N, N450D, L452W, N460K, T478K, N481K, Δ483/E484K, F486P, Q498R, N501Y, Y505H,** D614G, H655Y, N679K, P681H, N764K, D796Y, S939F, Q954H, N969K, P1143L
JN.1 (Omicron)	T19I, R21T, L24S, L24S/Δ25-27, S50L, Δ69/70, V127F, G142D, Δ144, F157S, R158G, N211I, Δ212, V213G, L216F, H245N, A264D, I332V, **G339H, K356T, S371F, S373P, S375F, T376A, R403K, D405N, R408S, K417N, N440K, V445H, G446S, N450D, L452W, L455S, N460K, S477N, T478K, N481K, Δ483, E484K, F486P, Q498R, N501Y, Y505H**, E554K, A570V, D614G, P621S, H655Y, N679K, P681R, N764K, D796Y, S939F, Q954H, N969K, P1143L

[1]The mutations present in XBB and XBB1.5 Spike are identical with an additional F486P mutation in XBB1.5, indicated with square brackets and an asterisk (*). [2]RBD mutations are highlighted in bold. [3]The Spike constructs underlined were also synthesised in the pcDNA3.1 expression vector, expressing a c-terminus FLAG tag (Biobasic, Canada).

Table 2.2: SARS-CoV-2 mutants built into a B.1 background in a pcDNA3.1 vector with a Δ19 truncation to assess immunogenicity and species tropism.

RBD-specific mutants used in Chapter 3 to assess immunogenicity.		
Alpha + E484K	K417N	L452R
N501Y	E484K	
NTD-specific mutants used in Chapter 3 to assess immunogenicity.		
Δ69-70	Δ143-145	Δ211
Δ69-70+ Δ143-145+ Δ211	Δ242-244	Δ156-157
Δ24-26	T19I	T19R
A27S	A67V	T95I
G142D	R158G	V213G
INS214EPE	D215G	
Spike mutants used in Chapter 4 to assess species tropism.		
N501Y	N501Y + Δ69-70	P618H
Δ144	A701V	***K417N***
E484A	***Q493R***	N501Y + Q493R
K417N + E484A	E484A + K417N + Q493R	E484A + K417N + Q493R + N501Y

Full-length codon optimised bat sarbecovirus Spike constructs were synthesised and subcloned into pcDNA3.1 (+) with a C-terminal FLAG tag (BioBasic, Canada). Human codon-optimised, Δ19-truncated Spikes of RhGB07 and RfGB02 were subcloned into pcDNA3.1 (+) (shared by Dr Kelvin Lau, EPFL, Switzerland) (**Table 2.3**) [74]. Codon optimised mammalian ACE2 constructs were subcloned into pDISPLAY with an N-terminal signal peptide (the murine Ig k-chain leader sequence) and HA-tag (BioBasic, Canada; Twist, USA, Twist Bioscience, USA) (**Table 2.4**).

Table 2.3: Bat sarbecovirus Spike constructs used in this study for receptor screens and neutralisation assays.

Bat Sarbecovirus Spike	Expression vector, tag	Accession number
SARS-CoV-2 (Wuhan-Hu-1)	pcDNA3.1, c-term FLAG	MN908947.3
BANAL-20-52	pcDNA3.1, c-term FLAG	UAY13217.1
BANAL-20-103	pcDNA3.1, c-term FLAG	UAY13229.1
BANAL-20-236	pcDNA3.1, c-term FLAG	UAY13253.1
RaTG13	pcDNA3.1, c-term FLAG	QHR63300.2
SARS-CoV-1	pcDNA3.1, c-term FLAG	AAR86775.1
WIV-1	pcDNA3.1, c-term FLAG	AGZ48828.1
Rs4231	pcDNA3.1, c-term FLAG	ATO98157.1
RhGB07	pcDNA3.1	WDQ27002.1
RfGB02	pcDNA3.1	WDQ27010.1
Rc-o319	pcDNA3.1, c-term FLAG	BCG66627.1
RacCS203	pcDNA3.1, c-term FLAG	QQM18864.1
RPYN06	pcDNA3.1, c-term FLAG	QWN56252.1
Rf1/2004	pcDNA3.1, c-term FLAG	ABD75323.1
Rp3/2004	pcDNA3.1, c-term FLAG	AAZ67052.1

Table 2.4: Codon optimised ACE2 expression plasmids used in this study for receptor screen and neutralisation assays

Mammalian ACE2	Species	Accession number
Human	*Homo sapiens*	BAB40370.1
Japanese Horseshoe bat	*Rhinolophus cornutus*	BCG67443.1
Least horseshoe bat	*Rhinolophus pusillus*	ADN93477.1
Pearson's horseshoe bat	*Rhinolophus pearsonii*	QKE49996.1
Big-eared horseshoe bat	*Rhinolophus macrotis*	ADN93471.1
Chinese rufous horseshoe bat	*Rhinolophus sinicus*	QMQ39219.1
Intermediate horseshoe bat	*Rhinolophus affinis*	QMQ39240.1
Shamel's horseshoe bat	*Rhinolophus shameli*	UBB59645.1
Greater horseshoe bat	*Rhinolophus ferrumequinum*	BAH02663.1
Halcyon horseshoe bat	*Rhinolophus alcyone*	ALJ94035.1
Greater false vampire bat	*Lyroderma lyra*	QKE49998.1
Flying fox bat	*Pteropus giganteus*	XP_039729365.1
Leschenault's rousette fruit bat	*Rousettus leschenaultii*	BAF50705.1
Black-bearded tomb bat	*Taphozous melanopogon*	UJP38391.1
Common vampire bat	*Desmodus rotundus*	XP_024425698.1
Pallid bat	*Antrozous Pallidus*	QJF77789.1
Little brown bat	*Myotis lucifugus*	XP023609438.1
Dog	*Canis lupus familiaris*	ACT66277.1
Cat	*Felis catus*	AAX59005.1
Pig	*Sus scrofa*	NP001116542.1

Mouse	*Mus musculus*	NP_001123985.1
Brown rat	*Rattus norvegicus*	NP001012006.1
Syrian Hamster	*Mesocricetus auratus*	XM005074209.3
Red fox	*Vulpes vulpes*	XP_025842513.1
Civet	*Paguma larvata*	AAX63775.1
Ferret	*Mustela putorius furo*	BAE53380.1
Pangolin	*Manis javanica*	XP017505752.1
American mink	*Neogale vison*	XP_044091953.1
Raccoon dog	*Nyctereutes procyonoides*	ABW16956.1
White-tailed deer*	*Odocoileus virginianus*	XP_020768965.1
Red deer	*Cervus elaphus*	XP_043752042.1
Marmoset	*Callithrix jacchus*	XP_008987241.1
Squirrel Monkey	*Saimiri boliviensis*	XP_010334925.2
Lemur	*Propithecus_coquereli*	XP_045394292.1
Rhesus macaque	*Macaca mulatta*	ACI04575.1

*chimera of white-tailed deer RBD, with rest of spike from red deer made using site-directed mutagenesis

2.2.2 Henipavirus plasmids

For the henipaviruses, pcDNA3.1 plasmids expressing codon optimised henipavirus fusion (F) and attachment (G) glycoprotein ORFs were used for functional assays including Cedar virus (CedV), Ghanaian bat henipavirus (GHNV), Mojiang virus (MojV), Hendra virus (HeV) (BioBasic, Canda), Melian virus (MeliV) (shared by Dr Piet Maes, KU Leuven, Belgium) and Malaysian Nipah virus (NiVM) and Bangladeshi Nipah virus (NiVB). Accession numbers for the whole genome, and the F and G glycoproteins can be found in **Table 2.5**. EphrinB2 from different species were subcloned into pcDNA3.1(+) between HindIII/NotI restriction sites and accession numbers for these EphrinB2 sequences can be found in **Table 2.6**.

Table 2.5: **GenBank IDs for henipavirus whole genome nucleotide, G and F protein sequences.**

Virus	Whole genome	G protein	F protein
Nipah virus Malaysia	NC_002728.1	NP_112027.1	NP_112026.1
Nipah virus Bangladesh	JN808864.1	AEZ01397.1	AEZ01396.1
Hendra virus	MN062017.1	AAC83193.2	AAC83192.2
Cedar virus	JQ001776.1	AFP87279.1	AFP87278.1
Ghanaian bat henipavirus	HQ660129.1	AFH96011.1	AFH96010.1
Mojiang virus	NC_025352.1	YP_009094095.1	YP_009094094.1
Melian virus	OK623353.1	UQM99519.1	UQM99518.1

Table 2.6: Codon optimised EphrinB2 expression plasmids used for parahenipavirus entry assays

Mammalian EphrinB2	Species	Accession number
Human	*Homo sapiens*	NC_000013.11
Rat	*Rattus rattus*	XM_032919537.1
Greater horseshoe bat	*Rhinolophus ferrumequinum*	XM_033104579.1

2.3 Pseudovirus-based assays

2.3.1 Generating pseudotyped viruses

Lentiviral based pseudoparticles (2nd genereation system) were generated as described previously [218]. For the Sarbecoviruses, HEK293T producer cells were seeded at $7.5x10^5$/well in 6-well dishes (Scientific Laboratory Supplies, Falcon™, cat# 252046) and transfected the next day with 900ng of Spike (**Table 2.1 and Table 2.3**), along with 600ng p8.91 (encoding for HIV-1 gag-pol) and 600ng CSFLW (lentivirus backbone expressing a firefly luciferase reporter gene) (lentivirus constructs shared by Dr Edward Wright, University of Sussex) using 10µL per well of 1µg/mL polyethyleneimine (PEI) transfection reagent (Merck, Cat# 408727) transfection reagent. For the henipaviruses, HEK293T cells were seeded at $2x10^6$/well in $10cm^2$ dishes (Fisher Scientific, Cat#11815272) and transfected the next day with 1000ng of each henipavirus F and G glycoprotein (**Table 2.5**), 100ng p8.91 and 1500ng CSFLW using 20µL dish of 1µg/mL PEI. A negative control was also set up using an empty pcDNA3.1(+) (ThermoFisher Scientific, Invitrogen™, Cat# V79020) plasmid (non-enveloped, NE) and a positive control using p-VSVG. Transfections were incubated at 37°C, 5% CO_2 overnight (32°C for HeV), after which the media was replaced with DMEM-10% to remove any residual transfection mix. Supernatants containing viral pseudotypes were harvested and pooled 48 and 72 hrs post-transfection, centrifuged at 1300*xg* for 10 mins at 4°C to remove cellular debris, aliquoted and stored at -80°C. To quantify the pseudotyped viruses, the sarbecovirus pseudoviruses were titrated 5-fold on HEK293T-hACE2 cells ($2x10^4$/well) and the henipavirus pseudoviruses on BHK-21 cells ($2x10^4$/well) in a white-bottomed 96-well plate (ThermoFisher Scientific, Nunc Microwell, Cat# 10182831) and incubated for 48 hrs at 37°C, 5% CO_2 after which Firefly luciferase was quantified. Media was removed and replaced with 50µL Bright-Glo™ Luciferase Assay System substrate (Promega, Cat# E2650) diluted 1:2 with PBS, incubated in the dark for 5 mins and read on a GloMax Multi+ Detection System (Promega, Cat# GM3000). Comma-separated values (CSV) files were then exported for analysis.

2.3.2 Micro-neutralisation tests (mVNT)

Neutralisation assays were conducted as described previously [218]. For the SARS-CoV-2 variants, sera from individuals immunised with up to 7 doses of a COVID-19 vaccine as part of the CONSENSUS study, or for the sabecoviruses and SARS-CoV-2 variants, pooled convalescent patient plasma from patients recovered from COVID-19 or negative control plasma (MHRA) were diluted in serum free DMEM for a final dilution of 1:40 and added in triplicate to a white-bottomed 96-well plate (ThermoFisher Scientific, Nunc Microwell, Cat# 10182831) and titrated three-fold. Sera from the CONSENSUS study were diluted dependent on the expected neutralisation titres [221]. Monoclonal antibodies (provided by

Katie Doores, Kings College London) were serially diluted, from a starting concentration of 50µg/ml. Sarbecovirus pseudoparticles were added in 50µL volume equivalent to 10^5-10^6 signal luciferase units and incubated for 1 hr at 37°C, 5% CO_2. Target HEK293T-hACE2 cells were added at a density of $2x10^4$ in 100µL and incubated at 37°C, 5% CO_2 for 48 hrs, after which Firefly luciferase activity was measured. Pseudotyped virus neutralization titres were expressed as calculating by interpolating the point at which there was a 50% or 80% reduction in luciferase activity, relative to untreated controls (inhibitory concentration, IC_{50}/IC_{80}; neutralisation dose, ND_{80}) for sera. For the mAbs, this IC_{50} was calculated as the percentage that yielded 50% inhibition relative to the untreated controls. CSV files were exported, and analysis was performed on GraphPad Prism v8.2.1.

For the henipaviruses, sera from immunised pigs, mice and hamsters were diluted in serum free DMEM and added to a 96-well plate in triplicate for a final dilution of 1:20 and titrated two-fold, or henipavirus-specific mAbs were used at 20µg/mL. Henipavirus pseudoparticles were added at a dilution equivalent to 10^6 signal luciferase units in 50µL volume and incubated for 1 hr at 37°C, 5% CO_2. BHK-21 target cells were then added at a density of $2x10^4$ in 100µL and incubated at 37°C, 5% CO_2 for 72 hrs after which Firefly luciferase activity was measured. Pseudotyped virus neutralization titres were calculated by interpolating the point at which there was a 50% reduction for the henipaviruses (ND_{50}), or an 80% reduction for SARS-CoV-2 (ND_{80}) variants in luciferase activity, relative to untreated controls. For the mAbs, this IC_{50} was calculated as the percentage that yielded 50% inhibition relative to the untreated controls. CSV files were exported, and analysis was performed on GraphPad Prism v8.2.1.

2.3.3 ACE2 receptor screen

Receptor usage screens were conducted as described previously [218, 219]. BHK-21 cells were seeded in 6-well plates at 7.5×10^5 /well in DMEM-10% 1 day prior to transfection with 500 ng of different species, ACE2-expressing constructs for the sarbecoviruses, EphrinB2-expressing constructs for the henipaviruses or a relevant empty vector (pDISPLAY™, ThermoFisher Scientific, Invitrogen™, Cat# V66020 or pcDNA3.1(+), ThermoFisher Scientific, Invitrogen, Cat# V79020, respectively) (**Table 2.4, Table 2.6**) in OptiMEM (ThermoFisher Scientific, Gibco™, Cat# 11058021) and *Trans*IT-X2® Dynamic Delivery System (Mirus Bio, Cat# MIR 6000) transfection reagent according to the manufacturer's recommendations. The next day, cells were harvested using 2mM EDTA (0.5M, pH8.01, RNase-free (ThermoFisher Scientific, Ambion®, Cat# AM9269G)) and re-plated into white-bottomed 96-well plates at $2x10^4$/well in DMEM-10% and infected with pseudoparticles equivalent to 10^5 to 10^6 relative light units (RLU) for 48 h at 37˚C, 5% CO_2.

To quantify firefly luciferase, media was replaced with 50 µL Bright-Glo™ Luciferase Assay System substrate (Promega, Cat# E2650) diluted 1:2 with PBS. The plate was incubated in the dark for 5 min and then read on a Glomax Multi+ Detection System (Promega, Cat# GM3000). CSV files were exported for analysis. Biological replicates were performed 3 times.

2.4. Cell-cell fusion-based assays

2.4.1 Cell-cell fusion assay

Cell-cell fusion assays were adapted from a previously described protocol [162]. HEK293T Lenti rLuc-GFP 1-7 cells (effectors) and BHK-21 Lenti rLuc-GFP 8-11 cells (targets) were seeded separately at $7.5x10^5$ per well in a 6-well dish in DMEM-10%. The following day, transfection mixes were set up in 200µL Opti-MEM (ThermoScientific, Gibco™, Cat# 11058021) with the *Trans*IT-X2® Dynamic Delivery System (Mirus Bio, Cat# MIR 6000) transfection reagent under manufacturer's recommendations. Viral glycoproteins were transfected (500ng each) into effector cells (500ng Spike (**Table 2.3**); 500ng F + 500ng G (**Table 2.5**)) and 500ng of the corresponding receptor into target cells (500ng ACE2 for the Sarbecoviruses (Table 2,4); 500ng EphrinB2 for the parahenipaviruses (**Table 2.6**)). A mock-transfected control was also included for both effector (pcDNA3.1 (+), (ThermoFisher Scientific, Invitrogen™, Cat# V79020)) and target cell (pDISPLAY™, ThermoFisher Scientific, Invitrogen™, Cat# V66020) populations. Transfections were incubated at 37°C, 5% CO_2 for 24-48 hrs after which cells were harvested and diluted to $2x10^5$/mL in DMEM-10%. Diluted effector and target cells were co-cultured by adding 100µL volume ($2x10^4$/well) of cells to each well of a white-bottomed, sterile 96-well plate plate (ThermoFisher Scientific, Nunc Microwell, Cat# 10182831) and incubated at 37°C, 5% CO_2. *Renilla* luciferase was quantified by replacing media with 60µL of Coelenterazine-H substrate, 1µM (Promega, Cat# S2011), diluted 1:400 in PBS. Plates were incubated in the dark for 2 mins then luminescence read on a GloMax Multi+ Detection System (Promega, Cat# GM3000). To quantify GFP-positive syncytia, cells were plated in a clear flat-bottomed 96-well plate and imaged every 4 hrs using the IncuCyte® S3 live cell imaging system (Satorius, Cat# 4647). Five fields of view were taken per well at 10x magnification and a representative field selected to depict GFP_+ syncytia. The total integrated intensity metric was used to measure GFP green count units (GCU) $µm^2$, as described previously [8].

2.4.2 Micro-fusion inhibition test (mFIT)

Henipavirus micro-fusion inhibition tests (mFITs) were set up as previously described [162], adapted from the cell-cell fusion assay outlined above. Henipavirus-specific mAbs (provided by Dr Keith Chappell and Dr Daniel Watterson, University of Queensland) at a

concentration of 20µg/mL were incubated with effector HEK293T Lenti-rLuc-GFP 1-7 cells overexpressing henipavirus glycoproteins for 1 hr at 37ºC with 5% CO_2. Target BHK-21 Lenti rLuc-GFP 8-11 were then co-cultured and incubated for 24 hrs at 37ºC with 5% CO_2. *Renilla* luciferase was quantified by replacing media with 60µL of Coelenterazine-H substrate, 1µM (Promega, Cat# S2011), diluted 1:400 in PBS. Plates were incubated in the dark for 2 mins then luminescence read on a GloMax Multi+ Detection System (Promega, Cat# GM3000) and CSV files were exported for analysis. Inhibition of fusion was calculated as the percentage that yielded 50% inhibition of fusion relative to the untreated controls (IC_{50}).

2.5 Molecular techniques

2.5.1 Western blotting

BHK-21 cells were transfected using Transit-X2 transfection reagent (Mirus Bio, Cat# MIR 6000), as per the manufacturer's instructions with 500 ng of different ACE2-expressing constructs (**Table 2.4**) or mock-transfected with empty plasmid vector (pDISPLAY™) and harvested 48 h post transfection. Producer cells transfected with sarbecovirus Spikes were harvested 48 h post transfection. All protein samples were generated using 2× Laemmli Sample Buffer (Bio-Rad, #Cat 1610737) and reduced at 95˚C for 5 min. Samples were resolved on 7.5% acrylamide gels by SDS-PAGE, using semidry transfer onto nitrocellulose membrane. Blots were probed with anti-human influenza hemagglutinin tag (HA) primary antibody (Miltenyi Biotech, Germany) for ACE2-transfected cells at 1:1,000 or with rat anti-FLAG primary antibody (BioLegend, USA) and anti-Spike primary antibody (Novus Biologics Cat# NB100-56578) at 1:,1000 for pseudovirus producer cells at 1:1,000 in PBS-Tween 20 (PBS-T, 0.1%) with 5% (w/v) milk powder overnight at 4˚C. Blots were also probed with mouse anti-GAPDH (Cell Signalling, 1:3,000, Cat# 97166S) as endogenous controls. Blots were washed in PBS-T and incubated with anti-mouse or anti-rabbit secondary antibody conjugated with horseradish peroxidase (Cell Signalling, Cat# 7076S or Cat# 7074S) at 1:2,000 in PBS-T for 1 h at room temperature. Membranes were exposed to Clarity Western ECL substrate (Bio-Rad Laboratories) according to the manufacturer's guidelines and exposed to autoradiographic film.

2.5.2 Depletion of RBD-specific antibodies

HIS-Select® Nickel Magnetic Agarose Beads (1.5mg) (Sigma, H9914) were conjugated to SARS-CoV-2 recombinant proteins expressing the His tag (20µg/ml protein) in binding buffer (100mM sodium phosphate pH8.0, 600mM NaCl, 0.02% Tween-20). This mixture was rotated on 10 mins at room temperature, then placed on a MagnaRack Magnetic Separation Rack (Thermofisher, Cat#CS15000) to pull out the RBD-bead conjugate and

washed three times in PBS + 0.05% BSA. Polyclonal sera was added to the SARS-CoV-2 RBD – beads conjugate in PBS + 0.05% BSA at a dilution of 3:1 beads:sera and rotated overnight at 4°C. The MagnaRack Magnetic Separation Rack was used to separate RBD-binding antibodies from the supernatant, leaving non-RBD binding antibodies, which were transferred into a new microfuge for use in downstream assays.

2.5 Protein assays

2.5.1 Protein expression

Secreted henipavirus G proteins (sG) were produced by cloning the ectodomain of the NiVB, HeV, CedV or GHNV G sequences (**Table 2.5**) into the pHLSec expression vector between the AgeI and KpnI sites (**Appendix 1**). NiVMsG was previously produced in the lab by Dr Dalan Bailey. Sarbecovirus RBDs were produced as Avitag-His-tag proteins by cloning into pOPINNTGneo expression vectors (**Appendix 2**) (shared by Dr Raymond Owens, University of Oxford, as described in [222]). PCR products were assessed by agarose gel electrophoresis to determine the correct size of DNA and sequenced to ensure incorporation with the correct gene. Primers use for cloning are listed in **Appendix 3.** These plasmids were then expressed in Expi293F cells using PEI40K transfection reagent (Polysciences, Cat# 24765-1) with additives the day after transfection (300mM valproic acid (Merck, Cat# P4543), 500mM of sodium propionate (Merck, Cat#P1880), 2.5M glucose (Merck, Cat# 49163-100ML)). Supernatants were harvested 4 days post-transfection, centrifuged for 45 mins at 6000 x *g* and filter through a 0.45μM filter. Presence of secreted protein was determined by Coomassie and by western blot for anti-His, as described above. Supernatants were purified using HisTrapHP columns (Cytivia, Cat# 17524802), desalted using Zeba Spin Desalting Columns (ThermoFisher Scientific, Cat# 89883) and concentrated using Amicon Ultra 15 columns (Merck Millipore, Cat# C7715). The proteins were then quantified using a Nanodrop and a Pierce BCA Protein assay (ThermoFisher Scientific, Cat# 23227) and run on an SDS-PAGE gel to assess protein purity by Coomassie stain.

2.5.2 Indirect ELISA with Henipavirus G proteins

Indirect ELISAs were performed by coating flat-bottomed 96-well plates with 50μL of an optimal concentration of antigen (1μg/ml for HeVsG and NiVsG, 5μg/ml for GHNVsG, CedVsG, MojVsG, MeliVsG), diluted in a carbonate/bicarbonate solution (0.6M, pH9.6) (Merck, Cat# 75335-1L) overnight at 4°C. The next day, the coating buffer was removed and plates were blocked with 100μL 5%milk in PBS for 2 hrs at 37°C. Sera (pig, mouse or hamster) was added at a starting dilution of 1:400 in duplicate in 2.5% milk in PBST and titrated two-fold down the plate to obtain the end-point titre. For the monoclonal m102.4, a

single concentration of 1µg/ml was tested. Incubation with primary antibody was carried out for 1hr at 37ºC after which the binding of IgG on the plate surface was detected on the plate using a HRP-linked secondary antibody - *pig sera*: anti-pig H+L IgG HRP, 1:10,000 (Merck, #Cat AP166P); *mouse sera*: anti-mouse IgG HRP, 1:5,000 (Cell Signalling, Cat# 7076S); *hamster sera*: anti-hamster H+L IgG HRP, 1:10,000 (Jackson Immuno, Cat# 107-035-142); *m102.4*: rabbit anti-human IgG, 1:10,000 (Merck, Cat# AP101). Samples were analysed after the addition of 3,3',5,5'-tetrametehylybezidine (TMB, Merck Cat# T4444) and evaluated the optical density (OD) at 450nm after addition of 1M sulphuric acid solution (Merck, Cat#258105). The cut-off was determined as the mean+3SD of negative controls.

2.5.3 Sarbecovirus RBD ELISA to measure antibody binding.

Recombinant RBD was coated onto 96-well ELISA plates at 1µg/ml per well in a carbonate/bicarbonate solution (0.6M, pH9.6) (Merck, Cat# 75335-1L) at 4ºC overnight. Plates were blocked for 1 hr at room temperature with PBS-T containing 1% bovine serum albumin (BSA, Merck, Cat# A3608), after which a dilution series of monoclonal antibodies (from Dr Katie Doores, King's College London, described in [223, 224]) or polyclonal sera (MHRA reference sera, see **Table 2.7**) were diluted in PBS was added for 1h, at 37ºC. Plates were washed 3 times with PBS-T, followed by the addition of anti-human-Fc HRP conjugate diluted 1:10,000 for 1h at 37ºC.1-step Ultra TMB (Merck Cat# T4444) was added to each well, incubated for 5-10 mins at room temperature and the reactions stopped with an equivalent volume of 2M sulphuric acid solution (Merck, Cat#258105), after which the optical density (OD) at 450nm was measured. Samples were analysed by plotting 50% effective concentration (EC_{50}) using GraphPad Prism (8.2.1) software.

Table 2.7: MHRA polyclonal sera used to establish WHO International Standards and Reference panels for anti-SARS-CoV-2 immunoglobulins.

Sample	MHRA code	Description
WT	S2-03	UK 2020, single individual, plasma - pre-VOC
	21/296	IRP for antibodies to SARS-CoV-2 variants - pre-VOC (pooled plasma)
Alpha	S2-01	Alpha sequence confirmed, serum
	S2-04	UK 2021, single individual, plasma - Alpha*
	21/300	IRP for antibodies to SARS-CoV-2 variants - Alpha* (pool plasma)
Gamma	S2-07	Brazil 2021, pool plasma - Gamma*
	22/126	IRP for antibodies to SARS-CoV-2 variants - Gamma (pool plasma)
Delta	21/312	IRP for antibodies to SARS-CoV-2 variants - Delta (pool sera from 19 individuals, Kenya)
Omicron	22/128	IRP for antibodies to SARS-CoV-2 variants - Omicron (pool plasma)
International Standard	20/136	1st WHO Standard
	21/338	2nd WHO International Standard (infected/vaccinated)
	21/340	2nd WHO International Standard
Vaccinee plasma	S2-05	Vaccinee plasma, low
	S2-02	Vaccinee plasma, high
Negative	S2-06	Negative plasma, pre-2019

IRP = International Reference Panel; *Assumed based on epidemiological data

2.6 Sera from pre-clinical animal studies and human studies.

2.6.1 Animal sera

Sera from mice, pigs, non-human primates, ferrets and hamsters immunised in pre-clinical vaccine studies for SARS-CoV-2 were obtained with the permission from the study lead for assessment of neutralising antibody responses using pseudoviruses bearing SARS-CoV-2 variant Spikes. The immunisation regime, study lead and relevant citations are outlined in **Appendix 4**.

2.6.2 Human sera

The UKHSA initiated a longitudinal audit of vaccinated individuals to examine antibody and T cell responses following COVID-19 vaccination (CONSENSUS study) [225]. Healthy participants ages 50-89 in January 2021 were recruited through North London primary care networks. Sera samples used in this study were taken at various timepoints after vaccination with up to 7 COVID-19 vaccinations. Serum samples were analysed in Roche Spike (indication of infection or vaccination) and Nucleoprotein-based (marker of previous SARS-CoV-2 infection) ELISAs. All sera were heat-inactivated at 56°C for 2 hrs before use in subsequent assays.

Serum samples were collected from 499 people who actively engage in bushmeat hunting, and their family members from 38 villages in Macenta prefecture of Guinea. Macenta is located in the historically forested Nzérékoré region and borders the Guéckédou prefecture, the index site of the 2013-2016 Ebola virus epidemic and the 2021 Marburg virus outbreak. Between February to December 2017, Toma-speaking villages in Macenta were purposively selected to include individuals affected and unaffected by the Ebola virus epidemic. Consenting participants were invited to local health centres, where following the completion of a sociodemographic questionnaire, 5ml peripheral blood was collected, centrifuged for 10mins at 200 *x g* and stored at -20°C [226]. These samples were run in a Luminex assay against different viral glycoproteins [227], in a study led by Miles Carroll, University of Oxford, with samples JAB356, JAB033 and JAB297 being approved for use in subsequent ELISA assays in this study.

2.7 Animals, Immunogenicity and Efficacy Studies

2.7.1 Mice - Henipavirus immunogenicity study

Inbred BALB/cOlaHsd (BALB/c) (Envigo) (n=5 to 7 mice per group), were immunized intramuscularly (i.m.) in the musculus tibialis with 2.5µg NiVBsG in Addavax (InvivoGen, Cat# vac-adx-10), GHNVsG in Addavax under homologous or heterologous prime-boost-boost regime. An equivalent volume of Addavax was also included as an adjuvant only control. Mice were boosted with the relevant vaccine candidate every 4 weeks. All mice were sacrificed 4 weeks after the final vaccination with serum samples collected by tail vein at weeks 4 and 8, and a cardiac bleed was taken at 12-weeks when animals were euthanised for analysis of humoral immunity. Spleens were collected for analysis of cell-mediated immunity.

2.7.2 Pigs – Henipavirus immunogenicity study

This study was performed as part of the Nipah virus vaccine for Pigs consortium led by Professor Simon Graham, The Pirbright Institute (*manuscript under review*). Forty-five, 8-10-week-old, female, large White-Landrace-Hampshire cross-bred pigs were randomly assigned to the same five treatment groups. Pigs were immunised by intramuscular inoculation of either 1×10^9 i.u. ChAdOx1 NiV G [191], 100 µg NiV sG in ZAF-001; 100 µg NiV mcsF [228] in ZAF-001; 100 µg HeV sG [194] in ZAF-001; or an equivalent volume (1 mL) of ZAF-001 (proprietary water in oil emulsion containing surfactants, ionic polymer and a synthetic immunomodulator, Zoetis Inc). After 3 weeks, 3 animals per group were euthanised by pentobarbital overdose and the remaining 6 animals per group received a homologous booster immunisation and were euthanised after a further 3 weeks. Serum

samples were obtained weekly, and the bio-banked sera from this study taken 42 days post-immunisation were used for subsequent analysis.

2.7.3 Hamsters – Henipavirus efficacy study

Golden Syrian Hamsters (n=12/group) received homologous prime-boost vaccinations of either 2.5µg NiVBsG or GHNVsG with Alhdrogel adjuvant, or an adjuvant only control. Animals were boosted 4-weeks apart and bleeds taken at day 0 and day 28 after initial immunisation. At 8-weeks, 6 animals were culled in each group and spleens and sera obtained (day 56) for analysis of humoral and cellular immunity. The remaining 6 animals were challenged with 10^2 $TCID_{50}$ NiVB and animals were euthanised when they reached humane endpoint, or 3-weeks post-challenge. Clinical scores, weight and temperature was measured throughout the study. Blood was taken for analysis of presence of viral RNA and tissue sections were obtained for histology.

2.8 Hamster tissue histology

2.8.1 Histopathology

Tissue samples from hamster lung, spleen, and the rostral part of the brain were fixed by immersion in 10% neutral-buffered formalin (NBF, Merck, Cat# HT501128) for 3 weeks and then routinely processed into paraffin wax and were decalcified with an EDTA based solution for seven days prior to embedding. 4 µm sections were cut and stained with haematoxylin and eosin (H&E). Stained slides were digitalised using a Hamamatsu S360 digital slide scanner (Hamamatsu Photonics K.K., Shizuoka, Japan) and examined with the ndp.view2 software (Hamamatsu Photonics K.K., v2.8.24). The severity of the lesions was recorded with a semi-quantitative score as follows, 0 = within normal limits; 1 = minimal histopathological lesions; 2 = mild histopathological lesions; 3 = moderate histopathological lesions and 4 = marked/severe histopathological lesions. The percentage of area histopathological lesions in the lungs was calculated using digital image analysis with Nikon-NIS-Ar software (Nikon, Instruments Inc., NY, USA).

2.8.2 NiV RNA in-situ hybridisation

Tissue samples were stained using the *in-situ* hybridisation (ISH) RNAscope technique to identify NiV RNA. The staining was automatically performed in a Leica BOND-RXm (Leica Microsystems, Milton Keynes, United Kingdom). Briefly, slides were pre-treated with hydrogen peroxide for 10 mins, target retrieval for 15 mins (98-101 °C), and protease plus for 30 mins (40 °C) (Advanced Cell Diagnostics, Cat# 322331). A NiV-specific probe (Advanced Cell Diagnostics, Cat# 439258) was applied and incubated for 2 hrs at 40 °C. Amplification of the signal was performed using the RNAscope 2.5 HD Detection Kit – RED

(Advanced Cell Diagnostics, Cat# 322360) following the manufacturer instructions. After mounting using EcoMount (Biocare Medical, Cat# EM897L), slides were digitally scanned with the Hamamatsu S360 digital slide scanner (Hamamatsu Photonics K.K). To quantify the presence of NiV RNA, tissues including lung, spleen, and brain were submitted to image analysis (Nikon NIS-Ar software) (Nikon, Instruments) to calculate the percentage of positivity (percentage area positively stained). Histopathology and *in-situ* hybridisation RNAscope technique were carried out in an ISO9001:2015 and GLP-compliant laboratory and evaluation was performed by two veterinary pathologists blinded to the study groups.

2.9 Analysing cellular immunity

2.9.1 Splenocyte isolation

Spleen were harvested from euthanised mice or hamsters and cut into small pieces (approx. 2mm^2) after removal of any fatty tissue. Cut spleens were then added to 5ml of digestion buffer for hamster spleens (1x HBSS (Gibco, Cat# 24020-091), 10mM HEPES (Gibco, Cat# 15630-056), 20µg/ml DNAseI (Merck, Cat# D5025-750KU), 2mg/ml Collagenase D (Roche, Cat# 11088882001), warmed to 37°C) or PBS for mouse spleens and slowly rotated on a MACSmix™ tube rotator (Miltenyi Biotec, Cat# 130-090-753) for 20 mins at 37°C, 5% CO_2. Following incubation, digested spleens were gently homogenised using a disposable pestle through a 100µm cell strainer into a new tube, rinsed through with 10ml wash buffer (RPMI-1640 (Gibco, Cat# 12633-012) + 10% foetal calf serum (FCS, Labtech, Cat# FCS-SA/500), 1% antimicrobial/antimycotic (anti-anti, Merck, Cat#A5955-100ML), 1% L-Glutamine (Merck, Cat# G7513), 30mM HEPES (Gibco, Cat# 24020-091), 5mM EDTA (Invitrogen, Cat# 10135423)) and centrifuged for 5 mins at 400 *xg*. Supernatant was discarded and red blood cells lysed with 5ml ACK lysis buffer (Gibco, Cat# A10492-01), then neutralised with addition of 25ml 1xPBS. Cells were then centrifuged for 5 mins at 400 *xg* and resuspended in wash buffer before pelleting and resuspending in 10ml culture media (RPMI-1640 (Gibco, Cat# 12633-012) + 10% FCS (Labtech), 1% anti-anti (Merck, Cat#A5955-100ML), 1% L-Glutamine (Merck, Cat# G7513) and 30mM HEPES (Gibco, Cat# 24020-091)). Cells were then counted for use in subsequent assays and remaining cells were frozen down in FCS + 10% dimethyl sulfoxide, DMSO (Merck, Cat# D8418) at -80°C.

2.9.2 IFNγ ELISpot

Mouse Splenocyte ELISpot

IFNγ antibody (Mabtech, Cat# 3321-2A) was diluted to 5µg/ml in carbonate/bicarbonate buffer, added to MAIP plates (Milipore, Cat# MAIPS4510) and incubated overnight at 4°C. Plates were then blocked in 100µl complete α-MEM (MEM α-modification (Merck, Cat# M-

4526), 10% FBS (Merck, Cat# F-2442), 1% pen/strep (Merck, Cat# P-0781), 1% L-Glutamine 4mM (Merck, Cat# G-7514), 0.1% 2-Mercapthoethanol (Gibco, Cat# BRL-31350-0100)) and incubated at room temperature for 1 hr. Splenocytes were added in triplicate at $1x10^6$/well to the top row and serially diluted 1:2 in complete α-MEM ($5x10^5$/well final), including a media only row. Splenocytes were stimulated with NiVB-G (3 pools, shared by Dr Rachel Kenneil, University of Oxford), GHNV-G (1 pool) or CedV-G (1 pool) 20-mers offset by 10 (Mimitopes) at 1µg/ml (**Appendix 5**) and incubated at 37°C for 18 hrs. A PMA and ionomycin (Fisher Scientific, Cat# 00-4970-03) positive control was added to each plate. Plates were washed 6x with PBS and incubated with 1µg/ml of rat anti-mouse IFNγ (Mabtech, Cat# 3321-2A) for 2hrs at room temperature in the dark. Plates were again washed 6x with PBS and 1µg/ml Streptavidin alkaline phosphatase polymer (Mabtech, Cat# 3321-2A) was added and incubated at room temperature for 1 hr. Plates were washed a further 6x with PBS and colour development was carried out with an AP conjugate sub kit (BioRad Cat# 170-5432) and incubated at room temperature for 5 mins. Plates were washed with tap water, the underdrain removed and left to dry overnight before counting spots (Mabtech, Cat# IRIS 2).

Hamster Splenocyte ELISpot

Pre-coated IFNγ plates (Mabtech, Cat#3102-2A) were rehydrated with PBS for a total of 4 washes and incubated at room temperature with complete RPMI-1640 ((RPMI-1640 (Gibco, Cat# 12633-012) + 10% foetal calf serum (FCS, Labtech, Cat# FCS-SA/500), 1% antimicrobial/antimycotic (anti-anti, Merck, Cat#A5955-100ML), 1% L-Glutamine (Merck, Cat# G7513), 30mM HEPES (Gibco, Cat# 24020-091), 5mM EDTA (Invitrogen, Cat# 10135423)) for 30 mins. Media was flicked off plates and peptide pools were added to relevant wells at 1µg/ml final concentration: NiVB-G (3 pools), GHNV-G (1 pool) or CedV-G (1 pool) 20-mers offset by 10 (Mimitopes) (**Appendix 5**). Cell stimulatory PMA and ionomycin (Fisher Scientific, Cat# 00-4970-03) positive control was added to relevant wells. Splenocytes were added in triplicate in RPMI ($5x10^5$/well final), including a media only row on each plate and incubated at 37°C for 18hrs. The next day, plates were washed 5x with PBS, then detection antibody diluted (Mabtech, Cat# 3102-2A) in 0.5% FBS-PBS was added and incubated at room temperature for 2 hrs. Plates were washed 5x with PBS and a streptavidin-ALP conjugate (Mabtech, Cat# 3102-2A) diluted in 0.5% FBS-PBS was added and incubated in the dark for 1 hr at room temperature. Plates were washed 5x with PBS and substrate added for 10 mins and colour development was stopped by washing with water. The underdrain was removed from plates and left to dry overnight in the dark at room temperature before counting spots (Mabtech, Cat# IRIS 2).

2.10 Ethics Statement

Animal studies were performed in accordance with UK Animals (Scientific Procedures) Act 1986 and approved by the relevant local Animal Welfare and Ethical Review Bodies (AWERB) (Mouse henipavirus study: Project License PP2352929 and University of Oxford AWERB; Hamster henipavirus study: Project License PP3877532 and UKHSA AWERB; Pig henipavirus study: Project License P9C86DC55 and The Pirbright Institute and Animal and Plant Health Agency AWERBs). The principles of the 3R's were applied for the duration of each study to uphold animal welfare. For the CONSENSUS study, the protocol was approved by UKHSA Research Ethics Governance Group (reference NR0253; 18/01/21) and permitted for use in this study. Participant samples were only analysed where informed consent was obtained. Ethical approval was obtained from the National Ethics Committee for Health and Research, Guinea (33/CNERS/15) and from the National Research Ethics Service UK for use of serum samples from individuals in the Macenta prefecture of Guinea and was ethically approved by the Board of UK Research Ethics Council and the National Research for Health Ethics Committee of Guinea (Permit: 012/CENRS/2017).

Chapter 3: Assessing the potential impact of emerging SARS-CoV-2 variants on COVID-19 vaccine efficacy.

3.1 Introduction and Aims

Severe respiratory syndrome coronavirus 2 (SARS-CoV-2) is a betacoronavirus with a single-stranded positive-sense RNA genome that emerged in late 2019 and is responsible for the COVID-19 pandemic [38]. Unlike most RNA viruses that have high mutation rates during replication due to the presence of an intrinsically error-prone RNA polymerase, coronaviruses possess some proof-reading capacity that allows for relatively accurate transcription and replication [229]. Nevertheless, there are still mutations. Although most of these mutations are synonymous or even, detrimental to the virus, some can confer an advantage to the virus by increasing or altering transmissibility, or immune escape, a phenomenon which has been evident throughout the pandemic [39]. Indeed, mutations in the SARS-CoV-2 genome have continued to emerge, both within and outside the surface Spike glycoprotein [40]. Mutations in the Spike protein are of particular interest as this protein is the main target of neutralising antibodies (nAbs), which are important for long-lasting immunity and the prevention of viral transmission following natural infection of immunisation [230]. Neutralisation of the virus particle occurs through inhibition of attachment, receptor engagement or virus uptake into the host cell, but there is also increasing emphasis being put on the importance of inhibition of cell-cell fusion, T-cell mediated immunity and the role of non-neutralising antibodies [162]. The development of nAbs is of particular interest when considering the evolution and emergence of new variants, in particular whether pre-existing immunity acquired by vaccination and/or infection can provide any degree of protection against these strains.

The monomeric unit of the trimeric Spike protein is subdivided, containing an N-terminal S1 domain, which is responsible for viral attachment to the proteinaceous host receptor, angiotensin converting enzyme 2 (ACE2), and a C-terminal S2 domain, which is anchored into the viral membrane, responsible for membrane fusion and entry following cleavage at S2` (**Figure 3.1A**) [231, 232]. The majority of nAbs are targeted against the S1 domain, in particular against the receptor binding domain (RBD) or regions closely adjacent to the ACE2-binding interface (**Figure 3.1A**) [233]. The RBD can exhibit two conformations: a locked “down” conformation, or an active “up” conformation, which exposes the receptor binding site [78]. However, there is also evidence that antibodies can potently bind “antigenic supersites” on the N-terminal domain (NTD) within S1, but this mode of action is less well characterised (**Figure 3.1A**) [232]. Collectively, these mutations have been implicated in immune escape and/or increased transmission of SARS-CoV-2 variants. For

example, the H69/V70 deletion in Alpha has been reported to increase infectivity, without evading antibody-mediated neutralisation [234]. Antibodies against S2 tend to be poorly neutralising [46, 235].

During the COVID-19 pandemic, mutations in the wildtype (WT) SARS-CoV-2 sequence have continued to emerge, both within and outside the Spike protein, with the earliest notable mutation being a change at amino acid position 614 in the Spike protein from an aspartic acid (D) to a glycine (G), giving rise to the D614G (Pango Lineage B.1) variant. This D614G mutation appears to result in breakage of a hydrogen bond between the S1 and S2 subunits, facilitating greater cleavage of the Spike protein, which translated to increased viral entry and transmission, but did not result in increased disease severity [41-43]. Viral genome sequencing efforts were established to track the evolution of the virus for collection of epidemiological data, such as the COVID-19 Genomics UK Consortium (COG-UK) and CoVariants enabled by data from GISAID [44]. This allowed close monitoring of the prevalence of new variants, and these were subsequently divided into categories by regulatory bodies such as the UK Health and Security Agency (UKHSA, formerly Public Health England) and the World Health Organisation (WHO) depending on the increased risk to global health, to prioritise monitoring, research and to inform the response to the pandemic as new variants continued to emerge.

Some of these variants, termed “Variants of Concern” (VOC) were subsequently given Greek letter identifiers by WHO, including Alpha/B.1.1.7, Beta/B.1.351, Gamma/P.1, Delta/B.1.617.2, and Omicron/B.1.529 and its subvariants (e.g. BA.1, BA.2, BA.5) [45]. These VOCs were considered to be of particular concern because they may be more transmissible, cause more severe disease or may escape neutralisation from pre-existing antibodies, based on the risk assessment of the amino acid changes detected [236-238]. Aside from the major VOCs, other variants emerged across the world and were classified as “variants under investigation” (VUIs; e.g., Theta/P.3, Mu/B.1.621, Lambda/C.37) or “variants under monitoring” (VUMs; e.g., Iota/B.1.526, B.1.1.318, C.1.2) (**Figure 3.1B**), but in May 2023, WHO declared that COVID-19 no longer represents a “global health emergency” so this naming convention was abandoned, although SARS-CoV-2 variants have continued to emerge.

In an effort to manage the transmission of SARS-CoV-2 and the effects of the COVID-19 pandemic, several public health strategies and non-pharmaceutical interventions were employed globally, including mask-wearing, minimising the movement of people (“lockdowns”), self-isolation of infected individuals and the development of antivirals and vaccines. Several vaccines were authorised and licensed for use in multiple countries,

including the Oxford-AstraZeneca (ADZ1222, Vaxzervria™) [90] and BioNTech/Pfizer (BNT162b2, Comirnaty®) [91] vaccines, designed to target the full-length Spike protein using the original SARS-CoV-2 sequence. These vaccines were shown to induce nAbs and in some cases, T cell responses to differing levels [92, 239], and were effective in reducing COVID-19 related hospitalisations and deaths [90, 91]. However, the emergence of SARS-CoV-2 variants resulted in reduced efficacy of the COVID-19 vaccines due to evidence of increased transmissibility and a reduction in nAb titres, resulting in infection and disease even in vaccinated or previously infected individuals, which has meant that in the UK, individuals are now receiving booster vaccinations with updated COVID-19 vaccines, although globally, most individuals do not receive boosters [49, 236].

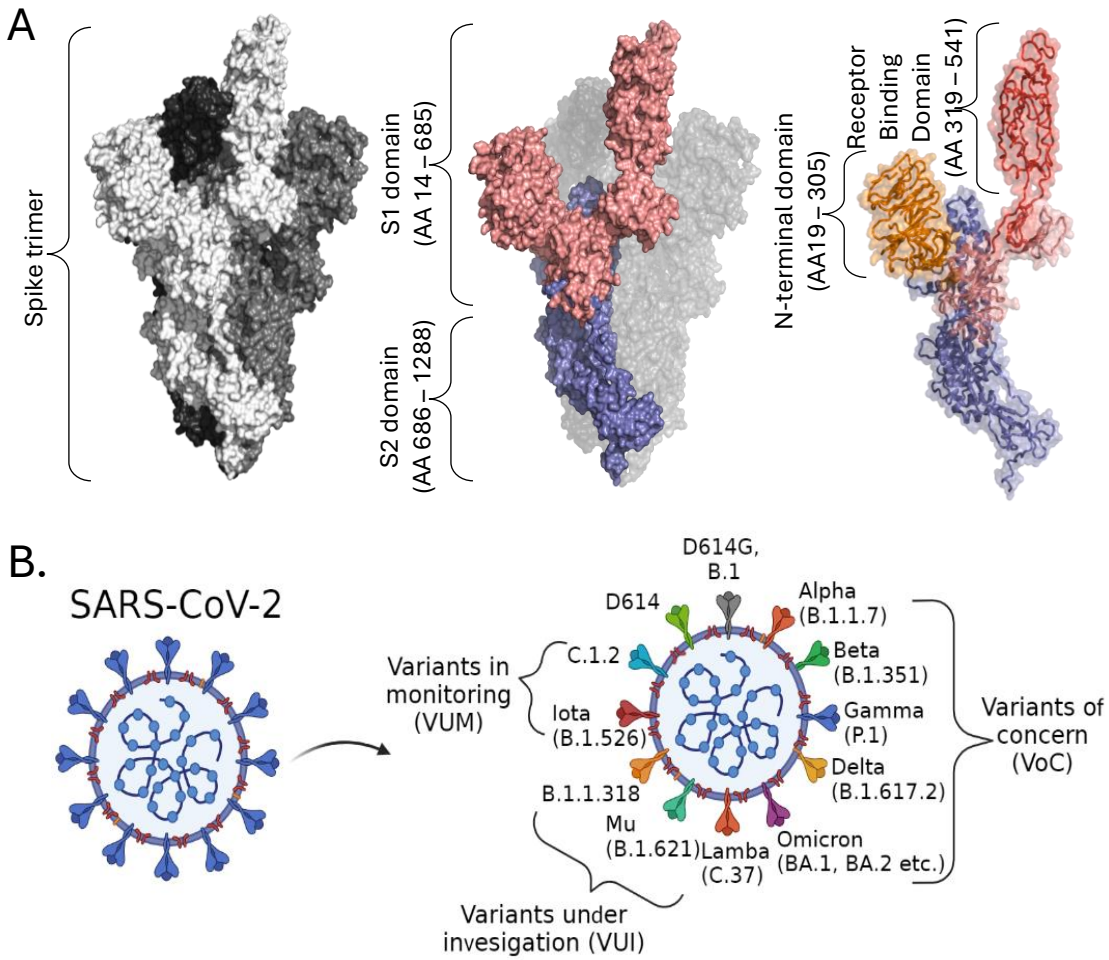

Figure 3.1: Schematic of SARS-CoV-2 Spike protein and classification of SARS-CoV-2 variants.
(A) Molecular surface representation of the trimeric SARS-CoV-2 Spike protein (PDB 6XM0), drawn using PyMOL, with each monomer coloured in a different shade of grey (left) and the RBDs depicted as a one "up", two "down" conformation. A single monomer is highlighted, depicting the S1 (pink) and S2 domains (blue) and the amino acid range each domain covers in the Spike sequence (middle). The S1 domain contains the N-terminal domain (NTD, orange) and the receptor binding domain (RBD, red), which span amino acids 19-305 and 319-541 in Spike, respectively (right). **(B)** Schematic of SARS-CoV-2 virion, including examples to represent variants that have emerged independently throughout the course of the pandemic. This includes the ancestral D614 and D614G/B.1 lineages, as well as variants assigned by the UK Health Security Agency (UKHSA) termed "variants of concern" (VOC; Alpha/B.1.1.7), Beta/B.1.351, Gamma/P.1, Delta/B.1.617.2/ and Omicron/BA.1/BA.2 etc.), "variants under investigation" (VUI; Lambda/C.37, Mu/B.1.612, B.1.1.318) or "variants under monitoring" (VUM; Iota/B.1.526, C.1.2) depending on the increased risk to global health, to prioritise the monitoring, research and response to the pandemic. Image was created using BioRender.

Owing to my expertise in virus pseudotyping, I was asked to help with assessing the humoral response to infection in difference animal models following immunisation with COVID-19 vaccines. Throughout the COVID-19 pandemic I examined the nAb responses using lentiviral pseudotypes using sera from mouse, pig, ferret, hamster and non-human primate animal models used to investigate the immunogenicity of the Vaxzervia™ vaccine. I also examined the capacity of a next generation COVID-19 vaccines (Oxford-AstraZeneca) expressing the Beta Spike (ADZ2816) in a mouse model (led by Dr Alexandra Spencer and Prof Teresa Lambe, University of Oxford) to neutralise variant Spikes, and in a larger pig model (pig studies led by Prof Simon Graham, The Pirbright Institute), where I could further examine the role individual mutations in the Spike proteins play in the neutralising response. Demonstrating a robust, durable and safe immune response in an appropriate animal model before a vaccine is taken to clinical trial is essential when developing a human vaccine.

I further examined the neutralising ability of sera from individuals vaccinated and boosted with the BioNTech/Pfizer BNT162b2 vaccine against different variants in pseudovirus-based neutralisation assays (in collaboration with Dr Kevin Brown and Gayatri Amirthalingam, UKHSA). I also examined the genetic determinants of immune escape in the Spike proteins of SARS-CoV-2 variants. These studies will help us to understand the breadth of immunity generated by current COVID-19 vaccines against the circulating VOCs and help to inform when new vaccines were needed and how they should be designed for other viruses with pandemic potential.

Most of the data outlined in this chapter have been published in several research articles [49, 240-243] and I can confirm that I am listed as co-first, or co-author for these publications. Where I am listed as co-first author, I can confirm I conducted the majority of the experiments described and performed the data analysis. Where I am listed as a co-author, I have included only experiments where I produced the data and have performed my own separate analyses and drawn independent conclusions. Where experiments were conducted by others, this has been indicated in the results, and included with permission of the author.

3.2 Results

3.2.1 Evaluation of neutralising antibody responses against WT SARS-CoV-2 in animal immunised with the ChAdOx-1 nCoV-19 (AZD1222) vaccine

In response to the COVID-19 pandemic, multiple candidate vaccines were developed to manage disease symptoms, including the chimpanzee adenovirus 1 (ChAdxOx-1) nCoV-19 (AZD1222) vaccine, which was tested in several animal models to demonstrate vaccine efficacy and safety, running in parallel to human clinical trials. These included mouse, pig, ferret and non-human primate models. In a preliminary animal study, inbred BALB/c and outbred CD1 mice aged 9-10 weeks of age were immunised by intramuscular (i.m.) injection of 10^8 infectious units (i.u.) of AZD1222 or ChAdOx-1-GFP in a prime-boost regime, where animals were boosted on day 0 and day 28 (study led by Prof Teresa Lambe and Dr Alexandra Spencer, University of Oxford, Project License P9808B4F1). Serum samples were taken 3-weeks after booster vaccination on day 49 which were analysed for nAb responses using pseudoviruses bearing the WT-Spike protein – the Spike variant encoded by the vaccine. Both BALB/c and Cd1 mice immunised with the AZD1222 vaccine showed robust and similar nAb responses against WT SARS-CoV-2, with no nAb response detected in ChAdOx-1-GFP immunised animals, indicative of an antigen-specific immune response (**Figure 3.2A**).

Separately, pigs aged 8-10 weeks old were immunised by i.m injection with 10^9 i.u. AZD1222 in a prime-only or prime-boost vaccination regime, with animals boosted on day 28 following the initial immunisation (study led by Prof Simon Graham, The Pirbright Institute, Project License PP1804248). Serum samples were obtained weekly until 42 days post immunisation to analyse nAb responses. Serum samples were assessed in pseudovirus neutralisation assays (conducted with support from Dr Carina Conceição, The Pirbright Institute; data adapted from [240]). In both the prime-only and prime-boost groups, an increase in nAb titre was observed from day 0 until day 14, where the Ab response peaked then began to wane by day 21 (**Figure 3.2B**). In the prime-only group, the nAb response continued to wane until day 42, whereas the prime-boost group showed a maintained, but non-boosted nAb response against WT SARS-CoV-2 pseudovirus, that was significantly greater than the prime-only group at days 35 and 42 post immunisation ($p<0.01$) (**Figure 3.2B**).

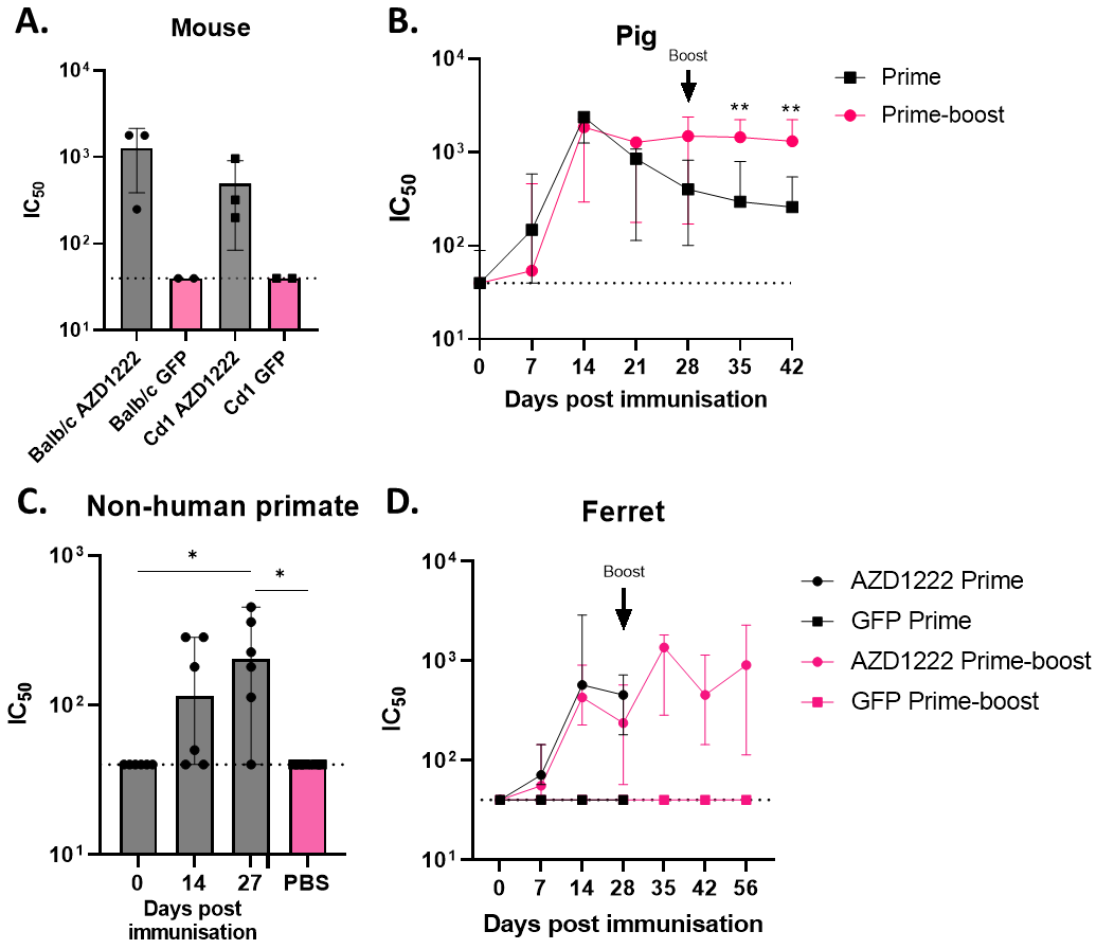

Figure 3.2: Vaccine studies to assess the immunogenicity of ChAdOx-1 nCoV-19 AZD1222 in animal models. (Adapted from Lambe T. et al., *Commun Biol* 2021 and Graham SP et al., *npj Vaccines* 2020). **(A)** 9-10-week-old inbred female BALB/cOlaHsd (BALB/c, circles) and outbred Crl:CD1 (CD1, squares) mice (Envigo and Charles River Laboratories, respectively) were immunised intramuscularly (i.m.) with 10^8 infectious units (iu) ChAdOx-1 nCoV-19 (AZD1222, black) or 10^8 iu ChAdOx-1-GFP vector control (pink) (n=3 AZD1222, n=2 ChAdOx-1-GFP for each group) under a prime-boost regime (boosted day 28) and serum samples taken on day 49 post-immunisation. **(B)** Six 8-10-week-old female Large White-Landrace Hampshire cross-bred pigs were immunised under a prime-only (n=3, black square) or prime-boost (n=3, pink circle) vaccination regime with i.m. immunisation of 10^9 iu AZD1222, boosted at day 28. Serum samples were taken weekly until day 42. A Student's *t*-Test was conducted to compared neutralising antibody titres between prime-only and prime-boost groups (** $p<0.01$). **(C)** Six non-human primates (rhesus macaques) received a single dose of $2.5x10^{10}$ virus particles (vp) AZD1222 i.m. (black circle) or phosphate-buffered saline (PBS) i.m. (pink square). Serum samples were taken every two-weeks for the AZD1222-immunised group and at day 14 only for the control group. A one-way ANOVA was conducted to compared differences in neutralising antibody titre at each time-point and between the AZD1222 and PBS-immunised groups (* $p<0.05$). **(D)** Twelve ferrets were immunised with $2.5x10^{10}$ vp of AZD1222 or ChAdOx-1-GFP i.m. After 28 days, half of the animals in each group (n=6) were boosted with an equivalent vaccine/control dose. Serum samples were taken weekly until day 56. Error bars represent median ± range. For bar graphs, each dot represents a single animal, and for line graphs, each dot represents the median in neutralising antibody titre. Neutralisation assays were conducted using lentiviral-based pseudoviruses bearing the WT SARS-CoV-2 Spike protein and titres were calculated by interpolating the point at which there was a 50% reduction in luciferase activity (IC_{50}). Dotted lines indicate the limit of detection.

Prior to advancing a vaccine to clinical trials, it is important to validate the vaccine in a larger animal closely related to humans, for example the non-human primate model. It is also desirable to show a reduction in disease severity and/or protection from infection with a single vaccine dose. Therefore, six adult rhesus macaques (three male, three female) were immunised i.m. with a single dose of $2.5x10^{10}$ virus particles (vp) of AZD1222, with an

equivalent group receiving phosphate-buffered saline (PBS) as a control (study led by Prof Teresa Lambe and Prof Sarah Gilbert, University of Oxford, data adapted from [241]). Serum samples were obtained at days 0, 14 and 27 post-immunisation for the AZD1222-immunised groups, and at day 14 for the control group. A significant increase in nAb titre was detected in these animals by day 27 and compared to the control group, for which there was no detectable nAb response ($p<0.05$) (**Figure 3.2C**).

Immunogenicity was further assessed in the ferret model, which was previously used as a model to study SARS-CoV-1 pathology and vaccine efficacy [244-246]. Ferrets were immunised with a single dose of $2.5x10^{10}$ vp of AZD1222 or an equivalent dose of ChAdOx-1-GFP and half of the animals in each group (n=6) were boosted 28 days post immunisation with a second vaccine dose (study led by Prof Teresa Lambe and Prof Sarah Gilbert, University of Oxford). Weekly serum samples were taken from ferrets until day 28 post-immunisation in the prime-only groups and until day 56 in prime-boost groups and were tested in pseudovirus-based neutralisation assays against WT SARS-CoV-2 (conducted with support from Dr Carina Conceição, The Pirbright Institute; data adapted from [241]). A significant increase in nAb response was detected 14 days post-immunisation in AZD1222 vaccinated animals, which increased in the AZD1222 prime-boost vaccinated group. As serum samples were not obtained for the prime-only group after day 28, comparison of a prime-only versus prime-boost vaccination schedule could not be conducted in this study. The control ChAdOx-1-GFP immunised groups did not exhibit any nAb reponses after one or two doses (**Figure 3.2D**). Examining safety, immunogenicity and/or efficacy of the AZD1222 vaccine in several animal models supported data produced in a separate phase 1/2 safety and immunogenicity trial with ChAdOx nCoV-19, which was eventually licensed as Vaxzervia™ [90]. However, as new SARS-CoV-2 variants emerged, there was evidence of reduced neutralising antibody responses against these variants with the licensed vaccine. As a result, vaccines with updated Spike antigens were developed and tested for their effectiveness against emerging variants.

3.2.2 Assessing the neutralising antibody response against SARS-CoV-2 variants using sera from mice immunised with ChAdOx1-vectored WT (AZD1222) or Beta (AZD2816) Spike vaccines.

Many of the SARS-CoV-2 VOCs express mutations within the Spike protein that result in a reduced ability of antibodies from people with pre-existing immunity or vaccination to neutralise these variants, which was first observed with the Beta variant (Pango Lineage B.1.351) which emerged in South Africa in December 2020 [247]. Therefore, in May 2021, sera from mice that had been immunised using a new ChAdOx1 vector vaccine harbouring a Beta Spike as the target immunogen (AZD2816, ChAdOx1 nCoV-19 B.1.351) was

examined (all mouse studies were led by Dr Alexandra Spencer and Prof Teresa Lambe, The University of Oxford). This vaccine was generated expressing key mutations in the Spike equivalent to the Beta VOC (**Table 1**) as described previously for AZD1222 (ChAdOx1 nCoV-19) [90]. BALB/c mice were immunised under different prime-boost regimens to mimic vaccination schedules that would be likely in the human population where individuals would have already received one or two doses of AZD1222, so we wanted to understand the benefit of boosting with the AZD2816 vaccine compared to AZD1222 (**Figure 3.3A**). Groups of mice were initially immunised with 10^8 iu of AZD1222 and then boosted 4 weeks later with 10^8 iu of AZD2186, or, not boosted. Mice were then sacrificed 3 weeks later, from which sera was obtained for use in pseudovirus-based neutralisation assays. One dose of AZD1222 against WT SARS-CoV-2 showed moderately low nAb responses, which were significantly higher with the two-dose regimen ($p<0.05$) (**Figure 3.3B, left**). The nAb responses of this sera against the Beta and Delta VOCs was also measured, which were below the limit of detection with one dose of AZD1222, but considerably higher in the two-dose regimen with AZD1222 and AZD2816 ($p<0.0001$) (**Figure 3.3B, middle and right).**

Next, the immunogenicity of BALB/c mice that had received a homologous AZD122 two dose regimen (10^8 i.u .each) 4 weeks apart was assessed, with a third dose of 10^8 i.u. AZD2816 4 weeks later or no booster; animals were sacrificed after 3 weeks to obtain sera. Neutralising antibody responses were detected in all vaccine groups against WT SARS-CoV-2 and Beta, but below the limit of detection against Delta (Spike constructs for Beta and Delta were generated by Dr Thomas Peacock, Imperial College London). Neutralisation titres were higher against the VOCs observed in animals boosted with AZD2816 in the three-dose regimen ($p<0.05$ for Beta and Delta) (**Figure 3.3C**). Finally, comparison of the neutralisation titres of BALB/c mice boosted with either 10^8 iu of AZD122 or AZD2816 following a homologous prime-boost with two doses of 10^8 iu AZD1222 was conducted to compare a homologous versus heterologous booster vaccination, as many individuals at this time would have already received at least two doses of AZD1222. Neutralisation assays were conducted using WT SARS-CoV-2, Beta and Delta lentiviral pseudoparticles as before and the nAb titres were marginally increased after boosting with AZD2186 against WT SARS-CoV-2, Beta and Delta, although titres were generally lower against Delta with both vaccine regimes **(Figure 3.3D)**. Overall, the data shows that a homologous boost with AZD1222 and then a heterologous booster vaccination with AZD2816 can further enhance antibody responses against WT SARS-CoV-2 and cross-neutralise other SARS-CoV-2 variants.

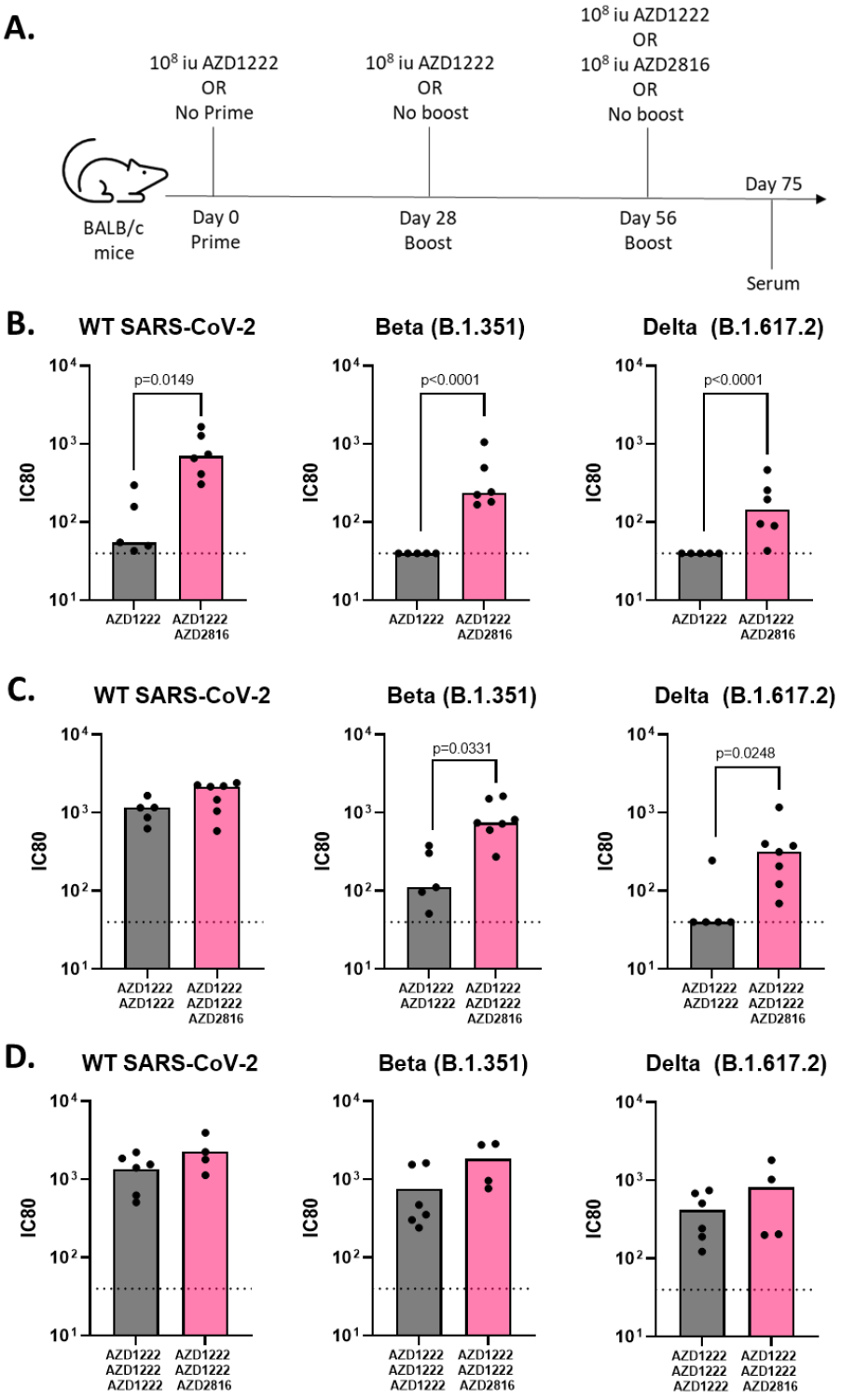

Figure 3.3: Immune response is boosted in mice by immunisation with three vaccine doses. (Adapted from Spencer A et al., *EBioMedicine* 2022).
(A) A schematic of the different immunisation schedules that were employed. BALB/c mice were immunised under different prime-boost regimes every 4 weeks and were then sacrificed 3 weeks later, and serum antibody responses measured. **(B-D)** The titre at which 80% neutralisation of virus is seen (IC80) is shown where sera from immunised mice were tested against pseudotyped viruses expressing G614D, Beta (B.1.351), Delta (B.1.617.2). Immunisation regimes included: **(B)** a single dose of 10^8 iu of AZD122 (ChAdOx1 nCoV-19) boosted 4 week later with 10^8 iu of AZD2816 (ChAdOx1 nCoV-19 B.1.351) or not boosted; **(C)** mice were boosted with 10^8 iu AZD122 and then again with 10^8 iu AZD2816 4 weeks apart (n=7) or did not receive a final boost (n=5); **(D)** Mice vaccinated with two doses of 10^8 iu of AZD1222, then boosted with 10^8 iu AZD1222 or AZD2816 (n=6). The lower limit of the assay is shown (dotted line). Data are represented as individual points per mouse with the bar indicating the median, and were analysed using an unpaired *t*-test, with significance between groups ($p<0.05$) indicated.

3.2.3 Immunisation of pigs with SARS-CoV-2 variant-based ChAdOx-1 vectored vaccines and determining key residues in Spike that result in immune evasion.

Next, the immunogenicity of AZD1222 and AZD2816 were examined in a pig model (led by Prof Simon Graham. The Pirbright Institute, data adapted from [240]). These two vaccines were tested under a homologous prime-boost regimen with different vaccination schedules. For AZD1222, three pigs were immunised with 10^9 iu vaccine at day 0 then boosted at day 28, with serum samples taken every week until day 56 where animals were sacrificed. The second experiment was conducted on a smaller scale, with the primary aim of generating positive AZD2186 sera for use in downstream assays. Three pigs were immunised with 10^9 iu AZD2816 at day 0, boosted at day 23 with AZD2816, then sacrificed at day 37, with serum samples being taken only at these time-points (**Figure 3.4A**).

Sera were selected at similar time-points (day 0, 21 and 35 from AZD1222 immunised pigs; day 0, 23 and 37 from AZD2816 immunised pigs) to test in neutralisation assays against the Spike variants used to generate the vaccines (WT SARS-CoV-2 and Beta) and against Delta, which showed the lowest nAb titres in mice (**Figure 3.3**). Beta and Delta were of particular interest as both VOCs exhibiting the greatest immune escape in the human population following their emergence, first detected in December 2020 in South Africa and in October 2020 India (Delta arose in the UK in March 2021), respectively [247, 248]. Under both vaccination regimens, neutralisation titres were below the limit of detection at day 0, as expected, but surprisingly also after a single immunisation (**Figure 3.4B-D**). However, after a second dose of AZD1222, there was a considerably large increase in nAb titre against WT SARS-CoV-2, which was comparable with those pigs immunised with AZD2816 ($p<0.05$) (**Figure 3.4B, 3.4E**). Pigs immunised with two doses of AZD2186 exhibited higher nAb titres against the Beta VOC, which were also greater than titres against WT SARS-CoV-2 (**Figure 3.4C, 3.4E**). Testing the sera against Delta, immunised pigs exhibited higher, but comparably lower nAb titres after two doses of AZD1222 or AZD2186 than against WT SARS-CoV-2 or Beta (**Figure 3.4D**).

It was also investigated whether the AZD2186 vaccine could cross-neutralise a Spike that harboured key mutations in Spike that have been suggested to be important for immune escape, D614G, N501Y and E484K (Alpha + E484K) – three of the mutations present in the Beta Spike. This mutant exhibited comparable nAb responses to what was observed against Beta in both vaccine groups (**Figure 3.4E**), suggesting that immunisation with the AZD2816 vaccine containing the N501Y/E484K change (Alpha + E484K) would be sufficient to induce high antibody titre responses in other variants that carry the same mutations, limiting the amount of booster vaccines required.

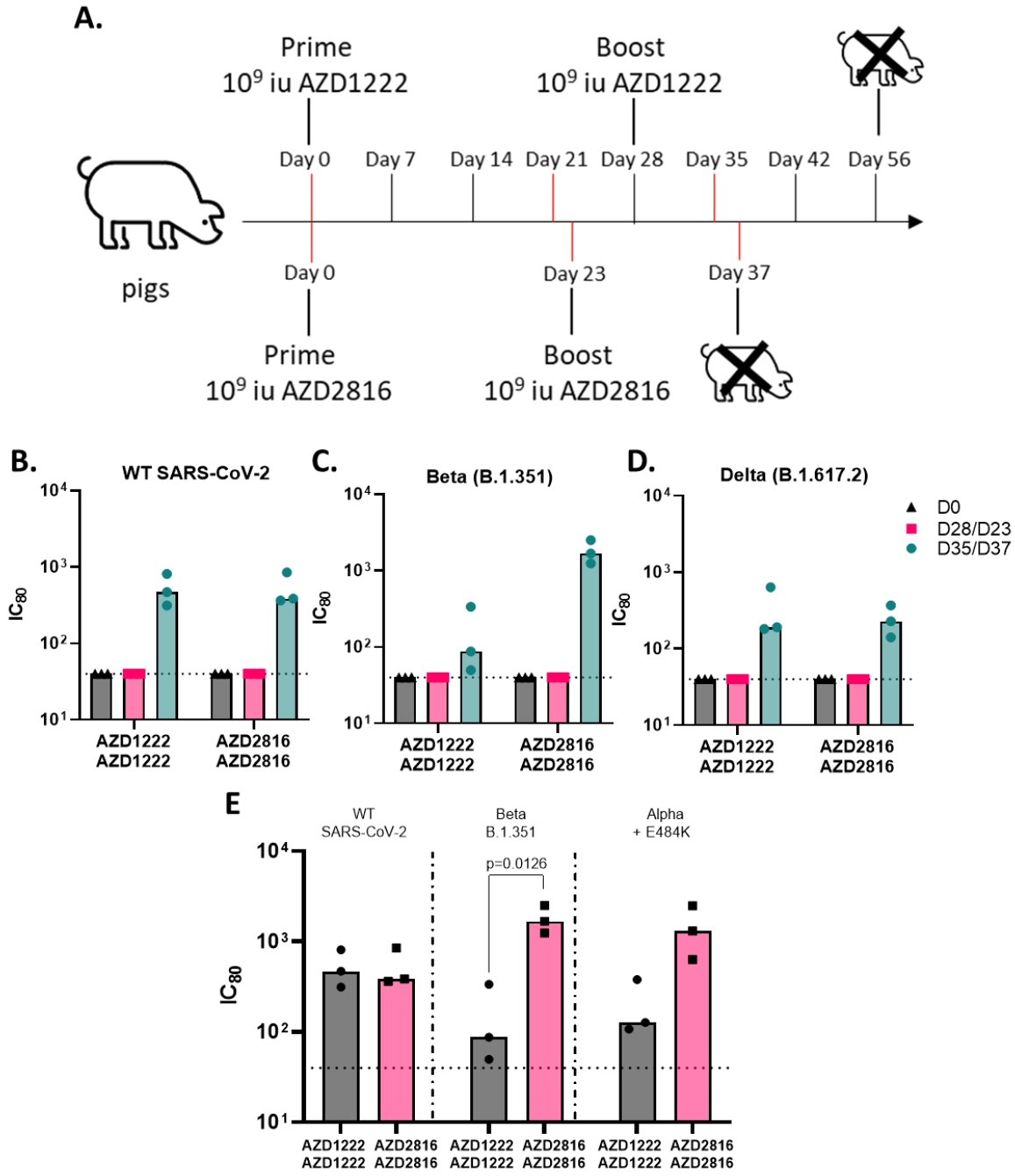

Figure 3.4: Immune responses are boosted in pigs immunised with AZD1222 or AZD2816 (Adapted from Graham SP et al., *npj Vaccines* 2020)

(A) A schematic of the different immunisation schedules that were employed. Three pigs were immunised under a homologous prime-boost regime with 10^9 IU of AZD1222 or AZD2816. Pigs were vaccinated with AZD1222 at day 0 and day 28, with serum samples taken weekly until day 56 where animals were sacrificed. AZD2186 vaccinated pigs were immunised at day 0, boosted at day 23 and culled at day 37, with serum samples being taken at these time-points. Sample timepoints that were assessed in neutralisation assays are indicated (red lines). Sera from immunised pigs were tested against pseudotyped viruses expressing **(B)** WT SARS-CoV-2 (vaccine variant, Vac), **(C)** Beta (B.1.351), **(D)** Delta (B.1.617.2) or **(E)** Alpha (B.1.1.7) with the D614G and an additional E484K mutation. The titre at which 80% neutralisation of virus is seen (IC_{80}) is shown. The lower limit of the assay is shown (dotted line). Data are represented as individual points per pig with the bar indicating the median, and were analysed using unpaired *t*-tests, with significance between groups ($p<0.05$) indicated.

3.2.4 Immunisation of hamsters with SARS-CoV-2 variant-based ChAdOx-1 vectored vaccines and assessing the antigenicity of key mutations in the SARS-CoV-2 RBD.

Recovery of Beta-specific nAb responses was observed in both mouse (**Figure 3.3**) and pig (**Figure 3.4**) immunogenicity studies in animals that had been primed with a vaccine containing the WT SARS-CoV-2 Spike as the target antigen (AZD1222) and boosted with a WT-SARS-CoV-2 (AZD1222) or Beta (AZD2816) Spike containing vaccine. However, at this point in late 2021, a large portion of the world's population were still unvaccinated or had only received one vaccine dose, particularly in lower-income countries [243]. Therefore, it was assessed whether a single or booster vaccination with AZD2816 would be preferential to distribute worldwide in place of AZD1222. This vaccination regime was tested in a hamster model, where animals were subsequently infected with either Beta or Delta virus as part of the same study (data not shown), as the hamster was established as an appropriate model to support SARS-CoV-2 infection, whilst mice do not support SARS-CoV-2 entry [249]. Eight 4-6-week-old Syrian Hamsters were immunised with either a single dose of $2.5x10^8$ i.u. AZD2186 (prime-only) or primed with $2.5x10^8$ i.u. AZD1222 and boosted with an equivalent dose of AZD2816 (prime-boost) (study led by Dr Neeltje van Doremalen and Dr Vincent Munster, National Institutes of Health, USA) (**Figure 3.5A**). Serum samples were collected 56 days after immunisation in the prime-boost group and after 28 days in the prime-only group for analysis in neutralisation assays with pseudoviruses bearing SARS-CoV-2 variant Spikes (conducted with the support of Dr Joseph Newman, The Pirbright Institute, data adapted from [243]). High nAb responses were detected against WT SARS-CoV-2, Beta and Delta in the prime-only group, that were marginally elevated in the prime-boost group against WT SARS-CoV-2 and Beta, but significantly greater against Delta ($p<0.05$); nAb titres were comparably low against Omicron BA.1 in both vaccine groups (**Figure 3.5B**).

The effect of single amino acid mutations in the Spike RBD present in the Beta, Delta and Omicron BA.1 variants: K417N, N501Y (present in Beta and Omicron BA.1), E484K (present in Beta, E484A in Omicron BA.1) and L452R (present in Delta) was also assessed. The presence of the L452R mutation recapitulated what was observed with the Delta Spike, and higher titres were observed against the E484K mutant in both vaccine groups (**Figure 3.5C**). The K417N and N501Y mutations showed increased neutralising antibody titres in the prime-boost group (**Figure 3.5C**). These data suggest a vaccine containing the Beta Spike is sufficient to induce robust immune responses against WT-SARS-CoV-2, Beta and Delta, but not against more antigenically distant variants, and a prime-boost response does not significantly increase neutralisation.

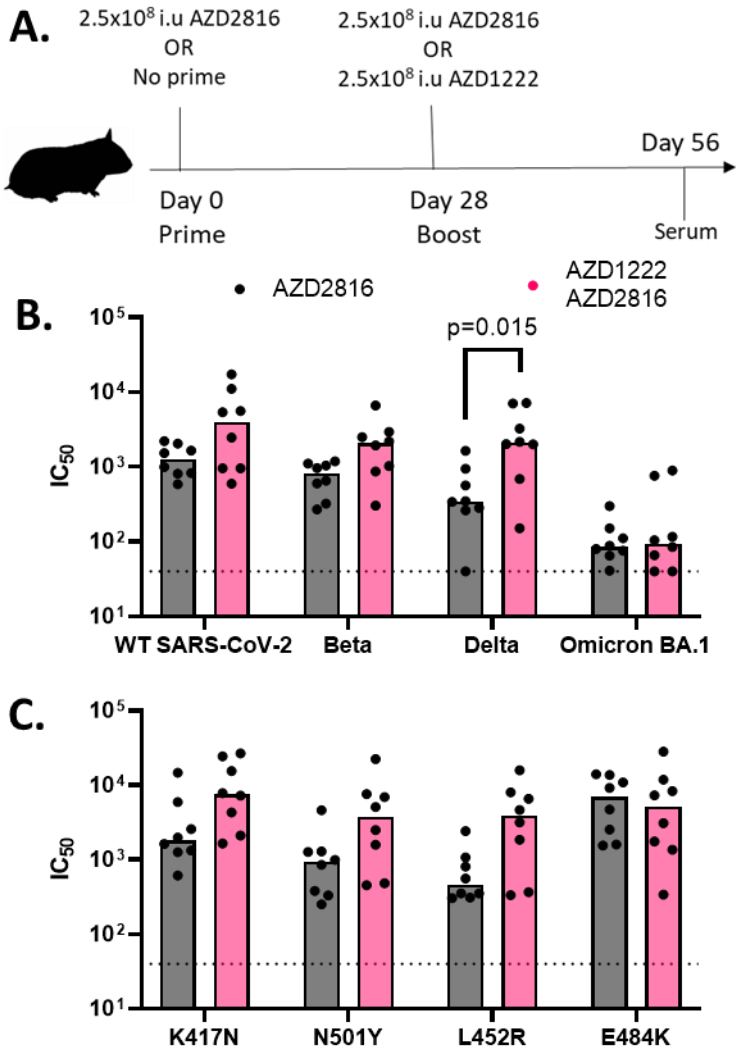

Figure 3.5: Immunisation with AZD1222 and AZD2816 vaccines in hamsters under prime-only and prime-boost regimes induce different levels of neutralisation. (Adapted from van Doremalen N et al., *Nature Comms* 2022).
(A) A schematic of the different immunisation schedules that were employed. Eight 4-to-6-week-old Syrian Hamsters were immunised under a prime-only or a prime-boost regime with 2.5x10^8 vp of AZD1222 or AZD2816. Hamsters were boosted 28 days after prime and serum samples taken at day 56. Sera from immunised hamsters were tested against pseudotyped viruses expressing **(B)** WT SARS-CoV-2, Beta (B.1.351), Delta (B.1.617.2), Omicron BA.1 variant Spikes or **(C)** mutant Spikes containing the K417N, N501Y, L452R or E484K change in Spike. The titre at which 50% neutralisation of virus is seen (IC_{50}) is shown. The limit of detection of the assay is shown (dotted line). Data are represented as individual points per animal and bars indicate the median, and were analysed using unpaired *t*-tests ($p<0.05$).

3.2.5 Analysis of human sera from trial participants vaccinated with COVID-19 vaccines following short- or long- interval prime-boost vaccination.

Initially in the UK, the mRNA-based Comirnaty® vaccine first and second dose vaccines were administered to many clinically vulnerable individuals, including older adults, with a short dosing interval 3-weeks apart. Faced with limited supplies of these vaccines, the UK then altered this schedule to maximise the number of people getting a single vaccination, with the intention to protect as many people as possible from developing serious disease. Accordingly, in the UK, vaccines were then administered up to 12-weeks apart for both

Comirnaty® and Vaxzervria™ due to evidence that a longer dosing interval would provide longer lasting immunity [90]. To understand the antigenicity of SARS-CoV-2 and SARS-CoV-2 variants, longitudinal analyses were performed of the nAb response in individuals following immunisation with COVID-19 vaccines using sera from a cohort of healthy older adults aged 50-90 years in January 2021 as part of the CONSENSUS study (led by Dr Kevin Brown, Dr Gayatri Amirthalingam and, Yung-Wai Chan, UKHSA). These individuals received either the mRNA-based BioNTech/Pfizer BNT162b2, Comirnaty® or the viral-vectored Oxford-AstraZeneca ADZ1222, Vaxzervria™ vaccine expressing the SARS-CoV-2 WT Spike protein as their first two doses.

As new SARS-CoV-2 variants emerged, the individuals in this cohort received booster vaccinations every Autumn and Spring from 2021 - 2023, receiving a homologous third booster, the Comirnaty® vaccine as their fourth booster, followed by vaccines with updated Spike antigens for subsequent boosters to overcome the immune escape that was being observed, particularly with Omicron subvariants. I contributed to efforts in the UK to monitor SARS-CoV-2 variants as they emerged to assess for vaccine effectiveness and immune escape, producing data which was fed back to regulatory bodies such as the Joint Committee on Vaccination and Immunisation and UKHSA. This data contributed to decisions that were made on policies for pharmaceutical and non-pharmaceutical interventions for the UK population. The sera received from the CONSENSUS study was used as part of this horizon scanning effort and included sera at several timepoints pre- and post- booster vaccination, analysed in Spike-based pseudotype neutralisation assays for the assessment of nAb responses (**Figure 3.6**). All experiments were performed alongside Dr Joseph Newman (The Pirbright Institute). Data produced for the 50–59 and 80–89-year-old age groups were led by Dr Newman, and data produced for the 60–69 and 70–79-year-old age groups were led by myself; however data for these cohorts have been combined for interpretation of vaccine efficacy.

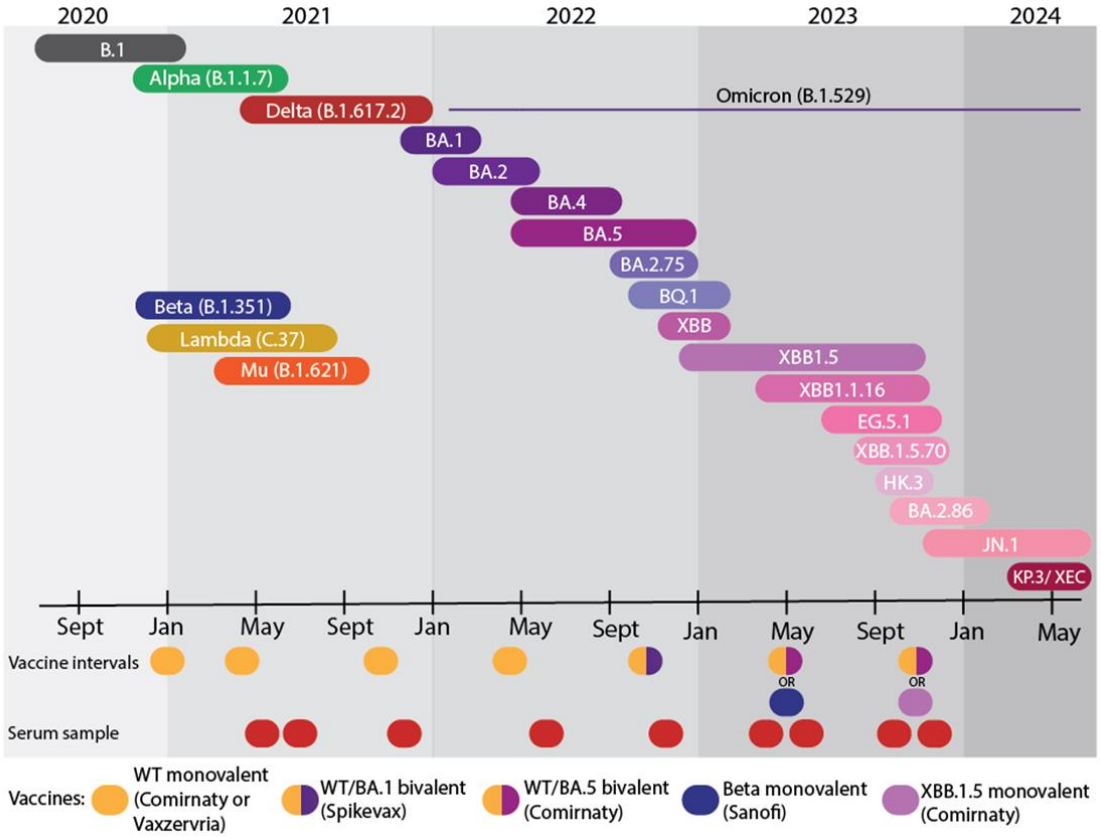

Figure 3.6: Emergence of SARS-CoV-2 variants over the course of the COVID-19 pandemic and vaccination schedule of individuals enrolled on the CONSENSUS trial.
Schematic of the timeline of the emergence of SARS-CoV-2 variants in the UK from September 2020 – May 2024, estimated based on sequence data deposited on https://covariants.org, depicted the month in which sequences first arose and ending when the variant was superseded by the next dominant circulating strain. The Beta (B.1.351), Lambda (C.37) and Mu (B.1.6.21) variants that were important in other parts of the world are also depicted. The CONSENSUS study is an audit of the antibody and T-cell responses in an older adult cohort in the UK, who received multiple doses of COVID-19 vaccines over the course of the pandemic, shown as coloured shapes with the colours depicting the vaccine strain. Individuals received their first two vaccines (WT Comirnaty™ or WT Vaxzervria©) either 3-weeks (short-interval) or up-to-12-weeks (long-interval) apart, then received booster vaccinations (third dose: homologous WT Comirnaty™ or Vaxzervria©; fourth dose: WT Comirnaty™; fifth dose: WT/BA.1 Spikevax™ bivalent; sixth dose: Sanofi Beta (VidPrevtyn®) or WT/BA.5 Comirnaty™; seventh dose: Comirnaty™ XBB.1.15 or WT/BA.5 bivalent) every Spring or Autumn. Serum samples were received pre- or post-vaccination and analysed in pseudotype-based neutralisation assays.

As part of horizon scanning efforts, the difference in nAb response was initially examined for these two vaccine regimes 3- and 20- weeks post-boost against the WT vaccine immunogen and the Delta (B.1.617.2) VOC, which was the dominant circulating variant in the UK in May 2021 (**Figure 3.6**). For the short interval group, the antibody response was examined of 37 individuals (age 70-79 *n*=13, age 80-89 *n*=24) and a median ND_{80} of 103.6 was observed at 3-weeks post vaccination, with a lower median titre observed for the older age group (70-79 age group median ND_{80}=129.1, 80-80 age group median ND_{80}=62.6) (**Figure 3.7A**). At 20-weeks post-second dose, waning of the nAb response was evident by 4.9x, with a significant decreased overall median ND_{80} of 21.3 (70-79 ND_{80}: 28.83, 80-89 ND_{80}: 16.0), with 8 of these individuals having no detectable nAb responses above the limit of detection in our assay (**Figure 3.7A**). The same sera was further examined against the

Delta Spike pseudotyped virus and a much lower median ND_{80} of 33.8 was noted at 3-weeks post-second dose (70-79 ND_{80}= 37.0, 80-89 ND_{80}= 12.4) (**Figure 3.7B**). As with the WT pseudotyped virus, a decrease in nAb titre was observed at 20-weeks post-second dose against the Delta Spike, with a fold change of 1.8x and reduced median ND_{80} of 19.6 (70-79 ND_{80}= 19.6, 80-89 ND_{80}= 12.5) (**Figure 3.7B**). The neutralisation titres remained high at both time points against both WT and Delta Spike for individuals who showed evidence of previous infection by SARS-CoV-2, calculated by the Roche N-ELISA (performed by Katja Hoschler, UKHSA) (**Figures 3.7A and B**).

Furthermore, comparison of the neutralisation against WT and Delta was carried out in individuals who received the extended-interval vaccination regime, analysing sera at similar timepoints as the short-interval vaccination group. Sera from 15 individuals was examined with ages ranging from 50-90 years old (age 50-59 *n*=2, age 60-69 *n*=8, age 70-79 *n*=4, age 80-89 *n*=1) who received two doses of either the Comirnaty™ or Vaxzervria© vaccine. A median ND_{80} titre of 66.9 was observed 3-weeks after vaccination with a 4.0x increase in median ND_{80} titre to 268.0 20-weeks post-2^{nd} dose against the WT Spike (**Figure 3.7C**). When comparing the two different vaccines administered, they elicited a comparable 4.4x increase in nAb response between 3- and 20-weeks post vaccination, indicating no advantage of one vaccine platform over the other (**Figure 3.7C**). Similar to the short-interval vaccinated group, at 3-weeks post-second dose, the extended-interval vaccinated group exhibited a lower nAb response against the Delta Spike (median ND_{80} 55.0 compared to WT) however, a 2.2x increase in median ND_{80} to 120.5 was observed 20-weeks post-second vaccination against the Delta Spike (**Figure 3.7D**). Previous infection did not appear to confer sustained higher nAb titres against WT and Delta Spike as was observed with the short interval vaccinated cohort (**Figure 3.7C and D**).

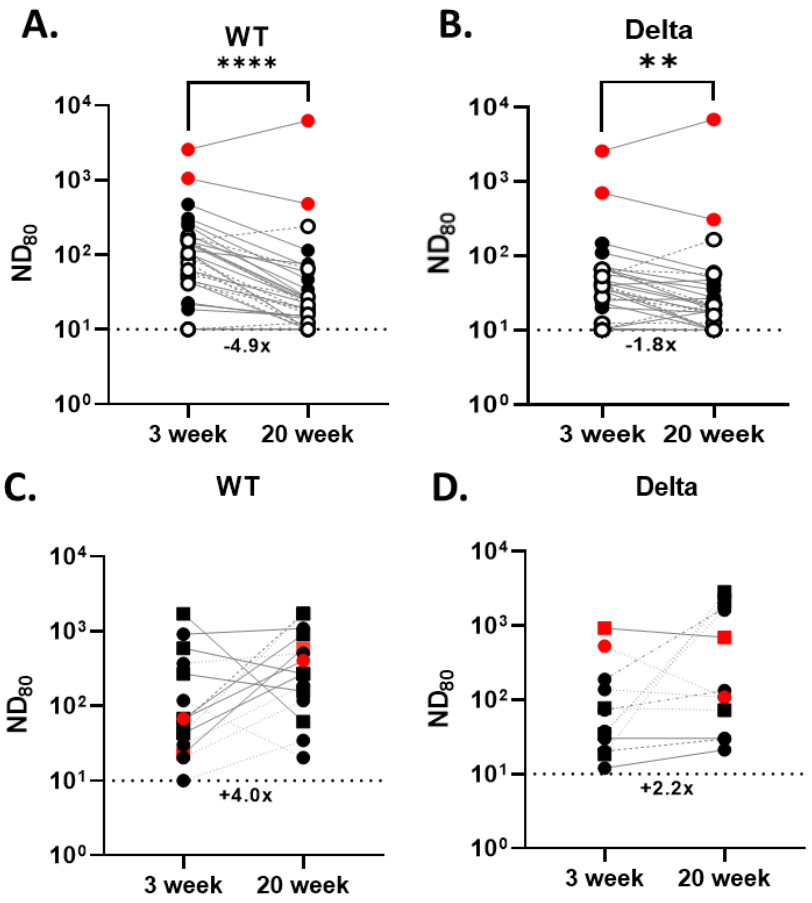

Figure 3.7: Neutralising antibody response generated following two doses of COVID-19 vaccination following a short-interval or extended-interval dosing regimen (adapted from Newman J, Thakur N et al., *Nat Microbiol* 2022).
Neutralisation titres calculated using pseudotypes bearing the **(A and C)** WT SARS-CoV-2 or **(B and D)** Delta Spike and sera from a cohort of individuals recruited as part of the UK CONSENSUS trial collected 3- and 20-weeks after second immunisation. **(A and B)** Comirnaty-vaccinated individuals aged 70–79 (*n* = 24, solid circles, solid line) or 80–89 (*n* = 13, open circles, dashed line), following immunisation with a short-interval vaccination regime of 3 weeks between first and second dose. **(C and D)** Comirnaty (*n* = 7, circle) or Vaxzervria (*n* = 8, square) immunised individuals aged 50-59 (*n* = 2, dot-dashed line), 60-69 (*8* = 2, dotted line), 70-79 (*n* = *4*, solid line) or 80-89 (*n* = 1, dashed line), following immunisation with an extended-interval vaccination regime up-to-12-weeks between first and second dose collected at 3 (*n* = 15 total) and 20 weeks (*n* = 12 total) after the second dose. Neutralisation titres were calculated by interpolating the point at which 80% reduction in luciferase activity was observed, related to no sera controls (ND_{80}). Statistical comparison of ND_{80} titres was performed using a Wilcoxon two-tailed matched-pairs signed rank test (**p < 0.01; ****p < 0.0001). Fold changes in median ND_{80} between 3 and 20 weeks are indicated. The detection limit of the assay is defined as a titre of 10 (dotted line). Convalescent sera are indicated in red, determined by N ELISA (Roche).

As new SARS-CoV-2 variants emerged, there was a concern of escape from vaccine-derived immunity, particularly in vulnerable cohorts such as older adults. Therefore, the same 3-week post second dose sera from the short-interval vaccinated group were used to investigate the neutralisation of SARS-CoV-2 variants with epidemiological relevance globally, including Alpha/B.1.1.7, Beta/B.1.351 and Delta/B.1.617.2 compared to the D614G-containing lineage B.1 pseudovirus responsible for the first wave of the pandemic. The median ND_{80} titre against B.1 observed was 193.7, slightly higher than what was calculated for the WT pseudovirus and a 1.3x increase in neutralisation was detected against the Alpha pseudovirus compared to B.1 (median ND_{80} 263.6), which is consistent

with published data showing robust neutralisation of Alpha in vaccinated individuals (**Figure 3.8A**) [48]. However, when analysing the nAb titres against Delta and Beta VOC Spikes, a 5.7x and 19.4x decrease in median titre was observed, respectively (Delta median ND_{80}=33.8; Beta median ND_{80}=10), with 24% of individuals against Delta and 73% of individuals against Beta exhibiting no detectable nAb response above the limit of detection (**Figure 3.8A**). A smaller subset of these sera (n=16) was also analysed with other VUIs that emerged in other parts of the world (Lambda/C.37, emerged November 2020 and Mu/B.1.621, emerged January 2021) or that arose much later after a second vaccine dose had been administered (Omicron BA.1 and BA.2, emerged in November 2021). A 1.2x increase in the median ND_{80} titre was observed against Lambda Spike, but a 3.0x decrease in titre against Mu compared to B.1 (Lambda median ND_{80}=167.55, Mu median ND_{80}=46.7); little to no antibody response was detected against BA.1 and BA.2 compared to B.1, with 32.5x decreases in median ND_{80} titre observed for both variants (BA.1 median ND_{80}=10.0, BA.2 median ND_{80}=10.0) (**Figures 3.8B and C**). It was noted that all individuals who were N-positive by ELISA sustained high nAb titres against all variants (**Figures 3.8A-C**).

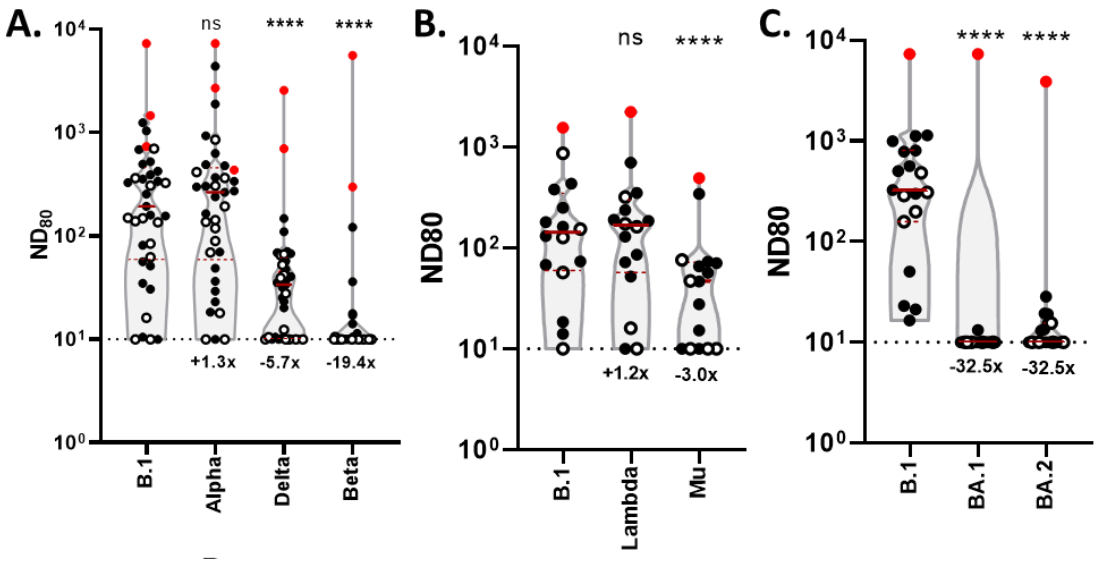

Figure 3.8: Neutralisation of SARS-CoV-2 VOCs and VUIs by sera from Comirnaty™-vaccinated individuals 3-weeks after second dose (adapted from Newman J, Thakur N et al., *Nat Microbiol* 2022).
Neutralization of pseudotypes bearing the SARS-CoV-2 **(A)** Alpha, Delta, Beta, **(B)** Lambda, Mu, or **(C)** BA.1, BA.2 Spike by sera (A: $n = 37$, B and C: $n = 16$ biologically independent samples) were compared in age-stratified cohorts: 70–79 years (A: $n = 24$, B and C: $n = 11$ solid circles) and 80–89 years (A:$n = 13$, B and C: $n = 5$ open circles). Statistical comparison of ND_{80} titres were performed using a Wilcoxon two-tailed matched-pairs signed rank test (****$p < 0.0001$; ns, not significant). Fold changes in median ND_{80} compared with B.1 are indicated (lower detection limit = 10 (dotted line). Medians are indicated with a solid line and upper and lower quartiles with dashed lines within the violin plots. Fold changes in median titre, compared with B.1 are indicated (lower detection limit = 100 (dotted line). Convalescent sera are indicated in red, as determined by N ELISA (Roche).

3.2.6 Assessing the effect of booster vaccinations in broadening the neutralising antibody response against SARS-CoV-2 Omicron subvariants.

The Omicron VOC emerged towards the end of 2021 and subsequent subvariants of Omicron have continued to emerge since. Over this period, individuals from the CONSENSUS trial received 4 more booster vaccinations in the Spring or Autumn of 2022 - 2023, and neutralisation assays were performed using sera post-boost to understand the breadth of immunity against the Omicron subvariants that were circulating at the same time (**Figure 3.6**). Individuals received a homologous boost of the Comirnaty™ or Vaxzervria© vaccines. An increase in nAb titres against Omicron was detected compared to post-second dose, where the antibody response was almost absent (**Figure 3.8B**). Compared to the homologous vaccine immunogen B.1 (median ND_{80}=2605.6), a significant decrease in median ND_{80} was observed against BA.1 (-11.7x, median ND_{80}=222.8), BA.2 (-9.3x, median ND_{80}=280.8) and BA.5 (-11.6x, median ND80=224.6), and all the samples showed neutralising titres above the limit of detection (**Figure 3.9A**). The BA.1, BA.2 and BA.5 variants contain several shared mutations in the RBD including E484A, K417N and N501Y that likely contribute to the reduced neutralising titres detected (highlighted in blue). BA.5 also contains the L452R mutation found in Delta, while BA.1 and BA.2 harbour the Q394R mutation (highlighted in red) however, these mutations do not appear to enhance immune escape (**Figure 3.9B**).

3.2.7 Assessment of sera from individuals receiving booster vaccinations with updated monovalent and bivalent Spiked-based COVID-19 vaccines.

Individuals in this cohort all received the Comirnaty™ vaccine as their fourth vaccine dose in Spring 2022 when BA.5 was the dominant circulating variant. The nAb responses were analysed against BA.5 pseudoviruses and Omicron subvariant pseudoviruses that later emerged, including BQ1.1, XBB, XBB1.5 and XBB1.16 (**Figure 3.6**). Compared to B.1 (median ND_{80}= 11911.3) a similar reduction in median nAb titre was observed against BA.5 (-10.4x, median ND_{80}=1147.6) after a fourth vaccine dose as was noted after a third vaccination, however the overall median titres were 1 log higher against both B.1 and BA.5 (**Figure 3.9C**). However, all the other Omicron subvariants analysed revealed large reductions in nAb response compared to the vaccine strain, despite the majority of these individuals being N-positive (BQ1.1 ND_{80}=207.9; XBB ND_{80}=139.0; XBB.1.5 ND_{80}=98.1; XBB.1.16 ND_{80}=83.7) (**Figure 3.9C**), but smaller decreases in median nAb titre were detected compared to BA.5, which was the preceding dominant variant (BQ.1.1: -5.5x, XBB: -8.3x, XBB.1.5: -11.7x, XBB.1.16: -13.7x) (**Figure 3.9C**). Most mutations in the RBD of Omicron subvariants were similar to those present in BA.5 (highlighted in blue), with a reversion at position 452 present in XBB, XBB.1.5 and XBB.1.16 (highlighted in orange), which could contribute to the more pronounced reduction in nAb titre compared to BQ.1.1,

which retains the L452R mutation (**Figure 3.9D**). The BQ.1.1 variant also harbours a K444T and N640K mutation, which could contribute to the decrease in neutralisation observed compared to BA.5, which is also present in the other subvariants (highlighted in red) (**Figure 3.9D**). Furthermore, XBB contains an additional Q493R mutation which is not present in the other variants, which may explain the difference in median ND_{80} observed for XBB compared to XBB.1.5. The mutations present in XBB.1.5 and XBB.1.16 RBDs are identical, so any differences in neutralisation may be attributed to mutations outside this region (**Figure 3.9D**).

In Autumn 2022, individuals in the CONSENSUS trial received a bivalent vaccine comprising the Moderna WT/BA.1 Spike (Spikevax™) as the target immunogens. The nAb response was analysed against the two homologously-matched vaccine Spikes along with Omicron subvariants that were circulating at the time (XBB, XBB.1.5, XBB.1.16 and XBB.1.5.70) (**Figure 3.6**). The nAb response against B.1 appeared saturated by a fifth vaccine dose (median ND_{80}=18124.1), likely attributed to the upper limit of detection of our assay. Inclusion of the BA.1 Spike in the vaccine formulation increased the overall nAb titre against the BA.1 pseudovirus, with only a -2.8x decrease in median ND_{80} compared to WT (median ND_{80}=6565.7) (**Figure 3.9 and E**). Similar to what was observed post-fourth dose, the nAb titres against the Omicron subvariants showed a large decrease compared to B.1 (XBB ND_{80}=234.2; XBB.1.5 ND_{80}=212.6; XBB.1.16 ND_{80}=461.3; XBB.1.5.70 ND_{80}=186.4), and to a lesser extent when compared against BA.1 (XBB: -28.0x, XBB.1.5: -30.9x, XBB.1.16: -14.2x, XBB.1.5.70: -35.2x), which is unsurprising giving that the nAb titres against BA.1 were lower than what was observed for B.1 (**Figure 3.9E**). When comparing the mutations present in the RBD of these variants to the BA.1 RBD, evidence of reversions at positions 394 and 496 were noted for XBB.1.15, XBB.1.16 and XBB.1.5.70 (highlighted in orange) which may contribute to the reduced nAb titres observed when compared to XBB (**Figure 3.9F**). The median nAb titres against XBB.1.16 were greater than XBB.1.5 despite both variants harbouring identical RBD mutations, suggesting that mutations outside the RBD may be important for the difference in neutralisation we are observing (**Figure 3.9E).** The XBB.1.5.70 variant also harbours a F456L mutation in the RBD, which could contribute to the scale of the immune escape seen when compared to the other subvariants (**Figure 3.9E**). Taken together, these data suggest that mutations in the RBD of SARS-CoV-2 variants contribute to a high degree of immune escape which can be overcome to a degree with booster vaccinations.

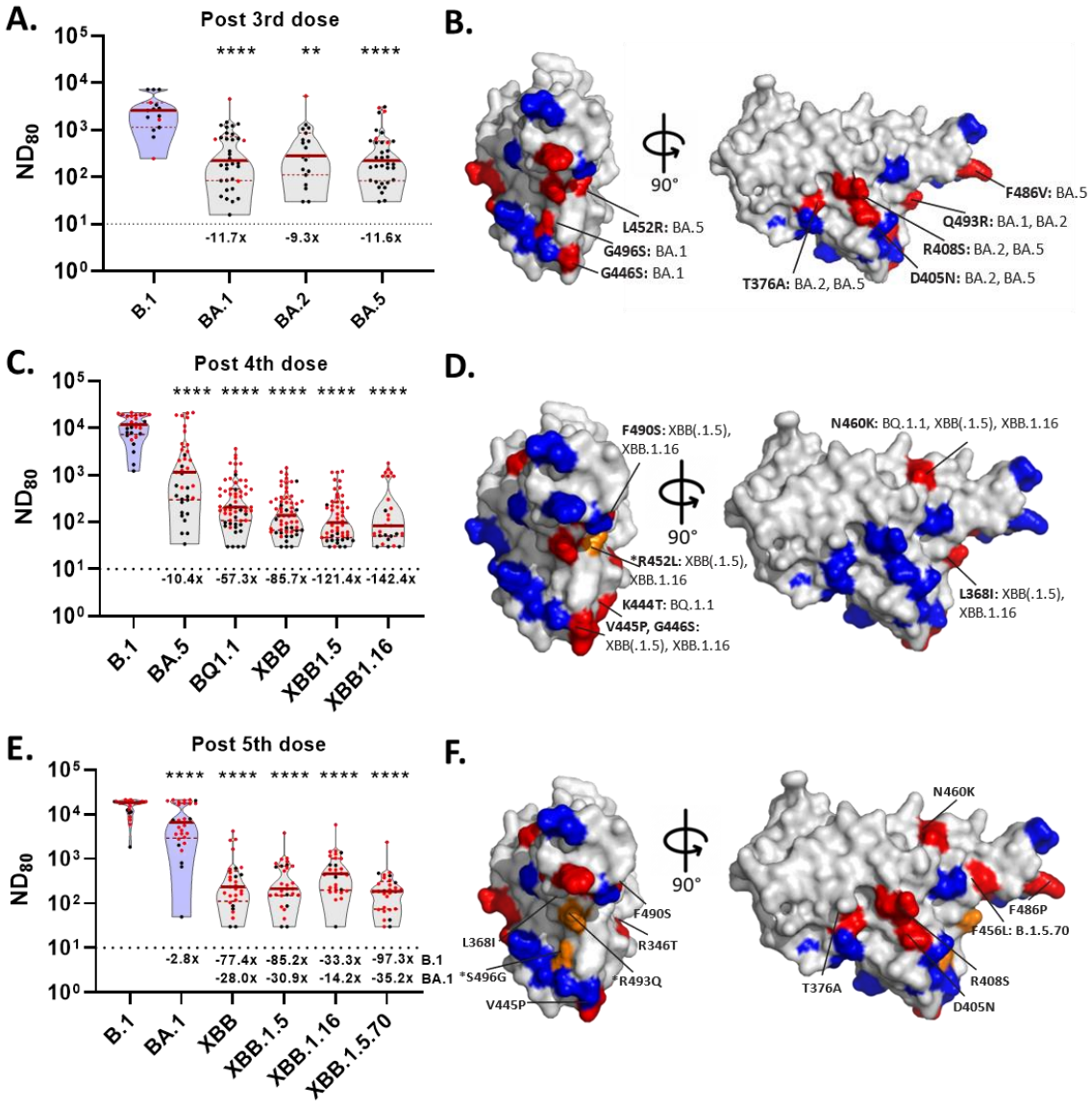

Figure 3.9: Longitudinal risk assessment of SARS-CoV-2 variants in an older adult population following several boost immunisations with COVID-19 vaccines.
Neutralisation of sera from individuals in the CONSENSUS trial following their **(A)** third (homologous Comirnaty™ or Vaxzervria© vaccine), **(C)** fourth (Comirnaty™) or **(E)** fifth (Spikevax WT/BA.1 bivalent) booster vaccination. Statistical comparison of ND_{80} titres were performed using a one-way ANOVA (****$p < 0.0001$; ** $p < 0.01$). Fold changes in median ND_{80} compared with B.1 or BA.1 are indicated (lower detection limit = 10 (dotted line). Medians are indicated with a solid line and upper and lower quartiles with dashed lines within the violin plots. Convalescent sera are indicated in red, as determined by N ELISA (Roche). (**B, D, F**) Molecular surface representation of the SARS-CoV-2 RBD (PDB 7UL0) generated in PyMOL in the "up" conformation, rotated 90° about the *x*-axis. Structures highlight matched (blue), differential (red) or revertant (orange) mutants relative to the comparator variant, with differential and revertant amino acid changes labelled. Comparison of (**B**) BA.1, BA.2 and BA.5 variant mutations relative to B.1; (**D**) BA.5, B.Q.1.1, XBB, XBB1.5 and XBB.1.16 variant mutations relative to B.1; and (**F**) XBB, XBB.1.5, XBB.1.16 and XBB.1.5.70 mutations relative to BA.1.

In Spring 2023, some individuals in this cohort were administered a sixth booster vaccination, receiving either the Sanofi VidPreventyn® Beta Spike vaccine or, the updated Comirnaty™ WT/BA.5 vaccine. Of note, only individuals in this vulnerable older adult cohort were in receipt of the VidPreventyn® monovalent vaccine in the UK. Serum samples pre- and post- boost were examined against the XBB.1.5 and BA.2.86 variant pseudotypes, representing the major variants circulating at the time. An increase in median ND_{80} against

all variants post-boost was noted with only small differences in response between the two different vaccine regimens. The bivalent Comirnaty™ vaccine yielded a 2.9x and 2.6x increase in mean ND_{80} titre, compared to a 2.1x and 2.3x increase with the VidPrevtyn® Beta monovalent against XBB.1.5 and BA.2.86 Spike, respectively (**Figure 3.10A and B**). Additionally, sera from immunisation with the VidPrevtyn® monovalent was analysed against E.G.5.1 Spike and the Comirnaty™ bivalent sera against XBB.1.16 Spike, and a 2.7x and 2.8x increase in nAb titres was noted, respectively (**Figure 3.10 A and B**). The RBD mutations present in the variants we tested that are also present in the vaccine immunogens were mapped out onto a WT SARS-CoV-2 RBD structure (blue = BA.5, green = Beta), and additional mutations in BA.2.86 were noted at positions 356, 403, 450, 481 and 483, and an L452W change (L452R in BA.5), which may have contributed to higher nAb titres detected post-boost (**Figure 3.10C**). The other mutations or the reversion at position 452 did not appear to have any significant impact on neutralisation (**Figure 3.10C**).

In Autumn 2023, some participants in the CONSENSUS study received either a Comirnaty™ XBB.1.5 monovalent or the Comirnaty™ WT/BA.5 bivalent as a seventh vaccine dose. Again, sera was analysed from before (pre-) and after (post-) this booster vaccination against Omicron subvariants circulating at that time, including E.G.5.1 and XBB.1.5.70, which arose prior to September 2023, and the BA.2.86 and JN.1 variants which emerged around the time the boosters were administered (**Figure 3.6**). Pre-boost, some of the individuals exhibited ND_{80} titres that were below the limit of detection for the assay against all Spike pseudotypes (monovalent: E.G.5.1 *n*=6, HK.3 *n*=8, BA.2.86 *n*=2, JN.1 *n*=4; bivalent: E.G.5.1 *n*=5, HK.3 *n*=7, BA.2.86 *n*=3, JN.1 *n*=6), which recovered post-boost (monovalent: E.G.5.1 *n*=2, HK.3 *n*=2, BA.2.86 *n*=1, JN.1 *n*=1; bivalent: E.G.5.1 *n*=3, HK.3 *n*=2, BA.2.86 *n*=0, JN.1 *n*=2), with similar fold changes observed with either the monovalent (E.G.5.1 +3.0x, HK.3 +2.3x, BA.2.86 2.5x, JN.1 +2.0x) or bivalent (E.G.5.1 +1.9x, HK.3 +2.0x, BA.2.86 +2.3x, JN.1 +1.7x) vaccines (**Figure 3.10D and E**). The ND_{80} titres against all Spikes appeared greater in individuals who were immunised with the Comirnaty™ XBB.1.5 monovalent vaccine compared to the Comirnaty™ WT/BA.5 bivalent vaccine (**Figure 3.10D and E**).

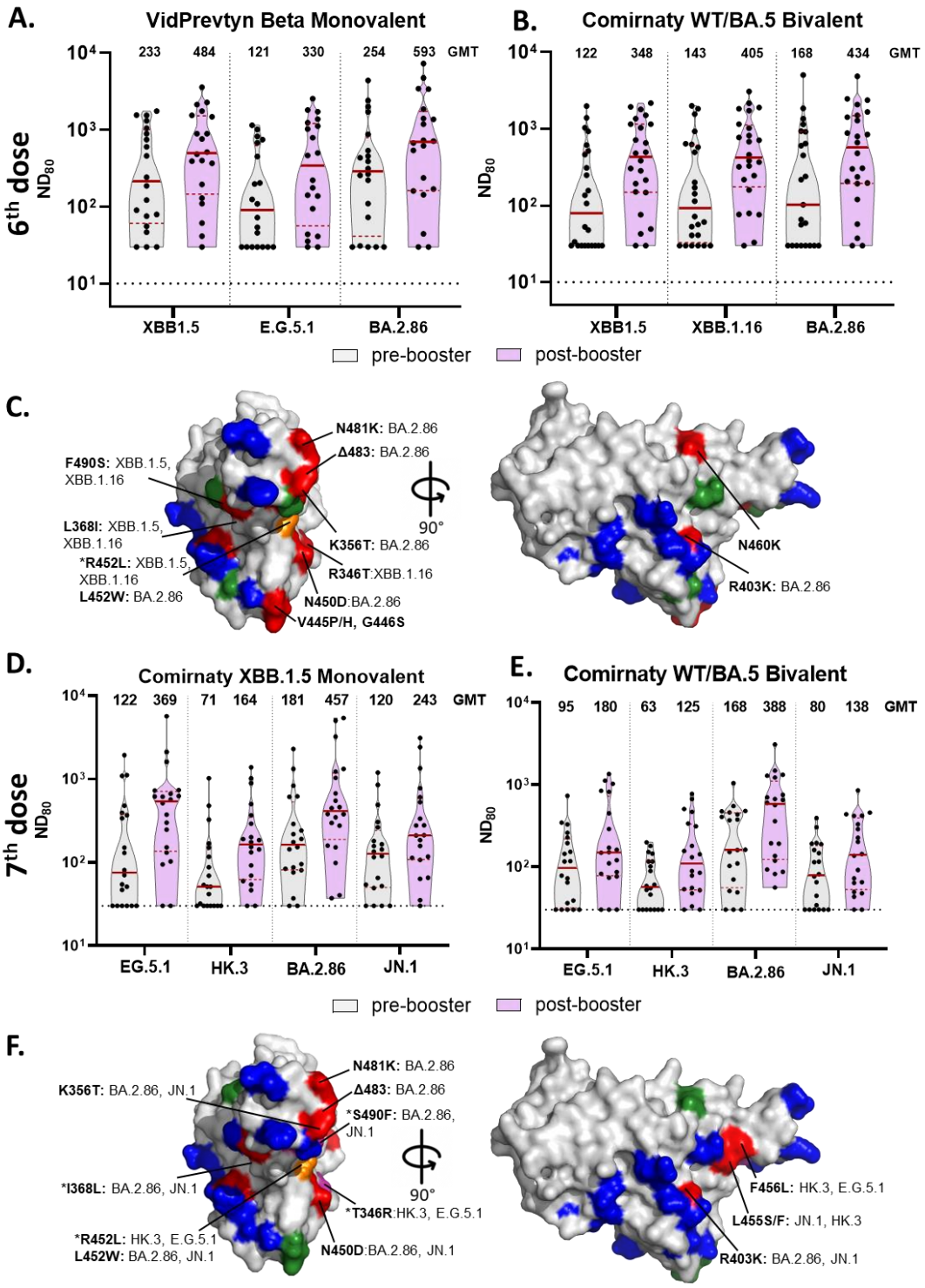

Figure 3.10: Analysis of SARS-CoV-2 Omicron subvariants following booster immunisations of COVID-19 vaccines with updated Spike immunogens.
Neutralisation of sera from individuals in the CONSENSUS trial following their **(A, B)** sixth or **(D,E)** seventh booster vaccination, pre- and post-vaccination. Geometric mean ND_{80} are shown for each sample group. (lower detection limit = 30 (dotted line). Medians are indicated with a solid line and upper and lower quartiles with dashed lines within the violin plots. Individuals were boosted with vaccines containing updated Spike immunogens: (**A**) Sanofi Beta VidPrevtyn ®, (**B,E**) Comirnaty™ WT/BA.5 bivalent or (**D**) Comirnaty™ XBB.1.5 monovalent, and tested against XBB.1.5, E.G.5.1, XBB1.16, BA.2.86, HK.3 or JN.1 Spike-pseudoviruses, as indicated. (**C,F**) Molecular surface representation of the SARS-CoV-2 RBD (PDB 7UL0) generated using PyMOL highlighting matched (blue compared to BA.5, green compared to (**C**) Beta or (**E**) XBB.1.5), differential (red) or revertant (orange compared to BA.5, pink compared to XBB.1.5) mutants relative to the comparator variant, with differential and revertant amino acid changes labelled.

This difference in neutralisation could potentially be attributed to the presence of key residues in XBB.1.5-based vaccine that overlap with substitutions found in E.G.5.1, HK.3, BA.2.86 and JN.1 (highlighted in green) (**Figure 3.10F**). Despite the presence of additional mutations in these variants, particularly BA.2.86 and JN.1 (red), and reversions at 452 compared to BA.5 (orange), or at positions 346, 368, 490 compared to XBB.1.5 (pink), mean nAb titres detected pre-and post-boost against all variants were similar (**Figure 3.10 D and E**), supporting the notion that the key mutations involved in immune modulation for these variants overlap with BA.5 (blue) and XBB.1.5 (green) e.g., N501Y K417N, E484A, Q498R (**Figure 3.10F**). These data suggest that the use of an updated Spike vaccine containing mutations at key RBD residues provides greater protection against new Omicron subvariants as they emerge, compared to multiple boosters with a WT-based vaccine.

3.2.8 Determining the role of SARS-CoV-2 NTD mutants in transmission and immune escape using NTD-specific monoclonal antibodies.

Although the majority of nAbs are directed towards the SARS-CoV-2 RBD, there is some evidence of neuralisation supersites in the NTD of Spike, but this mode of immune modulation is less well characterised [250]. Therefore, to investigate the role of SARS-CoV-2 NTD mutations in transmission and immune escape, I synthesised full-length Spike expression constructs of B.1, Beta, Delta, Omicron BA.1 and Omicron BA.2 VOCs, along with mutants representing individual NTD changes present in each of these variants in a B.1 background. These were designed with specific restriction sites on either side of the NTD (HindIII and KpnI) and the rest of Spike (KpnI and NotI) (**Figure 3.11A**). The mutants consist of single amino acid changes as well as recurrently deleted regions (RDRs): Δ 69-70 (RDR1), Δ 141-144 and Δ 146 (RDR2), Δ 210 (RDR3), and Δ 234-244 (RDR4) (**Figure 3.11B and C**) [250]. I initially ensured all the mutants were able to be incorporated into lentiviral pseudotypes and observed that relative to a vector-only negative control, all Spikes and mutants produced pseudoviruses with high-titres when used to infect HEK293T cells stably expressing human ACE2 (hACE2) (**Figure 3.11D**).

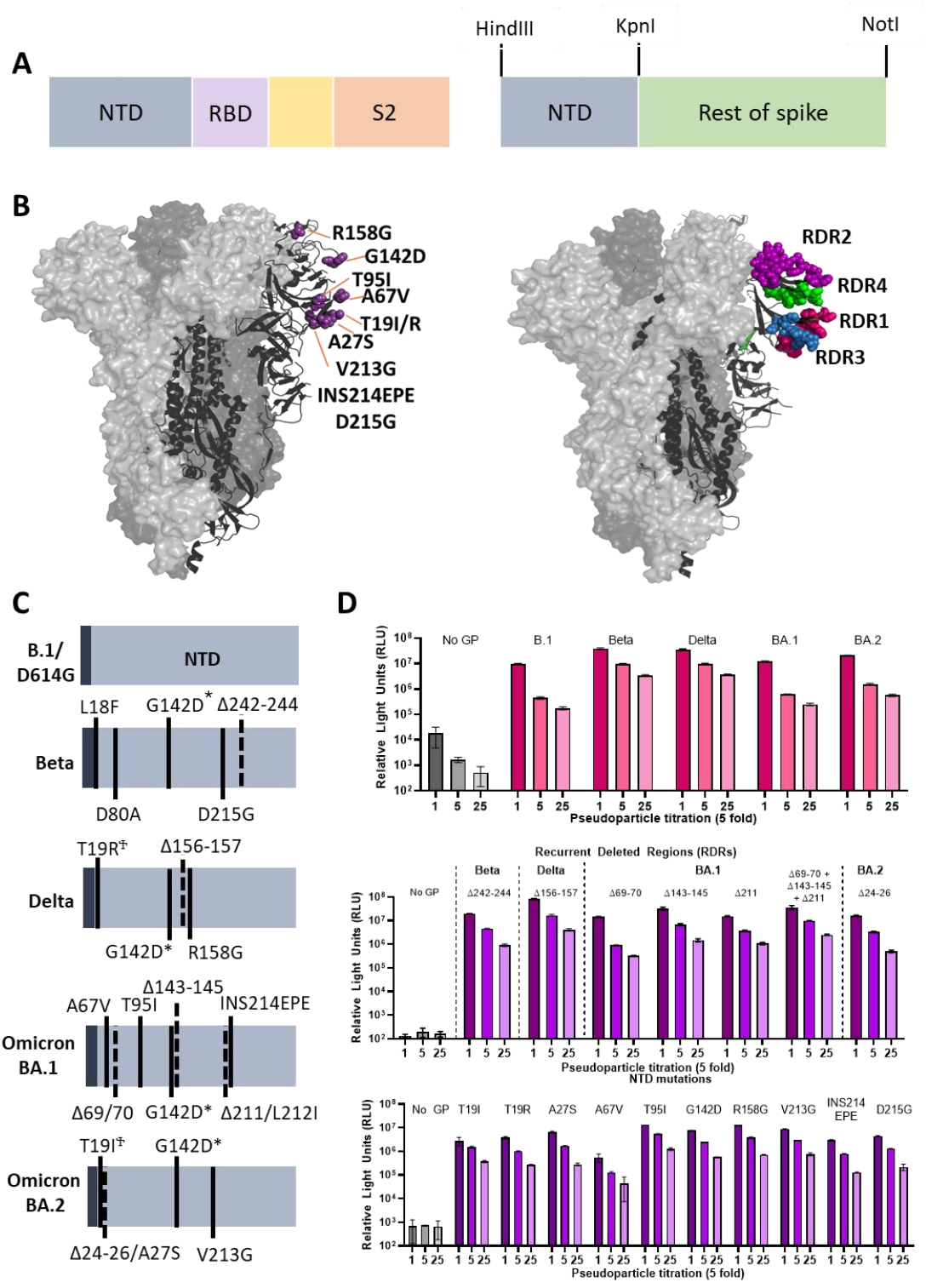

Figure 3.11 Rescue of SARS-CoV-2 NTD mutation/deletion lentiviral pseudotypes.
(A) Schematic of the Spike and mutant constructs generated to study the effect of SARS-CoV-2 N-terminal domain (NTD) mutants, outlining the restriction enzymes (HindIII, NotI, KpnI) included. Constructs were subcloned into a pcDNA3.1 backbone. **(B)** Structural map of SARS-CoV-2 Spike (PDB ID 6VYB) generated in PyMOL with variant NTD mutations and recurrent deleted regions (RDRs) denoted. RDRs are classified as: RDR1 (pink), RDR2 (purple), RDR3 (blue) and RDR4 (green). **(C)** Schematic of SARS-CoV-2 variant Spike (NTD) and their associated mutations and deletions. Depicted are the NTDs of WT/B.1, Beta, Delta, Omicron/BA.1 and Omicron/BA.2. Mutations present in multiple variants are highlighted: * = exact mutations, † = different amino acid mutation. **(D)** A lentiviral-based system was used to generate and rescue pseudoparticles bearing the Spike of different variants or their respective mutations or deletions, synthesised in a WT/B.1 background. All lentiviral pseudotypes were titrated 5-fold on HEK293T cells stably expressing human ACE2 and a vector only (no GP) pseudotype was also included as a negative control. Error bars represent mean + SD of triplicate values.

I then performed pseudovirus neutralisation assays to examine the effects of monoclonal antibodies (mAbs, provided by Dr Katie Doores, King's College London) isolated from SARS-CoV-2 breakthrough infections and to understand which key mutations in VOC Spike NTDs contribute to evading host immunity. The mAbs were previously characterised by competition ELISA compared to known mAbs that bind to different regions of the Spike protein and were subsequently grouped into different binding groups [224, 251]. I first assessed the neutralisation of Beta and Delta pseudoviruses as well as their respective individual NTD mutations and included B.1 as a comparator, using a panel of NTD-specific mAbs (group 5 and 6), RBD-specific mAbs and a commercial antibody, Imdevimab. The Beta Spike was neutralised by most group 5 mAbs (53-61%), which appeared to be mediated solely by the D215G mutation in NTD (**pink box**). The V1WT_13 monoclonal induced strong neutralisation (78%) against Beta Spike, which could not be attributed to a single NTD mutation as all NTD mutations yielded similar levels of neutralisation in the presence of this mAb (**Figure 3.12, left panel**). For Delta, poor neutralisation was observed with the group 5 mAbs V2D_16, V2D_36 and P008_51, but not V1WT_13, compared to B.1 (**Figure 3.12, left panel**). When introducing single point mutations present in Delta NTD into a B.1 background and testing them with the same mAbs, this escape from neutralisation appeared to be dominated by the Δ156-157 mutation (**Figure 3.12, left panel**).

Interestingly, for the group 6 monoclonals, the Δ242-244 mutation in Beta NTD completely escaped neutralisation (**turquoise box**), but this was not observed with the full-length Spike, which was neutralised well by the group 6 mAbs V1D_6, VA14_25 and V3Om_10 (75-85%), similar to what was observed against B.1 (55-72%). The opposite phenotype was seen for the group 6 mAbs against Delta Spike which poorly neutralised (0-27%); however, this immune escape could not be attributed to any specific individual mutation in the Delta NTD (**Figure 3.12, purple box**). Both Beta and Delta Spikes were not neutralised by P008_56, possibly attributed to the combinatorial effect of the individual NTD mutants in these Spikes (**Figure 3.12**). As expected, the RBD-specific mAbs were unaffected by mutations to the NTD (**Figure 3.12, right panel**).

I next took a subset of group 6 mAbs to further test against Omicron BA.1 and Omicron BA.2 pseudoviruses and their individual NTD mutations. For BA.1 I also synthesised a mutant that contained all three deletions present in the NTD. For BA.1 I observed a similar phenotype to Delta in that none of the mAbs were able to neutralise the full-length BA.1 Spike, however, I was able to attribute this neutralisation to the Δ143-145 mutation, either by itself or in combination with the Δ69-70 and Δ211 mutations, which by themselves were still efficiently neutralised by the group 6 mAbs (**Figure 3.13, turquoise boxes**). The BA.2 full-length Spike was neutralised well by the group 6 mAbs, and the Δ24-26 deletion had

little effect on neutralisation unlike what was observed with the deletions present in BA.1 (**Figure 3.13, pink box**).

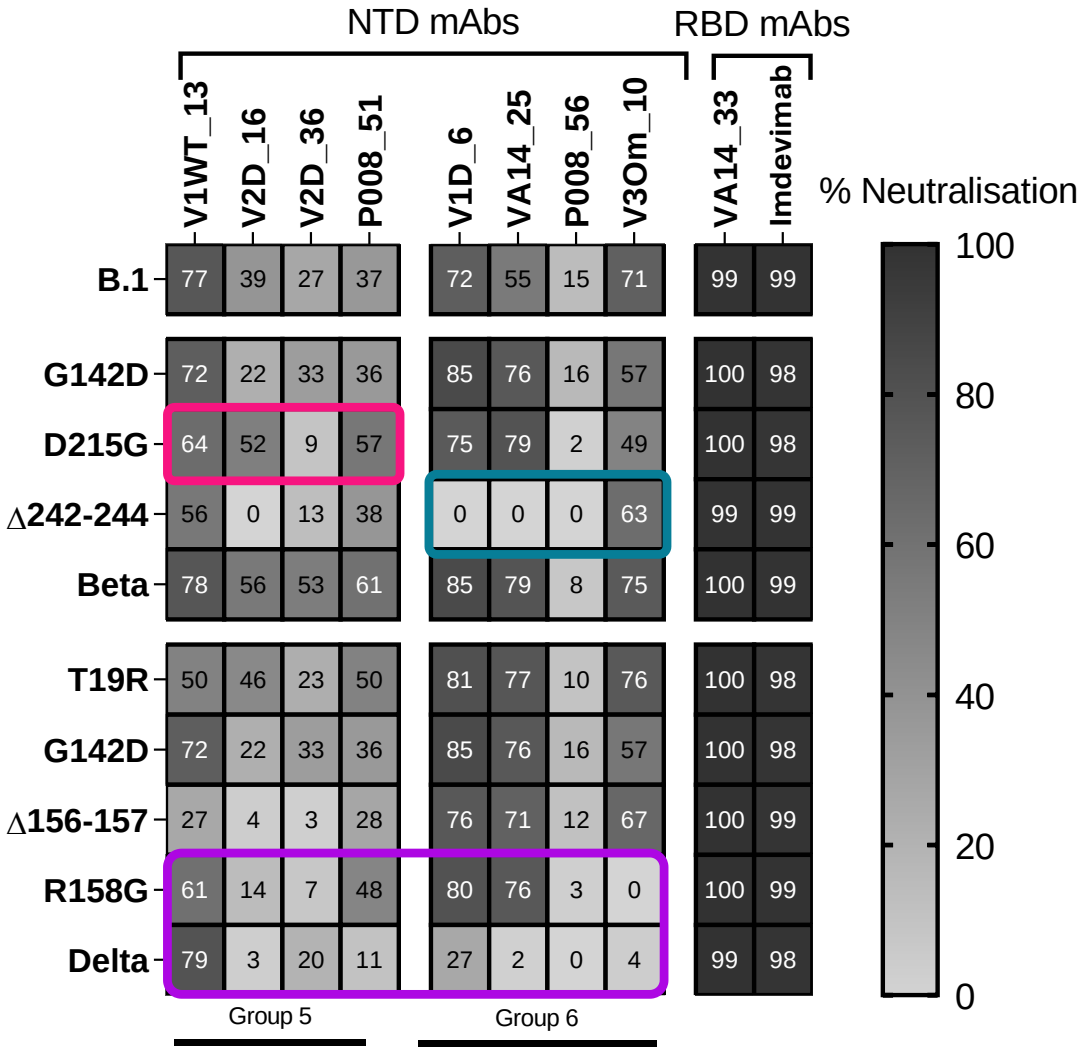

Figure 3.12 Mutations in Beta and Delta NTD Spikes show varied involvement in immune escape from NTD-specific monoclonal antibodies isolated from SARS-CoV-2 breakthrough infections.
Heatmap of neutralisation of B.1, Beta and Delta pseudotypes, along with their associated NTD mutations/deletions in the presence of monoclonal antibodies isolated from individuals of COVID-19 breakthrough infections. The monoclonal antibodies include those that specifically target the NTD (group 5: V1WT_13, V2D_16, V2D_36, P08_51, group 6: V1D_6, VA14_25, P008_56, V3Om_10), or the RBD (VA14_33, Imdevimab) used at a concentration of 10μg/ml. (C) Neutralisation was calculated a percentage of luciferase signal units, relative to no antibody control wells from triplicate values. Data of interest have been highlighted with coloured boxes (pink = D216G mutant with Beta, turquoise = Δ242-244 mutant with Beta, purple = Delta and associated Δ156-157 mutation).

As I observed with Delta and Beta Spikes, BA.1 and BA.2 were not neutralised by the P008_56 mAb, however the Δ211 mutation alone, which is present in BA.1 was neutralised 72% by this mAb, again suggesting a dominant effect of the Δ143-145 mutation, which completely reduced neutralisation with P008_56 either on its own, or in combination with the other BA.1 deletions ("all BA.1 dels") (**Figure 3.13**). These data were of particular interest due as we observed strong neutralisation against BA.2 Spike (82%) by the

commercial RBD-specific mAb, Imdevimab, whereas BA.1 was poorly neutralised (9%) (**Figure 3.13**). This was interesting as despite harbouring similar RBD mutations, there mutations present in BA.1 and BA.2 NTDs are largely different, suggesting a key role for these NTD mutants in immune escape.

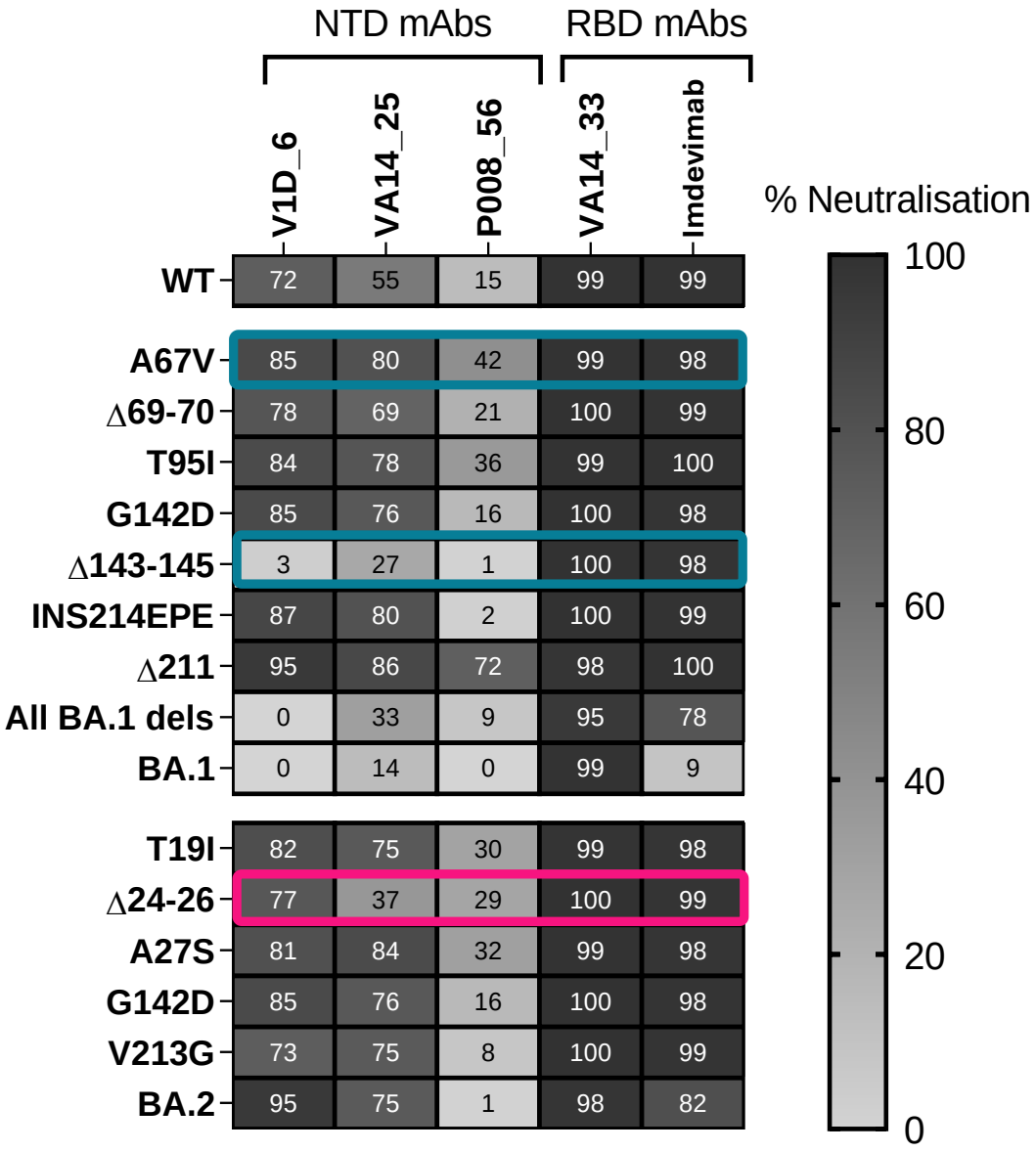

Figure 3.13 Mutations in Omicron NTD Spikes reveal significance of deletions in immune escape from NTD-specific monoclonal antibodies isolated from SARS-CoV-2 breakthrough infections.
Heatmap of neutralisation of B.1, Omicron/BA.1 and Omicron/BA.2Beta pseudotypes, along with their associated NTD mutations/deletions in the presence of monoclonal antibodies isolated from individuals of COVID-19 breakthrough infections. A mutant containing all the deletions in BA.1 was also included. The monoclonal antibodies include those that specifically target the NTD (group 5: V1WT_13, V2D_16, V2D_36, P08_51, group 6: V1D_6, VA14_25, P008_56, V3Om_10), or the RBD (VA14_33, Imdevimab) used at a concentration of 10µg/ml. (C) Neutralisation was calculated a percentage of luciferase signal units, relative to no antibody control wells from triplicate values. Data of interest are highlighted with coloured boxes (pink = Δ24-26 mutant with BA.2, turquoise = BA.1 and associated Δ143-145 mutation).

Owing to the differences in neutralisation observed with the whole VOC Spike compared to NTD-specific mutations in a B.1 background, particularly with Beta and Delta, I aimed to investigate whether mutations in the RBD of Spike played a role in immune evasion. Using single amino acid mutants present in different variants (Beta: N501Y, K417N, E484K; Delta: L452R; Omicron: N501Y, K417N, E484A) (**Figure 3.14A**), I tested a subset of group 6 NTD-specific mAbs (V1D_6, VA14_25, P008_56) against these mutants in pseudotype neutralisation assays. I observed that none of the mutants had any impact on neutralisation, exhibiting neutralisation percentages similar to B.1. These mutant pseudoviruses were also neutralised well by RBD-specific mAbs and as before, none of the mutants were neutralised by P008_56 (**Figure 3.14B**).

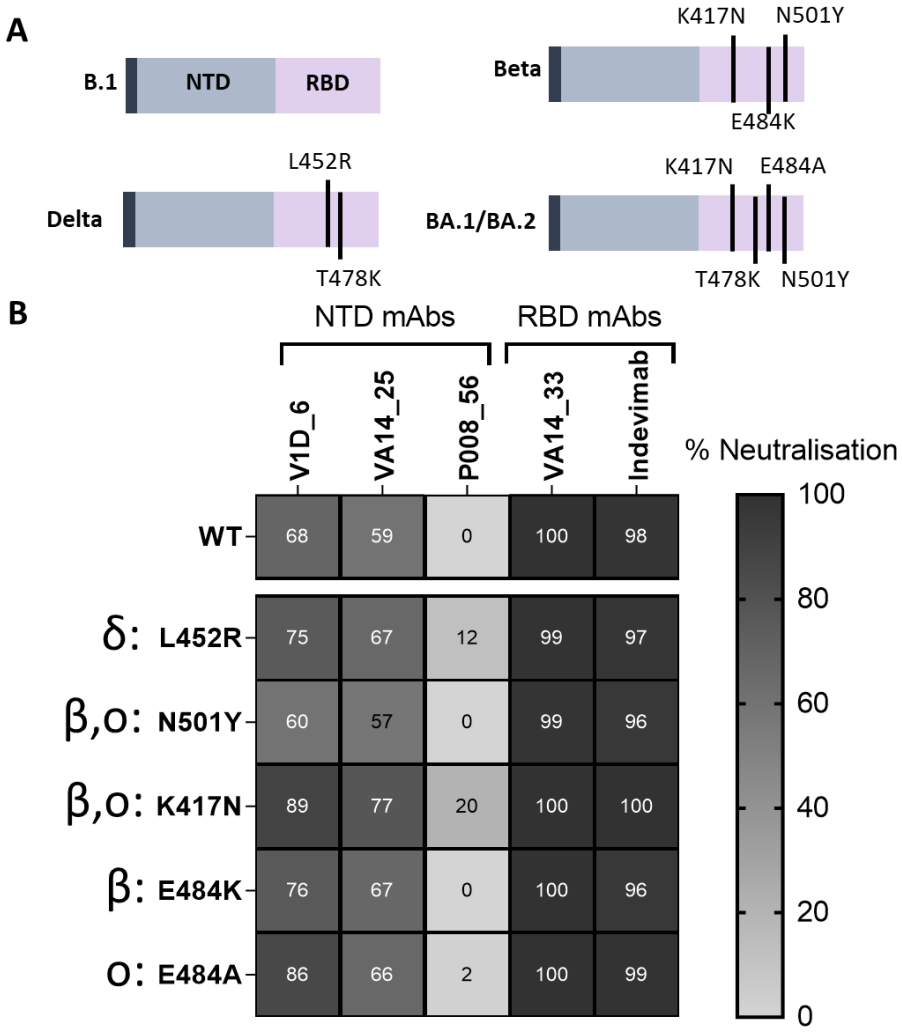

Figure 3.14 Mutations in the RBD of Spike do not contribute to immune escape from NTD-specific monoclonal antibodies isolated from SARS-CoV-2 breakthrough infections.
(A) Schematic of SARS-CoV-2 variant Spike RBDs and their associated mutations. Only mutations present in other VOCs are shown for Omicron. **(B)** Heatmap of neutralisation of B.1 receptor binding domain (RBD) mutations (WT/B.1 background) in the presence of monoclonal antibodies isolated from individuals of COVID-19 breakthrough infections. The monoclonal antibodies include those that specifically target the NTD (V1D_6, VA14_25, P008_56), or the RBD (VA14_33, Imdevimab) used at a concentration of 10µg/ml. Neutralisation was calculated a percentage of luciferase signal units, relative to no antibody control wells from triplicate values.

3.2.9 Determining the role of SARS-CoV-2 NTD mutants in antigenicity using sera from vaccinated animals.

Neutralisation of SARS-CoV-2 variant Spike pseudoviruses and their associated NTD-mutations revealed a significant role of deletions in immune escape, including Δ242-244 for Beta, Δ156-157 for Delta, Δ143-145 for Omicron BA.1 and Δ24-26 for BA.2 (**Figures 3.12 and 3.13**). I therefore wanted to assess the role of SARS-CoV-2 NTD mutants in antigenicity in polyclonal sera in a post-vaccination era using sera from vaccinated animals. However, as the majority of antibodies are directed against the RBD, I employed a method to specifically study the neutralisation phenotype of non-RBD specific antibodies present within the whole polyclonal response. Using late timepoint sera from 3 pigs immunised with two doses of the AZD1222 vaccine (shown in **Figure 3.2B**), I depleted B.1 RBD-specific antibodies from sera using HIS-tagged recombinant proteins conjugated to Ni-NTA beads. I then assessed the neutralisation phenotype of the SARS-CoV-2 variant and mutant pseudoviruses in the presence of non-RBD antibody depleted sera versus RBD-antibody depleted sera. The AZD1222 vaccine is based on the WT SARS-CoV-2 sequence, with B.1 being the closest matched variant and we observed a decrease in neutralising antibody titre in the RBD-antibody depleted sera and therefore concluded that the remaining neutralising response was likely confined to non-RBD specific antibodies (**Figure 3.15A**).

I observed a similar decrease in neutralising titres against full-length Beta Spike highlighting that the Beta NTD retains its antigenic similarity to B.1 following depletion of RBD-specific antibodies (**Figure 3.15B**), which I also observed using mAbs (**Figure 3.12)**. Although the antigenic differences between B.1 and Beta are not recapitulated with individual Beta NTD point mutants, I did observe a similar reduction in neutralisation in with the Δ242-244 both with polyclonal sera and mAbs (**Figure 3.12, Figure 3.15**), suggesting a combinatorial effect of the NTD mutations and the requirement of interaction with the RBD. The residual neutralisation of Delta Spike using RBD-Ab depleted sera was much lower compared to B.1 (**Figure 3.15C**), again consistent with what I observed with the mAbs (**Figure 3.12**), highlighting the antigenic differences between Delta and B.1 NTD. Neutralisation was almost completely absent against BA.1 and BA.2 Spikes using either RBD-specific Ab depleted or non-depleted sera, consistent with antibody selection against both sites in these viruses (**Figure 3.15D-E**). Depletion of RBD-Abs from sera allowed more sensitive and specific assessment of the effect of the individual mutants I generated, which were introduced into a B.1 background. In this context, I observed the Δ242-244 (Beta), G412D (Beta, Delta, BA.1, BA.2), Δ156-157 (Delta), Δ24-26 (BA.2) and Δ143-145 (BA.1) mutations all resulted in a decrease in neutralising antibody response compared to B.1 using RBD-Ab depleted sera (**Figure 3.15B-E**). Interestingly, I also tested different combinations of the deletions present in BA.1 and observed that the Δ143-145 mutation in combination with

Δ69-70 had comparable levels of neutralisation as Δ143-145 alone, but was slightly recovered in the presence of the Δ211 mutation (**Figure 3.15E**).

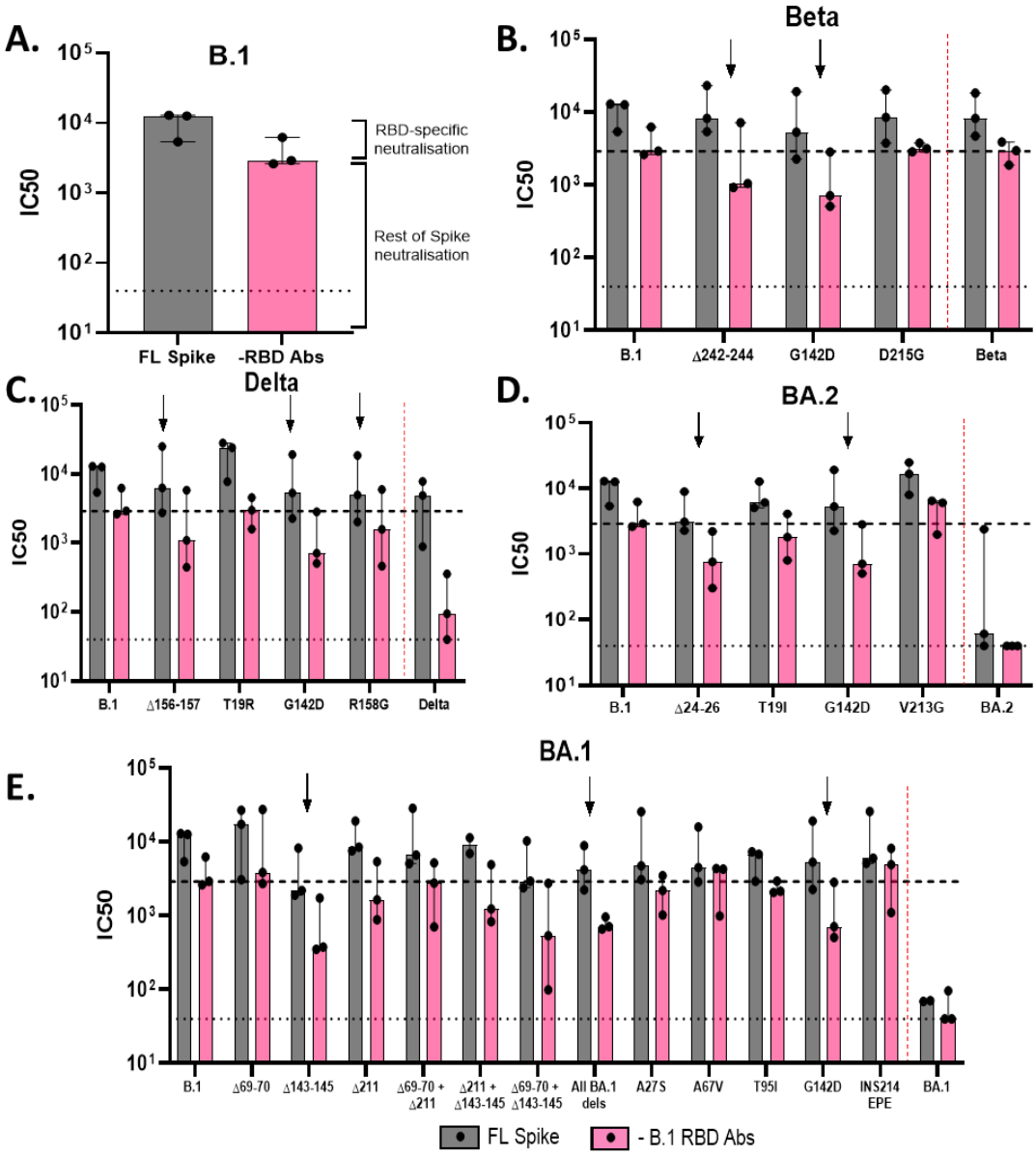

Figure 3.15 Neutralisation of SARS-CoV-2 pseudotypes bearing Spike NTD mutations following depletion of B.1-specific RBD neutralising antibodies.
Neutralisation of **(A)** B.1 **(B)** Beta, **(C)** Delta, **(D)** Omicron BA.2 or **(E)** Omicron BA.1 and their associated NTD mutations (built in a B.1 background), compared to B.1 in the presence of three late timepoint porcine sera immunised with 2 doses of the ChAdOx1 ADZ1222 vaccine that has either been non-depleted (grey) or depleted (pink) of B.1 RBD-specific antibodies. Error bars represent median ± range of triplicate values. The titre at which 50% neutralisation of virus is seen (IC50) is shown. Dotted line indicates limit of detection (LoD=40) for the assay. Dashed or lines indicate the IC50 relative to WT following depletion of B.1-specific RBD antibodies. Arrows indicate mutations of interest where a decrease in neutralisation was observed.

To further confirm the role of the RDRs in antigenicity, I depleted variant RBD-specific antibodies from matched vaccine regimes in CD1 mice. CD1 mice were received homologous prime-boost immunisation with a ChAdOx1-vectored vaccine bearing the B.1,

Beta or Delta Spikes (study led by Cameron Bissett and Professor Teresa Lambe, University of Oxford). Sera from these mice were depleted of RBD-specific antibodies with matched recombinant RBDs, which allowed us to assess the impact of the RDRs compared to the full-length Spike. As observed with the pig sera, depletion of RBD-specific antibodies in sera from B.1 immunised mice resulted in a decrease in neutralising antibody titre ($p<0.001$) (**Figure 3.16A**). When depleting Beta RBD-specific antibodies from Beta immunised mice, I observed a significant decrease in nAb titre ($p<0.005$) which was exacerbated with G142D and Δ242-244 containing pseudoviruses in a B.1 background ($p<0.05$), suggesting an important role for these mutants in Beta immune escape (**Figure 3.16B**). A similar trend was observed when depleting Delta RBD-specific antibodies from Delta immunised mice, where a large decrease in neutralising antibody titre was observed against full-length Delta Spike pseudovirus ($p<0.005$) and the G142D and Δ156-157 mutant containing pseudoviruses in a B.1 background also showed significantly large decreases in antibody titre ($p<0.005$), suggesting a dominant role of the RBD-specific antibodies and these two mutations in Delta antigenicity (**Figure 3.16C**).

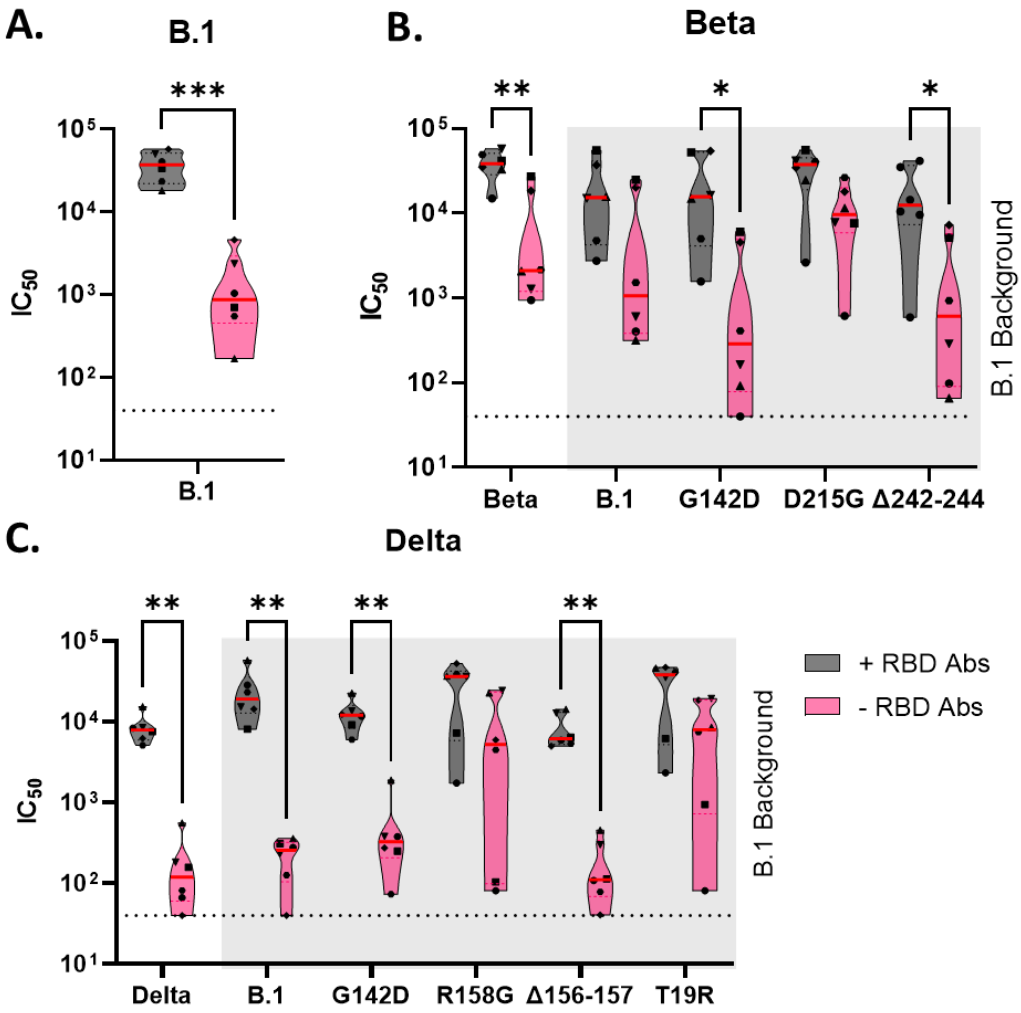

Figure 3.16 Neutralisation of SARS-CoV-2 pseudotypes bearing Spike NTD mutations following depletion of variant-specific RBD neutralising antibodies from immunised mice.
Neutralisation of (A) B.1 (B) Beta, and (C) Delta and their associated NTD mutations (built in a B.1 background) in the presence of sera from CD1 mice immunised under a homologous prime-boost regime with ChAdOx-1 vectored vaccines (A: B.1, B: Beta, C: Delta). Sera was either been non-depleted or depleted of (A)B.1, (B) Beta or (C) Delta RBD-specific antibodies. Error bars represent median ± range of triplicate values. The titre at which 50% neutralisation of virus is seen (IC50) is shown. Dotted line indicates limit of detection (LoD=40) for the assay. Statistical analysis was conducted using non-paired multiple Mann-Whitney *t*-tests (* = $p<0.05$, ** = $p<0.005$, *** = $p<0.001$).

3.3 Discussion

In response to the COVID-19 pandemic, several public health measures were put in place to try to manage virus spread and to reduce hospitalisation and mortality. One such measure was mass vaccination across many parts of the world with COVID-19 vaccines developed in different platforms. In an effort to fast-track the approval of vaccines, different phases of clinical trials were undertaken simultaneously including animal immunogenicity and efficacy studies, and human trials. One such vaccine platform was the viral-vectored ChAdOx-1 expressing the Spike protein of the WT SARS-CoV-2 virus (ADZ1222). We assessed the immunogenicity of this vaccine in mouse, pig, ferret and non-human primate animal models following prime-only or prime-boost regimes, and observed similar neutralisation titres using pseudotyped virus in all models; that being that control animals

did not mount a nAb response, but robust nAb titres were calculated in immunised animals (**Figure 3.2**). The most notable difference observed was the decrease in nAb titre in the prime-only immunised pigs by day 28, which was not detected in the ferret model. There also appeared to be a saturated nAb response in prime-boosted pigs, compared to prime-only immunised pigs; however, the nAb response increased post-boost in the ferret and NHP model (**Figure 3.2**).

Due to the decreased nAb responses that was seen against the Beta variant early in the pandemic both by us and others [49, 50, 236], there was significant concern that efficacy of the original ADZ1222 vaccine may be reduced against VOCs, however real-world data from both Canada and PHE showed that the vaccines were effective at preventing hospitalisation and death even with these reduced titres. Nonetheless, we tested sera from mice [242], pigs [240] and hamsters [243] vaccinated additionally with a ChAdOx-1 vaccine bearing the Beta (B.1.351) Spike protein (AZD2816) to assess immunogenicity (**Figure 3.3, Figure 3.4, Figure 3.5**). As priming of the immune response to the original Spike in AZD1222 may impact the ability to switch specificity of the response to Beta, we assessed nAb responses after one or two doses of the original AZD1222 vaccine in mice, followed by a single dose of AZD2816 to recapitulate the vaccination regime in 2022 in the global population. While a single dose of AZD1222 induced rapid antibody development specific to the WT vaccine variant, the nAbs responses against Beta and Delta were below the limit of detection. However, following a boost with either AZD1222, or AZD2816, these titres increased across all the VOCs tested (**Figure 3.3**). We also compared a homologous prime-boost-boost regimen with AZD1222 to a prime-boost with AZD1222 followed by an additional boost with AZD2816 to recapitulate the vaccination regime present at the time of assessment, where we measured the greatest nAb titres in the latter. The high nAb titres against WT SARS-CoV-2 induced by AZD2816 argues against the premise suggested by Lui et al, that the original vaccine may be better in inducing nAb responses in naïve populations than one encoding Beta [52]; we have shown the opposite to be true, suggesting that a heterologous booster may be just as effective as a homologous boost, if not better. T cells responses in these difference vaccine groups were also assessed, where high levels of effector and memory T cells and their associated cytokines were observed [242].

We examined sera from pigs immunised with homologous prime-boost regimens with either AZD1222 or AZD2816, and saw similar results then in mice, where nAbs responses were lower in AZD1222 vaccinated animals against Beta but increased in vaccinated AZD2816 animals (**Figure 3.4**). The Beta variant harbours 3 amino acid changed in the Spike RBD, which include N501Y, E4848K and K417N, thought to increase Spike RBD affinity for ACE2 [233, 252]. The N501Y mutation alone does not appear to affect sera neutralisation but

does in combination with D614G and E484K [252, 253]. Additionally, we tested the sera of immunised pigs against an Alpha variant carrying an additional E484K mutation (N501Y + E484K), where we observed similar nAb titres to those we saw against Beta (**Figure 3.4**). These data suggest that a Beta-specific vaccine may indeed cross-protect against other variants.

Similar results were also observed in hamsters immunised with a single AZD2816 vaccine or prime-boosted with AZD1222 followed by AZD2816. This showed negligible differences in titre against WT SARS-CoV-2 or Beta Spike, but the heterologous booster appeared more beneficial against the Delta variant and individual mutant Spikes containing the K417N, N501Y or L452R amino acid changes, at 56 days post immunisation (**Figure 3.5**). There was no significant difference in nAb titre observed against the E484K mutant after a prime-only or heterologous prime-boost vaccination, suggesting this mutation may be a key determinant of immune escape in the Beta VOC. This is supported by the nAb titres we detected against Omicron BA.1, which remained low with both vaccine regimes despite harbouring the K417N and N501Y mutations in Spike. BA.1 also contains an additional 13 Spike RBD mutations (37 mutations in the whole Spike), including an E484A mutation instead of the deterministic E484K mutations found in Beta. This suggests the importance of other mutations or a synergistic effect resulting in immune escape, which would therefore require additional booster or different target immunogens may be more beneficial in eliciting an immune response against the Omicron subvariants.

Whilst we observed these results using the ChAdOx-1 platform, it has been reported that other vaccines (and their platforms) behave differently in animal models. Hamsters immunised with a single dose of ADZ2816 or ADZ1222 followed by AZD2186 were fully protected against lower respiratory tract infection following infection with Beta, Delta and Omicron BA.1 with reduced gRNA and little to no detection of sgRNA [254]. However, Tostanoski et al., showed that vaccination of hamsters with an adenovirus-vectored vaccine encoding WT Spike (Ad26.COV2.S) resulted in reduced viral load after challenge with Beta VOC, but there was no significant difference in gRNA compared to the control group [255]. Furthermore, rhesus macaques vaccinated with Ad26.COV.S or the Moderna mRNA-1273 (encoding WT SARS-CoV-2 S) showed higher viral loads in nasal swabs and bronchoalveolar lavage when challenged with Beta VOC compared to WT SARS-CoV-2 [256-258]. In contrast, rhesus macaques immunised intranasally with prime-boost regimen of a WT followed by Beta S1 adjuvanted subunit vaccine were fully protected against Beta infection with significant reduction in viral replication [259]. These results suggest that whilst animal models are important to understand safety profile and immunogenicity of candidate vaccines, different vaccine platforms and animal models and even route of administration

can yield different results. Testing vaccines in the most appropriate model is therefore crucial to assess vaccine efficacy and the use of updated Spike immunogens may be more beneficial to increase protection against disease.

Vaccination against SARS-CoV-2 has been widely used in the UK population where many healthy individuals have received three or four doses of licenced vaccines and clinically vulnerable individuals receiving further boosters. In my studies I analysed a cohort of older adults highly susceptible to COVID-19 who have therefore received up to 7 vaccine doses, as of Autumn 2023. The licenced vaccines used in this cohort included monovalent or bivalent vaccines such as the Oxford/AstraZenena Vaxzervria© (WT monovalent) [90], the Pfizer/BioNTech Comirnaty™ vaccines (WT monovalent [91], WT/BA.5 bivalent, XBB1.5 monovalent), the Moderna Spikevax™ (WT/BA.1 bivalent) or the Sanofi VidPrevtyn® (Beta monovalent), which were administered as Spring and Autumn boosters as new SARS-CoV-2 variants emerged (**Figure 3.6**).

Initially, the vaccination regime in the UK was changed to extend the interval between the first and second dose from 3-weeks to ~12-weeks. We observed significantly lower nAb responses against WT SARS-CoV-2 and Delta in individuals who received a short-interval prime-boost with WT Comirnaty™ compared to those with an extended-interval prime-boost (**Figure 3.7**). Research conducted by Voysey et al. has also suggested that a longer duration between first and second dose demonstrated higher vaccine efficacy with Vaxzervria© [260], and other studies have shown that using extended dosing intervals of the WT Comirnaty™ vaccine enhanced nAb and helper T cell responses [96, 225]. This is likely due to the extended-interval vaccine regime allowing more time for generation of affinity matured B cells that can produce higher affinity nAbs and a more robust T cell response, which is particularly crucial in older adults who are known to have diminished immune responses to vaccines, especially in terms of their T cell responses. Studies investigating the immune response to the ChAdOx-1 nCoV-19 vaccine (ADZ1222) in aged mice have aimed to understand whether this vaccine could induce T cell responses, potentially offering insights into how to improve vaccine strategies for older adult populations. Following vaccinations aged C57BL/6 mice were also able to generate functional $CD8^+$ T cell responses. These studies highlighted the importance of T follicular helper (Tfh) cells for germinal centre formation in generating memory B cells and high-affinity antibodies, crucial in maintaining long-term immunity. Importantly these responses were vastly improved following booster immunisation, which enhanced both humoral and cell-mediated immune responses [261-263].

Further examination of individuals from the short-interval cohort double-vaccinated with the WT Comirnaty™ vaccine demonstrated significant reductions in neutralisation against the VOCs Beta, Delta, Omicron BA.1 and Omicron BA.2 relative to B.1, exacerbated by waning immunity (**Figure 3.8**). Systematic reviews of different publications on the potency of WT Comirnaty™ or Vaxzervria© vaccines in inducing neutralising antibodies against pre-Omicron SARS-CoV-2 VOCs identified similar trends in vaccinee and convalescent sera [264, 265]. We also identified a reduction in the neutralisation of VUI Mu, concordant with observations by Tada et al., [266] in individuals immunised with WT Comirnaty™, but differed from a study by Uriu et al., [267] who showed that Mu was more antigenically diverse than Beta in WT Comirnaty™ vaccine sera. Other studies have observed comparable decreases in neutralisation of over 30-fold against Omicron [55, 60, 232, 268], however, we also determined that a third or fourth booster with WT Comirnaty™ generates much higher nAb titres, albeit still ~10-12-fold lower than compared to B.1, corroborated by research from Garcia-Beltran et al., and Arbel et al., (**Figure 3.9**) [60, 269]. We also performed antigenic cartographic mapping on the collated ND_{80} titres against these SARS-CoV-2 variants. This revealed the largest antigenic distances between Beta (5.3 antigenic units (AU)), Mu (3.3AU) and Delta (3.1AU) compared to B.1 after a second vaccine dose, and against BA.1 and BA.2 after a third vaccine dose (3.3 and 3.1 AU, respectively), which consequently reduced the antigenic distance of earlier variants (data not shown) [49].

Differences in results could be attributed to experimental variation, particularly because our data was produced using pseudotyped viruses, which provide an effective, low-containment alternative to using live virus to rapidly screen sera sets and assess amino acid mutations. However, generally studies have shown comparable neutralisation titres between SARS-CoV-2 neutralisation tests using pseudoparticles or live virus, which can be used to complement classical serological assays like ELISAs [49, 270]. Alternatively, is has been demonstrated that SARS-CoV-2 virus-like particles (VLPs) are a good surrogate to assessing neutralisation in a more physiologically relevant manner as VLPs incorporate all the SARS-CoV-2 structural proteins bar the polymerase and this might prove a more viable alternative in the future [271]. In addition, the samples we have tested are from an older cohort of individuals aged 50-89, rather than younger people that represent a larger proportion of the population, however, the data we obtained is similar to that which has been described in other studies in older adults [272].

Acquisition of mutations in the RBD are thought to be deterministic for evasion of antibody-mediated immune responses. The Beta VOC contains N501Y, K417N and E484K mutations in the Spike RBD, of which the E484K mutation, and to a lesser degree K417N appear to contribute to immune escape based on binding data using VOC RBDs or single amino acid

RBD proteins with sera from the CONSENSUS study [49]. These mutations are also well associated with antigenic escape [233, 264, 265] (**Figure 3.8**). Class 1 and 2 antibody binding are affected by modifications at positions 417 and 484, respectively, which dominate the polyclonal response to the RBD of Spike [273]. Combining these changes with N501Y causes an additive effect, reducing nAb responses [264]. The Delta variant harbours an L452R mutations in the Spike RBD, which has been shown to have a slight increase in affinity for ACE2 and confers higher pathogenicity compared to B.1, but did not have a significant effect on neutralisation in our study [53, 274, 275].

The Omicron variant and its subvariants which did show substantial evidence of escape, also have mutations at these positions, with a number of additional mutations. All Omicrons have N501Y, K417N and E484A, whilst BA.5, BQ.1.1 and XBB.1.5 also harbour the L452R mutation, with BA.2.86 and JN.1 having a L452W mutation. Although we did detect some recovery of nAb responses against BA.1 and BA.2 following third and fourth vaccine doses, we observed an even greater increase when analysing sera in individuals who received the Moderna Spikevax™ [64] as their fifth vaccine - a WT/BA.1 bivalent (**Figure 3.9**). Nonetheless, Omicron subvariants that emerged later still exhibited lower nAb responses, even with boosters of updated bivalent vaccines bearing an Omicron Spike (Spikevax™ WT/BA.1; Comirnaty™ WT/BA.5 [65]) (**Figure 3.10**). The monovalent boosters however, either VidPrevtyn® Beta [62] or Comirnaty™ XBB.1.5 [276] resulted in higher nAb titres post-sixth or -seventh dose, respectively, particularly against the E.G.5.1 and BA.2.86 variants (**Figure 3.10**). This again highlights the importance of key mutants in the Beta VOC, similar to what we observed in our animal models, and for XBB.1.5 the presence of key mutations that overlap with the proceeding Omicron subvariants. It is worth noting however, that although these titres are reduced, they may still be sufficient to confer immune protection, and reduced disease severity, particularly because most participants by this point possessed both vaccine-derived and natural immunity following infection. Furthermore, detection of nAb responses is likely not the only correlate of protection, so cellular, non-neutralising antibodies and even mucosal immunity may also play key roles in determining protection.

The majority of nAb are targeted against the S1 domain of Spike, particularly the RBD or regions closely adjacent to the ACE2-binding interface, changes in which result in altered virus transmission and antigenicity [233]. Antibodies also potently bind to a “supersite” on the N-terminal domain (NTD [235], similar to what is known for other betacoronaviruses like MERS-CoV [277, 278] and that has been denoted in prior studies for influenza virus and HIV antibodies [279, 280]. This supersite is defined by 3 loops (amino acid positions: N1 (14-20), N3 (150-158), N5 (245-264)) within the NTD and corresponds to amino acids 13-

305 within S [46, 281]. The RBD and NTD are mutational hotspots [233], affecting the ability of nAbs to effectively access and neutralise at these sites. We therefore investigated the role of the Spike NTD and mutations that have arise in SARS-CoV-2 VOC NTDs to understand the impact they have on transmission, neutralisation and immune escape. The pseudotyped viruses we generated for B.1, Beta, Delta, BA.1 and BA.2 Spikes along with their associated NTD mutations were able to enter cells overexpressing hACE2. The presence of these mutations had little impact on entry, suggesting they do not affect transmission of the virus (**Figure 3.11**).

However, although full-length Beta Spike was neutralised well using NTD-specific mAbs derived from SARS-CoV-2 breakthrough infection individuals, we noted escape from neutralisation in group 6 mAbs with the Δ242-244 mutation which is adjacent to the N5 loop (**Figure 3.12**). This 3 amino acid deletion likely disrupts the structural arrangement of the N5 loop, which has been shown to prevent binding of mAbs [50, 236], but the additional presence of a R246I mutation within the same loop appears to suppress the structural rearrangement [46], which may explain why we are still able to detect neutralisation against the full-length Beta Spike. The opposite phenotype was noted against Delta, where group 6 mAbs resulted in immune escape against full-length Spike, but this could not be attributed to any of the NTD mutations, however the loop N3 G142D, Δ156-157 and R158G mutations did mirror the immune escape noted with full-length Delta Spike using group 5 mAbs (**Figure 3.12**). Of note, the group 5 mAbs are less potent neutralisers than the group 6 mAbs [223, 224], which could explain why the same phenotype is not observed with Beta and Delta. Additionally, the NTD supersite appears to only be accessible from a restricted angle from “above” by antibodies [46], so it is possible that the less potent group 5 mAbs likely bind distal to the supersite and require combinatorial mutations to have a profound effect, otherwise are not impacted as strongly by changes in the key NTD loops.

Examination of the Omicron BA.1 and BA.2 NTD mutations were of particular interest as both variant RBDs comprise similar RBD mutations, but their NTD mutations are vastly different. The neutralisation profile of these variants with NTD-specific mAbs also differed, where escape from neutralisation was observed against BA.1, attributed to the N3 loop Δ143-145 mutations. However, BA.2 was neutralised to a high degree by the same mAbs and the N1 loop deletion at positions 24-26 has little impact on its own on neutralisation (**Figure 3.13**). BA.1 also contains deletions at positions outside the NTD supersite (69-70 and 211), neutralisation of which was unaffected by NTD-specific mAbs by themselves, but the immune escape mediated by Δ143-145 appeared to dominate when expressed in combination with the Δ69-70 and del Δ211 mutations (**Figure 3.13**). The Δ69-70 mutation, present in loop N2, has been shown to compensate detrimental effects of other mutations

by increasing Spike incorporation and altering kinetics of cell-cell fusion [46, 234]. The only notable NTD mutation shared between all 4 VOCs examined is the G142D change, which may point to a dominant role of the N3 loop in mediating NTD-specific immunity.

These regions of deletions in the NTD have been termed “recurrent deleted regions” (RDRs), numbered arbitrarily from 5’ to 3’ based on the deletions examined by McCarthy et al., who showed that RDR4, representing the Δ242-244 mutant in Beta, was associated with the loss of mAb 4A8 binding, and that RDRs 2 and 4 in particular are associated with immune escape [250]. RDR2 and RDR4 coincide with the NTD supersites N3 and N5, respectively, which could explain the loss of neutralisation observed with mAbs at these sites. Furthermore, examining the NTD-specific mAbs with key RBD mutants present in the Beta, Delta and Omicron variants did not result in a reduction in neutralisation (**Figure 3.14**), which could indicate a synergistic role of both the NTD and RBD in antigenicity. To investigate this further, the expression constructs used have been designed as “cassettes” to allow us to generate chimeras of NTDs, initially with a B.1-specific rest of Spike sequence to understand the role of the combination of NTD mutations in each variant (**Figure 3.11**). Likewise, rather than assessing the effects of individual mutations in a B.1 background as we have shown here, mutants could be reverted to B.1 in the VOC backbones to examine whether an inverse phenotype is observed. In addition, we wanted to understand whether the NTD is necessary in virus entry, transmission and neutralisation by generating complete deletions of the NTD in our surrogate assays. This is of interest because a large deletion of the whole NTD naturally occurred in the Spike of the alphacoronaviruses Transmissible Gastroenteritis Virus (TGEV), which resulted in the emergence of Porcine Respiratory Coronavirus (PRCV), resulting in the loss of sialic acid binding and altered tissue tropism in pigs, from gut-tropic to respiratory tract-tropic) [35].

We also wanted to understand the role of the NTD, particularly the RDRs following vaccination and did so using sera from immunised animals. However, as most of the nAbs are directed against the RBD, we employed a technique to first deplete RBD-specific antibodies from polyclonal sera, which would allow more specific examination of non-RBD-specific antibodies and the possible epitopes that they bind. As with the mAbs, we noted decreases in nAb titres with the Δ242-244 (Beta), Δ156-157 (Delta), Δ24-26 (BA.2), Δ143-145 (BA.1) and G142D (all) mutations in the presence of WT SARS-CoV-2 (ChAdOx1 ADZ1222) immunised pigs (**Figure 3.15**), and in mice homologous prime-boosted with Beta or Delta-specific ChAdOx1-vectored vaccines (**Figure 3.16**). However, the effects are less prominent in the WT-immunised sera, which were depleted with VOC-specific RBDs, whereas Beta- or Delta- immunised mouse sera was depleted with matched RBDs. This difference in titre is likely attributed to the lack of Beta or Delta-specific antibody epitopes

following immunisation with WT SARS-CoV-2. Additionally, nAbs can also be directed towards the S2 portion of Spike, albeit to a lesser extent, which is more conserved than S1 [282, 283], and depletion of RBD-specific antibodies does not account for S2-specific antibodies, which will contribute to the nAb response we are detecting.

To summarise, the antigenic escape properties of the variants we examined are due to combined changes in the Spike protein, particularly the RBD, but with evidence of NTD-involvement, which likely work in concord and potentially in an additive manner to evade vaccine or monoclonal-derived immunity. The NTD contains a single supersite of antibody recognition, which may result in resistance and may be selectively favoured by future emerging variants to evade neutralisation. The results we obtained in the CONSENSUS older adult cohort highlight the vulnerability of this group of individuals, with reduced antibody titres even after 7 vaccine doses, as well as the need for continual booster vaccinations. Understanding how antibody titres correlate with immunity is crucial for assessing future vaccine design for SARS-CoV-2 variants or other viruses with pandemic potential, with a focus on rational vaccine design to incorporate more antigenically distant viruses to broaden the antibody repertoire.

Chapter 4: Assessing the species tropism of sarbecoviruses for mammalian ACE2.

4.1 Introduction and Aims

SARS-CoV-2, the virus responsible for the COVID-19 pandemic, is thought to have originated from an as yet unidentified *Rhinolophus* bat species, given its high sequence similarity to other sarbecoviruses, particularly at the receptor binding domain (RBD) level (e.g., RaTG13 (96% similarity), BANAL-20-52 (97% similarity)) [106, 216, 284]. It is also thought that SARS-CoV-2 emerged in the human population via an intermediate host, similar to the origin of SARS-CoV-1 in 2002 via palm civets, and MERS-CoV via camels in 2012 [285, 286]. Natural infections of a range of species including cats, dogs and mink, along with experimental infection of ferrets, mice, primates, hamsters and other animals suggest that SARS-CoV-2 may also have broader host range than just bats and humans [219, 287-289].

Understanding SARS-CoV-2 host range is important to assess the risk of disease in other animals that could act as intermediate reservoirs for the virus, but also to help establish and validate animal models used to study virus pathogenesis or to test therapeutics and vaccines. Functional and structural studies identified angiotensin-converting enzyme 2 (ACE2) as the proteinaceous receptor for entry for SARS-CoV-2 and RaTG13, which in early 2020 was the most closely related beta-coronavirus [290-292]. These studies demonstrated high affinity for the N-terminal peptidase domain of ACE2 by the SARS-CoV-2 Spike RBD, which was shown to be deterministic for SARS-CoV-1 cross-species infection and pathogenesis [293].

Prior to the commencement of this DPhil, our group previously functionally assessed the host tropism of 21 different species, published in Conceiçao C, Thakur N et al., (*PLoS Biology,* 2020) [219], where I am listed as joint first author, the findings of which have been adapted and summarised in **Figure 4.1**. In this study, expression constructs for 21 ACE2 orthologues were synthesised from different species, including human, companion animals (dog, cat, rabbit, hamster, horse, rat, ferret, chinchilla), livestock (chicken, cattle, sheep, goat, pig, turkey, buffalo), bats (horseshoe-bat, fruit bat, little brown bat) and potential intermediate hosts (civet, pangolin), which showed 62-99% sequence identity at the amino acid level and a high level of divergence at the SARS-CoV-2 – ACE2 binding sites (**Figure 4.1A**). We examined whether these ACE2s could support the entry of SARS-CoV-2, SARS-CoV-1 and RaTG13, using codon-optimised Spike expression constructs [294]. The modelled structure for RaTG13 aligned with SARS-CoV-2 showed a high level of structural

conservation, but also identified several variable residues which interact directly with ACE2 within the RBD at the sequence level (**Figure 4.1B**).

We employed two surrogate virus entry assays: a lentivirus-based pseudotype virus-based assay to mimic receptor engagement and particle entry [218], and a quantitative fusion assay to assess subsequent Spike-mediated cell-cell spread [162]. We observed that SARS-CoV-2 had broad tropism for mammalian ACE2 in both assays, particularly human, hamster, cat, dog, rabbit and many livestock species, but had notable restrictions with rat, bat and bird ACE2s (**Figure 4.1C, left panel**). SARS-CoV-1 showed a similar pattern of ACE2s usage as SARS-CoV-2, however RaTG13 appeared to have more restricted host range (**Figure 4.1C, middle and right panel**). Mutants generated at variable amino acid residues between SARS-CoV-2 and RaTG13 RBDs identified in **Figure 4.1B**, revealed that these residues played a critical role in hACE2 usage, and may contribute to the difference in species tropism observed for these two viruses (**Figure 4.1D**).

As the COVID-19 pandemic progressed, the ancestral SARS-CoV-2 strain evolved due to repeat infections in humans, breakthrough infections and immune selection pressure, giving rise to SARS-CoV-2 variants, some of which grew to global dominance, described in **Chapter 3**. Some of these variants exhibited the propensity to infect new animal reservoirs, for example, variants like B.1.2, B.1.582 and B.1.596 were detected in white-tailed deer resulting in onward transmission [295-297], and some SARS-CoV-2 lineages harboured mutations that resulted in circulation of the virus in ferret and mink [298, 299].

Later, the BANAL bat sarbecoviruses isolated in Laos were identified as being more closely related to SARS-CoV-2 than RaTG13 at the protein level. These virus Spikes have high affinity for ACE2, which appears to be an ancestral trait of these viruses [216]. Since 2020, many other sarbecoviruses, have also been identified and isolated in parts of Asia, Africa and Europe that cluster phylogenetically into different clades: clade Ia which includes SARS-CoV-1, clade Ib which includes SARS-CoV-2, clade III – V viruses, and the clade II viruses which do not use ACE2 as their entry receptor [69, 70, 74, 300-304]. Due to the emergence of SARS-CoV-2 in the human population and our initial assessment of the broad tropism of SARS-CoV-2, we undertook further characterisation of the species tropism of SARS-CoV-2 variants and other sarbecoviruses to determine the reverse zoonotic potential of these viruses into other animals and any onward risk to humans.

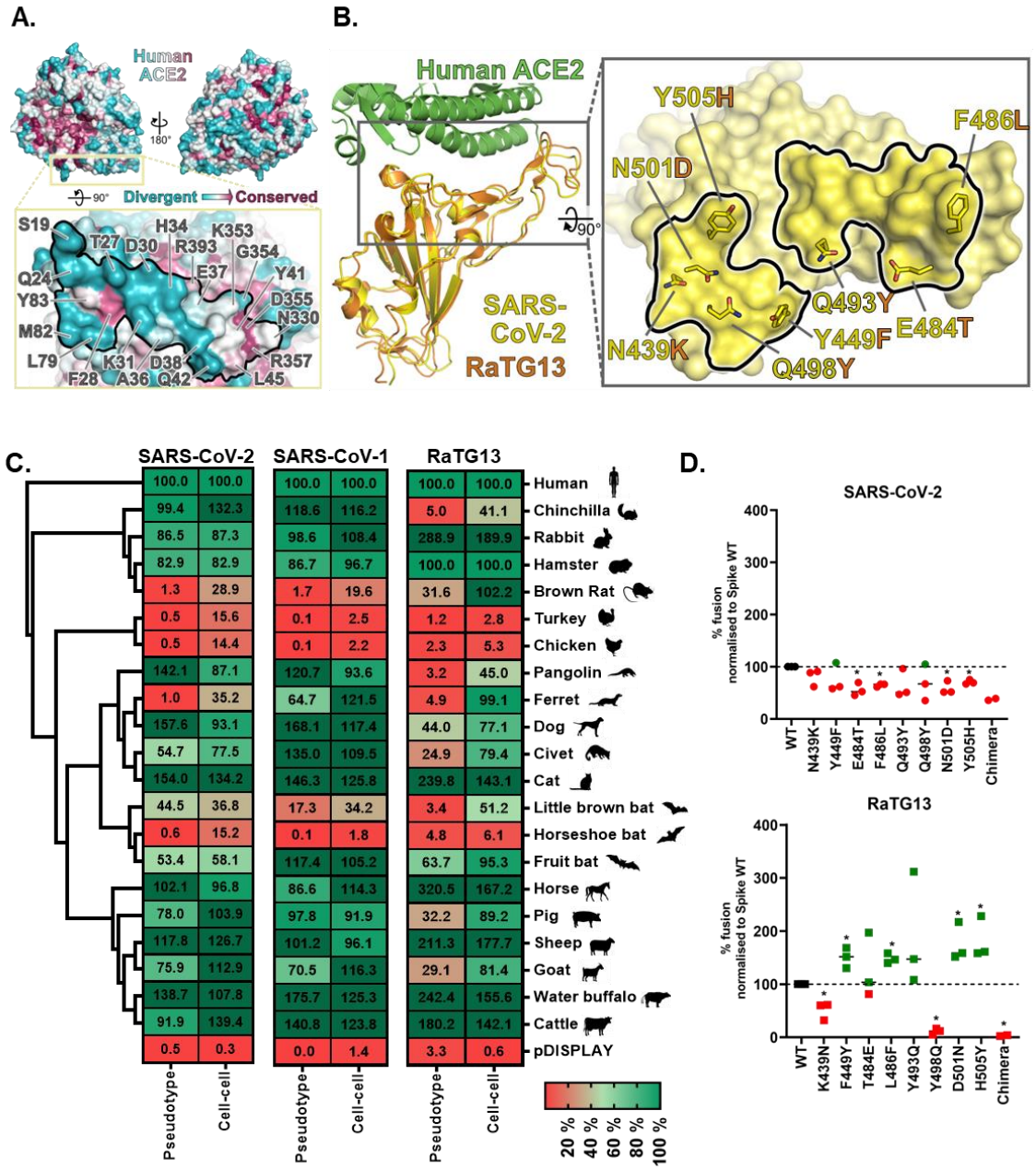

Figure 4.1: SARS-CoV-2 has broad tropism for mammalian ACE2 (adapted from Conceiçao C, Thakur N et al. *PLoS Biol* 2020)
(A) Conservation of mammalian ACE2 amino acid residues, mapped onto the surface of the human ACE2 ectodomain, with divergent (blue) and conserved (pink) residues shown. The inset shows the residues involved in the ACE2 – SARS-CoV-2 RBD binding interface (highlighted). **(B)** Comparison of the RBD structures of SARs-CoV-2 and RaTG13 Spike proteins, with the inset highlighting key amino acid changes between SARS-CoV-2 (yellow) and RaTG13 (orange) that interact directly with ACE5. **(C)** A heatmap illustrating the receptor usage profile of SARS-CoV-2, SARS-CoV-1 and RaTG13 in entry assays (pseudotype and cell-cell fusion) with mammalian and bird ACE2s. The data in each row is normalised to human ACE2 (top row), and a pDISPLAY control was included to demonstrate specificity. **(D)** The specific amino acids that interact with ACE2 that were different between SARS-CoV-2 (top) and RaTG13 (bottom) were mutated to generate chimeric Spike proteins and examined in a cell-cell fusion assay on cells expressing human ACE2. Fusion activity was normalised to the level of fusion seen with the wildtype Spike, and green or red points indicating an increase or decrease in fusion, respectively. Data is representative of 3 individual replicates with a Student *t* test performed compared to WT (*p <0.05).

Building on previous work, and as part of my DPhil, I expanded our analysis of species tropism using a library of 15 bat sarbecovirus and 10 SARS-CoV-2 variant Spike proteins. I tested these Spikes with 35 different host ACE2 receptors which included human ACE2

(hACE2), 15 bat ACE2s and a panel of 18 ACE2s covering livestock, wildlife, companion animals and potential intermediate hosts. The ACE2s selected represent species that are implicated in SARS-CoV-2 zoonosis (e.g., *Rhinolophus* bats, pangolin, raccoon dog), or those that have acquired SARS-CoV-2 tropism following the emergence of new variants (e.g., mouse, white-tailed deer, mink) [31, 299, 305]. Furthermore, I also identified key amino acid residues within the RBD of these viruses that are deterministic in the receptor usage tropism we observed. Lastly, I assessed the antigenicity of these viruses using convalescent sera and monoclonal antibodies from SARS-CoV-2 infected individuals to understand the breadth of COVID-19-derived immunity against SARS-CoV-2 variants, or against other sarbecoviruses, i.e. to understand risk should they emerge in the human population. This seems a likely possibility given the previous outbreak of SARS-CoV-1 in 2002-2004, and because the discovery of other bat sarbecovirus with high genetic identity to human coronaviruses has demonstrated the ability of naturally circulating bat viruses to bind hACE2 with high affinity *in vitro* [303, 306].

The data outlined in Figures 4.2, 4.4 and 4.6 in this chapter for the Alpha, Beta, Gamma and Delta SARS-CoV-2 variants have been published in: Thakur N et al., SARS-CoV-2 variants of concern have extended ACE2 receptor host ranges (*Journal of General Virology,* 2024) [305]. Data for Omicron within these same figures is novel and I can confirm that I am listed as first author for this publication. All other data is yet unpublished and I conducted the majority of the experiments described and performed the data analysis. Where experiments were conducted by others, this has been indicated in the results, and included with permission of the author.

4.2 Results

4.2.1 Investigate the altered host range of SARS-CoV-2 variants for non-human mammalian ACE2s.

For SARS-CoV-2, the emergence of a D614G mutation in Spike gave rise to the B.1 lineage virus, which was responsible for the first wave of the COVID-19 pandemic. This was followed by subsequent waves of infections with genetically, and often antigenically, divergent D614G-containing SARS-CoV-2 variants. These included the Alpha, Beta, Gamma and Delta variants, and the phylogenetically distant Omicron variant, and its subvariants, defined by the introduction of a large number of mutations in the viral genome, particularly concentrated within the Spike protein. The structural maps shown in **Figure 4.2** highlight the amino acid differences between the variants of concern (VOC), mapped onto the wild-type ancestral strain of SARS-CoV-2 Spike (WT, PDB: 6XM4); each map shows individual Spike trimers in the down formation coloured in grey, black or a distinct colour to distinguish each variant (Alpha (B.1.1.7), red; Beta (B.1.351), green; Gamma (P.1), blue;

Delta (B.1.617.2), yellow; Omicron BA.1, purple, Omicron BA.2, pink), with the mutations present in these variants compared to WT labelled and highlighted in red (**Figure 4.2**; mutations sourced from https://covariants.org/).

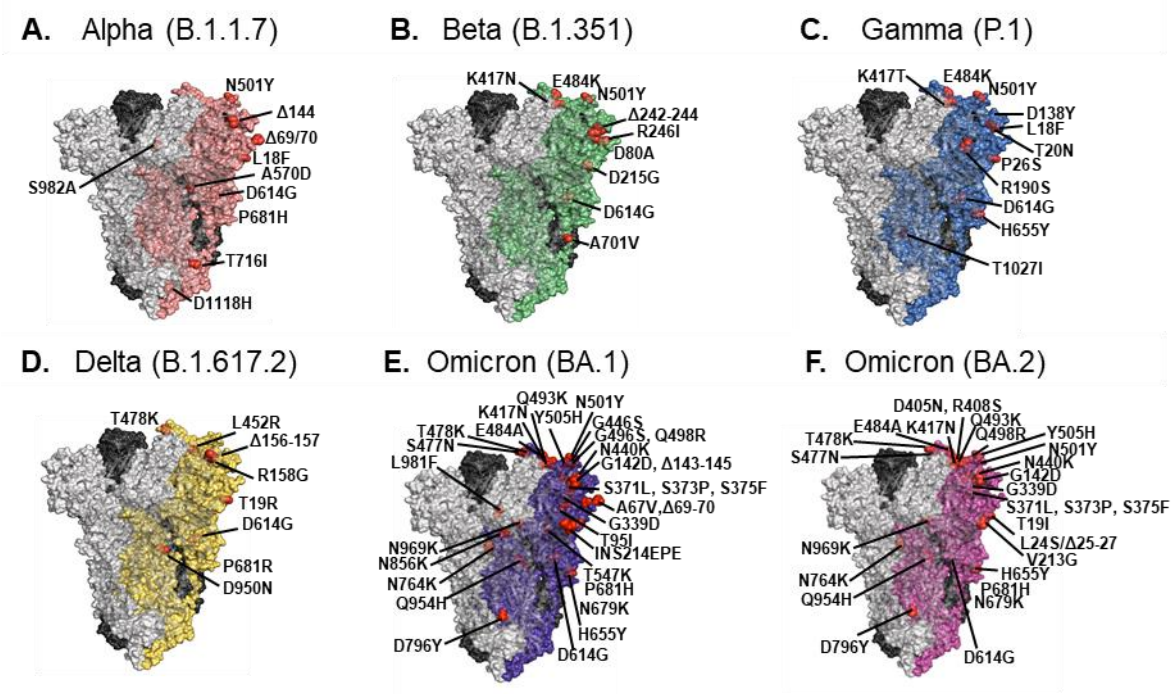

Figure 4.2: Emergence of SARS-CoV-2 variants of concern and their associated spike mutations (adapted from Thakur et al., *JGV* 2021).
Molecular surface representation of the trimeric spice protein is shown (PDB 6XM4), with each monomer shown in a different colour – grey, black, or differential colours to distinguish the **(A)** Alpha (B.1.1.7), red; **(B)** Beta (B.1.351), green; **(C)** Gamma (P.1), blue; **(D)** Delta (B.1.617.2), yellow; **(E)** Omicron (BA.1), purple; or **(F)** Omicron (BA.2), pink. The coloured monomer in each case is depicts mutations present in each variant compared to the lineage B wild-type SARS-CoV-2 strain, indicated by red spheres, and each individual mutation is labelled. Structures were generated in PyMOL.

Codon optimised variant Spike constructs were generated by site-directed mutagenesis, or synthesised into expression vectors, based on the SARS-CoV-2 lineage B, WT reference sequence, with an additional Δ19 truncation of the cytoplasmic tail. Schematics of the Spike constructs are shown in **Figure 4.3**, outlining the various domains within the monomeric Spike protein: the N-terminal S1 domain (which consists of the N-terminal domain (NTD) and RBD and a C-terminal S2 domain, separated by an S1/S2 furin cleavage site. Schematics are shown for B.1, Alpha, Beta, Gamma, Delta, Omicron BA.1, Omicron BA.2, and BA.2 sublineages BA.5, XBB, XBB1.5 and BA.2.86, with the mutations present in each of these variants annotated, relative to WT – the D614G mutation is highlighted in blue, RBD mutations in red, and mutations present in previous iterations of BA.2 are highlighted in grey (**Figure 4.3**). These constructs were made by Dr Thomas Peacock (Imperial College London) and distributed as part of the Genotype-to-Phenotype UK (G2P-UK) consortium.

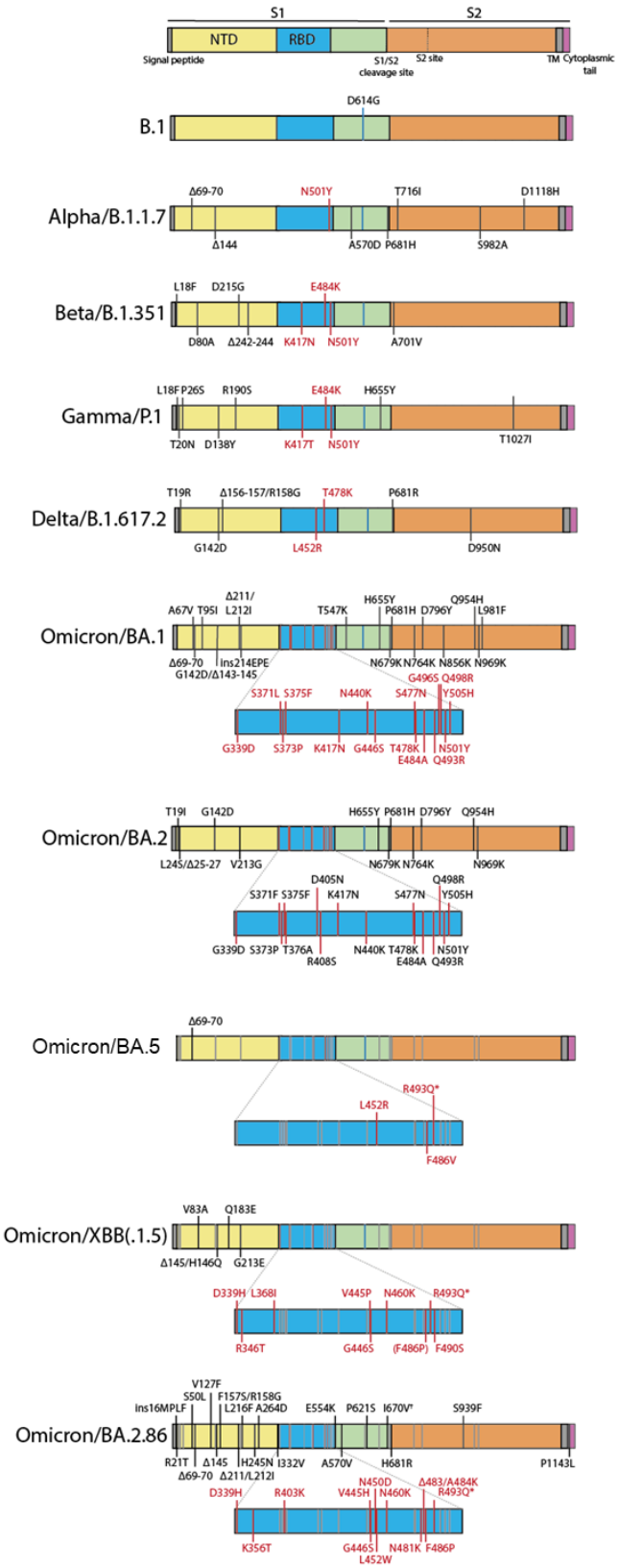

Figure 4.3: Schematics of SARS-CoV-2 variant Spike constructs.
Schematic of the Spike constructs for B.1, Alpha (B.1.1.7), Beta (B.1.351), Gamma (P.1), Delta (B.1.617.2), Omicron (BA.1, BA.2, BA.5, XBB, XBB1.5, BA.2.86). Key regions of the N-terminal domain (NTD), receptor binding domain (RBD), S1 and S2 are indicated, and the mutations, insertions and deletions present in each variant compared to WT are annotated. The D614G mutation is highlighted in blue. XBB, XBB1.5 and BA.2.86 are sub-lineages of BA.2, so common mutations are depicted by grey lines, with additional mutations labelled. These sub-lineages also have a reversion of the mutation at position 493 from R back to Q, indicated by an asterisk (*).

These variant Spike constructs were used to generate lentiviral-based pseudoviruses to assess whether SARS-CoV-2 variants exhibit altered species tropism compared to the WT or B.1 strain. We initially tested a subset of ACE2s, in addition to hACE2, where we have previously observed differences in host tropism [219], animals that could be potential reservoirs for virus (civet, intermediate host; rat, through excreted sewage) or animal models used to study SARS-CoV-2 transmission and pathogenesis (ferret, hamster, mouse).

ACE2s were overexpressed in BHK-21 cells – which are naturally refractory to SARS-CoV-2 infection – and infected with WT, Alpha, Beta, Gamma, Delta and Omicron BA.1 pseudoviruses, and virus entry measured by quantifying luciferase signals. As with previous findings, mouse and rat ACE2 usage was restricted with WT virus, but significant increases in entry were observed for mouse ACE2 with all variants, and with Alpha, Beta and Gamma for rat ACE2 (**Figure 4.4**). Human, civet and ferret ACE2 exhibited significantly higher levels of entry with Beta compared to WT (**Figure 4.4B**). Additionally, ferret ACE2 usage was marginally greater with Alpha and Delta, but also significantly enhanced with Gamma (**Figure 4.4A, C and D**). There was no significant difference in pig or hamster ACE2 usage by these variants, apart from for hamster ACE2 with Omicron BA.1, which interestingly, showed a significant reduction in ACE2 usage compared to WT (**Figure 4.4E**).

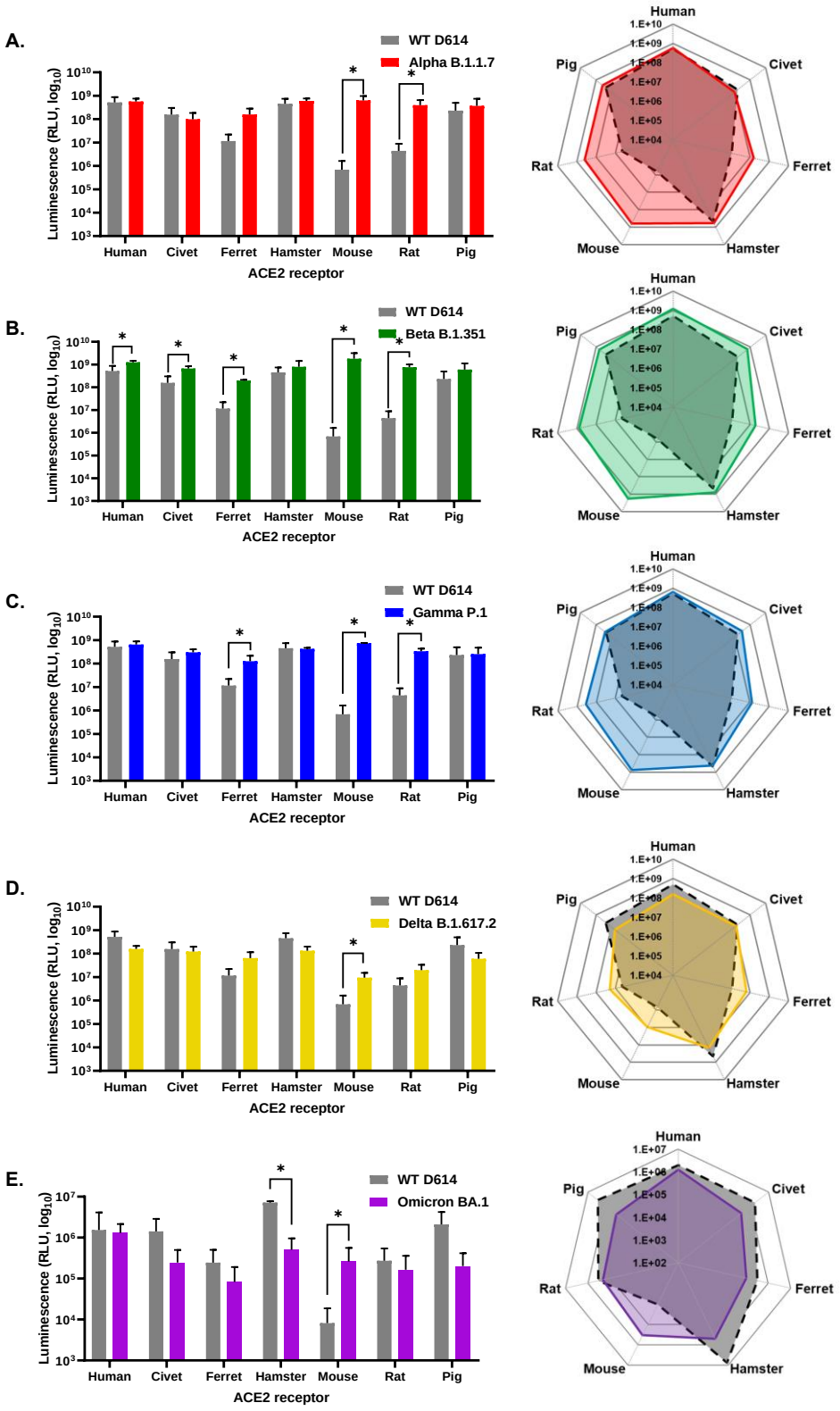

Figure 4.4: ACE2 receptor usage with SARS-CoV-2 variant spikes show altered species tropism (adapted from Thakur et al., *JGV* 2021).
Receptor usage of SARS-CoV-2 variant spikes pseudotypes **(A)** Alpha (B.1.1.7), **(B)** Beta (B.1.351), **(C)** Gamma (P.1), **(D)** Delta (B.1.617.2) and **(E)** Omicron BA.1, compared to wildtype SARS-CoV-2 (WT) with BHK-21 cells overexpressing human, civet, ferret, hamster, mouse, rat and pig ACE5. Viral entry is shown by luciferase activity. The right panels show the same data replotted as radar plots, with the grey plots indicating the receptor usage for WT, and the coloured plots depicting the change in receptor usage. Each experiment was conducted on 3 separate occasions, with the mean luciferase values shown. Statistical significance was measured using a Students *t*-test compared to WT (*p <0.05).

As previously stated, the WT strain of SARS-CoV-2 was quickly replaced by the D614G-containing B.1 strain, from which all subsequent SARS-CoV-2 variants ultimately originated from. We further expanded our ACE2 library and tested a broader range of variants to assess shifts in host range compared instead to the B.1 virus, to reflect the post-human emergence era. The expanded ACE2 library consisted of 16 bat ACE2 receptors selected based on previously published data [73] which showed varied levels of WT SARS-CoV-2 pseudovirus entry with a panel of bat ACE2 orthologues. This included ACE2s from *Rhinolophus* species where SARS-CoV-2 is suspected to have originated (*Rh. cornutus, Rh. pusillus, Rh. macrotis, Rh. sinicus, Rh. pearsonii, Rh. affinis, Rh. shameli, Rh. ferrumequinum, Rh. Alcyone*), and representative bat species from other families (*L. lyra, P. giganteus, R. leschenaultii, T. melanopogon, D. rotundus, A. pallidus and M. lucifugus).* Moreover, a range of 19 other animals were selected to test in addition to hACE2, including some of the animals tested previously with WT, to understand whether there are any differences in ACE2 usage with B.1. The Chinese hamster sequence was also replaced with the Syrian hamster sequence (97% amino acid identity), which is the primary animal model used to study SARS-CoV-2 transmission. To this end, ACE2s were tested from livestock/pets (dog, cat, pig), rodents (mouse, rat, Syrian hamster), potential intermediate reservoirs (red fox, civet, ferret, pangolin, mink, raccoon dog, white-tailed deer, red deer), and monkeys (marmoset, squirrel monkey, lemur, macaque).

Initially, receptor screens were carried out with SARS-CoV-2 variants with a panel of bat ACE2s to try to better understand the likely natural host of WT SARS-CoV-2, but also to determine whether other bat species could support entry of SARS-CoV-2 variants that act as reservoirs for reverse zoonoses. Varied levels of entry were noted compared to hACE2, observing an increased fold change in bat ACE2 usage with the Alpha, Beta and Delta variants to equivalent or greater levels than was detected for hACE2. The greatest increase in bat ACE2 tropism was seen with Omicron BA.1 and to a lesser degree, with Omicron BA.5. Interestingly, the converse was observed with many of the other Omicron variants tested (BA.2, XBB, XBB.1.5 and BA.2.86), with a reduction or complete loss of receptor usage of several bat ACE2 species, relative to hACE2 as compared to B.1 (**Figure 4.5, top panel**). In contrast, the species tropism for mammalian ACE2s with different SARS-CoV-2 variants remained broad, with restrictions in virus entry seen for only a few variants with new world monkey ACE2s (marmoset and squirrel monkey) and ferret ACE2, relative to hACE2 (**Figure 4.5, bottom panel**). For the animal ACE2s we had tested previously with WT SARS-CoV-2 in **Figure 4.1** (indicated by an asterisk in **Figure 4.5**), a similar trend in ACE2 usage was observed with B.1, indicating that the D614G mutation does not play a significant role in host tropism.

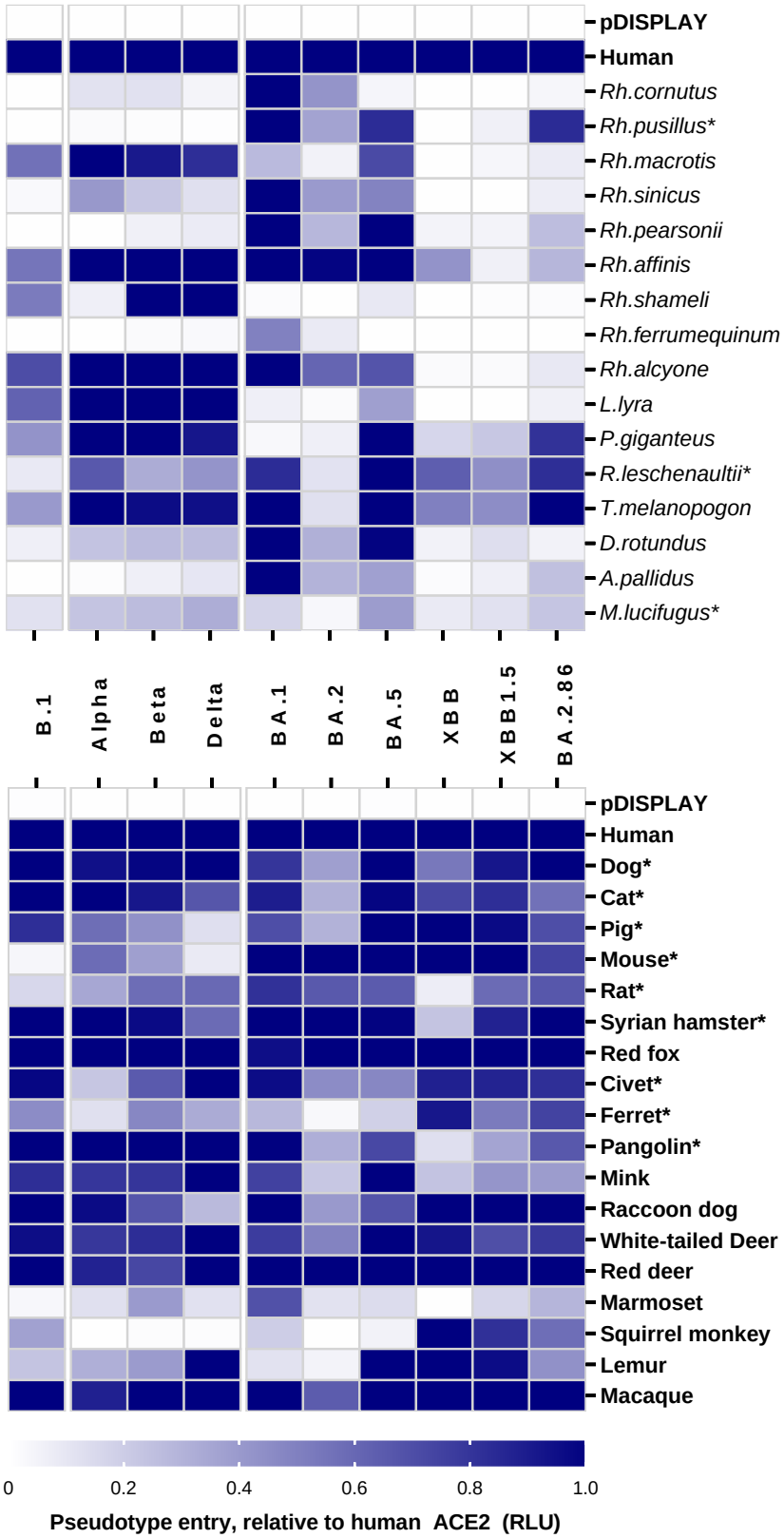

Figure 4.5: SARS-CoV-2 Spike variants show restricted usage of bat ACE2 receptors, but broad species tropism of mammalian ACE2 receptors.
Heatmap showing the bat (top) and mammalian (bottom) ACE2 usage of SARS-CoV-2 variant Spike pseudotypes with B.1, Alpha, Beta, Delta, BA.1 and BA.2 and its subvariants (BA.5, XBB, XBB.1.5, BA.2.86). Data is shown as the mean fold change in pseudotype entry, relative to human ACE2. Data is representative of 3 independent replicates, which the mean luciferase data shown. The baseline value of 1 indicates entry equivalent to human ACE2, with an increase in entry shown in blue, and decrease transitioning to white. * indicates receptors that have been examined in previous studies and were tested again here [219, 305].

4.2.2 Determining key mutations in the RBD responsible for changes in SARS-CoV-2 variant species tropism.

The genetic determinants responsible for the altered species tropism observed with SARS-CoV-2 variants were investigated, particularly focusing on the mutations present within the RBDs of Alpha and Omicron BA.1 that directly interact with sites on ACE2 (**Figure 4.3**). For Alpha, an increase in host range was observed for mouse and rat ACE2, but not for civet ACE2 (**Figure 4.4**). The Alpha variant evolved a single mutation at position 501 in SARS-CoV-2 RBD from an asparagine to a tyrosine (N501Y). Sequence analysis revealed that residue 501 in Spike RBD interacts with amino acid positions N41 and K353 in hACE2, which instead is replaced by a histidine in mouse and rat ACE2 (H353). This could explain the limited ACE2 usage of WT SARS-CoV-2 with these rodent receptors as the histidine residue at position 353 in rodent ACE2 forms shorter side chains, which disrupts hydrogen bonds and hydrophobic interactions with side chains of G496 and Q498 in the RBD (**Figure 4.6A**) [219].

Changes in SARS-CoV-2 host range could result in the emergence of new intermediate hosts that could allow further mutations to arise in the virus through adaption of its new host or could act as amplification reservoirs for sustained virus transmission. To functionally examine the role of amino acid changes in Spike in overcoming host range restrictions, receptor usage screens were performed with plasmids expressing mutations built into a WT SARS-CoV-2 background, selecting mutations across the whole Spike found in Alpha: Δ 69/70, Δ144 (NTD), N501Y (RBD), P618H (furin cleavage site) (mutant plasmids were generated by Dr Thomas Peacock, Imperial College London, UK). Lentiviral-based psuedotypes expressing these mutant Spike plasmids were used to infect cells overexpressing mouse, rat or civet ACE2. For both mouse and rat ACE2, the N501Y change was sufficient to overcome the restriction observed with WT pseudovirus with these receptors, allowing entry equivalent to Alpha, with a ~1.6 log and ~3 log increase in pseudtype entry observed for mouse and rat ACE2, respectively, relative to WT (**Figure 4.6B and C**). Changes to the furin cleavage site (P618H) or deletions of in the NTD (Δ 69/70, Δ144) appeared to have little effect on entry; of note the Δ69/70 mutation was examined in an N501Y-containing background, which could potentially obscure the standalone effects of the Δ69/70 mutation (**Figure 4.6B and C**). None of the mutations present in Alpha increased use of civet ACE2 – in fact, the mutations appeared to have an inhibitory effect on entry, with up to ~1log decrease in entry observed, relative to WT (**Figure 4.6D**).

A.

SARS-CoV-2 RBD binding sites	K417	E484	Q493	Q493	Y505	G496 Q498	Q498 N501	Q498	N501 Y505	Y505	Y505
ACE2 binding sites	30	31	34	35	37	38	41	42	353	354	393
Human	D	K	H	E	E	D	Y	Q	K	G	R
Mouse	N	N	Q	E	E	D	Y	Q	H	G	R
Rat	N	K	Q	E	E	D	Y	Q	H	G	R
Civet	E	T	Y	E	Q	E	Y	Q	K	G	R

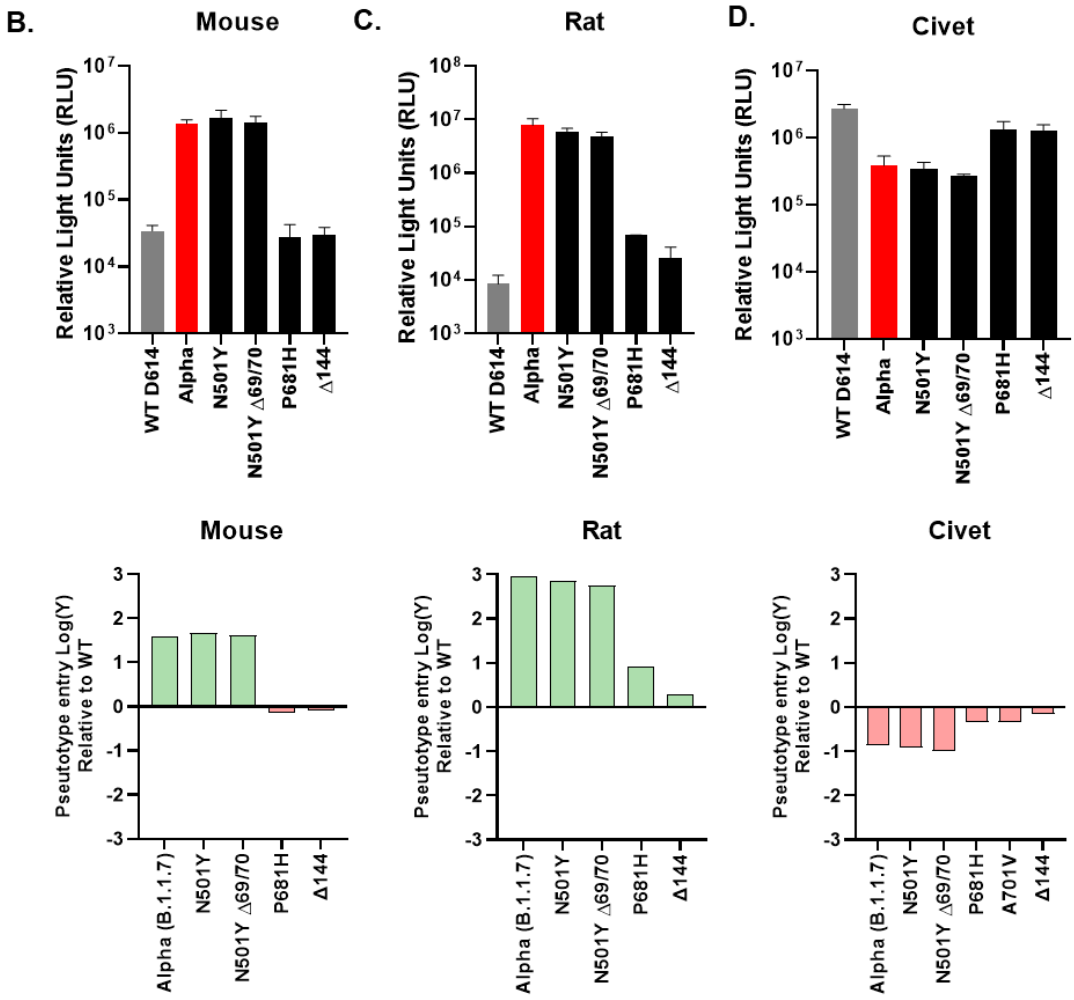

Figure 4.6: Mutational analysis of the WT SARS-CoV-2 RBD identifies the N501Y mutation as critical for extending rodent ACE2 usage. (adapted from Thakur et al., *JGV* 2021).
(A) Table highlighting SARS-CoV-2 amino acids and the interacting residues in human ACE2. The ACE2 amino acids at these positions have been listed for human, mouse, rat and civet ACE2, with the red boxes highlighting residues that interact with position 501 in Spike. The entry efficiency of pseudotypes bearing SARS-CoV-2 spikes with individual or combinations of mutations found in Alpha for **(B)** mouse, **(C)** rat and **(D)** civet ACE2-expressing cells, compared to WT SARS-CoV-2 (grey bar) or Alpha (red bar). The mean relative light unites (RLU) (middle panel) of three individual experiments are shown, with error bars representing mean + SD. The bottom panel shows pseudotype entry relative to WT for Alpha or mutant pseudoviruses with mouse, rat and civet ACE2, with green or pink bars representing and increases or decreases in entry, respectively.

Due to the significant differences in entry seen with the bat ACE2s infected with B.1 and Omicron BA.1 pseudotypes (**Figure 4.5**), the varying amino acid residues between these two variant Spike proteins was also investigated. Compared to B.1, Omicron BA.1 has a significant number of amino acid substitutions in the Spike protein, exhibiting 13 mutations in the RBD alone (**Figure 4.3**). Again, I focused on those RBD residues that interact directly with ACE2, and those that have been previously documented to contribute to altered

species tropism [219, 307]. To this end, mutants of B.1 were generated and introduced changes at positions 417, 484, 493 and 501 in the Spike proteins, either individually or in combination with other mutations (K417N, E484A, Q393R, N501Y) and it was observed that all mutants were functional when titrated on cells stably-expressing hACE2 (**Figure 4.7A**).

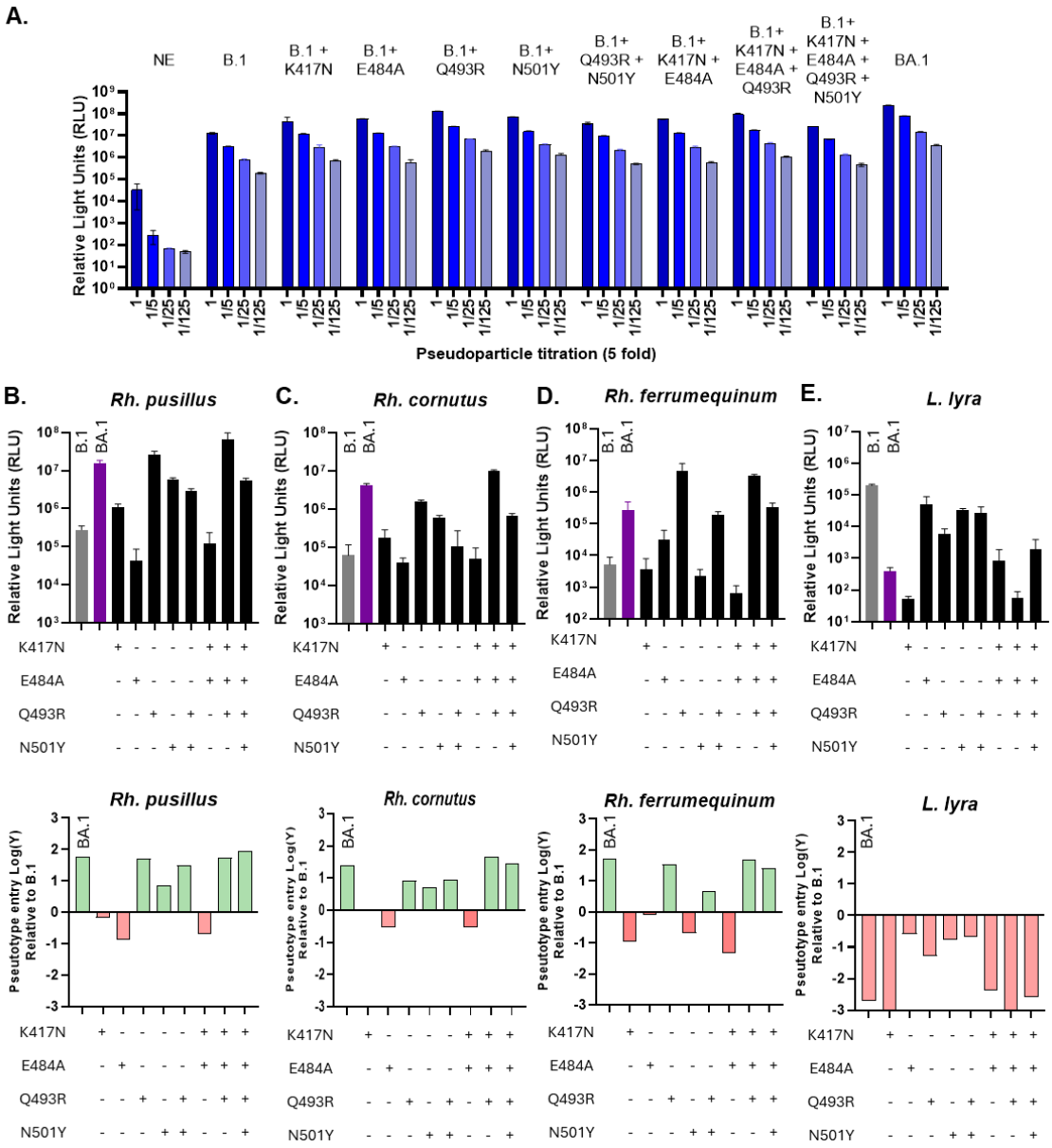

Figure 4.7: Mutational analysis of the B.1 RBD identifies key residues in Omicron BA.1 that contribute to altered bat ACE2 usage.
(A) Infection of HEK293T cells stably expressing hACE2 with SARS-CoV-2 B.1 and BA.1 pseudoparticles, along with individual mutants generated with mutations at positions 417, 484, 493 and 501, either singly or in combination. Virus was titrated 5-fold on cells and Firefly luciferase signals measured (relative light units, RLU); a negative control (non-enveloped, NE) was also included. Specific amino acids within the B.1 RBD were mutagenised to make the RBD more BA.1-like, introducing the K417N, E484A, Q493R or N501Y mutations, either by themselves or in combination. Entry of these mutants was tested with **(B)** *Rh. pusillus,* **(C)** *Rh. cornutus,* **(D)** *Rh. ferrumequinum*, and **(E)** *L. Lyra* ACE2s and compared to WT SARS-CoV-2 (grey bar) or Omicron BA.1 (purple bar). The mean relative light units (RLU) (middle panel) of three individual experiments are shown, with error bars representing mean + SD. The bottom panel shows pseudotype entry relative to B.1 for BA.1 or mutant pseudoviruses for the same bat ACE2s, with green or pink bars representing increases or decreases in entry, respectively.

The entry phenotype of these mutants was then assessed with representative bat ACE2s that showed an increase (*Rh. cornutus, Rh. pusillus, Rh*. *ferrumequinum*) or a decrease in receptor usage (*L. lyra)* with BA.1 compared to B.1 (**Figure 4.5**). Whilst the K417N and E484A mutants on their own, or in combination, had no impact on receptor tropism, the Q493R and N501Y mutations, either in isolation or in combination with other mutations, resulted in increased receptor usage of *Rh. pusillus* (~1.8log) and *Rh. cornutus* (~1.4log), compared to B.1 (**Figure 4.7B and C**). The Q394R mutation alone, or in combination with other mutations appeared to be sufficient to increase *Rh. ferrumequinum* ACE2 usage (~1.7log) (**Figure 4.7D**). For *L. lyra*, a decrease in receptor usage was observed when all 4 mutations were present, which appeared to be dominated particularly by a change at position 417 (~4.7log) (**Figure 4.7E**). Together, these data examining the rodent ACE2 restrictions with Alpha and the bat ACE2 restrictions with Omicron BA.1 highlight the importance of RBD-mutations in altering and extending the ACE2 species tropism of SARS-CoV-2 variants.

4.2.3 Assessing the receptor usage of bat sarbecoviruses with different bat and mammalian ACE2 species.

I next wanted to determine the ACE2 receptor usage of other bat sarbecoviruses to understand if they also exhibit broad tropism like SARS-CoV-2, which could suggest that these viruses also have the propensity to spill-over into an animal or human population. Spike sequences were selected of 110 bat sarbecoviruses from NCBI and aligned their RBD amino acid sequences, revealing these viruses cluster phylogenetically into distinct clades. This includes clade Ia viruses, which account for 13.6% of the 110 sequences analysed (yellow), clade Ib viruses (6.7%, orange), clade II viruses (57%, blue), clade III viruses (11.8%, green), clade IV viruses (10%, purple), and a clade V virus (0.9%, red). (**Figure 4.8A**). Representative viruses from each clade were selected for analysis (highlighted in red) based on experimental data in publications [72, 75, 216, 301]. The viruses have been isolated primarily in Asia (clade I, II, IV and V), and in parts of Europe and Africa (clade III), coloured in blue on the world map shown, with other sarbecoviruses included in the initial phylogenetic tree also labelled (**Figure 4.8B**). The bat species these that viruses have been isolated from are globally widespread, with shaded areas depicting their existing geographic distribution (**Figure 4.8B**). The Rhinolophus species have been grouped together and it should be noted that the *Rhinolophus* (teal)*, P. giganteus* (yellow)*, L. lyra* (purple)*, R. leschenaultia* (green) *and T. melanaopogon* (red) bat species overlap in their geographic distribution, particularly in Southeast Asia, whereas the *D. rotundus* (blue)*, A. pallidus* (orange) and *M. lucifugus* (pink) species intersect in their range in the Americas (**Figure 4.8B**).

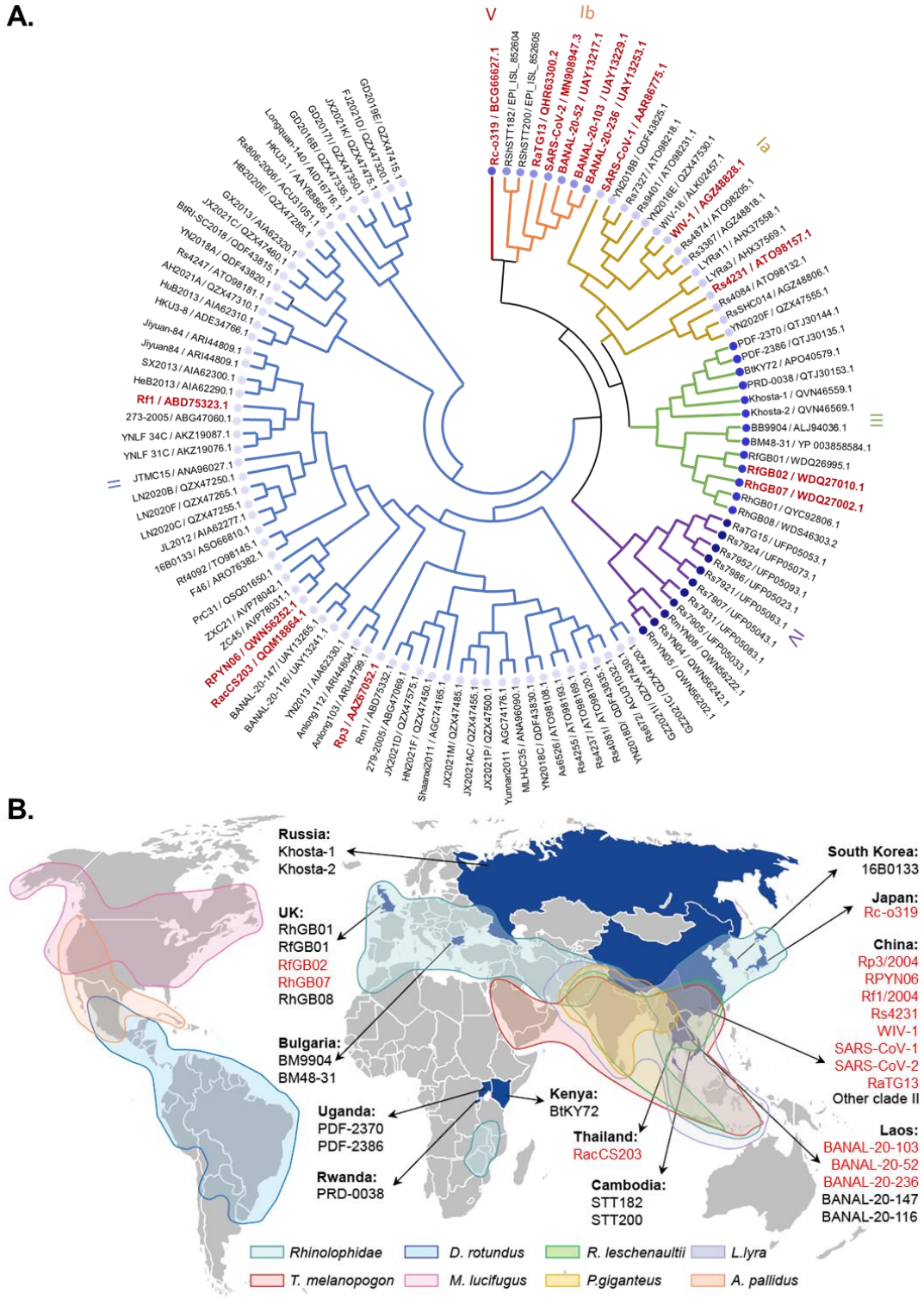

Figure 4.8: Phylogeny and geographic distribution of bat sarbecoviruses.

(A) Evolutionary history of bat sarbecovirus RBDs (NCBI reference shown for 110 amino acid sequences) was inferred by using the Maximum Likelihood method and Whelan and Goldman model. Initial tree(s) for the heuristic search were obtained automatically by Neighbour-Join and BioNJ algorithms estimated using the JTT model with discrete Gamma distribution (5 categories (+G, parameter = 0.3460)) [308]. Evolutionary analyses were conducted in MEGA 11 [309]. Of note, the HKU3-7 and HKU3-8, and the HKU3-1, 2, 3, 4, 5, 6, 7, 9, 19, 11 and 12 Spike sequences are identical, so the HKU3-8 and HKU3-1 sequences were used as representatives, respectively. Bat sarbecovirus clades are shown: clade Ia (yellow), clade Ib (orange), clade II (blue), clade III (green), clade IV (purple) and clade V (red). Spike sequences were acquired from GenBank, based on published data [69, 74, 216, 291, 303, 306]. **(B)** World map highlighting the geographic location where the sarbecoviruses included in (A) were first isolated (coloured in blue), along with the distribution of the bat species these were isolated from (https://www.iucnredlist.org/). Viruses selected for analysis in this study are highlighted in red.

The selected bat sarbecoviruses were aligned by their RBD sequences and include SARS-CoV-1, WIV-1 and Rs4231 (clade Ia), SARS-CoV-2, RaTG13, BANAL-20-52, BANAL-20-236 and BANAL-20-103 (clade Ib), RacCS203, RPYN06, Rf1/2004 and Rp3/2004 (clade II), RhGB07, RfGB02 (clade III) and the clade V virus Rc-o319. Clade IV viruses were not included in this analysis due to the unavailability of Spike sequences at the time of virus selection (**Figure 4.9A**). These bat sarbecoviruses show high levels of divergence at the RBD-ACE2 binding interface when compared to the SARS-CoV-2 RBD (PDB 7UL0), in particular deletions at positions 446, 449 and 486 in the clade II viruses and a single deletion at position 449 in the clade III viruses (**Figure 4.9B and C**). Full-length Spikes were subsequently synthesised and codon optimised for mammalian expression in a pcDNA3.1 vector backbone with a c-terminal FLAG tag; RhGB07 and RfGB02 were untagged (synthesised and distributed by Dr Kelvin Lau, EPFL, Switzerland).

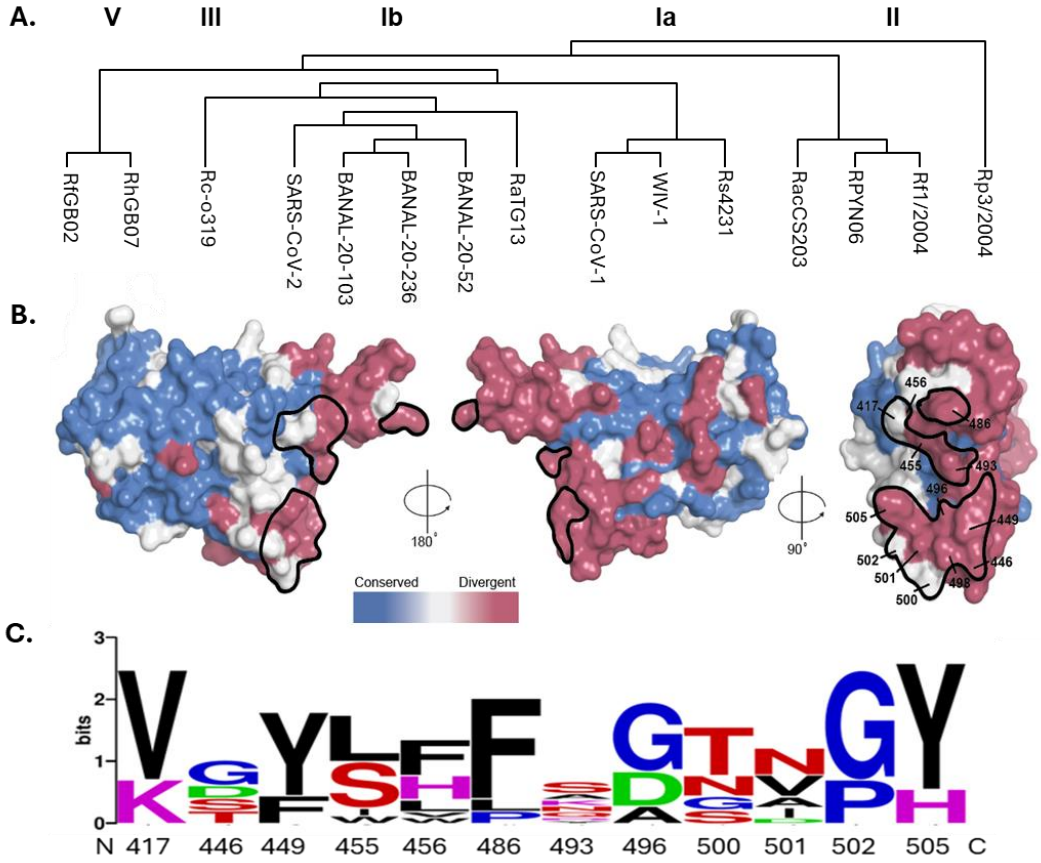

Figure 4.9: Bat sarbecovirus RBDs are highly divergent.
(A) Phylogenetic tree of ACE2 proteins assembled using the Maximum Likelihood method and Whelan & Goldman model conducted in MEGA11 (Temple University, USA) [308, 309]. The tree is drawn to scale, with the highest log likelihood (-2118.09) shown, obtained by applying Neighbor-Join and BioNJ algorithms estimated using the JTT model with a discrete Gamma distribution (5 categories, +G parameter = 0.4154). **(B)** Structural map of SARS-CoV-2 Spike RBD (PDB 7UL0) mapped with conserved (blue) and divergent (pink) amino acid residues of the bat sarbecovirus RBDs under investigation. The ACE2- binding sites are also outlined in black in 3 conformations, and binding residues are labelled. **(C)** WebLogo (University of California, Berkeley, USA) plots summarising the amino acid divergence at the ACE2-binding interface within the bat sarbecovirus RBDs. The single letter amino acid code is used with vertical height representing prevalence at each position are colour representing similar physiochemical properties (pink = positive charge, green = negative charge, red = uncharged, black = hydrophobic, blue = other). Deletions are represented by an "X" and were disregarded from the analysis.

To assess the bat species tropism of these different sarbecoviruses, a receptor usage screen was conducted in cells overexpressing a library of ACE2 receptors, including the 16 bat ACE2 orthologues described, along with hACE2. BHK-21 cells overexpressing these receptors were infected with different bat sarbecovirus Spike-based pseudotypes. Prior to this, I ensured sufficient entry and expression of the pseudotyped bat sarbecovirus Spike proteins. To do this, pseudoviruses were titrated five-fold on HEK293T cells stably expressing hACE2, starting with neat pseudovirus. Compared to the negative control (non-enveloped, transfected with a pcDNA3.1 control vector), high levels of entry were detected with SARS-CoV-2, BANAL-20-52, BANAL-20,236, BANAL-20-103, SARS-CoV-1 and WIV-1, and moderate entry with RaTG13, Rs4231 and RhGB07; no entry was detected with RfGB02, Rc-o319, RPYN06, RacCS203, Rp3 and Rf1 (**Figure 4.10A).** Since entry was not detected for some sarbecovirus Spikes, to confirm that these Spike had been incorporated into the pseudovirion, protein expression levels were also confirmed in lysates from pseudovirus producer cells for both SARS-CoV-2 Spike and the FLAG-epitope tag. FLAG expression was detected for all Spikes to varying levels. Blotting with an anti-SARS-CoV-2 Spike antibody was able to cross-detect most of the other sarbecovirus Spike proteins, either as full-length (S) or cleaved (S1/S2) Spike. RhGB07 and RfGB02 are not FLAG-tagged but were detected by the anti-Spike antibody (**Figure 4.10B**). BHK-21 cells overexpressing bat ACE2 receptors were used to assess protein expression using the encoded HA-epitope tag by immunoblotting. Lysates were probed with an anti-HA antibody which showed good expression of all HA-tagged bat ACE2 proteins (**Figure 4.10C**).

Receptor tropism of viruses here has been defined as either being broad and able infect several different species within different mammalian orders (i.e., a generalist), or viruses are restricted to use of one or a small number of species receptors from distinct animal orders (i.e., a specialist) [220]. This study revealed that clade Ib viruses, which includes SARS-CoV-2, are more generalist in their bat ACE2 usage and demonstrate broad receptor tropism, with RaTG13 being a notable exception. Clade Ia, III and V viruses are more specialist in their ACE2 usage, primarily using their cognate bat ACE2, i.e., the host receptor from which these viruses were isolated, highlighted with a red square. For example, Both WIV-1 and Rs4231 were isolated from *Rh. sinicus*, and both viruses showed robust usage of this ACE2 receptor. Clade II viruses were unable to use any of the bat ACE2 receptors tested (**Figure 4.11A**). The absence of a red square is indicative of the lack of a cognate receptor in our screen, either due to the unavailability of an ACE2 sequence, or because the original bat host is yet unknown (RhGB07: *Rh. hipposideros*; SARS-CoV-2, SARS-CoV-1: unknown; BANAL-20-52: *Rh. malayanus*; BANAL-20-236: *Rh. marshalli*; RacCS203 – *Rh. acuminatus*).

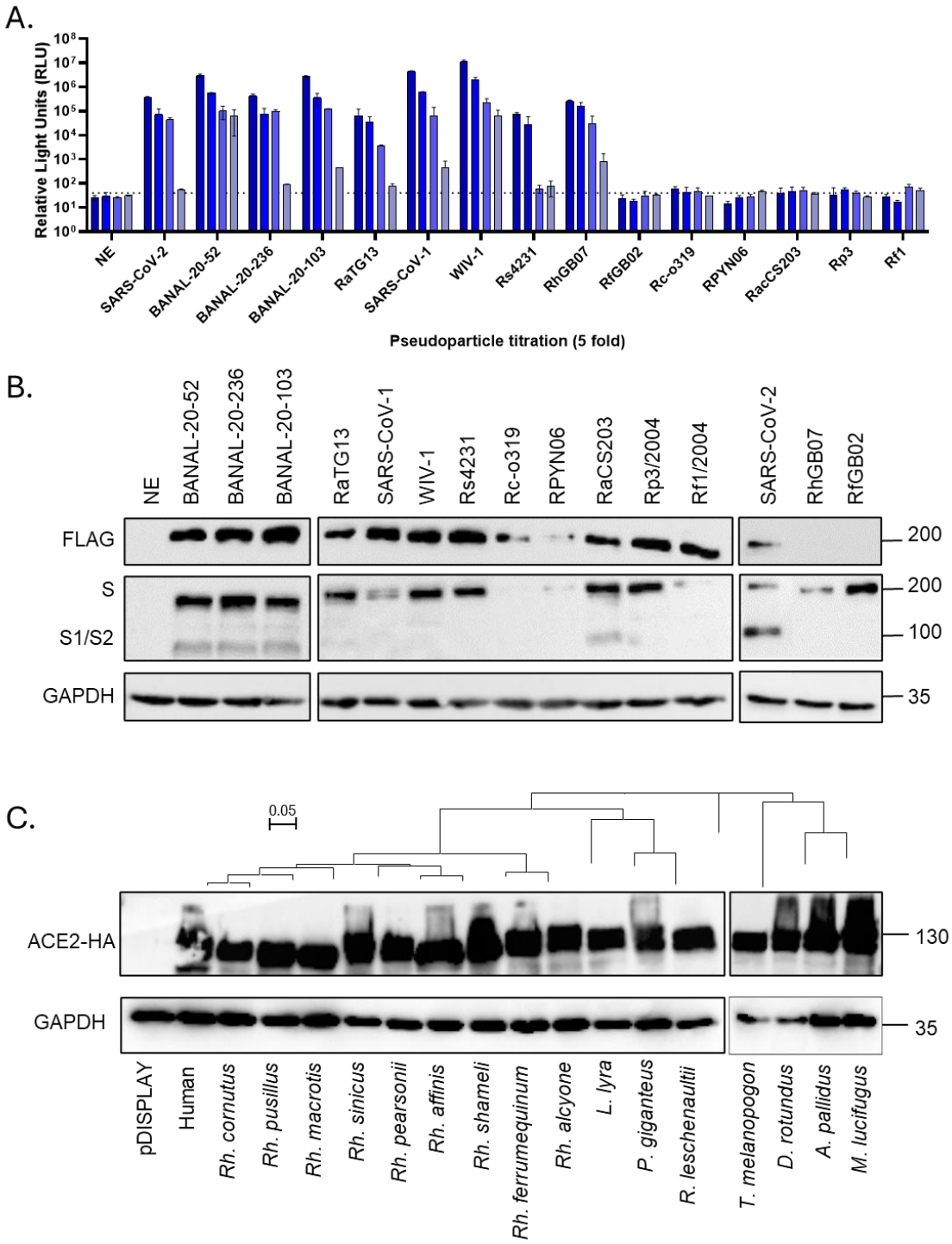

Figure 4.10: Assessing the expression of bat sarbecovirus Spike and bat ACE2 constructs.
(A) Bat sarbecovirus Spikes expressed in a lentiviral-based pseudotype system were titrated on HEK293T cells stably expressing human ACE2. Pseudoviruses were titrated five-fold, starting at neat ceoncentration, and Firefly luciferase signals measures (relative luciferase units, RLU). A non-enveloped (NE, no Spike) negative control was included to establish background luciferase signals (dotted line), and error bars represent the mean ± standard deviation of 3 triplicate values. Immunoblots from SDS-PAGE gels of lysates from **(B)** producer cells of lentiviral pseudotypes, blotted with an anti-FLAG and anti-SARS-CoV-2 Spike (full-length Spike, S; cleaved Spike, S1/S2) antibody or **(C)** BHK-21 cells transfected with bat ACE2 orthologues blotted with an anti-HA antibody. Anti-GAPDH was used as an internal loading control, and mock samples (NE for Spike, pDISPLAY for ACE2) were included to show specific expression. Values indicate predicted size in kDa of the proteins.

Coronaviruses are also known to induce cell-cell fusion causing the formation of multinucleated syncytia. Therefore, we also measured bat sarbecovirus usage of bat ACE2 receptors in a quantitative cell-cell fusion assay, which showed a similar trend of broad host range for the clade Ib viruses, and narrower host range for the clade Ia, III and V viruses. Again, fusion was note detected with the clade II viruses (**Figure 4.11B).** This cell-cell fusion assay also showed high concordance with the pseudotyped-based entry assay by Pearson's correlation (RfGB02: r= 0.8244, p<0.0001; RhGB07: r=0.9335, p<0.0001; Rc-o319: r=0.9467, p<0.0001; SARS-CoV-2: r = 0.6684, p=0.0024; BANAL-20-103: r=0.5308, p=0.0234; BANAL-20-236: r=0.6096, p=0.0072; BANAL-20-52: r=0.7343, p=0.0005; RaTG13: r=0.7719, p=0.0002; SARS-CoV-1: r=0.9005, p<0.0001; WIV-1: r=0.7724, p=0.0002; Rs4231: r=0.8259, p<0.0001) (**Figure 4.11C**).

Due to the broad receptor usage we observed with bat sarbecoviruses and different bat ACE2s, the receptor tropism and spillover potential of these viruses was also assessed with other mammalian ACE2s to understand whether the pattern of specialist vs generalist ACE2 usage extended to a wider selection of mammalian ACE2s. The receptor tropism was assessed of bat sarbecovirus Spikes for the mammalian ACE2s initially screened in **Figure 4.5**, excluding the clade II viruses that do not use ACE2. Similar to what was observed with the bat ACE2s, clade Ib viruses exhibited broad tropism for the majority of mammalian ACE2s tested, with notable restrictions for SARS-CoV-2 with mouse, rat, ferret, mink, marmoset and squirrel monkey ACE2. RaTG13 also appeared to have restricted mammalian ACE2, as did the clade III viruses RfGB02 and RhGB07. Unlike with bat ACE2s, clade Ia viruses appeared to also have broad mammalian ACE2 receptor usage, and interestingly, Rc-o319 did not use any of the mammalian ACE2s tested (**Figure 4.12A**). These mammalian ACE2 receptor orthologues show high levels of divergence in ACE2 at the RBD-ACE2 binding interface, in particular at amino acid positions 24, 30, 31, 32, 41, 52, 79, 82, 353 and 354 (**Figure 4.12B**).

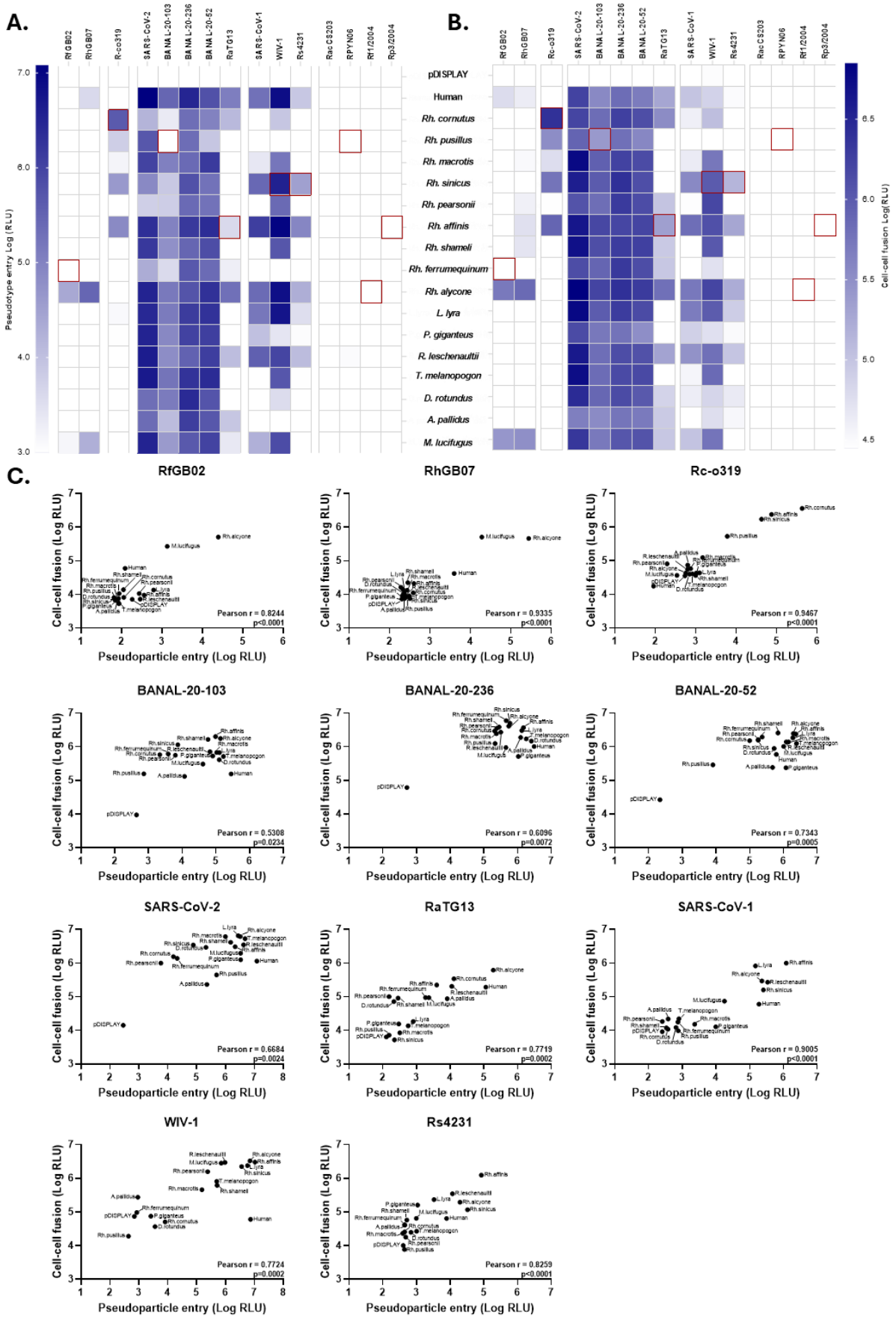

Figure 4.11: Assessing the human and bat ACE2 tropism of bat sarbecovirus Spike pseudotypes. Heatmaps illustrating receptor usage are shown for two entry assays, representing the mean log RLU of 3 separate experiments. A vector only control (pDISPLAY) was included to demonstrate specificity and to set the

background signal. The cognate bat receptor for each virus, where possible is highlighted with a red box. **(A)** Bat sarbecovirus Spikes were used to generate lentiviral-based pseudotypes and used to infect BHK-21 cells overexpressing different bat ACE2s or human ACE2. **(B)** Cell-cell fusion was measured of bat Sarbecovirus Spikes with bat ACE2 receptor orthologues using a split GFP-*Renilla* luciferase system. **(C)** XY scatter plots for each of the pseudoviruses, correlating the log(RLU) of pseudoparticle entry (X) against cell-cell fusion entry (Y). Clade II viruses that do not use ACE2 as their entry receptor were excluded. Each data point is labelled with the corresponding ACE2 receptor and a Pearson's correlation calculated with 95% confidence intervals (Pearson r value and p value are shown).

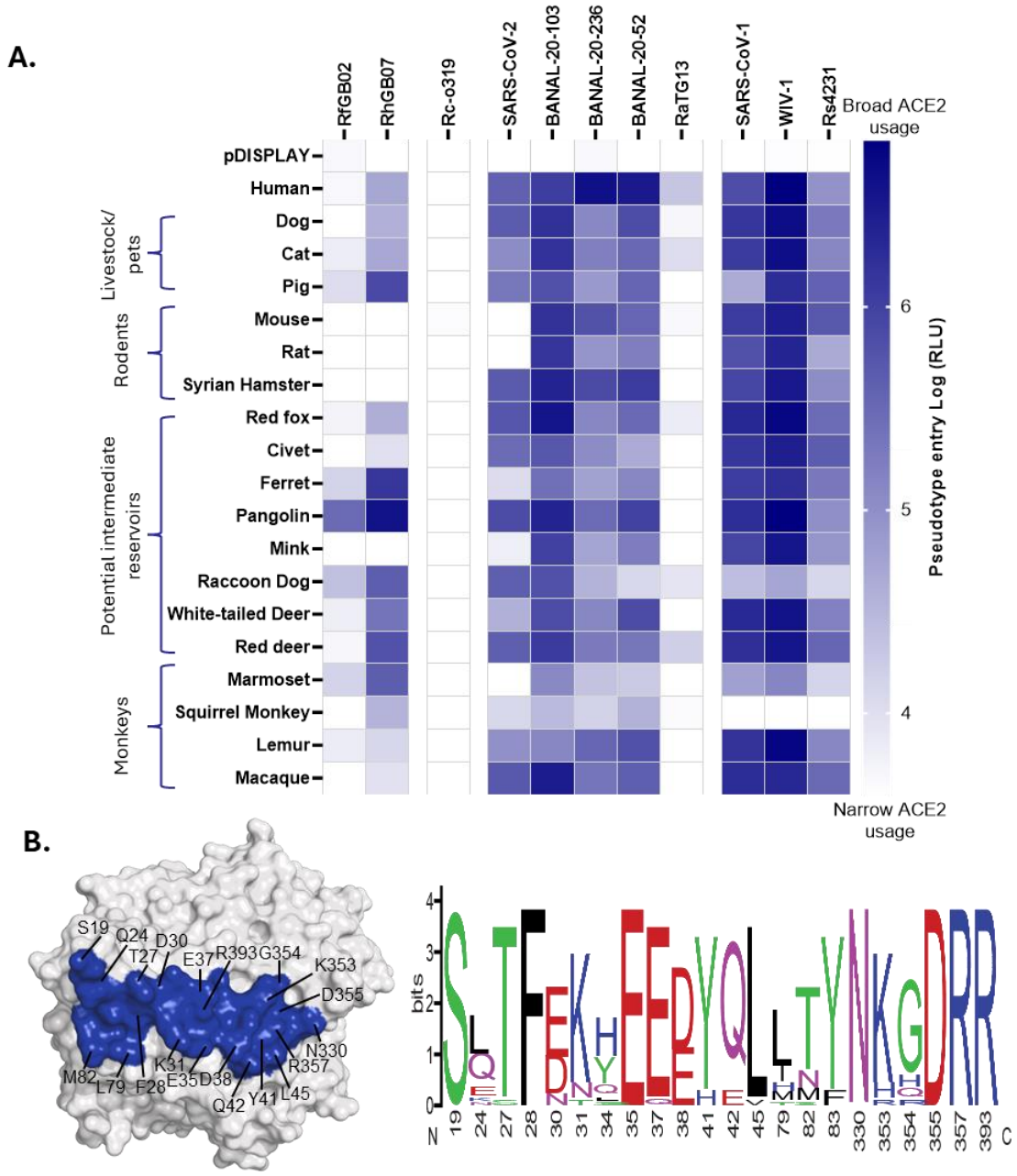

Figure 4.12: Assessing the mammalian ACE2 tropism of bat sarbecovirus Spike pseudotypes.
(A) Heatmap showing the receptor usage of bat sarbecovirus pseudotyped viruses with mammalian ACE2s, including human, livestock/pets, rodents, potential intermediate hosts and monkeys. The mean log RLU is shown of 3 separate experiments and a pDISPLAY control was included to determine the background levels of entry. **(B)** Structural map of human ACE2 (PDB 6M0J) mapped (generated in PyMOL) with the residues that make contact with the SARS-CoV-2 RBD-binding site. WebLogo (University of California, Berkley, USA) plots summarising the amino acid divergence within the mammalian ACE2 sequences in this screen. The single letter amino acid code is used with the vertical height presenting the frequency of each amino acid at that position. The positions at which ACE2 interacts with SARS-CoV-2 RBD are shown from N-terminal to C-terminal, with the different colours representing amino acids with similar biochemical properties.

4.2.4 Investigating the antigenicity of bat sarbecoviruses using sera and monoclonal antibodies from individuals with COVID-19 immunity.

As several of the bat sarbecoviruses showed broad host range for mammalian ACE2s, in particular for hACE2, this suggested there is potential for these viruses to spill-over into the human population, which has already been observed for SARS-CoV-1 and SARS-CoV-2. We therefore wanted to ascertain whether pre-existing immunity following infection with SARS-CoV-2 would provide any level of cross-protection for other sarbecoviruses with the propensity to use hACE2. Initially, the antigenicity of bat sarbecoviruses was examined with a panel of sera and plasma obtained from the Medicines and Healthcare products Regulatory Agency, UK (MHRA, formally the National Institute for Biological Standards and Control, NIBSC, UK; more information found here: https://nibsc.org/science_and_research/idd/cfar/covid-19_reagents.aspx), which includes the World Health Organization (WHO) International standards for anti-SARS-CoV-2 immunoglobulins, and reference panel material for SARS-CoV-2 variants of concern B.1 (wild-type, WT), Alpha, Gamma, Delta, and Omicron BA.1. Plasma was also tested from vaccinees with high and low nAb antibody titres, and negative plasma, which is a pool of plasma from individuals pre-2019 (**Table 4.1**).

Table 4.1: WHO International Standards for anti-SARS-CoV-2 immunoglobulin and Reference Panel for antibodies to SARS-CoV-2 variants of concern.

Sample	MHRA code	Description
WT	S2-03	UK 2020, single individual, plasma - pre-VOC
	21/296	IRP for antibodies to SARS-CoV-2 variants - pre-VOC (pooled plasma from 4 individuals, USA)
Alpha	S2-01	Alpha sequence confirmed, serum
	S2-04	UK 2021, single individual, plasma - Alpha*
	21/300	IRP for antibodies to SARS-CoV-2 variants - Alpha* (pool plasma from 3 individuals, UK)
Gamma	S2-07	Brazil 2021, pool plasma - Gamma*
	22/126	IRP for antibodies to SARS-CoV-2 variants - Gamma (pool plasma from 6 individuals, Brazil)
Delta	21/312	IRP for antibodies to SARS-CoV-2 variants - Delta (pool sera from 19 individuals, Kenya)
Omicron	22/128	IRP for antibodies to SARS-CoV-2 variants - Omicron (pool plasma from 9 individuals, South Africa)
International Standard	20/136	1st WHO Standard
	21/338	2nd WHO International Standard (infected/vaccinated)
	21/340	2nd WHO International Standard
Vaccinee plasma	S2-05	Vaccinee plasma, low
	S2-02	Vaccinee plasma, high
Negative	S2-06	Negative plasma, pre-2019

IRP = International Reference Panel; *Assumed based on epidemiological data

Using an in-house ELISA, high levels of human IgG binding (EPT) was observed with the clade Ia and Ib RBDs (recombinant RBDs were produced by Dr Jospeh Newman, The Pirbright Institute, UK; RhGB07 recombinant protein was provided by Dr Kelvin Lau, EPFL), which also exhibited moderate-to-high neutralisation titres (IC_{50}) using pseudotyped viruses harbouring full-length Spike compared to SARS-CoV-2, using cells stably expressing hACE2 as the target receptor (BANAL-20-103, BANAL-20-236: ns; BANAL-20-52, * $p<0.05$; Rs4231: ** $p<0.005$; WIV-1: *** $p<0.0005$) (**Figure 4.13**). Of note, SARS-CoV-1 and RaTG13 – which were initially screened for receptor usage – were excluded from this analysis due to the inability to generate purified RBD proteins, and only RhGB07 was shown to use hACE2, so RfGB02 was also excluded. Strong binding of the RhGB07 and Rc-o319 RBDs was also noted with most of the sera tested. The binding of samples 22/126, 21/340 and S2-05 (low) were not examined with RhGB07 RBD owing to the inaccessibility of additional sera for this finite resource (**Figure 4.13A, bottom panel**). As Rc-o319 and RhGB07 exhibited low usage of hACE2, alternative receptors were used as target receptors in neutralisation assays. Cells were transiently transfected with *Rh. cornutus* ACE2 for Rc-o319 and *Rh. alcyone* ACE2 for RhGB07 neutralisation assays and lower neutralisation titres were noted for RhGB07 (***, $p<0.0005$), and little to no neutralisation against Rc-o319 (***, $p<0.0005$) (**Figure 4.13A, top panel, Figure 4.13B**). The binding and neutralisation phenotype for these two viruses, which are the most antigenically distant compared to SARS-CoV-2, were comparable to what we observed with the SARS-CoV-2 variant Omicron BA.1, a virus that emerged under human antibody selection pressure (**Figure 4.13**). Interestingly, binding was not detected in some instances (e.g., S2-03 did not bind to RhGB07 RBD, 21/296 and S2-04 did not bind to WIV-1 RBD), but neutralisation was still observed of these viruses with these sera, suggestive of neutralisation epitopes outside the RBD (**Figure 4.13**).

The identification of conserved antibody binding or neutralising epitopes on Spike, particularly those with high potency, is of great interest for development of broad-spectrum therapeutics or vaccine design. Due to the cross-reactivity and cross-neutralisation observed with polyclonal sera against different sarbecoviruses, the importance of the RBD in this conserved antigenicity was further investigated, since this region is known to be a major target of neutralising antibodies. Using a panel of monoclonal antibodies (mAbs) isolated from SARS-CoV-2 breakthrough infections (generated and provided by Dr Katie Doores and Dr Jeoff Seow, King's College London, UK) the nAb responses against bat sarbecovirus Spike pseudoviruses was further examined. The mAbs used in this screen have been grouped based on their binding profile to the SARS-CoV-2 RBD, formed based on competition ELISAs with antibodies with known RBD specificity, which aligned with antibody classes that have been previously classified (Group 1 [class IV], 2 [class I/II], 3

[class I/II], 3.5 [class I/II], 4 [class III] and 8 [non-RBD binder]) (**Figure 4.14**) [223, 251, 310, 311].

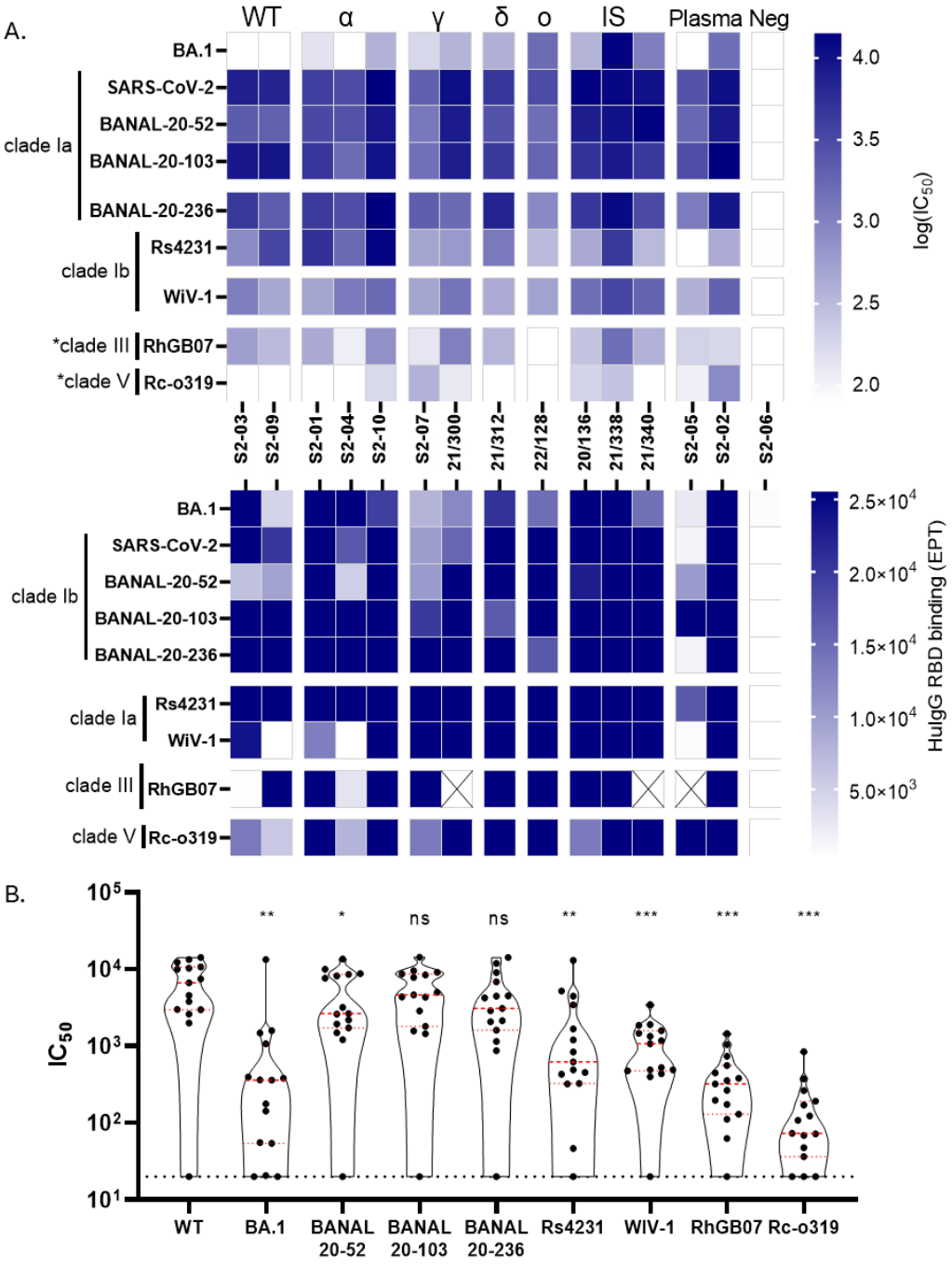

Figure 4.13: Assessing binding and neutralisation of bat sarbecovirus Spike with SARS-CoV-2 convalescent sera.
(A) Heatmap showing the log (IC50) values for neutralisation (top) and human IgG RBD binding end-point titres (EPT, bottom) of SARS-CoV-2, BANAL-20-52, BANAL-20-103, BANAL-20-236, Rs4231, WIV-1, RhGB07, Rc-o319 and BA.1 in the presence of the indicated sera in **Table 4.1**. HEK293T cells stably expressing human ACE2 were used for all neutralisation assays, apart from RhGB07 and Rc-o319, where cells overexpressing *Rh. alcyone* or *Rh. cornutus* were used, respectively (indicated by an asterisk). Boxes with crosses indicate a condition that was not tested. **(B)** Violin plots showing collated IC50 values, with the median, upper and lower quartiles (red lines) and limit of detection (black dotted line) shown. A one-way ANOVA with Dunnet's multiple comparison was performed, compared to SARS-CoV-2, with significance values indicated (* = p<0.05, ** = p<0.005, ***= p<0.0005, ns = non-significant).

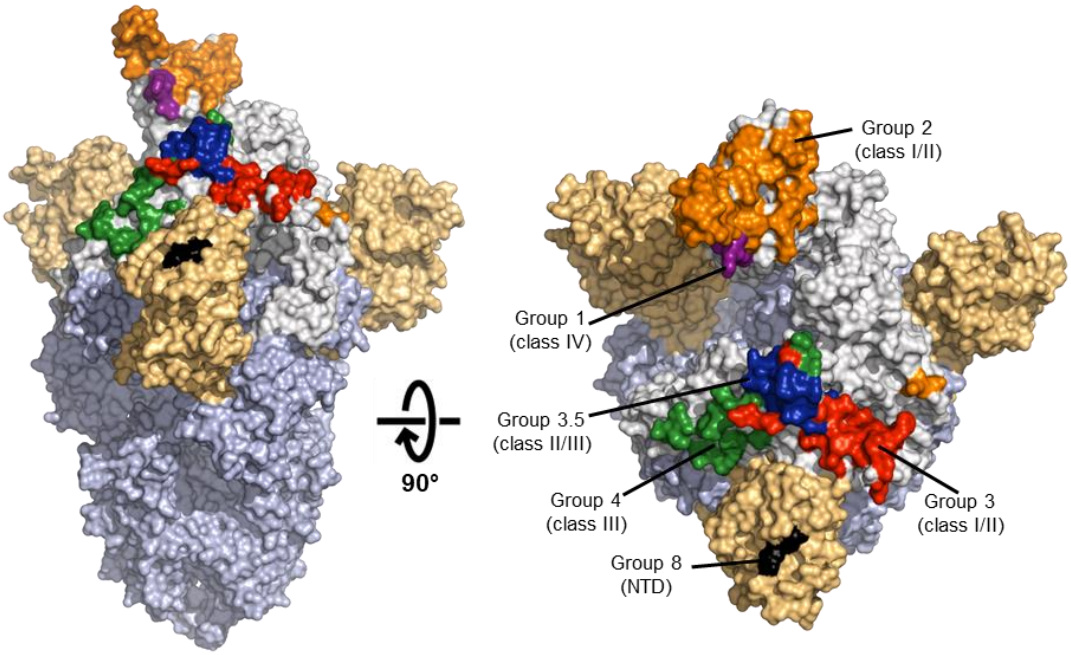

Figure 4.14: Monoclonal antibodies isolated from SARS-CoV-2 breakthrough infections cluster into distinct binding groups on the Spike protein.
Molecular surface representation of the trimeric SARS-CoV-2 Spike protein (PDB 6XM0) coloured in light blue. The N-terminal domain (NTD) is coloured in cream and the receptor binding domain (RBD) in grey. Epitopes of characterised antibody binding groups are shown: Group 1 (Class IV), purple; Group 2 (Class I/II), orange; Group 3 (Class I/II), red; Group 3.5 (Class II/III), blue; Group 4 (Class III), green; Group 8 (Non-RBD, NTD), black [310]. Of note, Group 3.5-binding mAbs overlap with the Group 3 and 4 binding sites. A front view and top view are shown. Structures were generated in PyMOL.

The binding and neutralisation of bat sarbecoviruses was investigated using mAbs from different antibody binding groups. As with the sera tested, SARS-CoV-2, BANAL-20-52 and BANAL-20-236 RBDs exhibited high binding with all mAbs tested across the different binding groups. In contrast, WIV-1, Rs4231, Rc-o319 and RhGB07 RBDs exhibited poorer binding with these mAbs, but all still bound to a high degree to VA14_16 (except RhGB07, group 2), V1WT_41 (group 3) and V1WT_06 (group 4). Interestingly, these 3 mAbs were also able to bind the RBD of the non-ACE2 using clade II virus, RacCS203, albeit to a lesser degree. As expected, none of the group 8 mAbs (NTD-specific) were bound by any of the RBDs (**Figure 4.15**). The neutralisation of the sarbecovirus Spikes showed a similar trend to binding, with the majority of clade Ib viruses exhibiting strong binding EC50s and neutralisation IC50s of <0.08 µg/ml, which was not observed for clade Ia, III and V virus RBDs and Spikes, suggesting a dominant role of the RBD in immune evasion (Table 4.2). Elucidating where these mAbs bind on the Spike RBD can help determine important conserved antibody binding epitopes that could be targeted for future therapeutics or vaccines, and differential binding epitopes that could be used to predict immune escape.

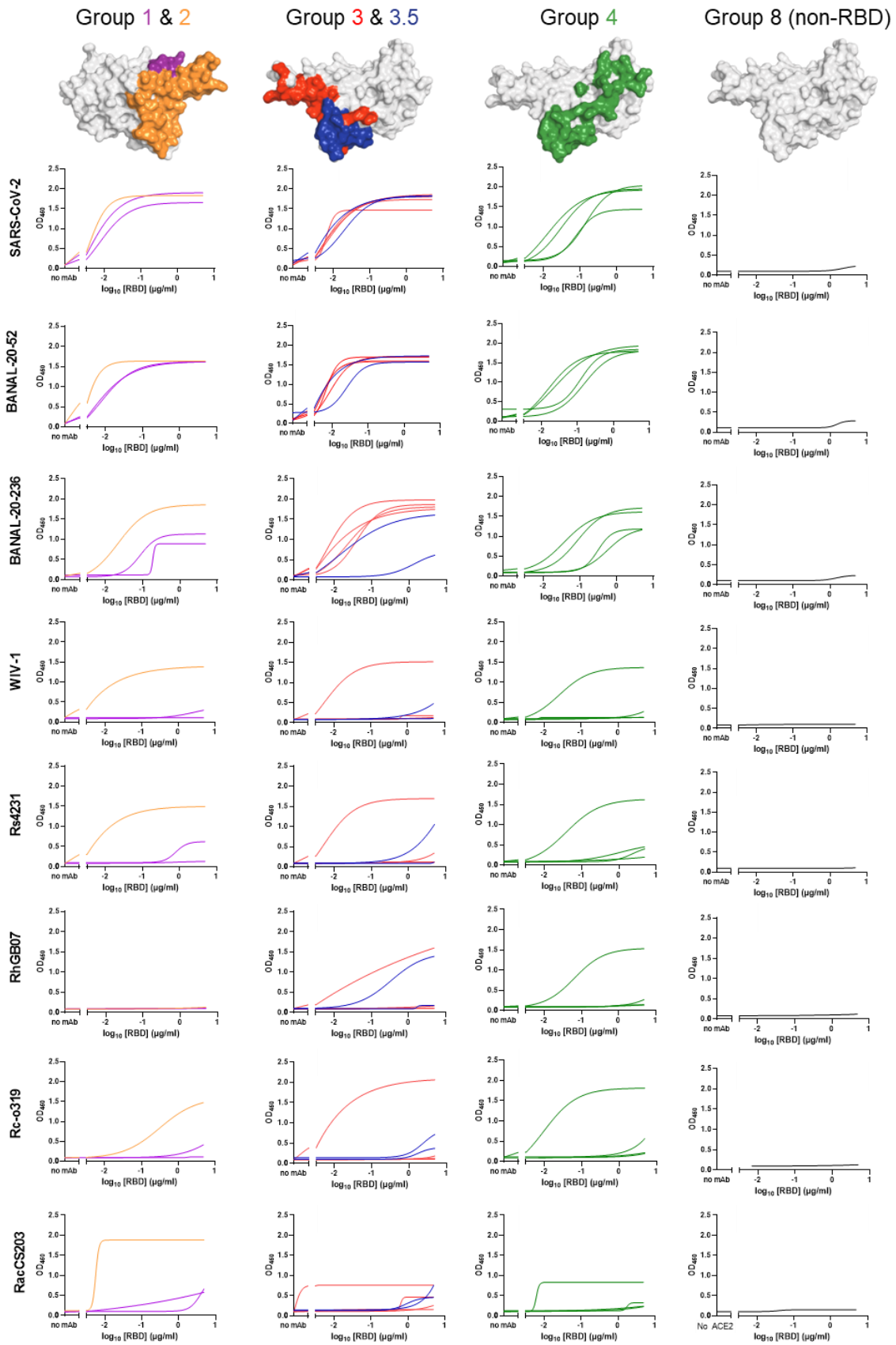

Figure 4.15: Monoclonal antibodies isolated from SARS-CoV-2 breakthrough infections bind differentially to bat sarbecovirus RBDs.
RBD structure of SARS-CoV-2 (PDB 7UL0) with the binding epitopes of the different mAb groups is shown (Group 1 = purple, Group 2 = orange, Group 3 = red, Group 3.5 = blue, Group 4 = green, Group 8 = non-RBD, NTD-specific, defined previously [310]. Each of the plots shows mAb binding, coloured by their designated binding group in an ELISA using purified sarbecovirus RBDs (Clade Ib: SARS-CoV-2, BANAL-20-52, BANAL-

20-236; Clade Ia: WIV-1, Rs4231; Clade III: RhGB07; Clade V: Rc-o319; Clade II: RacCS203). Curves were calculated using a least squares regression non-linear fit in GraphPad Prism.

Table 4.2: Binding and neutralisation of bat sarbecovirus RBDs in the presence of monoclonal antibodies isolated from individuals with SARS-CoV-2 breakthrough infections.

		Group 1		Group 2	Group 3				Group 3.5		Group 4			
		V3WT_20	V1WT_26	VA14_26	V2D_12	V3OM_37	V2D_48	V1WT_41	V3WT_01	V1WT_09	V1WT_06	V1D_22	V3OM_03	V3WT_02
SARS-CoV-2	Binding (EC50, µg/ml)	<0.08	<0.08	<0.08	<0.08	<0.08	<0.08	<0.08	<0.08	<0.08	<0.08	<0.08	0.14	<0.08
	Neutralisation (IC50, µg/ml)	0.28	0.26	0.12	<0.08	<0.08	<0.08	0.15	<0.08	0.10	0.76	0.24	0.42	1.46
BANAL-20-236	Binding (EC50, µg/ml)	0.19	0.08	<0.08	<0.08	<0.08	<0.08	<0.08	0.10	1.38	<0.08	0.57	0.31	0.09
	Neutralisation (IC50, µg/ml)	0.82	0.19	<0.08	<0.08	<0.08	<0.08	<0.08	<0.08	9.83	<0.08	0.40	<0.08	0.18
BANAL-20-52*	Binding (EC50, µg/ml)	<0.08	<0.08	<0.08	<0.08	<0.08	<0.08	<0.08	<0.08	0.08	<0.08	<0.08	0.15	0.12
	Neutralisation (IC50, µg/ml)	>50	0.71	<0.08	<0.08	<0.08	<0.08	<0.08	<0.08	0.18	1.22	0.46	0.50	0.17
BANAL-20-103*	Binding (EC50, µg/ml)	<0.08	<0.08	<0.08	<0.08	<0.08	<0.08	<0.08	<0.08	0.08	<0.08	<0.08	0.15	0.12
	Neutralisation (IC50, µg/ml)	4.26	0.24	<0.08	<0.08	<0.08	<0.08	<0.08	<0.08	0.26	<0.08	0.75	0.30	0.20
WIV-1	Binding (EC50, µg/ml)	>5	4.84	<0.08	0.63	0.46	>5	<0.08	>5	0.08	<0.08	>5	0.08	4.00
	Neutralisation (IC50, µg/ml)	8.85	0.54	<0.08	>50	>50	>50	<0.08	>50	>50	<0.08	>50	>50	>50
Rs4231	Binding (EC50, µg/ml)	0.71	0.79	<0.08	>5	<0.08	0.20	<0.08	>5	>5	<0.08	1.09	4.00	4.33
	Neutralisation (IC50, µg/ml)	37.64	0.36	<0.08	>50	>50	>50	<0.08	>50	>50	<0.08	>50	>50	>50
Rc-o319	Binding (EC50, µg/ml)	1.84	>5	0.32	>5	>5	>5	<0.08	4.40	1.71	<0.08	>5	>5	>5
	Neutralisation (IC50, µg/ml)	>50	>50	>50	>50	>50	>50	14.90	>50	>50	11.60	>50	>50	>50
RhGB07	Binding (EC50, µg/ml)	<0.08	<0.08	>5	<0.08	<0.08	>5	<0.08	0.34	1.69	<0.08	>5	>5	0.72
	Neutralisation (IC50, µg/ml)	>50	>50	>50	<0.08	>50	>50	1.09	<0.08	>50	<0.08	>50	>50	>50

*The same ELISA data is used for BANAL-20-52 and BANAL-20-103 as the RBD sequences for these two proteins are identical.
Antibody groups are coloured to match the structural images shown in **Figure 4.14** and **Figure 4.15**.
IC50 and EC50 represent the half-maximal effective concentration of neutralisation and binding (µg/ml), respectively, calculated using a non-linear fit of regression on GraphPad Prism. Red boxes indicated monoclonal antibodies of interest with broad cross-reactivity.

4.3 Discussion

Recognising potential animal reservoirs and the risk of viral infection in suspected natural and intermediate hosts is important to understand the spillover capacity of viruses with pandemic potential, such as sarbecoviruses that could result in sustained transmission. In addition, when new viruses emerge, it is also important to establish relevant animal models for infection that best replicate the disease seen in people and animals following natural infection. Understanding the genetic determinants of host range can further help predict future zoonotic events and pathogenesis, e.g., identifying differences in receptor usage between closely related viruses and the key amino acid substitutions that underpin this restriction. Here, we investigated these differences at an intraspecies level with SARS-CoV-2 and its variants, and at an interspecies level to understand how these species tropism trends extend to other sarbecoviruses.

SARS-CoV-2 variants evolved over the course of the COVID-19 pandemic, with an increasing number of mutations, particularly in the Spike protein. The largest number of mutations has been seen in Omicron variants and subvariants, which have repeatedly grown to global dominance (**Figure 4.2, Figure 4.3**). The mutations present in these

variants have profound epidemiological effects, have exhibited altered host tissue tropism (Omicron) [312], and resulted in altered species tropism [71, 305], the latter is unsurprising given the high level of natural divergence in amino acid residues of mammalian ACE2 orthologues at the ACE2-RBD binding interface (**Figure 4.1A**) [312, 313]. An example of this is evident when comparing different rodent species. WT SARS-CoV-2 was restricted in its use of mouse and rat ACE2 but could enter cells overexpressing hamster ACE2 to high levels (**Figure 4.1C, Figure 4.5**). We subsequently demonstrated how the N501Y mutation in Alpha was sufficient to overcome the WT and B.1 restriction seen with mouse and rat ACE2. This can be attributed to the presence of a histidine residue at position 353 in mouse/rat ACE2, as opposed to the lysine present in hACE2 (**Figure 4.6**) [305]. The N501Y mutation may confer an advantage to SARS-CoV-2 binding H353 in rodent ACE2. Subsequent SARS-CoV-2 variants all contain the N501Y mutation and have maintained their ability to enter cells overexpressing mouse and rat ACE2 (**Figure 4.3, Figure 4.5**). However, whether SARS-CoV-2 variants are more pathogenic in rodents is an area of ongoing investigation, for example, there are ongoing concerns that rodents could transmit SARS-CoV-2, acquired in contaminated wastewater [314].

Importantly, rodent animal models are valuable for studying SARS-CoV-2 transmission, pathogenesis and for testing vaccines/ therapeutics. Initially wild-type mouse models were shown to be refractory to SARS-CoV-2 infection, so transgenic models were established to study SARS-CoV-2 infection, for example using the K18-human ACE2 model [315]. However, if SARS-CoV-2 variants result in increased pathogenicity due to their acquired ability to use mouse/rat ACE2, which has been demonstrated in Alpha- and Beta-infected mouse models, this can complicate the interpretation and comparison of infection data between different variants, especially comparisons to WT/B.1 [316]. Furthermore, the hamster model has been established as the primary animal model to study SARS-CoV-2 pathogenesis. The ferret model, used previously to study SARS-CoV-1 pathogenesis [244-246], does not immediately support SARS-CoV-2 infection because of a restricted host range for mustelid ACE2, supported by our receptor usage data (**Figure 4.1, Figure 4.5**) [298].

The narrower host range of SARS-CoV-2 variants in the bat ACE2 screen is surprising, given that SARS-CoV-2 likely originated in Chiroptera bat species [31, 204, 304] supported by evidence of SARS-CoV-2 infection of bat ACE2 expressing cells *in vitro* and experiments that suggest that SARS-CoV-2 RBD binding bat ACE2 with high affinity [317]. However, certain restrictions in bat ACE2 usage with B.1 were overcome with Omicron BA.1, due to the presence of a Q493R mutation in Spike, either by itself or in combination with other RBD-specific mutations, such as N501Y, E484A and K417N (**Figure 4.7**). The loss of *L.Lyra*

ACE2 usage by BA.1 could also be attributed to a K417N mutation (**Figure 4.7**). The Q493R mutation has been shown by others to be important in overcoming bat ACE2 restrictions due to increased affinity of the Omicron RBD for residues at positions 35 and 31 in bat ACE2, which have been described as key determinants for bat ACE2 usage, along with ACE2 amino acid positions 27 and 42 [73, 318]. Interestingly, in the BA.5 variant the amino acid at position 493 is reverted (R493Q), and a loss in *Rh. cornutus* and *Rh. ferrumequinum* ACE2 usage was observed, but not for *Rh. pusillus* (**Figure 4.5**), suggesting that these key mutations likely have a combinatorial synergistic role in altering host range. This is also evident when comparing the bat ACE2 usage of XBB, which retains the Q493R mutation and can use *Rh. affinis* ACE2, to XBB.1.5 where it reverts back to WT and loses *Rh.affinis* ACE2 tropism. However, restrictions were also noted in XBB and XBB.1.5 with other Rhinolophus ACE2s and *L. Lyra*, potentially attributable to the R346T and I368L mutations present only in these Omicron subvariant Spikes, compounding effects on nearby mutations that interact with ACE2. It would also be interesting to investigate whether mutating BA.1 back to B.1 reverts the bat ACE2 usage phenotype observed, however mutational analysis focused on Spikes from B.1 to BA.1 as this was the natural direction of emergence.

Other notable restrictions observed were with the platyrrhines ACE2s (marmoset and squirrel monkey), which exhibited lower levels of pseudotype entry with different SARS-CoV-2 variants compared to hACE2, restrictions which were not seen for catarrhines ACE2s (lemur and macaque) (**Figure 4.5**). It has been suggested that ACE2 residues 41 and 42 are predictive of primate ACE2 restriction to SARS-CoV-2, where binding to positions 446 and 500 in Spike are abrogated due to loss of hydrogen bonds (H41 and Y42 in platyrrhine ACE2s, but Y41 and Q42 in hACE2 and catarrhine ACE2s) [319]. Therefore, the need for continued surveillance and testing in livestock, pet and wildlife is crucial in understanding the possibility of the spillover or even spillback potential of SARS-CoV-2, SARS-CoV-2 variants, and even related viruses within the same genus or subgenus.

The data presented here indicate that at an intraspecies level, SARS-CoV-2 is a generalist ACE2 using virus (**Figure 4.1, Figure 4.4**), with SARS-CoV-2 variants exhibiting even broader host range, attributable to a few key amino acid changes in the SARS-CoV-2 RBD which enhance ACE2 binding. This has been observed naturally with SARS-CoV-2 divergent variants exhibiting the ability to infect new animal hosts, such as white-tailed deer in the USA [295, 297], mink in Denmark [299], and hamsters in China [320]. Therefore, this spectrum of generalist vs specialist species tropism was assessed at the interspecies level for other bat sarbecoviruses. These viruses cluster phylogenetically into distinct clades with the majority being isolated in regions of China, where there is great ecological overlap of different bat species that roost in these regions (**Figure 4.8**). The representative sequences

selected were based on sequence availability and data from similar studies [66, 68, 69, 74, 75, 306], however this approach is biased and may overrepresent clades of viruses where there is already a lot of data available (e.g. the clade I viruses), but neglects to give us a broader understanding of other clades. Moreover, for the clade Ia viruses selected, SARS-CoV-1, WIV-1 and Rs4231 branch separately within their clade based on their RBD sequences. Should this type of analysis be performed again, it would be useful to use more unbiased criteria to select the sarbecoviruses which more fairly captures the diversity within the sarbecovirus genus, as described in a study on alphacoronaviruses, where Spike sequences were selected based on a Greedy maximum genetic distance algorithm [220].

As with SARS-CoV-2, other clade Ib viruses were also mostly generalists in their bat ACE2 usage. Clade Ia and even more so, clades III and V were more specialised, using primarily the ACE2 receptor of the bat species from which the virus was isolated (**Figure 4.11**). Nevertheless, the clade Ia viruses were able to exhibit more generalist mammalian ACE2 usage, similar to the clade Ib viruses, despite the high level of divergence in the sequences of the ACE2 orthologues tested at the RBD-ACE2 binding interface (**Figure 4.12**). However, although both proteins were expressed well (**Figure 4.10**), BANAL-20-103 did not use the predicted cognate *Rh. pusillus* ACE2 receptor in pseudotype entry assays but did to a low level in a cell-cell fusion assay (**Figure 4.11**), suggesting that ACE2 isolates deposited on GenBank may not be the one used by BANAL-20-103, or that the cognate receptor for this virus is a different bat ACE2. Although generally, good concordance was observed between the two assays, the discrepancy in results may be due to overexpression of both Spike and ACE2 in the cell-cell fusion assay, which may have exaggerated any low-level interaction that was formed. This means that more Spike is likely expressed on the surface of an effector cell in the fusion assay than would be in a pseudovirus virion, increasing the chances of Spike-receptor engagement events.

Interestingly, RaTG13 showed a distinct, more restricted pattern ACE2 usage despite sharing 98% amino acid similarity with SARS-CoV-2 and clustering in the same clade as SARS-CoV-2 and the BANAL viruses (**Figure 4.11, Figure 4.12**). This is likely due to amino acid substitutions at key ACE2-binding sites, for example a F486L substitution in RaTG13 compared to SARS-CoV-2 results in weakened hydrophobic interactions between side chain residues L79, M82 and Y83 in ACE2 [219]. Correlating entry of bat sarbecoviruses with binding could also be useful in defining the importance of affinity between RBDs and ACE2 in receptor usage. This could be investigated using purified recombinant RBDs and performing binding assays or measuring protein-protein interactions. RaTG13 also contains similar amino acid changes that have arisen in SARS-CoV-2 variants, such as a Q493Y and Y505H. Although these confer an advantage for the variants, they appear to be

detrimental to RaTG13 host range. These residues bind to regions distal to position 31 and 353 in ACE2, which we have already described as significant for ACE2 receptor utilisation for SARS-CoV-2 variants, but were also previously identified for SARS-CoV-1 [66, 293]. The more restricted host range of RaTG13 may confer an evolutionary advantage for this virus as a result of adaptation and sustained infection of its natural host, *Rh. affinis.*

The clade II Spikes that were assessed derived from SARS-CoV-1 related (Rp3 and Rf1) or SARS-CoV-2 related (RacCS203 and RPYN06) lineages. Consistent with other studies, the clade II viruses did not use ACE2 as a functional receptor, despite the Spike protein being expressed well (**Figure 4.10, Figure 4.11**). This can largely be attributed to two regions deletions in the RBD spanning amino acids 443-447 (region 1) and 473-488 (region 2) relative to SARS-CoV-2 RBD. However, other determinants outside these loop deletions also restrict ACE2 usage since substitutions of these regions, or the entire receptor binding motif with the SARS-CoV-2 sequence, still failed to achieve any detectable ACE2 binding or entry [71, 216].

Clade III viruses RhGB07 and RfGB02 also had restricted bat and slightly broader mammalian ACE2 usage, with only RhGB07 able to utilise hACE2 (**Figure 4.11, Figure 4.12),** as previously described [74]. Of note, the RBD sequences of RfGB02 and RhGB07 are identical, which indicates there are differences outside the RBD that confer the differences in hACE2 observed [74]. When aligned to SARS-CoV-2 RBD, a deletion at position 449 (region 1) is noted in RhGB07 and RfGB02, which potentially disrupts electrostatic interactions formed with positions 38 and 42 of ACE2, which have been shown to be important for bat ACE2 receptor usage. Notable restrictions in these clade III viruses are seen with rodent and mink ACE2s, likely attributed to various RBD amino acid changes that disrupt interactions with key ACE2 binding sites, for example the isoleucine change at position 501 results in weak interactions with position 353 in ACE2 [71].

Others have shown similar results with related clade III viruses, such as PRD-0038, which branches separately from RhGB07 and RfGB02 [68]. Although this virus uses hACE2 poorly, its host range extends to geographically relevant bat species, *Rh. alcyone*, *Rh. landeri* and specific alleles of *Rh. ferrumequinum* ACE2. One or two amino acid substitutions in Spike – T487W and K482Y – are sufficient to increase tropism for these bat ACE2s [68]. Conversely, Khosta-2 was shown to be able to bind hACE2 in structural models and infect human cells *in vitro* using full-length Spike in the presence of trypsin [66, 67]. The clade V Spike Rc-o319 exhibited similar restrictions in bat ACE2 usage and was unable to use human or other mammalian ACE2s (**Figure 4.11, Figure 4.12**). Rc-o319 contains a 10 amino acid deletion in region 2 (481-499), which likely contributes to this specialist

receptor usage profile. The fact that the deletions in region 1 are shorter than region 2 but appear to have a greater impact on restricting host range suggests that region 1 deletions exhibit more diverse sequence changes crucial for ACE2 binding.

Of note, viruses from clade IV were not included due to the unavailability of complete sequences at the time of study commencement. Other studies have investigated the tropism of a clade IV virus, RaTG15, which shares 72.6% amino acid identity with SARS-CoV-2 RBD. There is a short deletion is present in RaTG15 at amino acid positions 444-447, and residues within the RBD also vary that are crucial for SARS-CoV-2 binding to the ACE2 receptor (486, 493, 494, 501), of which residues 493 and 501 have been shown here to be deterministic of host range. RaTG15 RBD had detectable binding to *Rh. affinis* and Malayan pangolin ACE2, and full-length Spike pseudoviruses were able to enter cells overexpressing these receptors, however, no obvious binding or entry with hACE2 was detected [75].

This study focused analyses on sarbecoviruses isolated from bat species, however SARS-CoV-1 and SARS-CoV-2 related viruses have been isolated from *Paguma larvata* (palm civet, e.g., SARS CoV SZ3 in China) and *Manius javanica* (pangolin, e.g., BetaCoV/P4L in China), respectively [69]. These species were proposed as potential intermediate reservoirs of SARS-CoV-2, along with the raccoon dog, so future analysis should include these sarbecoviruses to understand the breadth of species tropism of possible virus intermediates. Indeed, a SARS-CoV-like virus was isolated from palms civets, raccoon dogs and Chinese ferret-badger in an animal market in 2003 in China [321].

The continued evolution of SARS-CoV-2 in the human population raises concerns of antigenic escape from immunity, through vaccination and/or natural infection. Due to the broad host range that was observed for many of the sarbecovirus Spikes investigated, particularly for viruses that were able to effectively enter cells overexpressing hACE2, we wanted to understand the breadth of protection COVID-19 derived immunity could provide against other sarbecoviruses, should they emerge in the human population. A similar trend in binding and neutralisation was observed with convalescent sera analogous to the receptor usage profile of the sarbecovirus Spikes, particularly with clade I viruses, where viruses with more generalist ACE2 usage were also neutralised more broadly with convalescent sera (**Figure 4.13**). This suggests that although sarbecoviruses with broad host range could result in spillover into new hosts and onwards transmission of the virus, current immunity against SARS-CoV-2 may be sufficient in providing cross-protection against these viruses. We also noted some evidence of neutralisation against more specialist ACE2 users, RhGB07 and Rc-o319, mirroring the neutralisation observed for the

antigenically distant SARS-CoV-2 variant BA.1 (**Figure 4.13**). Considering what is known about immune escape with BA.1, it is therefore likely that pre-existing immunity against SARS-CoV-2 will confer low level neutralisation of clade III or clade V sarbecoviruses. We previously discovered that RaTG13 Spike pseudotypes were neutralised better than SARS-CoV-2 in the presence of sera from vaccinated healthcare workers, both with and without prior infection [106]. CryoEM structure of the RaTG13 Spike revealed a more stable conformation of the trimeric protein and binding assays demonstrated lower affinity for hACE2 than SARS-CoV-2 [294, 322]. This could mean that nAbs are able to displace ACE2-binding more potently and therefore confer greater antigenicity against RaTG13. Therefore extending this analysis to include sera from vaccinated individuals in the UK would also be of interest to understand whether vaccine-derived immunity can enhance binding and neutralisation of bat sarbecoviruses, similar to what we observed using convalescent sera (**Figure 4.13**). This would nicely represent the situation if a UK bat sarbecovirus (e.g., RhGB07) were to emerge, but would require examination of vaccinee sera from other parts of the world to understand better what this would mean in Southeast Asia, i.e. where many of these bat sarbecoviruses have been identified.

This analysis was expanded to investigate the binding and neutralisation of sarbecovirus Spikes by monoclonal antibodies derived from SARS-CoV-2 breakthrough infections and discovered that group 2 (apart from RhGB07), 3 and 4 mAbs were able to bind all sarbecovirus RBDs to varying degrees, including the non-ACE2 using RacCS203. These mAbs have been classified through competition ELISAs with known mAbs, so being able to map the exact location at which they bind would be useful to understand the regions of Spike that could be targeted to produce pan-sarbecovirus therapeutics. To begin to decipher these key residues, RBD swaps of a generalist and specialist sarbecovirus could be conducted, introducing point mutations singly or in combination to try to recapitulate the change in binding that was also observed (e.g., which mutation would allow RhGB07 to be bound by class II mAb VA14_26). This would also provide vital information to understand which epitopes are important, for example, in designing broad-spectrum, pan-sarbecovirus therapeutics.

Taken together, these data indicate the need for increased virus surveillance and sampling, particularly in livestock, wildlife and companion animal populations where high levels of ACE2 usage are observed. These animals could act as reservoirs for zoonosis, reverse zoonosis or sustained transmission of sarbecoviruses. However, ACE2 usage for a particular species may not always result in infection and disease in the animal host. A relevant example is pigs, which we showed can be used by sarbecovirus Spikes to a high degree (**Figure 4.4, Figure 4.5, Figure 4.12**) [219, 305]. Pigs are refractory to SARS-CoV-

2 infection, despite having been established as reservoirs for other viruses like influenza, Nipah virus and porcine coronaviruses [323]. Understanding post-entry barriers to infection, either in terms of virus uncoating, protease specificity (e.g., TMPRSS2), co-receptors or host innate immunity is also important in determining the risk sarbecoviruses pose to different animal populations. Furthermore, understanding whether other sarbecoviruses have zoonotic potential and can establish themselves in animal amplification reservoirs in a way that is consequential to human public health still remains important. To this end, determining whether pre-existing COVID-19-derived immunity can provide any degree of cross-protection against these sarbecoviruses, should they emerge in the human population is also of extreme importance.

Chapter 5: Quantifying the cross-neutralisation phenotypes of antibodies raised by heterologous henipavirus vaccination.

5.1 Introduction and Aims

Henipaviruses are taxonomically classified within the *Paramyxoviridae* family and *Henipavirus* genus. Nipah virus (NiV) and Hendra virus (HeV) cause severe and often fatal encephalitis and respiratory disease in human populations and in animals (both naturally and experimentally) (**Figure 5.1**) [110, 158]. This high pathogenicity means these viruses are classified at Biosafety Level 4 (BSL4). NiV in particular has pandemic potential since it can infect humans directly from the natural host (*Pteropodidae* Old world fruit bats), from animal reservoirs and also transmit between humans [132, 324]. There are two major clades of NiV, consisting of strains isolated from different countries: the NiV-Malaysia (NiVM) clade contains sequences from virus strains isolated from Malaysia and Cambodia, and India and Bangladesh strains form the NiV-Bangladesh (NiVB) clade Isolates from Thailand have mixed sequences that cluster with either NiVM or NiVB based on their nucleoprotein (N) sequence (**Figure 5.2**) [131].

There are currently no vaccines or therapeutics licenced for use against NiV, but a limited number of candidate vaccines are currently entering human clinical trials, including a recombinant HeV subunit vaccine expressing the attachment (G) protein (HeVsG) [117]. There is a similar licensed subunit vaccine against HeV-G (EquiVac® HeV, Zoetis) for use in horses, but despite this vaccine protecting both ferrets and African green monkeys against experimental NiV challenge, it failed to protect pigs which were identified as an intermediate reservoir for NiVM [176, 178]. Other vaccine candidates include a recombinant vesicular stomatitis virus (VSV) expressing NiVB-G; a chimpanzee adenoviral vector (ChAdOx1) expressing NiVB-G; and an mRNA vaccine encoding a monomer of NiVM-G covalently linked to the fusion (F) protein as a secreted prefusion stabilised protein [117]. The monoclonal antibody (mAb) m102.4 against the HeV-G protein, is also currently in human clinical trials for use against NiV infection, and has been administered to humans in the past on compassionate grounds, for individuals at high-risk of HeV infection [117, 163]. There is evidence of some level of cross-protection and cross-neutralisation against NiV infection using HeV-specific therapeutics, including m102.4 [196, 325].

Other viruses such as Cedar virus (CedV) isolated from Grey-headed flying foxes in Australia (*Pteropus alecto*) [140], Ghanaian bat henipavirus (GHNV) detected in the faeces of African Straw-coloured fruit bats (*Eidolon helvum*) [144] and the divergent Henipavirus, Angavokely henipavirus (AngV) identified in the urine sample of a fruit bat (*Eidolon*

duprenum) in Madagascar [145] have subsequently been taxonomically classified within this genus (**Figure 5.1, Figure 5.2**). Analysis of the polymerase (L) protein amino acid sequence of AngV reveals that it clusters separately from other bat-borne viruses [145] (**Figure 5.1**). Unlike the majority of Henipaviruses, which have been identified in flying fox bats, GHNV and AngV were identified in fruit bats. Evidence for human infection, disease and cross-neutralisation is limited with these viruses, despite the presence of cross-reactive antigenic regions. Preliminary studies in guinea pigs and ferrets showed that CedV was able to replicate in these animals, but failed to cause clinical disease, unlike HeV and NiV, and this absence in pathogenicity is attributed to the lack of the RNA editing region in the P gene of CedV [140].

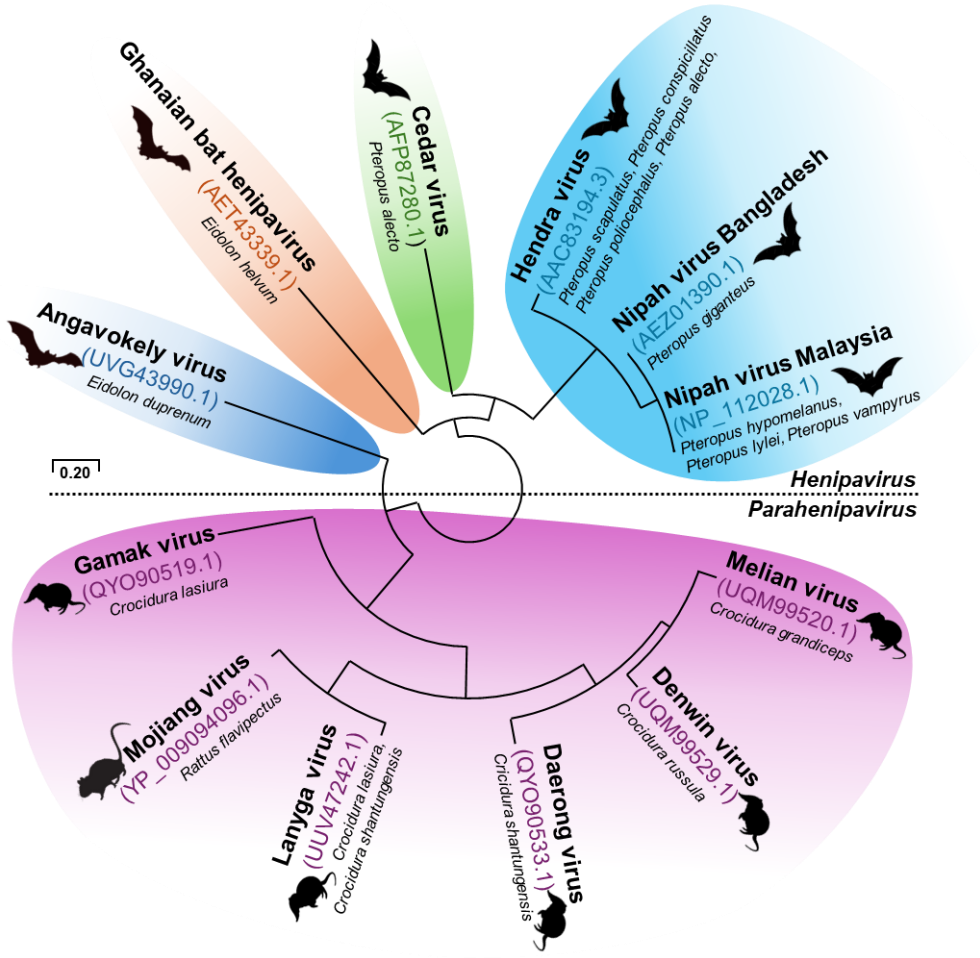

Figure 5.1: Phylogenetic analysis of henipaviruses and parahenipaviruses.
The evolutionary history was inferred by using the Maximum Likelihood method and Le_Gascuel_2008 model [326], obtained automatically by applying Neighbour-Join and BioNJ algorithms to a matrix of pairwise distances estimated using the JTT model. A discrete Gamma distribution was used to model evolutionary rate differences among sites (5 categories (+*G*, parameter = 0.9828)). The tree is drawn to scale, with branch lengths measured in the number of substitutions per site. This analysis involved 12 polymerase (L) protein amino acid sequences (6 henipaviruses, 6 parahenipaviruses), with a total of 2213 positions in the final dataset. Evolutionary analyses were conducted in MEGA11 [309]. Accession numbers of the L protein sequences used are shown, along with the species each virus was first identified in, either bat-borne for the henipaviruses (*Pteropus* or *Eidolon*), or rat/shrew-borne for the parahenipaviruses (*Rattus* or *Crocidura*).

A group of “henipa-like” viruses were recently reclassified into a separate genus, now recognised as *Parahenipavirus*, distinguished by the presence of an extra ORF within the F gene that encodes a transmembrane protein, an alternative entry receptor other than the EphrinBs, and a different natural host of rodent/shrew origin, rather than bat [152]. Viruses within this genus include Mojiang virus (MojV) [147] and Langya virus (LayV) [148], both of which have been associated with disease in humans. MojV was first identified following an outbreak in Chinese mine workers who succumbed after contracting severe pneumonia, while Langya virus (LayV) was also isolated in China, associated with infection resulting in non-fatal febrile illness in 35 individuals [147, 148]. MojV was identified by PCR from rat rectal swabs (*Rattus flavipectus*) and LayV-specific RNA was detected in shrews (*Crocidura lasiura* and *Crocidura shantungensis*) (**Figure 5.1, Figure 5.2**). Other phylogenetically distinct “henipa-like” viruses have been isolated such as Gamak virus (GAKV) and Daerong virus (DARV) in Korea, with the same shrew species as LayV (*C. lasiura* and *C.shantungensis*, respectively) being identified as the natural reservoir for these viruses [149]. Furthermore, Melian virus (MeliV) isolated in Guinea, and Denwin virus (DewV) isolated in Belgium were both also identified in shrews (*Crocidura grandiceps* and *Crocidura russula,* respectively) and both cluster together phylogenetically, despite circulating in different continents (**Figure 5.1, Figure 5.2)** [150].

More recently, the complete genomes of other Henipa-like viruses identified in China have been submitted to GenBank including from striped field mice, *Apodemus agarius* (GenBank ID: MZ328276.1), shrews; *Chodsigoa smithii* (GenBank accessions: OM030316.1), *C. attenuate* (GenBank ID:OM030317.1) or *C. shantungensis* (GenBank ID: OM030314.1, OM030315.1) [152]. Partial sequences of novel Henipa-like viruses have also been deposited, including Peixe-Boi virus (PBV) detected in Brazilian opossums (*Marmosa demerarae*), suggesting the presence of yet another independent henipa-like subclade [153]. Additionally, phylogenetic analysis of the L gene amino acid sequences of viruses isolated from wild rodents and shrew in Zambia identified a high prevalence of sequences branching from paramyxovirus lineages leading to the henipaviruses [154].

The attachment (G) and fusion (F) surface viral glycoproteins present on the surface of the *Henipavirus* virions facilitate viral entry following binding of the proteinaceous cellular receptor EphrinB2. Binding triggers a conformational change of the prefusion F and insertion of the fusion peptide into the host cell membrane. The receptor for the parahenipaviruses is still unknown [158, 327, 328]. The viral glycoproteins are embedded into the surface of the enveloped henipavirus virion, with the majority of the protein being presented on the virion exterior. Thus, the viral glycoproteins are also, unsurprisingly, major targets for neutralising antibodies (nAbs), the development of which are considered pivotal

for long-lasting immunity and the prevention of viral transmission following natural infection, or immunisation. Neutralisation of the virus particle usually occurs by inhibiting attachment, receptor engagement or virus uptake into the host, but can also be mediated through inhibition of cell-cell fusion [162].

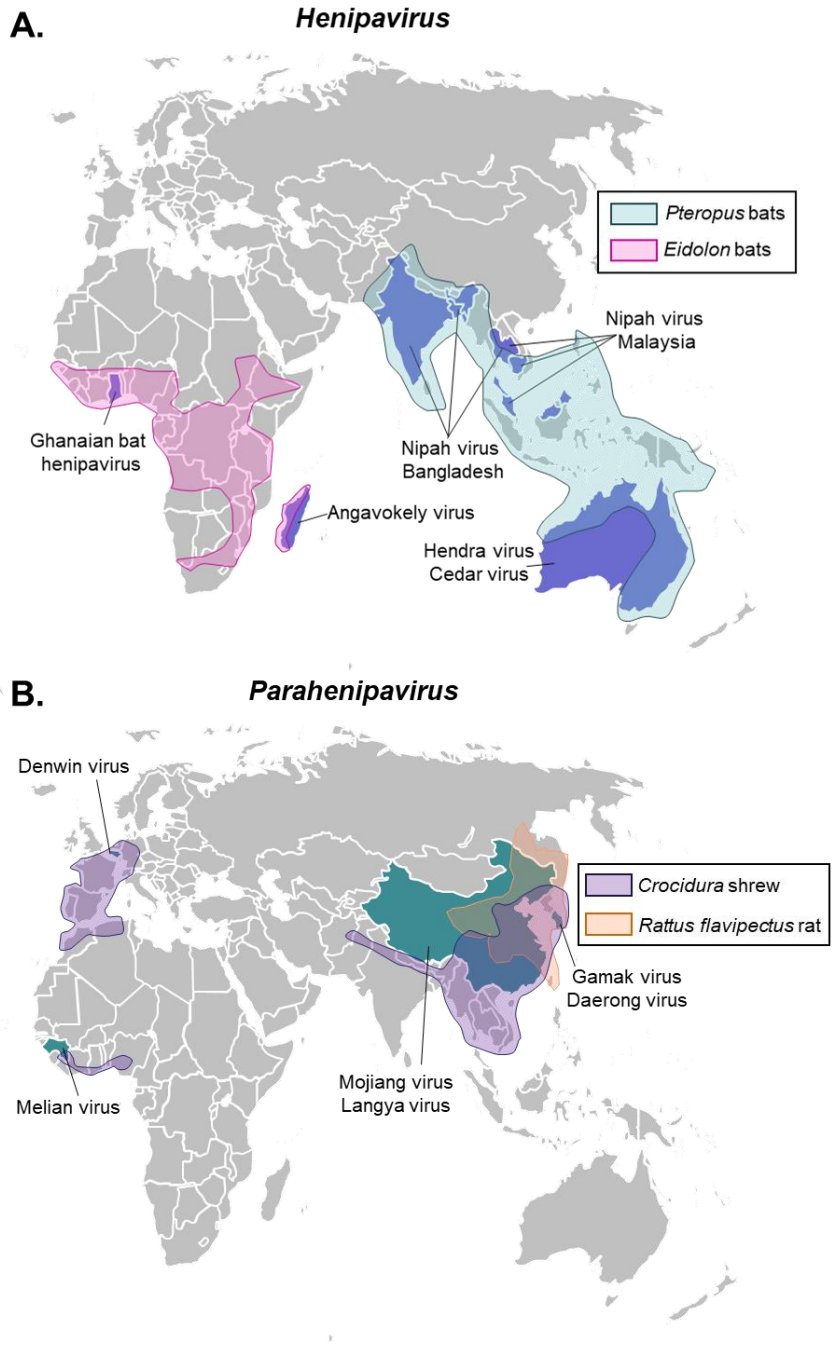

Figure 5.2: Geographic distribution of henipaviruses and parahenipaviruses.
World map highlighting the geographic location where (A) henipaviruses (Nipah virus, Hendra virus, Cedar virus, Ghanaian bat henipavirus) and (B) parahenipaviruses (Mojiang virus, Langya virus, Melian virus, Denwin virus, Gamak virus, Daerong virus) were first isolated, coloured in blue and teal, respectively. The distribution of the species from which these viruses were isolated from or identified in is also depicted: *Pteropus* bats (green), *Eidolon* bats (pink), *Crocidura* shrew (purple), *Rattus flavipectus* rat (orange) (https://www.iucnredlist.org/).

The development of nAbs is of particular interest when considering new and emerging viruses, specifically whether pre-existing immunity can provide any degree of cross-protection. This is particularly pertinent when considering the 2022-2026 strategy outlined by Coalition for Epidemic Preparedness (CEPI) to develop safe, effective and globally accessible vaccines for emerging viruses, “Disease X”, in as little as 100 days [329]. This could apply to the emergence of a known unknown, such as a novel henipavirus that results in severe morbidity and mortality, or of a known henipavirus acquiring the ability to cause severe disease and death in humans that could lead to the next epidemic or pandemic.

In this chapter, I aimed to characterise the breadth of immunity generated by henipavirus-derived infection or vaccination and whether existing vaccination strategies are likely to provide protection against emerging, related henipaviruses. In addition, it will shape our understanding of risk, when and where new vaccines are needed, and how they should be designed, particularly against novel henipaviruses that might emerge in the future. To do this, I have established binding and entry assays for the henipaviruses to examine the cross-reactivity and cross-neutralisation phenotype of both mAbs and sera generated from various vaccine studies. The sera tested were developed from different animal models including pig and mouse, in which the immunogenicity of candidate henipavirus vaccines was assessed. A hamster-based efficacy study was also performed to understand the cross-protective capacity of these vaccines.

Most of the data and analysis outlined in this chapter has been produced by me. The establishment of the cell-cell fusion assay for Nipah virus described herein has already been published, and I am listed as first author: Thakur N et al., Micro-fusion inhibition tests: quantifying antibody neutralization for virus-mediated cell-cell fusion (*Journal of General Virology,* 2020) [162]. All other data is unpublished. Where experimental setup up and data acquisition has been performed by others, this has been indicated in the results, and included with permission of the author.

5.2 Results

5.2.1 Development of low biocontainment assays to measure antibody responses against henipaviruses.

NiV and HeV are classified as biosafety level 4 (BSL-4) pathogens, making research on these viruses difficult without access to BSL-4 research labs. Furthermore, the only other henipavirus that has been isolated is CedV; for GHNV only the genetic sequence is available, but no viral isolate. Therefore, to expand our immunological toolbox, my first aim was to establish low biocontainment assays for the henipaviruses for high throughput analysis across the whole genus at containment level 2 (CL2). To do this, I aimed to

establish binding and entry assays using the surface F and G glycoproteins that mediate cell-entry. Molecular phylogenetic analysis was carried out using amino acid sequences obtained from GenBank for the henipavirus NiVM, NiVB, HeV, CedV and GHNV-F and -G proteins, along with the F and G of parahenipaviruses MojV and MeliV (**Figure 5.3**). The sequences for NiVM, NiVB and HeV-F and -G proteins showed the highest pairwise similarity (**Figure 5.3, blue**). MojV and MeliV-F and -G (**Figure 5.3, pink**) were more distantly related to the other henipavirus sequences. In general, the F sequences appear to be more conserved than the G proteins; interestingly, the F sequence for GHNV shares greater homology with HeV and NiV, than CedV (**Figure 5.3A, orange and green, respectively**), whereas for the G sequences, the opposite is true (**Figure 5.3B**).

Full-length ORFs representing the F and G sequences for NiVM, NiVB, HeV, CedV and GHNV (**Table 5.1**) were cloned into a pcDNA3.1 expression vector for use in entry assays. Viral pseudotypes have been widely employed as a surrogate for live virus assays through incorporation of a trans-encapsidated viral glycoprotein of interest, vectored by another virus. One example is a lentiviral-based system which requires co-transfection of the following plasmids encoding: (i) the HIV-1 structural/replicase proteins *Gag* and *Pol,* (ii) a firefly luciferase reporter gene flanked by HIV-1 regulatory regions and the packaging signal, and (iii) the heterologous viral glycoprotein to be trans-encapsidated [218]. Pseudotypes were generated using this lentiviral-based system and used to infect target BHK-21 cells, which have previously been shown to support NiV entry without requiring overexpression of the proteinaceous EphrinB2 receptor [330]. Firefly luciferase was quantified as a measure of virus infection and productive infection was detected for NiVM ($p<0.0001$), NiVB ($p<0.001$), CedV ($p<0.0001$) and GHNV ($p<0.01$) above 10^6 signal light units; VSV-G was used a positive control ($p<0.0001$) and a non-enveloped (NE), pcDNA3.1 mock-transfected control was used to determine background luciferase signals (**Figure 5.4A**). HeV pseudoparticles yielded luciferase signals only slightly higher than background, suggesting HeV did not pseudotype efficiently (**Figure 5.4A**). This may be due to the highly fusogenic nature of the HeV-F glycoprotein which led to extensive cell-cell fusion in the HEK293T producer cells, used for lentivirus synthesis.

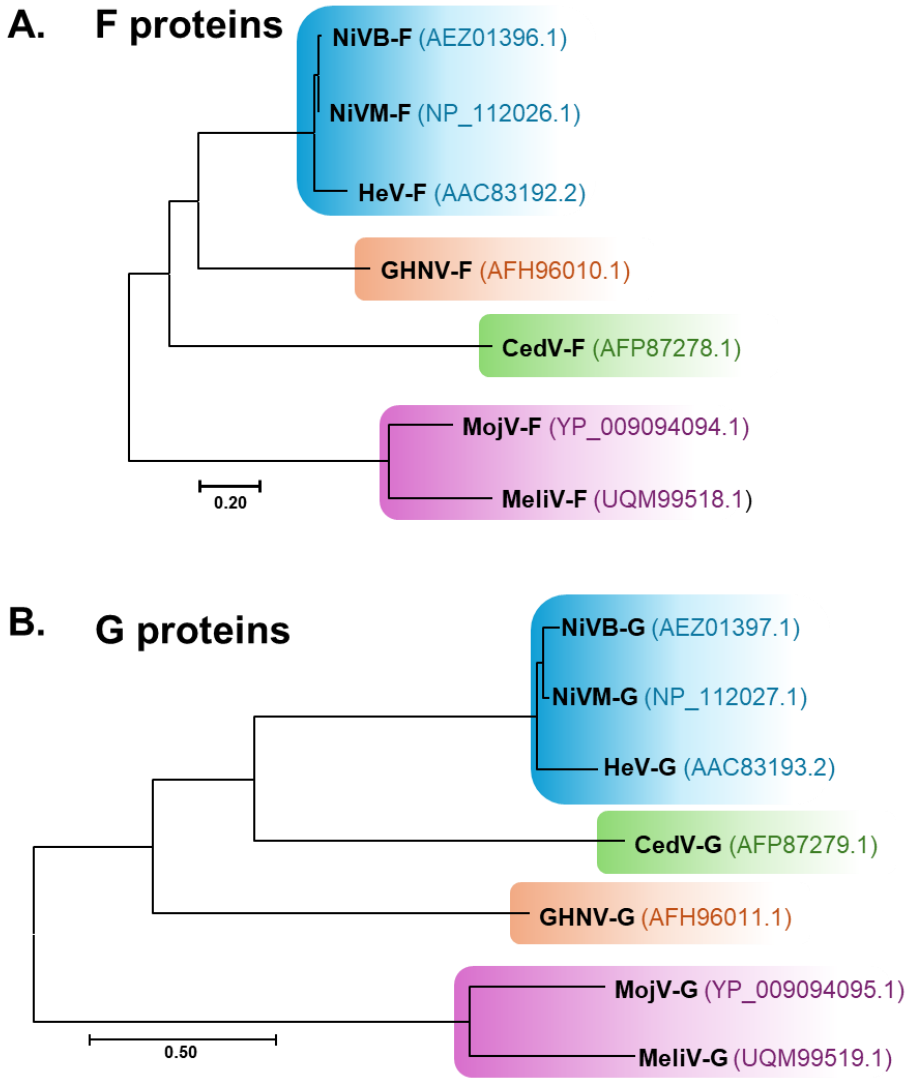

Figure 5.3: Phylogenetic analysis of henipaviruses and parahenipaviruses F and G proteins.
The evolutionary history was inferred by using the Maximum Likelihood method and **(A)** Whelan And Goldman + Freq. model (7 F protein amino acid sequences, 572 positions) [308] or **(B)** Le_Gascuel_2008 model (7 G protein amino acid sequences, 539 positions) [326], obtained automatically by applying Neighbor-Join and BioNJ algorithms to a matrix of pairwise distances estimated using the JTT model. A discrete Gamma distribution was used to model evolutionary rate differences among sites (5 categories (+*G*, parameter: F proteins = 3.3411, G proteins = 2.0079)). The tree is drawn to scale, with branch lengths measured in the number of substitutions per site. Evolutionary analyses were conducted in MEGA11 [309]. Accession numbers of the F and G protein sequences used are shown.

Table 5.1: GenBank accession numbers for Henipavirus F and G proteins to clone into expression plasmids.

pcDNA3.1(+) plasmid expressing viral glycoprotein	Accession number	
	F protein	G protein
Nipah virus Malaysia	NP_112026.1	NP_112026.
Nipah virus Bangladesh	AEZ01396.1	AEZ01397.1
Hendra virus	AAC83192.2	AAC83193.2
Cedar virus	AFP87278.1	AFP87279.1
Ghanaian bat henipavirus	AFH96010.1	AFH96011.1
Mojiang virus	YP_009094094.1	YP_009094095.1
Melian virus	UQM99518.1	UQM99519.1

To optimise the pseudotyping of HeV, the temperature at which producer cells were left to incubate after transfection of the glycoproteins was lowered from 37°C to 32°C to reduce the growth rate of the producer cells. This is also likely reduces the probability of premature triggering of F, therefore minimising the likelihood of fusion events occurring. Indeed, infection of BHK-21 target cells with HeV pseudoparticles that had been incubated at 32°C were able to yield productive infection of ~10^5 luciferase signal units ($p<0.05$), and there was a visibly marked reduction in fusion in HEK293T producer cells (**Figure 5.4B**). NiVM pseudoparticles were included as a comparator, where a 1-log reduction was observed in luciferase titre of pseudoparticles produced at 32°C ($p<0.05$) compared to those produced at 37°C but still significantly greater (3-log, $p<0.0001$) than the NE control (**Figure 5.4B**).

HeV and NiV can also spread to neighbouring cells by cell-to-cell fusion, causing the formation of multinucleated syncytia that contribute to the clinical pathology observed with such viruses and a mechanism of sustained viral syncytia [331]. Therefore a quantitative fusion assay based on a split *Renilla* luciferase-GFP system was also established and optimised, assays which have been employed for various surface glycoproteins in our lab, including measles virus [332], respiratory syncytial virus (human and bovine) [162], and betacoronaviruses [162, 219], and NiV [162]. This cell-cell fusion assay was adapted for the other Henipaviruses, transfecting equal amounts of the F and G glycoproteins into effector cells (HEK293T rLuc–GFP1-7) stably expressing half of a split *Renilla*-GFP luciferase reporter, and co-culturing them with target cells (BHK-21 rLuc–GFP-8-11), stably expressing the other half of the split reporter. Successful cell-cell fusion was detected for all henipaviruses compared to mock-transfected controls (pcDNA3.1 no glycoprotein, GP), although was markedly lower for GHNV, measured by *Renilla* luciferase expression (**Figure 5.4C**) (NiVM $p<0.001$, NiVB $p<0.0001$, HeV $p<0.0001$, CedV $p<0.001$) and the formation of GFP-positive syncyctia over time (**Figure 5.4D and E**).

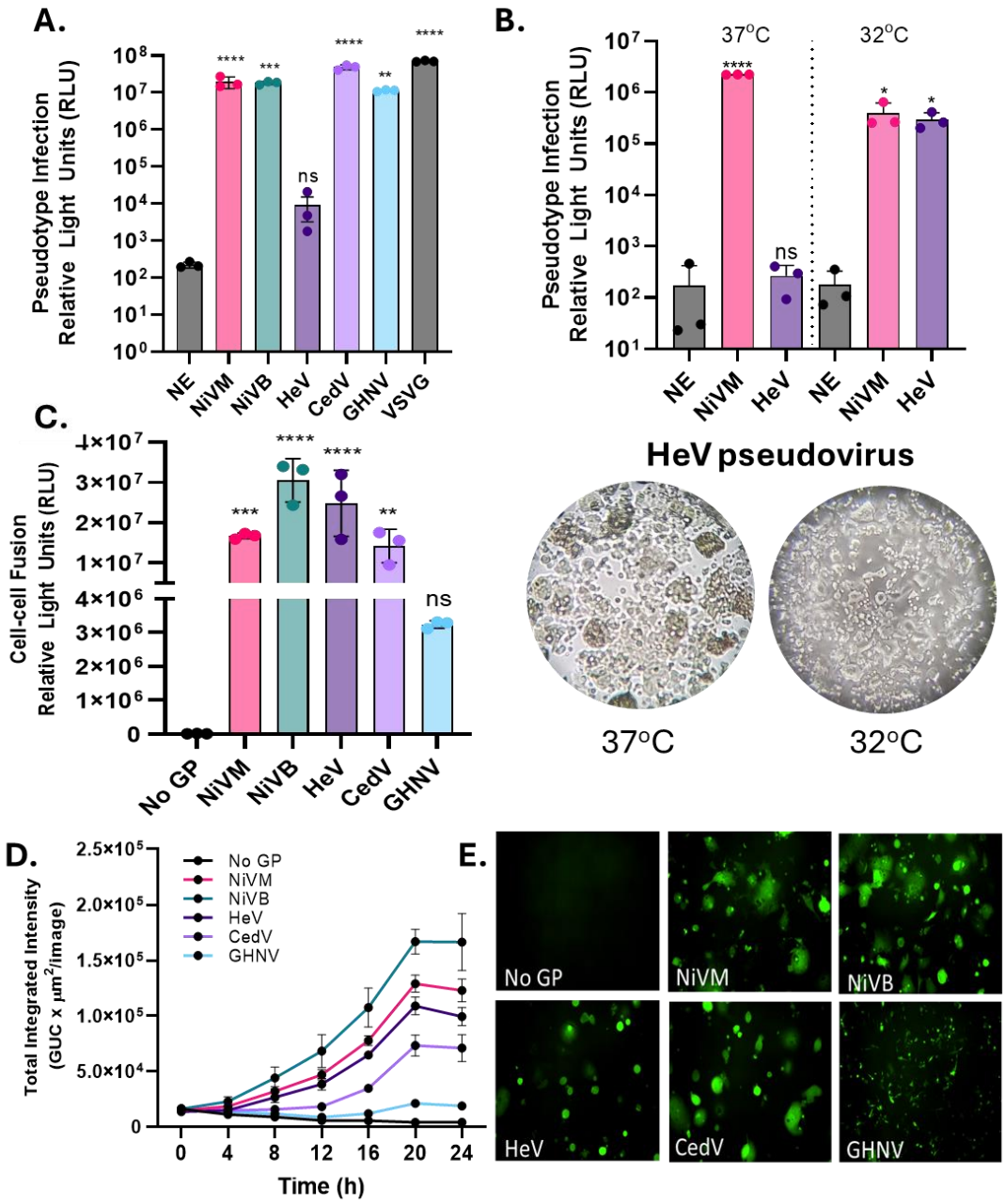

Figure 5.4: Establishing henipavirus entry assays.
(A) Luciferase signals of henipavirus pseudotypes NiVM, NiVB, HeV, CedV and GHNV. VSVG was included as a positive control. **(B)** Optimisation of HeV pseudoparticles by incubating transfections at 37°C or 32°C, with microscope images included of syncytia formation at both temperatures 2-days post transfection (10X magnification). **(C)** Successful cell-cell fusion for henipaviruses expressing the F and G of NiVM, NiVB, HeV, CedV or GHNV was determined by measuring luciferase signal and **(D and E)** quantifying and visualizing the formation of GFP-positive syncytia (x10 magnification). Representative data is shown for 3 repeats, and error bars represent mean ± SD. A one-way ANOVA was used to compare viral pseudotypes to the NE control (*p<0.0001* ****, *p<0.001* ***, *p<0.01* **, ns non-significant).

In addition to assessing the ability of NiV- and HeV-based vaccines to induce cross-neutralising antibody responses across the henipavirus genus, I also wanted to establish an ELISA to look more broadly at binding antibodies to henipavirus attachment (G) proteins with vaccine sera and known mAbs. To achieve this, I cloned the ectodomain of our proteins of interest (NiVM-G, NiVB-G, HeV-G, GHNV-G, CedV-G) into an expression vector containing a secretion signal. These plasmids were then transfected into suspension

Expi293 cells, after which the supernatants were harvested and the presence of secreted protein was determined by blotting for 6x-tag His antibody and through Coomassie protein staining. The secreted proteins (sGs) were then purified and concentrated before being used in subsequent functional assays (**Figure 5.5A**). Representative data is shown for expression of secreted NiVB-G (NiVBsG), with the other proteins produced in the same manner. A pcDNA3.1 plasmid expressing full-length NiVB-G was amplified over the ectodomain region and the correct size band (~1.6kB) was excised and cleaned-up following agarose gel electrophoresis (**Figure 5.5B**). The NiVB-G ectodomain insert was ligated into the pHLSec protein expression vector by HiFi DNA assembly, and the correct insertion of the NiVB-G ectodomain sequence was verified by performing a digest using the cloning restriction sites, AgeI and KpnI, and by Sanger sequencing (**Figure 5.5C**).

Following expression in Expi293F cells, secretion of NiVB-G was confirmed by immunoblot to detect the anti-His tag at the correct size, ~70kDa (**Figure 5.5D**). Purification of the secreted protein supernatant was performed by immobilised metal ion affinity chromatography using a Nickel-His column and fractions of protein were collected by eluting in increasing concentrations of imidazole (125 – 1000 mM) and identified by Coomassie staining (**Figure 5.5E**). Positive fractions were pooled, concentrated and buffer-exchanged into PBS and quantified by Nanodrop based on the molecular weight and extinction co-efficient of the protein (NiVB-G: MW= 70kDa, ε = 72,770, determined by Expasy ProtPram https://web.expasy.org/protparam/). Expression of purified NiVBsG was verified by Coomassie stain for 1µg protein (**Figure 5.5F**).

The recombinant proteins produced were used as antigens to coat plates in indirect ELISAs. The optimal concentration of antigen was first assessed, using 0, 1, 2 and 5 µg/mL of NiVBsG in the presence of a fixed dilution of unconjugated anti-His antibody, and optical density (OD, 450nm) measured after the addition of an HRP-linked secondary antibody. The minimal concentration for NiVBsG to yield an OD above 1 was determined to be 1µg/mL based on the cut-off value (**Figure 5.5G**). The optimal concentration of the other recombinant proteins, determined in the same manner was 1µg/mL for NiVMsG and HeVsG, and 5µg/ml for CedVsG and GHNVsG.

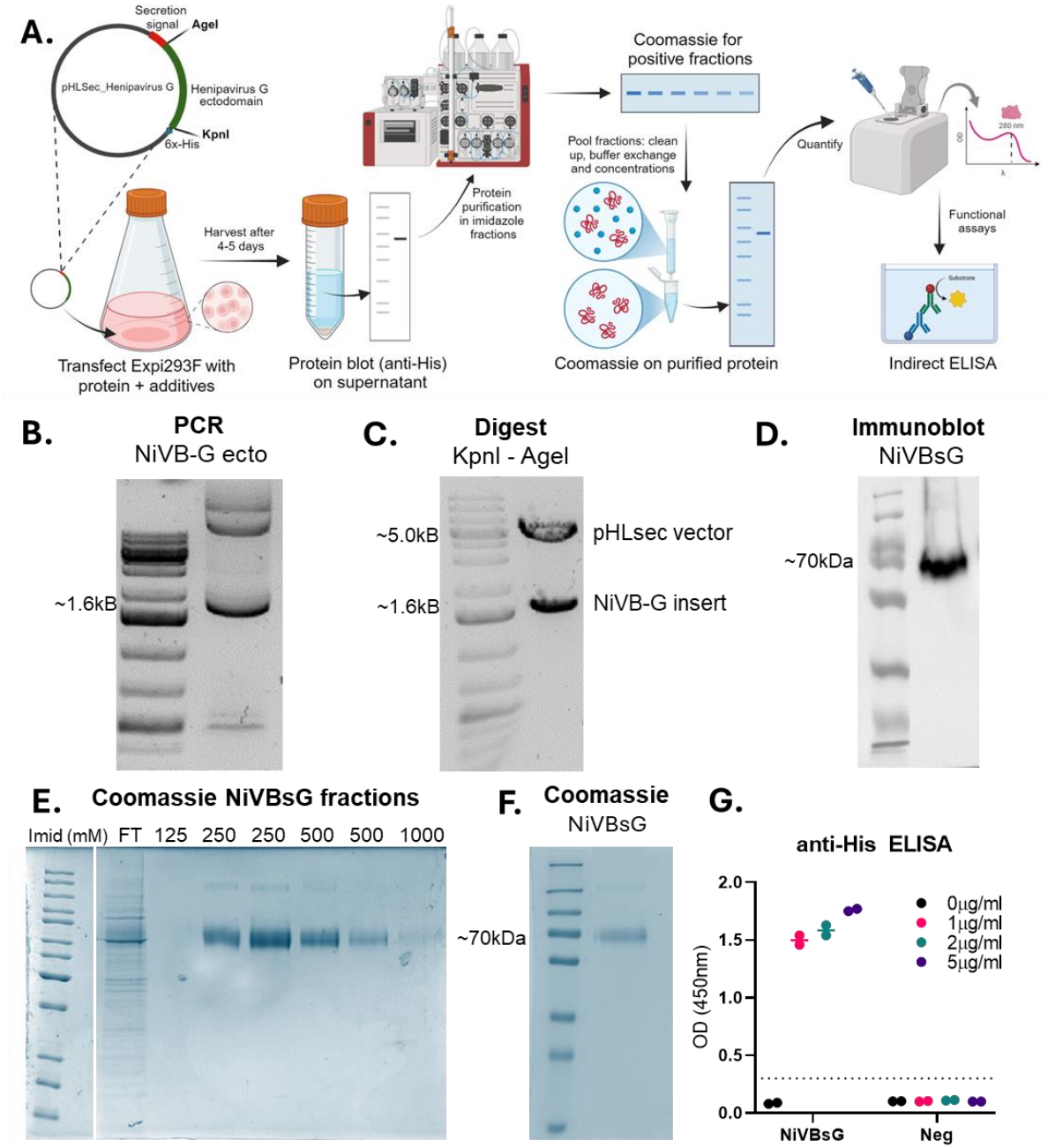

Figure 5.5: Production of secreted recombinant protein expressing henipavirus G.
(A) Schematic outlining protein expression and purification process, produced in BioRender. **(B)** DNA gel showing PCR of NiVB-G ectodomain with primers listed. **(C)** Diagnostic digest of pHLSec-NiVB-G plasmid with AgeI and KpnI to determine correct ligation of insert and vector. **(C)** Anti-His tag immunoblot to determine expression of NiVBsG following protein expression and purification. **(E)** Coomassie stain of protein fractions of NiVBsG with increasing concentrations of imidazole (mM). **(F)** Coomassie stain of concentrated and buffer-exchanged purified NiVBsG protein (1µg). Proteins run by SDS-PAGE under reducing condiitions. **(G)** Indirect ELISA optimization using 0, 1, 2, 5 µg/ml NiVBsG in the presence of a fixed dilution (1:1000) of an anti-His unconjugated antibody. Data points show OD (450nm) with mean OD shown and the dotted line indicated the cut-off value (mean + 3SD of negative).

5.2.2 Optimisation of binding and entry assays for parahenipaviruses.

Additionally, I also attempted to establish binding and entry assays for the parahenipaviruses MojV and MeliV to understand the entry mechanisms and breadth of cross-reactivity and cross-neutralisation of these related viruses. Using a lentiviral-based pseudotype platform, I transfected equivalent amounts of parahenipavirus F and G into

producer cells before infection of a library of target cells. MojV was isolated from rats, so I tested various rodent cells including hamster (BHK-21, DEDE, CHO), mouse (McCoy, RAW264.7) and rat (PC12) cell lines. MeliV was isolated in shrew, however I did not have access to shrew cell lines so assessed the MeliV pseudoviruses in rodent cell lines also. I also included the human epithelial cell line HEK293T as both MojV and MeliV have been suggested to be linked with infection in the human population. I was unable to detect any appreciable level of pseudovirus infection in any of the cell lines examined, above the non-enveloped (NE) control (**Figure 5.6A**). I did however observe infection with a VSV-G pseudovirus positive control with all the cell lines, to varying degrees (**Figure 5.6A**).

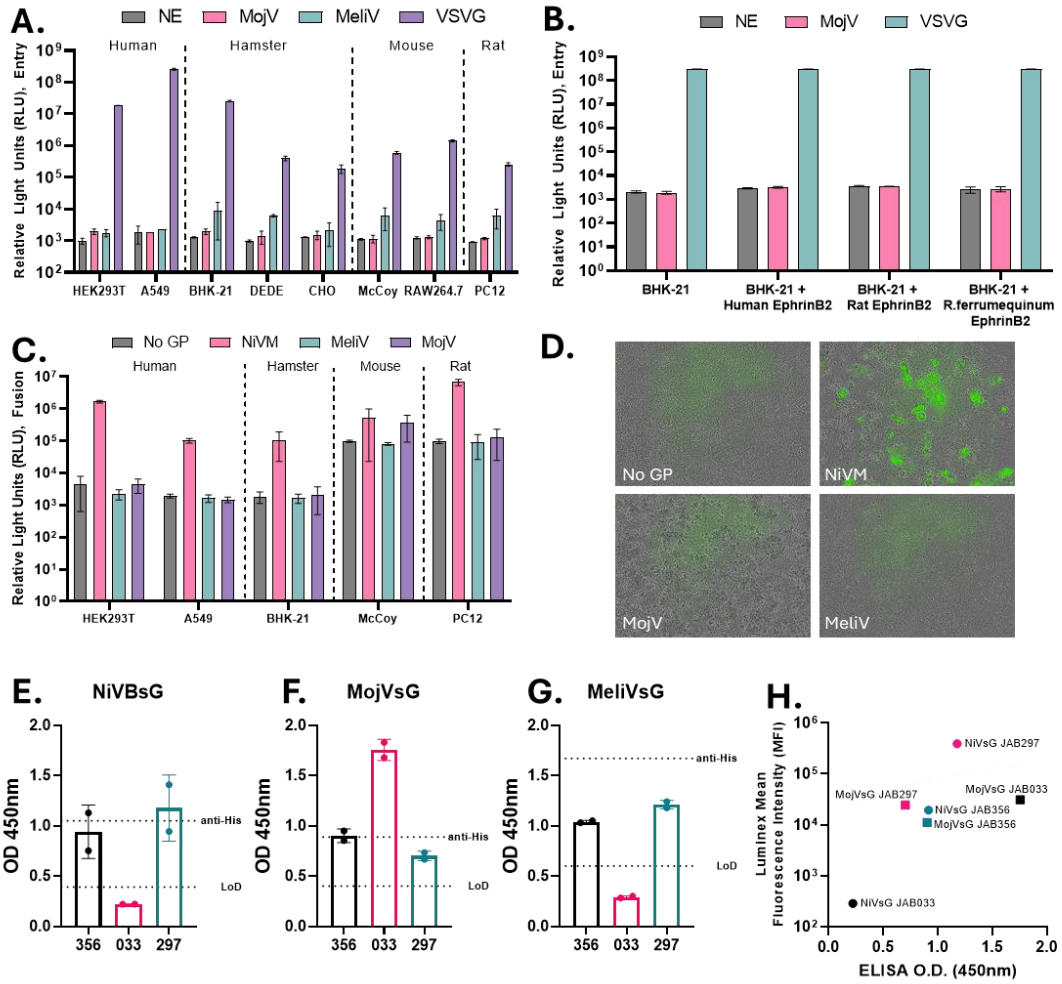

Figure 5.6: Optimisation of entry and binding assays with parahenipaviruses.
Lentiviral pseudotype entry assays for MojV and MeliV using different target cells of **(A)** HEK293T, A549, BHK-21, DEDE, CHO, McCoy, RAW264.7, PC12, or **(B)** BHK-21 cells transiently transfected with human, rat or *Rhinolophus ferrumequinum* EphrinB2. VSV-G was included as a positive control. Non-enveloped, NE particles were used to establish background luciferase levels. **(C)** Cell-cell fusion assay for NiVM, MojV, MeliV using HEK293T, A549m BHK-21, McCoy or PC12 cells as targets. NiVM was included as a positive control and mock-transfected cells to establish background luciferase (no glycoprotein, GP). **(D)** GFP images (10x magnification) for fusion assays using BHK-21 target cells. Indirect ELISAs showing OD (450nm) for sera tested for reactivity against **(E)** NiVBsG, **(F)** MojVsG or **(G)** MelisG using serum samples from individuals who actively engage in bushmeat hunting in Guinea and screened positively for *Henipavirus* G proteins by Luminex [226]. Limit of detection (LoD) is indicated, determined as the mean + 3SD of negative sera. The OD value for anti-His is included as a positive control. **(H)** *XY* correlation for indirect ELISA vs Luminex mean fluorescence intensity (MFI) for binding of sera to NiVBsG and MojVsG secreted proteins and tetramers, respectively.

The parahenipaviruses do not use the Ephrin receptors for entry and the entry receptor is yet unknown, but to understand whether the EphrinB2 receptor from other species could support infection with MojV pseudovirus, I transiently transfected BHK-21 cells with human, rat or *Rhinolophus ferrumequinum* EphrinB2, the latter two species inhabiting the cave in which MojV was identified [147]. However, MojV pseudovirus entry was not observed above background (NE) in any of the receptor conditions although I could detect entry with a VSV-G pseudovirus positive control (**Figure 5.6B**). I therefore attempted to instead establish a cell-cell fusion assay for the parahenipviruses, transiently transfecting effector cells expressing rLuc-GFP1-7 with equimolar ratios of MojV or Meli F and G, which were co-cultured with target cells expressing rLuc-GFP-8-11. I assessed entry with human (HEK293T, A549), hamster (BHK-21), mouse (McCoy) and rat (PC12) cell lines and detected cell fusion with NiVM but not for MojV or MeliV – with either luciferase or GFP – for any cell line, above the no glycoprotein (GP) background control (**Figure 5.6C and D**).

As I was unable to establish entry or cell-cell fusion assays for the parahenipaviruses, I instead generated secreted proteins for MojV-G and MeliV-G, in the same manner as described in **Figure 5.5,** to measure binding antibodies and determined the optimal concentration of MojVsG and MeliVsG to be 5µg/ml giving OD values of between 1.0 – 1.5 with an anti-His antibody conjugate (**Figure 5.6E-G**). Serum samples were collected from 499 households whose individuals actively engage in bushmeat hunting in the Macenta prefecture of Guinea, a region that was the index site of the 2013-1016 Ebola epidemic and the 2021 Marbury virus outbreak. These samples were initially screened in a Luminex assay against several viral glycoproteins, including henipavirus G proteins (study led by Prof Miles Carroll, University of Oxford) [226, 227]. The specificity of NiVBsG, MojVsG and MeliVsG was examined with a small subset of this sera (JAB356, JAB033 and JAB297) determined to be positive for these respective antigens by Luminex.

I was able to detect IgG antibody responses against NiVBsG, MojVsG and MelisG with JAB356 and JAB297, but JAB033 only had specificity only for MojVsG (**Figure 5.6E-G**). Our indirect ELISA data correlated well with the Luminex data obtained by Grace Hood (University of Oxford) using NiVB-G and MojV-G tetramers, suggesting detection of virus-specific IgG antibodies in these sera (**Figure 5.6H**). Due to the lack of productive infection in our pseudotype and cell-cell entry assays, these assays were not used in subsequent analyses. Instead, I focused on using secreted proteins in indirect ELISAs to detect cross-reactive antibodies following henipavirus vaccination or infection.

5.2.3 Examining antibody responses against henipaviruses using bio-banked sera from NiV/HeV-immunised pigs and monoclonal antibodies.

Using the low-biocontainment assays established, the ability of sera from pigs vaccinated with NiV- and HeV-based vaccines to elicit cross-neutralisation of different henipaviruses was assessed. This is important to understand the utility of current vaccines being designed in eliciting cross-protection against other henipaviruses, known or unknown, should they emerge in the human population. These sera were generated as part of an Innovate NiV immunogenicity study (led by Prof. Simon Graham and Dr Rebecca McLean, The Pirbright Institute, *manuscript in preparation*) and included a recombinant, secreted variant of NiV-G (NiVMsG); a molecular clamp stabilised NiV-F protein (NiVmcsf) [228]; a replication deficient chimpanzee adenovirus-vectored NiV-G (ChAdOx-1 NiV G) [191]; and a soluble recombinant HeV-G (HeVsG) protein, based on the protective antigen in EquiVac® vaccine licenced for use in horses [194]. Of note, since the pig acted as an amplification host for the initial outbreak of NiV in Malaysia, all porcine vaccines were based on the NiVM sequence as the immunogen (**Figure 5.7A**).

I selected late timepoint (day 42) sera from each vaccine group (n=6 pigs per group) vaccinated under a homologous prime-boost regime as this is when I would expect to detect the highest antibody response. To confirm this, I tested these sera in our in-house indirect ELISAs against each henipavirus recombinant protein. As expected, sera from pigs vaccinated with a matched subunit protein and immunogen produced the highest IgG-specific responses (i.e. NiVMsG vaccinated pig sera with NiVMsG, and HeVsG vaccinated pig sera with HeVsG). There was also high cross-reactivity with NiVBsG (**Figure 5.7B**). Sera from the NiVMsG vaccinated group showed variable IgG responses to HeVsG, with sera from the NiVMsG vaccinated group yielding the highest endpoint titres compared to other vaccine groups (**Figure 5.7B**). I also detected cross-reactive antibodies against CedVsG and GHNVsG (**Figure 5.7B**). Sera from the ChAdOx1-NiVG and HeVsG vaccine groups also had similar IgG responses against NiVMsG, NiVBsG and GHNVsG albeit to a lesser extent that the NiVMsG vaccine group, while sera from the HeVsG group had detectable IgG against all 4 sG proteins (**Figure 5.7B**). There were no detectable IgG responses against CedVsG in the ChAdOx1-NiVG vaccine group, nor for any of the antigens in the NiVmcsF immunised group (**Figure 5.7B**). Due to the differences in antigen preparations and concentrations used, and since there is no standard curve to normalise to, I was unable to make direct comparisons between the signals obtained for each ELISA antigen. I also tested the human monoclonal m102.4, which was raised against a soluble form of the HeV-G protein in indirect ELISAs. This mAb interacts with the receptor binding domain of HeV and NiV attachment protein and has been shown to cross-react with high

affinity to both viruses [165]. I found that m102.4 had high detectable binding responses against both NiVMsG and HeVsG, but not against CedVsG or GHNVsG (**Figure 5.7C**).

Using pseudotype neutralisation assays (mVNT assays) I examined the same sera from each vaccine group for the presence of cross-neutralising antibodies. Assays were performed with NiVM, NiVB, HeV, CedV, and GHNV pseudotyped viruses. The NiVMsG vaccinated pigs exhibited robust nAb responses against both NiVM and NiVB pseudotypes (**Figure 5.7D**). The same was also observed for NiVmcsF and ChAdOx1-NiVG vaccinated pigs, with similarly high IC50 seen against NiVB and NiVM (**Figure 5.7D**). Interestingly, both NiVM- and NiVB-specific nAbs were detected in animals vaccinated with a HeV antigen, but there were no nAbs detected against CedV or GHNV above the limit of detection for any of the vaccine groups (**Figure 5.17D**). I also assessed the nAb response against HeV pseudoviruses, including NiVM as a comparator, and found that comparable titres were obtained against HeV and NiVM in the HeVsG vaccinated groups. However, pigs immunised with NiV-based vaccines elicited low nAb responses against HeV pseudoviruses (**Figure 5.7E**). These findings highlight that both HeV- and NiV-vaccinated pigs can elicit a cross-protective nAb response to different strains of NiV (NiVM and NiVB), however this does not translate to the more distantly related viruses within the genus.

Separately, I examined the ability of two mAbs to inhibit virus entry and cell-cell fusion. I again tested m102.4 and additionally, mAb 5B3 which binds to the NiV- and HeV-F proteins and ‘holds’ them in their pre-fusion state, inhibiting membrane fusion (mAbs provided by Daniel Watterson and Keith Chappell, University of Queensland) [170]. I demonstrated that both 5B3 and m102.4 were able to robustly inhibit viral entry of NiVM and NiVB by >50%, but only m5B3 was able to inhibit fusion of these viruses by >50% in micro fusion inhibition tests (mFITs), as demonstrated previously [162] (**Figure 5.7F and G**). Both m5B3 and m102.4 were able to inhibit fusion of HeV, consistent with previously published data [165, 170] (**Figure 5.7F and G**). Inhibition of pseudoparticle entry or cell-cell fusion was not observed with any of the other henipaviruses, nor against the VSVG pseudotype control (**Figure 5.7F and G**).

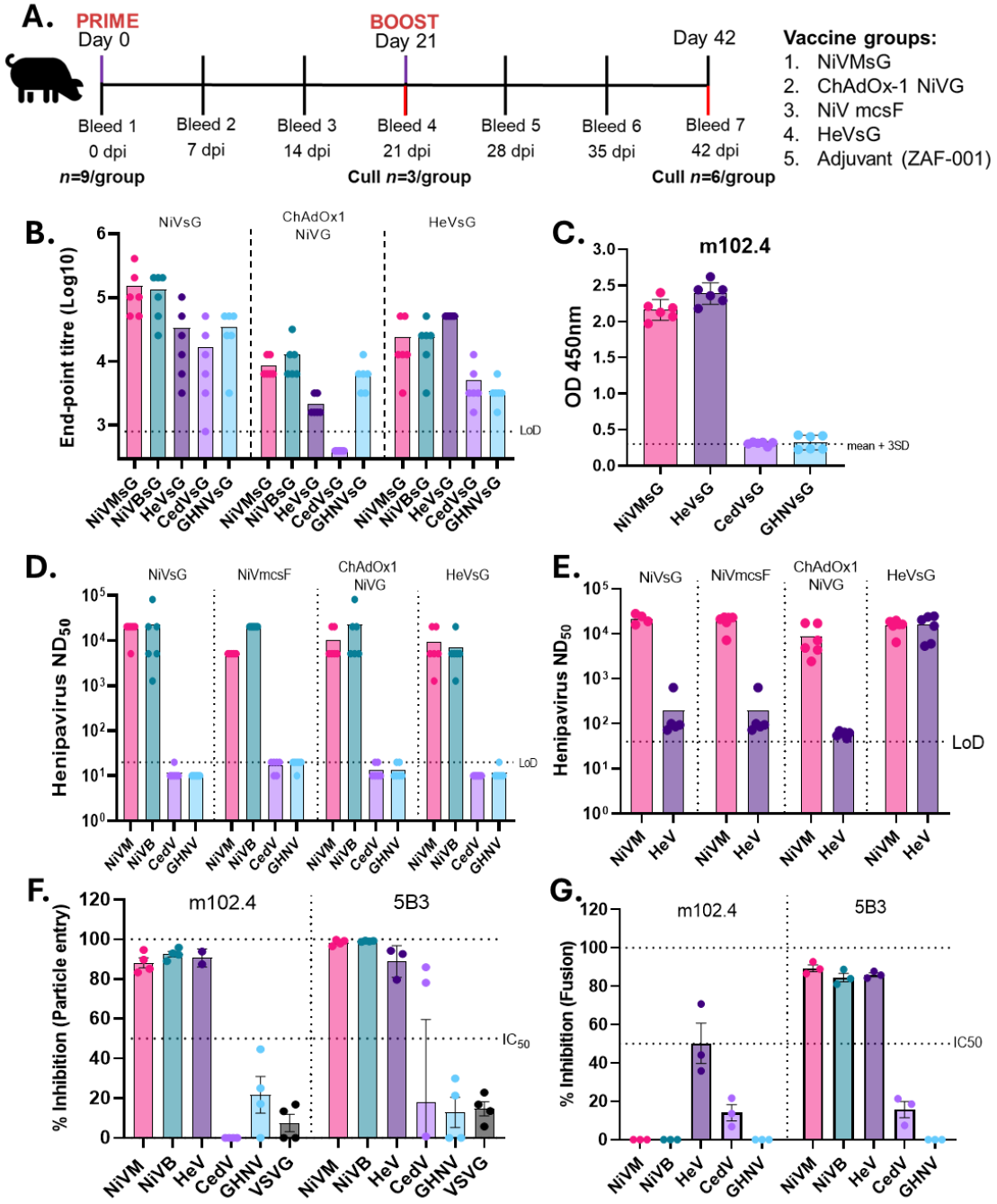

Figure 5.7: Antibody assays using NiV or HeV vaccinated-pig sera and monoclonal antibodies.
(A) Schematic outlining pig immunogenicity study. Forty-five 8-10-week-old female cross-bred pigs were immunised i.m. under a prime-boost regime 3-weeks apart with 1 × 10^9 IU ChAdOx1 NiV-G, 100 µg NiVsG in ZAF-001; 100 µg NiVmcsF in ZAF-001; 100 µg HeVsG in ZAF-001; or an equivalent volume (1 mL) of ZAF-001. Serum samples were obtained weekly and animals were euthanized as indicated (n=3/group day 21, n=6/group day 42). Indirect ELISAs to detect IgG binding against NiVMsG, NiVBsG, HeVsG, CedVsG and GHNVsG for **(B)** day 42 sera from immunised pigs or **(C)** for the anti-human G-specific monoclonal m102.4 (1µg/ml), with end-point titres shown. **(D)** NiVM, NiVB, CedV, GHNV and **(E)** HeV mVNTs carried out using late time-point sera. Inhibition was calculated as the inhibition at which 50% inhibition of no sera controls was seen (ND_{50}), interpolated from a line of best fit. **(F)** A virus neutralisation test using pseudotypes (mVNT) and **(G)** a fusion inhibition test (mFIT) were carried out in the presence of the anti-F mAb 5B3 or the anti-G mAb m102.4. For the mVNT **(F)**, 2µg/mL of each antibody was incubated with NiVM, NiVB, HeV, CedV and GHNV pseudotypes equivalent to 10^6 signal luciferase units. For the mFIT **(G)**, 20µg/ml of each mAb was incubated with effector cells expressing henipavirus F and G viral glycoproteins for NiVM, NiVB, HeV, CedV and GHNV. Inhibition of entry or fusion was calculated as a percentage that yielded 50% inhibition (IC_{50}) relative to untreated controls (i.e. no mAb). Each bar represents the median OD or titre within a group, with each point representing a single animal; error bars represent mean ± SD. The dotted line represents the limit of detect of the assay (mean + 3SD for ODs, limit of detection (LoD) for titres).

5.2.4 Assessment of candidate henipavirus vaccines in a mouse immunogenicity study.

Due to the cross-reactive but non-neutralising antibody response detected in sera from NiV/HeV-vaccinated pigs against more distance henipaviruses, I wanted to determine whether this was true for other henipaviruses. The theoretical basis for this study was to understand which henipavirus antigen, or combination of antigens, if any, could provide the widest degree of cross-protection during an outbreak of known or an unknown henipavirus. Therefore, homologous or heterologous vaccinations were conducted using the G protein of two distantly related henipaviruses, NiVB and GHNV. I decided on using the subunit G platform as this is where the highest antibody responses was observed in our pig model (**Figure 5.7**). BALB/c mice (n=6 per group) were immunised intramuscularly under a prime-boost-boost regime, with 4-weeks between each booster vaccination. Mice received either homologous immunisations of an adjuvanted subunit vaccine (sG) expressing NiVBsG or GHNVsG, or heterologous immunisations of NiVB-sG – GHNVsG – GHNVsG or GHNVsG – NiVBsG – NiVBsG (**Figure 5.8A**). Serum samples were obtained prior to each boost, with cardiac bleeds obtained when animals were culled 12-weeks post prime for analysis of antibody responses and spleens harvested to investigate T-cell responses (**Figure 5.8A**). Animal handling, immunisations, bleeds and take-downs were performed by Barabara Dema Jimenez and Marta Ulaszewska, University of Oxford.

I initially analysed the total IgG binding response by indirect ELISA to understand the antigen-matched responses in the different vaccine groups. After a single immunisation with either NiVBsG or GHNVsG, I was only able to detect binding antibodies against the matched immunogen, however cross-reactive antibodies were detected in all vaccine groups against both NiVBsG and GHNVsG after the first boost (**Figure 5.8B and C).** The total IgG response against NiVBsG was comparable between different vaccine regimes and did not increase further after a second-boost and a similar response was detected against GHNVsG when GHNVsG was given as the first immunogen. In contrast, immunising with NiVBsG first only showed a moderate increase in antibody titre after a first-boost, and increased further after a second boost, to levels comparable to the homologous immunised GHNVsG group and the GHNVsG – NiVBsG – NiVBsG group (**Figure 5.8B and C).**

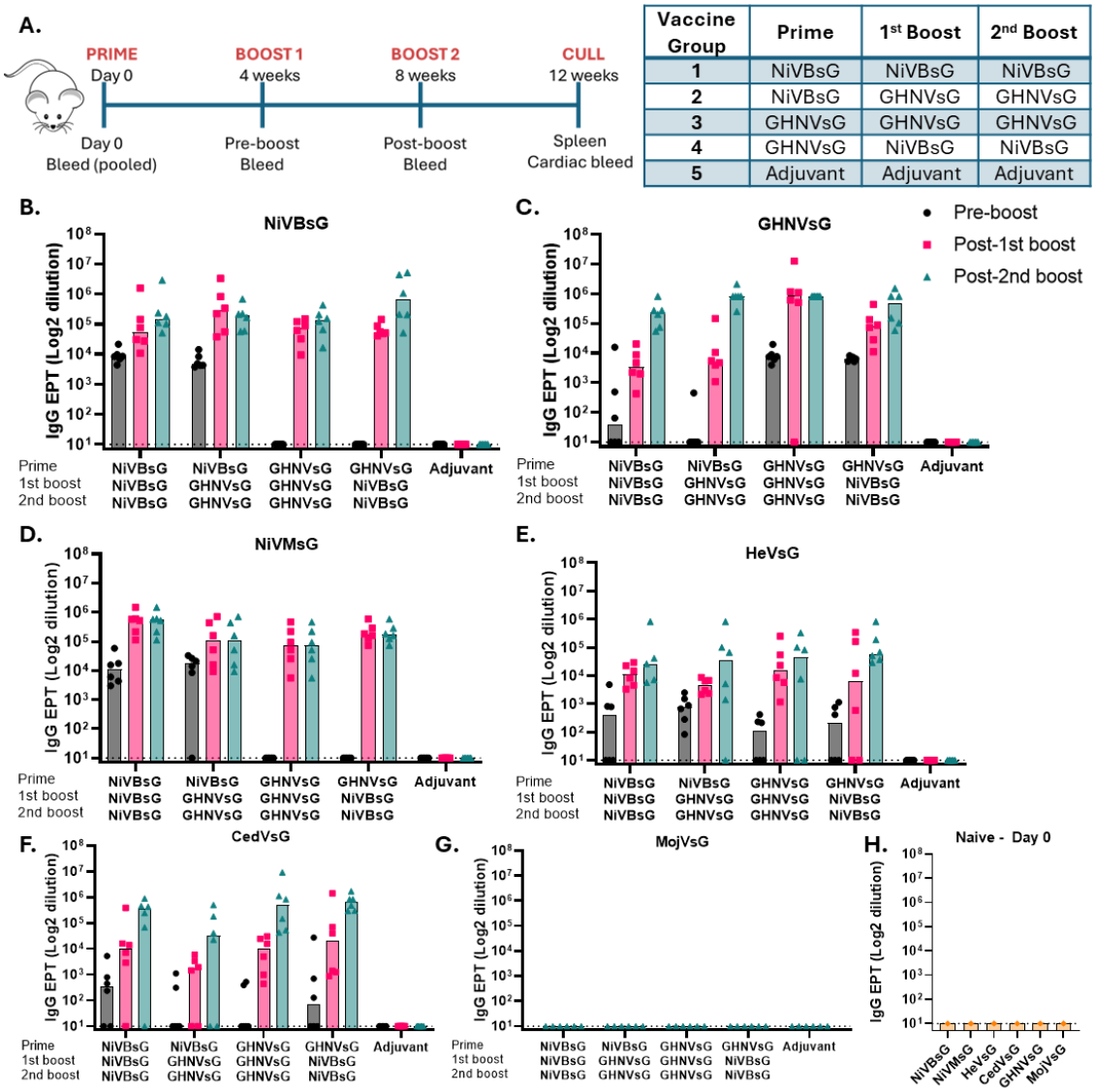

Vaccine Group	Prime	1st Boost	2nd Boost
1	NiVBsG	NiVBsG	NiVBsG
2	NiVBsG	GHNVsG	GHNVsG
3	GHNVsG	GHNVsG	GHNVsG
4	GHNVsG	NiVBsG	NiVBsG
5	Adjuvant	Adjuvant	Adjuvant

Figure 5.8: Mouse immunogenicity study using henipavirus vaccines under homologous and heterologous vaccinations reveals broad cross-reactivity against different henipaviruses.
(A) Schematic of experimental plan. BALB/c mice (n=6/group) were immunised i.m. with 2.5µg adjuvanted NiVB or GHNV subunit proteins using a homologous or heterologous regime, as described in the table adjacent. Mice received booster vaccines 4 and 8 weeks apart. An adjuvant only group was also included. Bleeds were taken prior to each boost and at 12-weeks after prime for use in subsequent analysis. Spleens were also harvested from euthanised animals for use in functional assays. Indirect ELISAs were conducted on pre-boost, post-1st boost and post-2nd boost sera against the **(B)** NiVBsG, **(C)** GHNVsG, **(D)** NiVMsG, **(E)** HeVsG and **(F)** CedVsG antigens. **(G)** Indirect ELISAs were also carried out (G) on post-2nd boost sera against MojVsG antigen and on **(H)** pooled sera from naïve mice (n=6) at day 0 pre-immunisation against all antigens. End-point titres (EPTs) are shown calculated by transforming the interpolated values from a nonlinear least squares regression standard curve. Each point represents an individual animal. Dotted lines represent the limit of detection for the assay and bars represent median EPTs.

I next examined the total IgG response against related henipavirus sGs, noting comparable antibody titres against NiVMsG to those observed for NiVBsG. A similar trend was also observed against HeVsG but with lower titres (**Figure 5.8D and E).** Interestingly, I was able to detect cross-reactive antibody responses against HeVsG after one immunisation with either NiVBsG or GHNVsG, with modest increases in titre with subsequent boosters (**Figure 5.8E).** The antibody response against CedVsG was the lowest out of all the henipavirus G proteins tested following a single immunisation. Nevertheless, I noted the

greatest increase in total IgG response in groups where GHNVsG was administered as the first vaccine, but also in the NiVBsG homologous group. I was still able to detect cross-reactive antibodies against CedVsG in the NiVBsG – GHNVsG – GHNVsG immunised group, but to a lesser extent than the other vaccine groups (**Figure 5.8F).** No cross-reactive antibodies were detected in the adjuvant only immunised group against any of the antigens (**Figure 5.8B-F).** I also wanted to understand if this cross-reactive phenotype extended to the parahenipaviruses, but were not able to detect any total IgG responses against MojVsG (**Figure 5.8G**). I also analysed pooled naïve sera from mice taken at day 0 prior to immunisation and did not note any specific IgG antibody responses, as expected (**Figure 5.8H**).

Due to the high level of cross-reactivity I observed against all the henipavirus G proteins in ELISA, I wanted to understand whether the antibodies also had neutralising capability, considering I also detected cross-reactive antibodies in pigs vaccinated with NiV-G, which were non-neutralising (**Figure 5.7**). Hence, I performed neutralisation assays using lentiviral pseudotypes bearing different henipavirus glycoproteins, initially examining the response against the vaccine-matched viruses, NiVB and GHNV. Similar to what was observed by ELISA, after prime only nAb responses against NiVB were detected when NiVBsG was administered as the first immunisation, but not GHNVsG. However, after a first- or second-booster vaccination, robust nAb responses were detected against NiVB in all vaccine groups, albeit lower in the GHNVsG homologous group (**Figure 5.9A**). In contrast, nAbs against GHNV were only detected in the GHNVsG homologous group, which were considerably lower than the titres calculated against NiVB. A marginal nAb response was also noted against GHNV in the NiVBsG – GHNVsG – GHNVsG vaccinated group after second-boost, and titres just above the limit of detection in the NiVBsG- GHNVsG – GHNVsG immunised group (**Figure 5.9B**).

Next, the cross-neutralising capacity of this sera was examined against other henipaviruses using only sera from post second boost (due to the limited availability of sera from the other timepoints). A similar pattern in the nAb response was noted against NiVM that was detected for NiVB (**Figure 5.9C**)**.** Cross-neutralising antibodies were also detected against HeV, which were strongest in the groups where a NiVBsG vaccine was received two or three times (i.e., NiVBsG homologous group or GHNVsG – NiVBsG – NiVBsG group), compared to when a GHNVsG vaccine was delivered (i.e., GHNVsG homologous group or NiVBsG – GHNVsG – GHNVsG group) **(Figure 5.9D**). Similar to the porcine immunisations, no cross-neutralising antibodies were detected against CedV pseudoviruses with any of the vaccine groups, despite the presence of a robust total IgG antibody response (**Figure 5.9E**).

No nAb responses were detected with pooled naïve day 0 sera against any of the henipavirus pseudoviruses (**Figure 5.9F**).

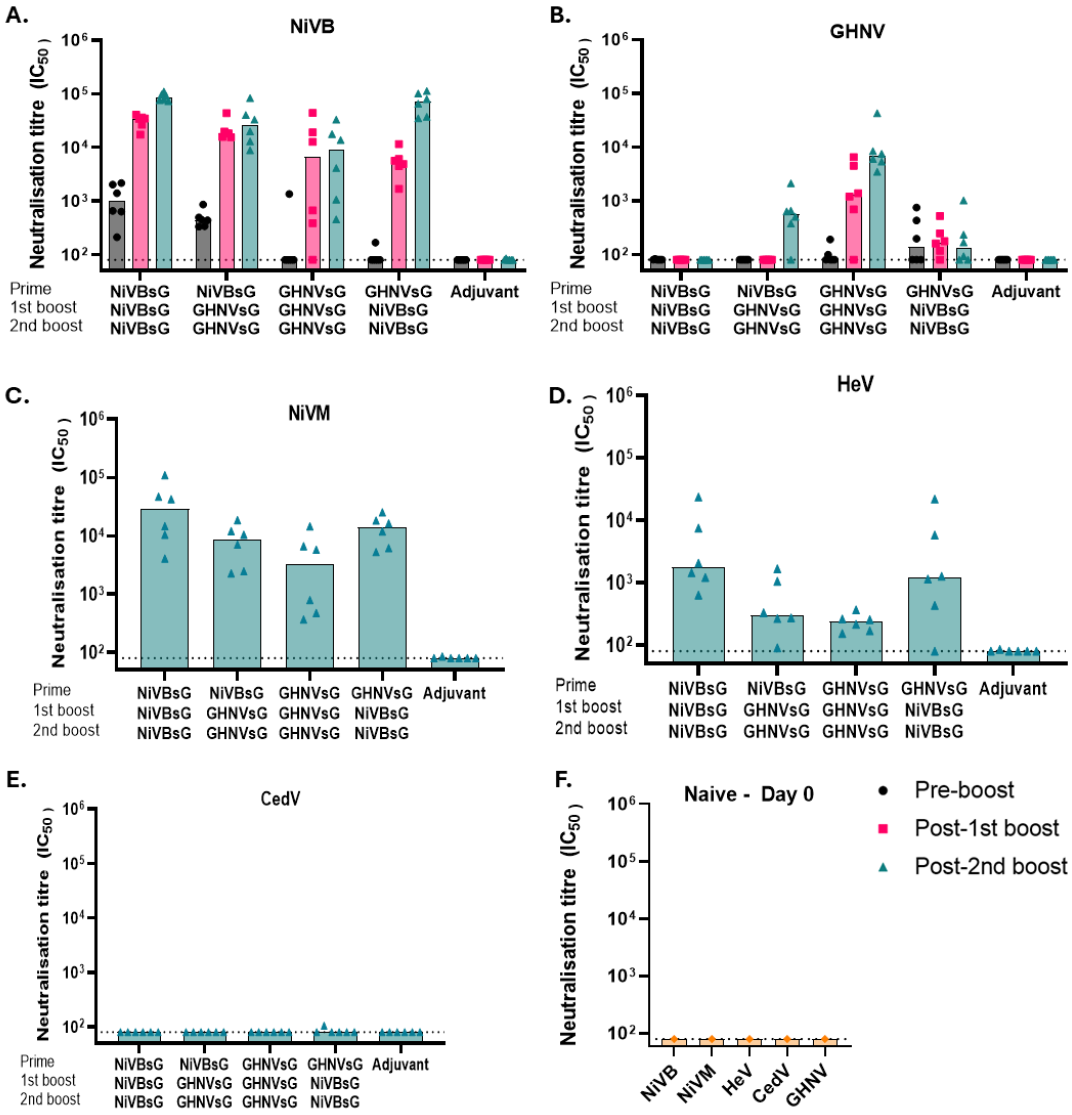

Figure 5.9: Mouse immunogenicity study using henipavirus homologous and heterologous vaccination regimes reveals cross-neutralisation of henipaviruses.
Lentiviral-based pseudotype neutralisation assays were conducted on pre-boost, post-1st boost and post-2nd boost sera from immunised animals against **(A)** NiVB and **(B)** GHNV. Further neutralisation tests were carried out on post-2nd boost sera against **(C)** NiVM, **(D)** HeV and **(E)** CedV, and **(F)** on naïve pooled day 0 sera against all henipavirus pseudoviruses. Inhibition was calculated as the point at which 50% inhibition of no sera controls was seen (ND_{50}), interpolated from a line of best fit with each data point representing an individual animal. The dotted line indicated the limit of detection (LoD) of the assay and the bars represent median ND_{50} titre.

Finally, I wanted to understand whether these vaccines could also induce antigen-specific T-cell responses, which are known to play a critical role in durable memory immune responses and in providing help to B-cells for generation of high affinity antibodies [333]. Therefore, splenocytes isolated from immunised animals were stimulated with pools of overlapping synthetic peptides representing NiVB-G, GHNV-G or CedV-G and enumerated IFNγ secreting cells by ELISpot (**Figure 5.10A**). Interestingly, similar trends in the IFNγ

response across was observed in the different vaccine groups to those that were seen for the nAb responses, with the strongest response detected in the homologous matched vaccinated group i.e., the NiVBsG group stimulated with NiV-G peptides ($p<0.0001$), and the GHNVsG homologous group with GHNV-G peptides ($p<0.0001$). Additionally, the lower numbers of IFNγ secreting cells were detected in the NiVBsG vaccinated group following stimulation with GHNV-G peptides, and vice versa (**Figure 5.10B and C**).

The IFNγ response detected in the heterologous prime-boost-boost groups were comparable and fell in a range between that of the NiVBsG and GHNVsG homologous vaccine groups (**Figure 5.10B and C**). Of note, a single peptide pool was used for CedV-G and GHNV-G, but for NiVB-G the data shown was acquired from peptide pools spanning 3 regions of the G protein. In the NiVBsG homologous prime-boost-boost immunised group, the IFNγ response was generally comparable between all peptide pools, but greatest with peptides that span the stalk region and the C-terminal of the globular head (**Figure 5.10D**). For both the heterologous immunisation groups, the IFNγ response was greatest when stimulated with NiVB-G peptide pool 3, which spans towards the end of the globular head and is the region in which the receptor binding motif is located (**Figure 5.10D**). Strong IFNγ responses were also detected against CedV-G peptides, particularly in the NiVBsG homologous and GHNVsG – NiVBsG – NiVBsG groups ($p<0.001$), which were conversely considerably lower in the two vaccine groups where GHNVsG was the more frequently used antigen. No substantial IFNγ response was noted in the adjuvant only group (**Figure 5.10B-E**).

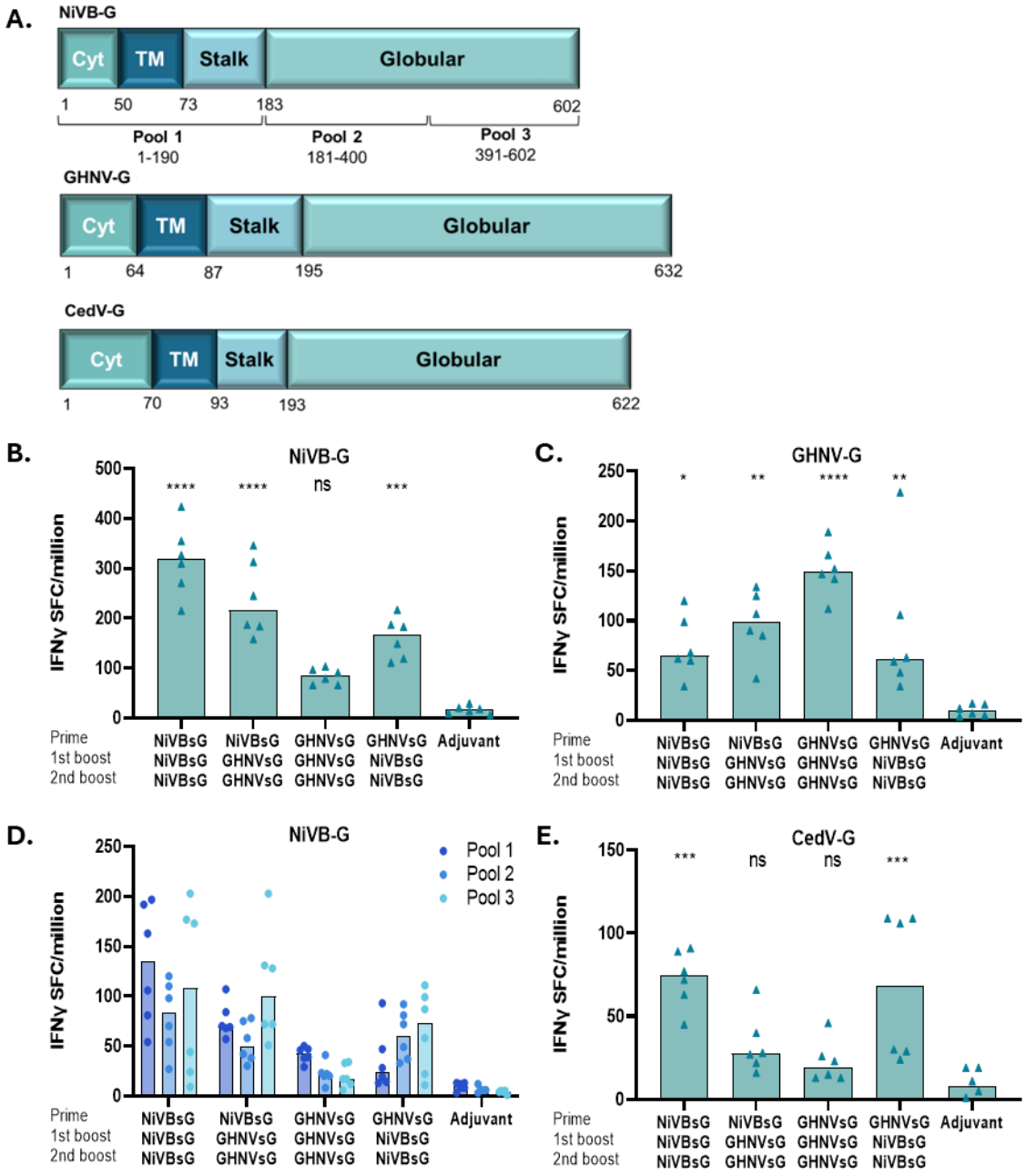

Figure 5.10: Mouse immunogenicity study using Henipavirus vaccines under homologous and heterologous vaccination regimes induce IFNγ T-cell responses.
(A) Schematics depicting synthetic peptide libraries (20-mers offset by 10 amino acids) used to stimulate splenocytes from immunised animals. The NiVB-G library was split into 3 pools, and the CedV-G and GHNV-G libraries were single pools and used at 2µg/ml in subsequent assays. The schematics outline the amino acid length of different regions of the G-protein including the cytoplasmic tail (Cyt), the transmembrane domain (TM), the stalk domain (stalk) and the globular head in which the receptor binding motif is found (globular), based on published data [334-336]. Of note, the vaccine immunogens had their Cyt and TM regions (white text), removed to allow for production of secreted proteins, therefore the data from the ELIspots excludes stimulation from amino acids 1-73 for NiVB-G, 1-86 for GHNV-G and 1-92 for CedV-G. IFNγ ELIspots were carried out on splenocytes from animals, harvested 4-weeks post 2nd boost after stimulation with **(B [total] and D [individual pools])** NiVB-G, **(C)** GHNV-G and **(E)** CedV-G peptides. Bars show the number of IFNγ secreting splenocytes in spot forming cells (SFC)/million, with each data point representing a single animal. A one-way ANOVA was used to compare IFNγ responses compared to adjuvant only controls (*p<0.0001* ****, *p<0.001* ***, *p<0.01* **, ns non-significant).

5.2.5 Efficacy study in hamsters to assess protection against NiV infection following immunisation with candidate henipavirus vaccines.

Owing to the vaccine-induced cross-reactive and cross-neutralising antibody responses and broad T-cell responses detected in our mouse immunogenicity study, particularly with GHNVsG vaccination against NiVB (**Figure 5.7-5.10**) I wanted to investigate whether immunisation with a GHNVsG vaccine would also protect against NiVB infection. This was particularly interesting for us to investigate due to the lack of bi-directionality of neutralisation between NiVB and GHNV in our mouse study (i.e., GHNVsG immunisation neutralises NiVB, but NiVBsG immunisation does not neutralise GHNV) (**Figure 5.9**), similar to the lower levels of neutralisation observed against HeV with NiVMsG vaccination in pigs (**Figure 5.7**), which suggests that NiVB may not be the best immunogen to induce cross-protection against the henipaviruses. Standard laboratory mice strains do not develop disease following NiV infection via the intraperitoneal (i.p.) or intranasal (i.n.) routes, however infection of golden Syrian hamsters with NiV is well established to result in disease and pathology similar to that seen in humans [118]. Therefore, golden Syrian hamsters were used as models to assess vaccine efficacy in our study. Animals were immunised with homologous prime-boosts of either an adjuvanted (Alhydrogel) NiVBsG or GHNVsG vaccine, or adjuvant only control 4-weeks apart (*n*=12/group). A vaccine requiring multiple booster vaccinations to induce robust immunogenicity and protection against infection is less likely to obtain funding approval due to increased cost, inefficacy and logistics of distribution, so unlike our mouse study, I opted to exclude a third vaccination to understand vaccine efficacy after only two doses. I also opted for homologous prime-boost regimes of NiVBsG and GHNVsG rather than heterologous vaccination due to the low nAb titres against GHNV in the heterologous vaccine groups (**Figure 5.9B**). The adjuvant used was determined following a preliminary hamster immunogenicity study testing NiVMsG and HeVsG antigens with different adjuvants (led by Steve-Findlay Wilson and Stuart Dowell, UKHSA [180]). A further 4-weeks later, half of the animals were euthanised to examine the vaccine-derived immune response (*n*=6) (**Figure 5.11A**)

Sera was obtained from all 12 hamsters in each group at pre-immunisation (Day 0), pre-boost (Day 28) and post-boost (pre-challenge, Day 56) and analysed by indirect ELISA against the vaccine-matched antigens NiVBsG and GHNVsG. A boosting in IgG antibody responses was observed against NiVBsG in the NiVBsG immunised group (**Figure 5.11B**). A similar trend was noted in the GHNVsG immunised group against GHNVsG, however the increase in IgG antibody response after boosting was minimal (**Figure 5.11C**). Conversely, unlike our pig and mouse data (**Figure 5.7, Figure 5.8**), cross-reactive IgG antibodies could not be detected in the NiVBsG vaccinated group against GHNVsG, nor in the GHNVsG immunised group against NiVBsG (**Figure 5.11B and C**). The total IgG antibody response

against NiVM and HeV was also examined. A similar trend in total IgG antibody response against NiVMsG (*n*=12) and HeVsG (*n*=6) was also noted, but with end-point titres calculated ~1-2log lower than against NiVBsG, respectively (**Figure 5.11E and F**). The lower total IgG antibody response against HeVsG in hamsters compared to NiV was similar to what was observed in our pig (~2log reduction) and mouse (~1log reduction) studies (**Figure 5.7, Figure 5.8**). However, unlike data from our pig and mouse studies, total IgG antibodies were noted detected in any of the serum samples above the limit of detection against CedV (**Figure 5.11G**), or indeed in Day 0 samples or in adjuvant only vaccinated groups (**Figures 5.11 B-G**). Next, the nAb response against NiVBsG and GHNVsG was analysed, and a similar trend was noted to what was observed in the indirect ELISA, whereby NiVB pseudovirus was only neutralised by sera from NiVBsG-immunised hamsters with an increase in IC50 titre after boosting, and GHNV pseudovirus was only neutralised by GHNVsG-immunised hamsters, with little boosting effects seen following a second immunisation (**Figure 5.11H and I**). Cross-neutralising antibody responses were not detected against GHNV pseudovirus with NiVBsG vaccine sera, against NiVB pseudovirus with GHNVsG vaccine sera, or against either pseudovirus in the adjuvant only group (**Figure 5.11H and I**).

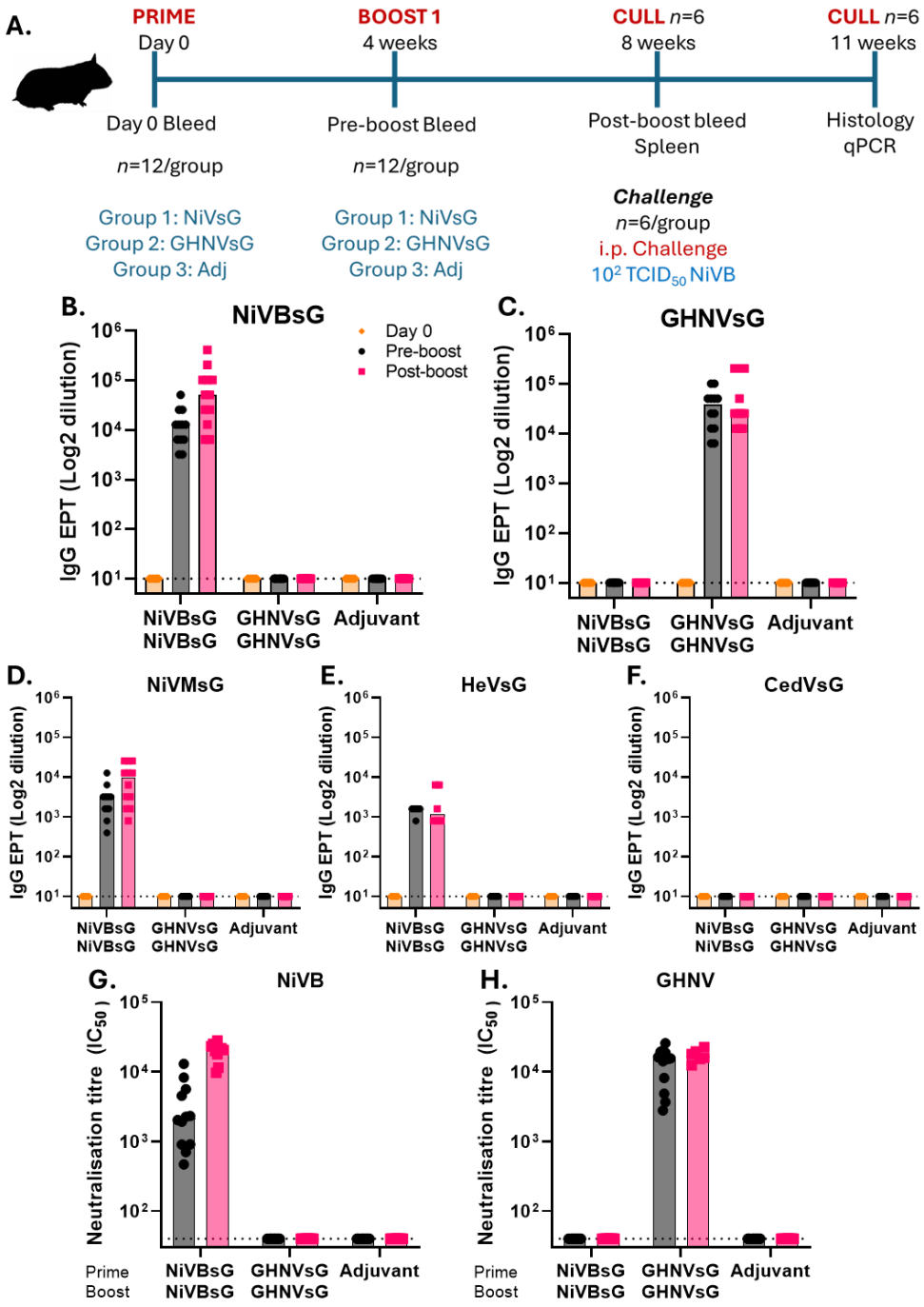

Figure 5.11: Hamster efficacy study using henipavirus vaccines under homologous vaccination regimes induce homotypic antibody responses.
(A) Schematic of experimental plan. Syrian hamsters (*n*=12/group) were immunised i.m. with 2.5µg adjuvanted (Alhydrogel) NiVB or GHNV subunit proteins using a homologous prime-boost regime 4-weeks apart. An adjuvant only group was also included. Bleeds were taken at day 0, day28 (pre-boost) and day 56 (pre-challenge). At 8-weeks, 6 animals were culled for analysis of the immune response. Spleens were also harvested from euthanised animals for use in functional assays. The remaining 6 animals were challenged i.p with 10^2 $TCID_{50}$ NiVB and animals were euthanised when they reached humane endpoint, or 3-weeks post challenge. Indirect ELISAs were conducted on day 0, 28 and 56 sera against the **(B)** NiVBsG, **(C)** GHNVsG, **(D)** NiVMsG, **(E)** HeVsG and **(F)** CedVsG antigens. End-point titres (EPTs) are shown, calculated by transforming the interpolated values from a nonlinear least squares regression standard curve. Each point represents an individual animal. Dotted lines represent the limit of detection for the assay and bars represent median EPTs. Lentiviral-based pseudotype neutralisation assays were conducted on day 28 and 56 sera from immunised animals against **(G)** NiVB and **(H)** GHNV. Inhibition was calculated as the point at which 50% inhibition of no sera controls was seen (ND_{50}), interpolated from a line of best fit. Each data point represents an individual animal. The dotted line indicates the limit of detection (LoD) of the assay and the bars represent median ND_{50} titre.

To measure vaccine-derived T-cell responses, spleens were obtained from the 6 euthanised hamsters at day 56 post-prime for analysis of stimulated splenocytes (the same peptides used in **Figure 5.10**). IFNγ in the splenocytes from the NiVBsG vaccinated group, when stimulated with NiVB-G peptides were quantified, but not in the GHNVsG or adjuvant only immunised groups (**Figure 5.12A**). In contrast, low but comparable numbers of IFNγ secreting cells were detected in both vaccine groups when splenocytes were stimulated with GHNV-G peptides (**Figure 5.12B**). The data generated from the NiVB-G stimulated splenocytes were summed from 3-separate peptide pools, and most of the IFNγ response observed was directed towards the N-terminal of the globular head region (**Figure 5.12C**). A low IFNγ response from splenocytes in the GHNVsG immunised group was also detected when stimulated with CedVsG peptides, but little to no response in the NiVBsG immunised group (**Figure 5.12D**). Of note, the hamster ELISpot assays have not been well optimised, and media controls for these ELISpots yielded high background values, and although the data presented is following media correction, the results per animal are extremely varied so caution must be taken before drawing any meaningful conclusions based on this data.

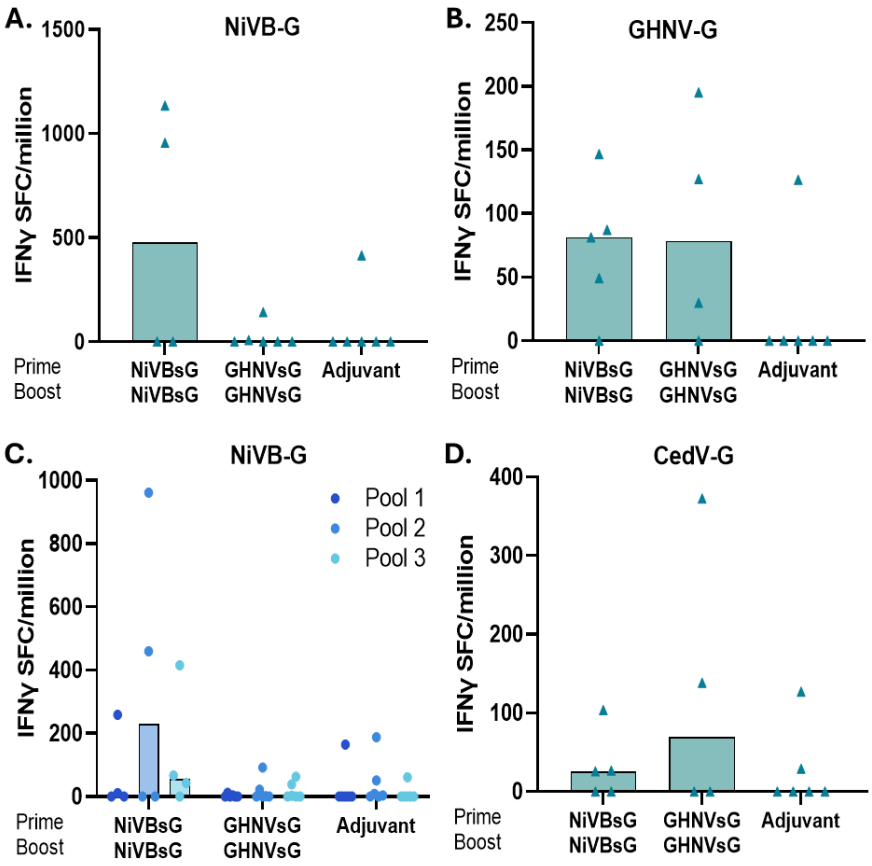

Figure 5.12: IFNγ T-cell responses in hamsters vaccinated with henipavirus vaccines under homologous vaccination regimes.
IFNγ ELIspots were carried out on splenocytes from animals, harvested 4-weeks post-boost after stimulation with **(B [total] and D [individual pools])** NiVB-G, **(B)** GHNV-G and **(D)** CedV-G peptides (as described in **Figure 5.10**). Bars show the number of IFNγ secreting splenocytes in spot forming cells (SFC)/million, with each data point representing a single animal. A one-way ANOVA was used to compare IFNγ responses compared to adjuvant only controls, which were non-significant.

Four-weeks after receiving a homologous booster vaccination, the remaining hamsters (*n*=6/group) were challenged via the intraperitoneal route (i.p.) with 10^2 $TCID_{50}$ NiVB. If animals were not already removed from the experiment because of reaching their humane end point then they were euthanised after 3-weeks and tissue was obtained for histology, sera and nucleic acid isolation (**Figure 5.11A**). The dose of virus used for challenge was determined in a preliminary study (conducted by Emma Kenndey and Lucy Flett, UKHSA) infecting hamsters i.p. with different doses of NiVB (10^5, 10^4, 10^3, 10^2 $TCID_{50}$, *n*=4/group), and selecting the lowest dose where all animals survived to end of the study. This was to ensure any protective effects of the vaccines could be elucidated, without animals reaching premature humane endpoints due to high infection doses. Of note, the 10^2 TCI50 dose selected was also in concordance with infectious doses used in previous NiVB hamster challenge studies (data not shown) [191, 337].

In the adjuvant control group, 100% of hamsters (6/6) met their humane clinical endpoint (HCE) by 12.5 days post-challenge (dpc) (**Figure 5.13A**). In the immunised groups, all hamsters (6/6) immunised with NiVBsG showed 100% survival post-NiVB challenge (*p*=0.0015, Log-Rank Mantel-Cox survival analysis test), but only 16.7% of hamsters (1/6) immunised with GHNVsG survived to day 22 post-challenge (**Figure 5.13A**). Clinical signs were recorded in all 6 unvaccinated animals (100%) starting at 7 dpc, with evidence of ruffled fur, laboured breathing and neurological sequelae and tremors (**Figure 5.13B**). Similar signs were observed in 5/6 animals (83%) immunised with GHNVsG starting at 8 dpc, with 1/6 animal also showing symptoms of dehydration. No clinical signs were observed in the 6 animals (100%) immunised with NiVBsG while 1/6 animals (17%) immunised with GHNVsG, remained healthy for the duration of the study post-challenge (**Figure 5.13B**). Animals immunised with NiVBsG showed a gradual increase in weight after challenge, whereas hamsters immunised with GHNVsG had generally stable weights throughout (**Figure 5.13C**). The weights of hamsters in the adjuvant control group increased slightly up to 4 dpc, then gradually decreased as animals began reaching HCE and finally dipped at day 9. After day 9 the weight shown represents only a single animal, which increased until the animal reached HCE (**Figure 5.13C**). Temperatures remained relatively consistent for all animals in the NiVBsG and GHNVsG vaccine groups but showed a steeper decline in temperature in the adjuvant vaccine group from 1 dpc, then recovered to values similar to the other two vaccine groups by 6 dpc (**Figure 5.13D**).

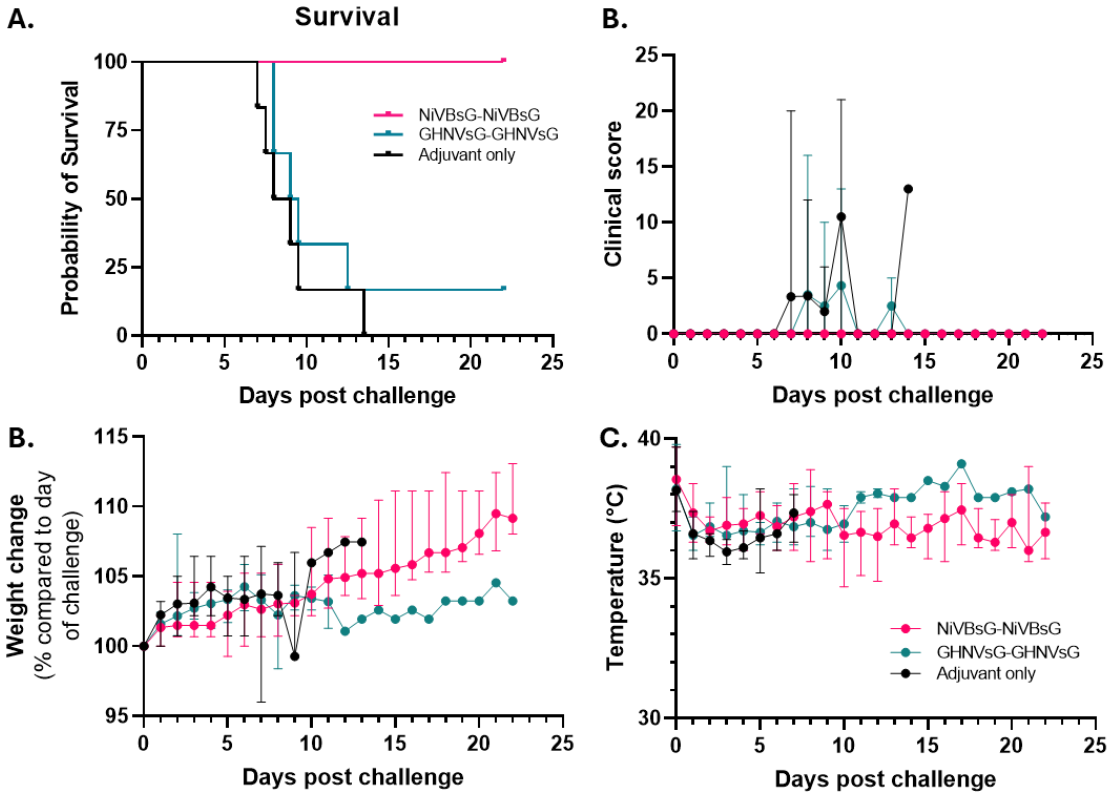

Figure 5.13: Clinical readouts from hamster efficacy study of animals immunised with henipavirus vaccines.
Clinical readouts from hamsters immunised with adjuvanted NiVBsG, GHNVsG or an adjuvant only control using a prime-boost strategy and challenged i.p. with 10^2 $TCID_{50}$ NiVB. **(A)** Kaplan-Maier survival plot with Log-Rank Mantel-Cox statistical test (p=0.0015). **(B)** Clinical score observation. **(C)** Weight change compared to the day of challenge**. (D)** Temperature changes. Data shows mean values with errors bars denoting ± standard error (n=6/group).

NiV infection results in gross respiratory and neurological disease and pathology [110]. To characterise this in more detail, histopathological staining (procedure and image processing conducted by Ines Ruedas Torres and Francisco Javier Salguero, UKHSA) was performed on lung, brain and spleen tissue from infected animals in each vaccine group, with no changes observed in any of the organs in the NiVBsG immunised group (**Figure 5.14 A-C, D, G and J**). Lung pathology was noted in the GHNVsG immunised group, with lesions consisting of thickening of the alveolar wall, characteristic of broncho-interstitial pneumonia (**Figure 5.14A and E).** In the adjuvant control group, there was evidence of necrosis of the alveolar and bronchiolar epithelium and the presence of immune infiltrates and cell debris (**Figure 5.14A and F**). Lesions were observed in GHNVsG immunised and control groups in the spleen (**Figure 5.14B**), with evidence of mild to moderate depletion of lymphoid cells, particular in the control group (**Figure 5.14H and I, insets**). In the brain, lesions were observed in the GHNVsG immunised and adjuvant control groups (**Figure 5.14C**), with evidence of meningitis (**Figure 5.14L, arrow**), accompanied by leukocyte aggregation in the perivascular space (**Figure 5.14K, arrows**), which was most prominent in samples from the animals in the control group (**Figure 5.14L, inset**).

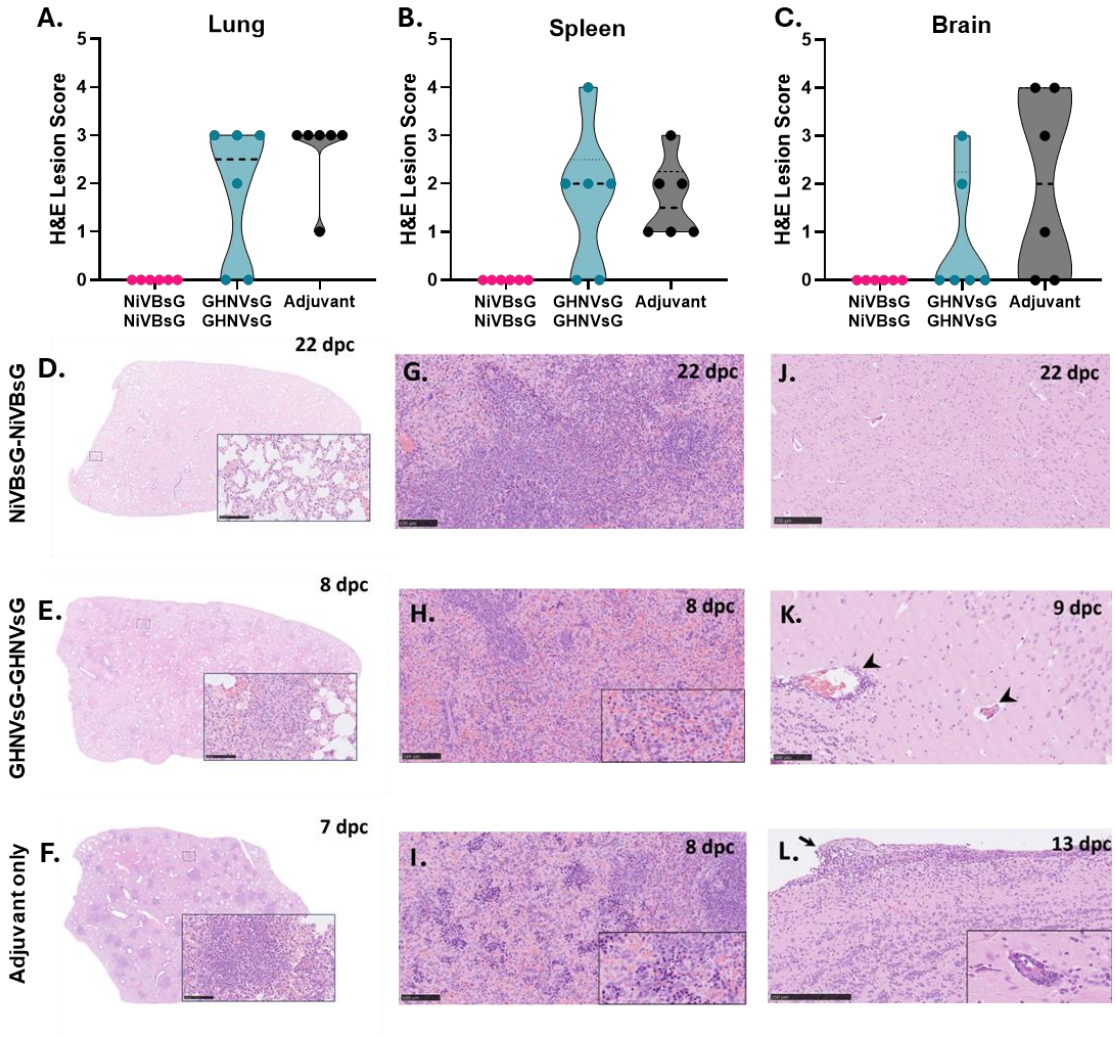

Figure 5.14: Lung, spleen and brain histopathological score and representative H&E images following NiV challenge.
Cumulative histopathological scores for **(A)** lung, **(B)** spleen and **(C)** brain tissues in immunised animals following challenge. Representative tissue section H&E staining for **(D, E, F)** lung, **(G, H, I)** spleen and **(J, K, L)** brain tissue post challenge for animals immunised with **(D, G, J)** NiVBsG (22 dpc), **(E, H, K)** GHNVsG (8-9 dpc), or **(J, K, L)** an adjuvant only control (9dpc). Data points show individual animals with violin plots denoting median and quartiles, *n*=6. dpc, days post-challenge. Insets and arrowheads indicate areas of interest. Bar = 100µm.

The presence of NiV infection in any of the tissues was determined where pathology was detected to understand whether the vaccines used reduced virus dissemination in the tissue. The presence of NiVB RNA was detected by RNAscope *in situ* hybridisation (ISH) (procedure and image processing conducted by Ines Ruedas Torres and Francisco Javier Salguero, UKHSA) and was not observed in any of the organs in animals immunised with NiVBsG (**Figure 5.15A-C, D, G and J**). In tissue sections from animals in the GHNVsG immunised and adjuvant control groups, viral RNA was observed to varying degrees in most challenged animals (**Figures 5.15A-C**). In the lung, small amounts of viral RNA was detected in the lesion regions from 4/6 GHNVsG immunised animals (**Figure 5.15A, E**), but was more prominent in the adjuvant control group with 6/6 animals showing evidence of the presence of viral RNA (**Figure 5.15A, F**), which was particularly high in one animal (**Figure**

5.15F). The viral RNA was observed in inflammatory infiltrates in areas where broncho-interstitial pneumonia was prevalent (**Figure 5.15E and F, arrowheads and inset**). In the spleen, small amounts of viral RNA was detected (**Figure 5.15B**) mostly in immune cells from the red pulp (**Figure 5.15 H and I, arrowheads**). In the brain, viral RNA was detected in small amounts in the GHNVsG immunised group but was more widespread in the adjuvant control group (**Figure 5.15C**), detected mainly in neurons (**Figure 5.15L, arrowhead**), accompanied by neutrophil infiltrates within the mid-brain areas (**Figure 5.15 K and L**).

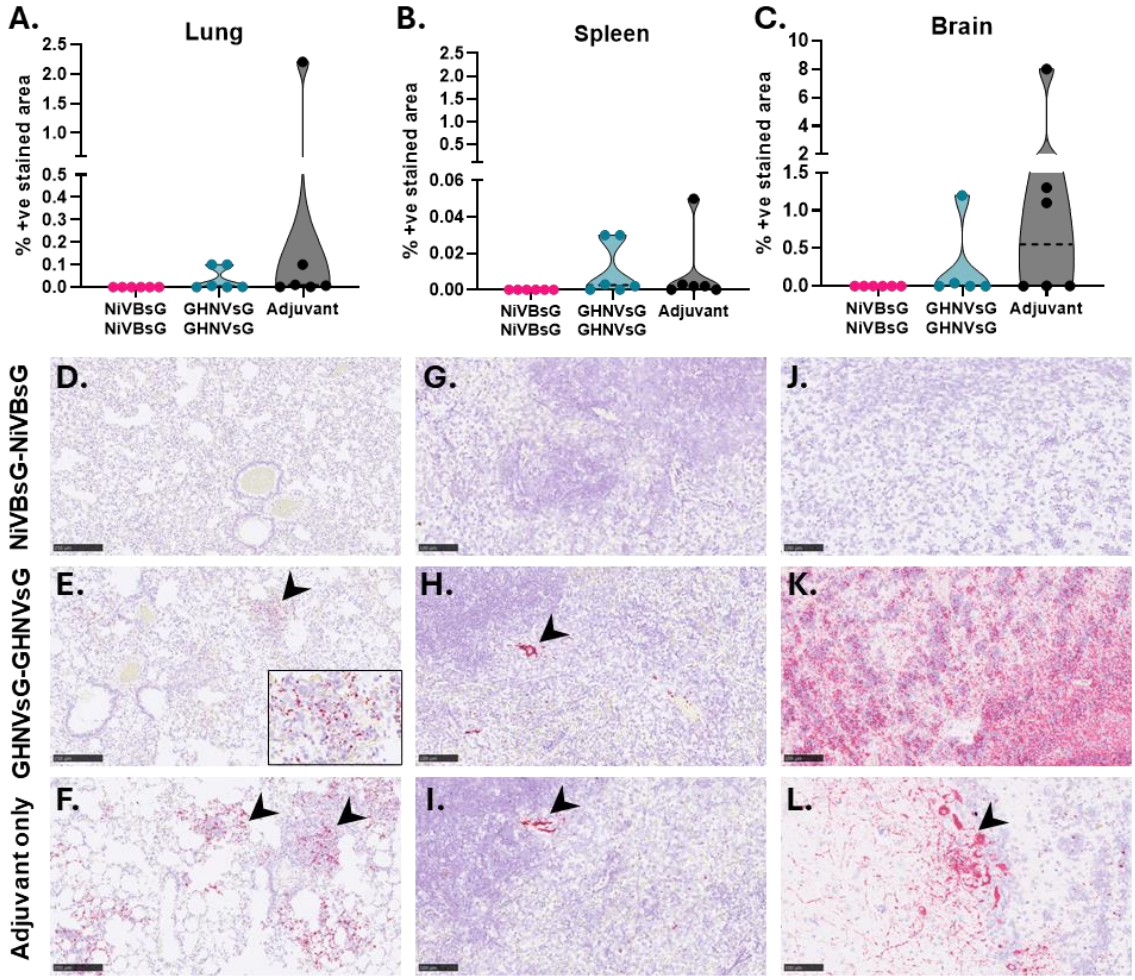

Figure 5.15: Quantification of NiVB RNA in lung, spleen and brain tissue sections (RNAscope). Digital image analysis (percentage area positively stained for NiV RNA by *in situ* hybridisation (ISH) in **(A)** lung, **(B)** spleen and **(C)** brain tissue. Representative ISH RNA-scope for **(D, E, F)** lung, **(G, H, I)** spleen and **(J, K, L)** brain tissue post challenge for animals immunised with **(D, G, J)** NiVBsG (22 dpc), **(E, H, K)** GHNVsG (8-9 dpc), or **(J, K, L)** an adjuvant only control (9dpc). Data points show individual animals with violin plots denoting median and quartiles, *n*=6. dpc, days post-challenge. Insets and arrowheads indicate areas of interest. Bar = 100µm.

5.3 Discussion

There are currently no licensed vaccines or therapeutics approved for use in humans against the henipaviruses, despite the pandemic potential of NiV and the identification of related parahenipaviruses, like MojV and LayV which have shown evidence of disease in

humans [147, 148]. I therefore wanted to understand the breadth of utility of vaccines already in development for NiV against other henipaviruses, in effect mimicking events that may occur during future spillovers of henipaviruses. These data can help shape future design of vaccines against related henipaviruses and parahenipaviruses, either known or unknown, should they emerge in the human population. The utility of these vaccines likely depends on the respective similarity between viral genomes. CedV is the closest related *Henipavirus* to NiV and HeV and exhibits identity <33% at the amino acid level in the F and G glycoproteins (F: 32-33% identity, G: 29-30% identity, compared to NiV and HeV, respectively), and 50% identity compared to the L protein [140] (**Figure 5.1, Figure 5.3**). In contrast, GHNV-f exhibits 56% sequence identity to NiV-F and GHNV-G exhibits only 26% identity to NiV-G [146]. CedV was therefore a good model to investigate whether homologous or heterologous vaccinations with NiV and/or GHNV could in addition, protect against infection from a currently apathogenic henipavirus. Based on the data observed in the animal studies presented here, it appears that if CeV or other viruses even more divergent than CedV were to ever emerge, the utility of current vaccination and therapeutic strategies, although not designed for heterologous use, would be unlikely to provide any degree of cross-neutralisation should they be required in an emergency outbreak situation.

Phylogenetic analysis carried out comparing the henipavirus and parahenipaviruses surface glycoproteins revealed that the F sequences are more closely related than the G sequences (**Figure 5.3**), suggesting that the ability of henipaviruses to cause disease in human and animal species may be attributed to sequence divergence of the attachment and/or fusion proteins resulting in functional constraints or immune pressure at accessible sites. This could include differences in attachment to the receptor binding site by engaging at sites distal or suboptimal for sufficient attachment, resulting in inefficient engagement with the F protein to trigger entry. Alternatively, it is possible that another receptor or a co-receptor is required for sustained and substantial infection to occur, which is likely the case for the parahenipaviruses like MojV and MeliV, which do not appear to utilise EphrinB2 (**Figure 5.5**) or EphrinB3 [338]. The F and G glycoproteins from MojV and MeliV were also unable to induce cell-cell fusion in different target cells, or when overexpressing EphrinB2 from difference species (**Figure 5.6C**), data which does not correlate with previously published data that showed cell-cell fusion of MojV with A549, BHK-21 and HEK293T cells relative to no glycoprotein controls [338]. However, the data that was shown in the published study was expressed relative to the controls, with ~10-fold increase in fusion, whereas our data is shown using raw luciferase values, which was deemed to be a more appropriate measure of fusion due to the sensitivity of the assay, although the presence of GFP^+ syncytia was not detected in the assay (**Figure 5.6D**).

Although the parahenipaviruses are most closely related to the henipaviruses, they are structurally very different, so it may be worth investigating the capacity of parahenipavirus glycoproteins to interact with other established paramyxovirus receptors, particularly from the rat and shrew species from which they were first identified. This approach has been evidenced with other virus families, such as the coronaviruses. Alphacoronaviruses generally use APN as their functional receptor for entry; however, within this genus NL63 instead enters using ACE2, which is a common receptor for the betacoronaviruses, highlighting the possibility of cross-receptor usage within the same virus family [339]. Whilst GHNV only uses EphrinB2 as its functional receptor for entry [334], CedV has been shown to enter cells *in vitro* via human EphrinB1, EphrinA2 and EphrinA5 in addition to EphrinB2 [335]. Furthermore, CedV is able to use mouse EphrinA1 but not human EphrinA1, which differ by 1 residue in the receptor binding region [335]. Da Silva et al., demonstrated some evidence of cell-fusion mediated by MojV F and G glycoproteins with human EphrinA5, rat EphrinA4 and mouse EphrinA1 however at much lower levels compared to the henipaviruses. For example, the authors showed mouse EphrinA1 usage by MojV was 2-fold greater than a no-receptor control, compared to a 1,200-fold difference in fusion seen for CedV [340]. As there are differences in receptor usage between the henipaviruses, generating secreted proteins of these receptors and using them in conjunction with other henipavirus sG proteins to look at binding rates and affinity. This could be achieved by flow cytometry, ELISA or bio-layer interferometry, which will also allow us to elucidate how preferential receptor usage can play a part in transmission and disease progression of the henipaviruses.

Transmission of the henipaviruses also occurs via cell-cell fusion, which contributes to disease progression through the formation of syncytia. Cell-cell fusion is mediated by surface expression of the F and G glycoproteins on neighbouring cells, which can therefore also be a target for nAbs. For the cell-cell fusion assay conducted, the suggested variation in the G attachment protein sequences may require use of more of this protein in comparison to the fusion protein for fusion to occur. Going forward, tagging the glycoproteins to confirm they are being expressed using flow cytometry or Western blot analysis. This would confirm whether the glycoproteins are being incorporated into the pseudovirus at all, and if the correct receptor or target cell is being tested. Additionally, screening the parahenipavirus proteins, particularly MojV-G and LayV-G on high-throughput receptor screening platforms may reveal novel interactions of these parahenipavirus proteins with other human proteins that could be candidates for receptors for these viruses. We currently have an ongoing collaboration with University of York (led by Professor Gavin Wright) to screen the parahenipavirus sGs with ~1900 human transmembrane proteins to investigate this.

HeV and NiV also caused the greatest syncytia formation in cells, compared to GHNV where the syncytia and fusion detected were far less prominent (**Figure 5.4E**). It is plausible that the reduced ability to cause syncytia formation could be linked to an inability of these more distant viruses to cause disease in humans, likely attributed to the thermostability of the F protein, which translates as reduced cell-cell fusion, and in turn results in less severe pathogenesis. It had been demonstrated that the cytoplasmic tail of GHNV-G modulates the fusogenicity of GHNV-F and truncation of GHNV-G enhances the fusion activity of GHNV-F [341]. Additionally, NiV and HeV, unlike the other henipaviruses, also utilise EphrinB3 as a receptor in the brain, which is linked to increased disease severity [158]. Indeed, it has been shown that two key residues in the NiV and HeV attachment protein are critical for the use of EphrinB3 as an alternative receptor [342, 343]. Identifying such residues and building mutants of GHNV-G and CedV-G that have these amino acid changes, or of HeV-G and NiV-G that lack these changes will allow us to assess whether there is an increase or decrease in infectivity. Such differences at the amino acid level would be important to investigate should a new, related henipavirus emerge.

Established henipavirus binding and entry assays were adapted to perform neutralisation assays with sera from animals immunised with henipavirus vaccine candidates. Sera from a bio-banked pig vaccination study, where animals were immunised against NiVM or HeV, were able to cross-neutralise both viruses. However, differences were observed when using the subunit vaccine platform whereby sera obtained from pigs immunised with a HeVsG vaccine were able to potently neutralise both NiV and HeV, but sera from NiVMsG vaccination sera did not neutralise HeV as well (**Figure 5.7D and E**). This suggests that HeV-based of even GHNV-based vaccines may be better than NiV-based vaccines in inducing a broader nAb response against antigenically different viruses. Going forward it would be interesting to investigate whether there are binding epitopes present on HeV that differ to NiV that account for this difference in total IgG and nAb response seen. Indeed, it has been demonstrated that a single dose of adjuvanted HeV-G protein subunit is able to protect against lethal challenge with NiVB in African green monkeys, and other studies have shown complete protection against both NiV and HeV in HeVsG immunised ferrets, horses and cats [110, 163]. A formulation of HeVsG is now in phase I clinical trials for use in humans against NiV-related infection and disease.

Additionally, similar levels of neutralisation were detected against NiVM, NiVB and HeV using the ChAdOx1 vector-based platform, although the binding antibodies against these antigens were generally lower than those detected in the subunit vaccine immunised groups

(**Figure 5.7**). The ChAdOx1 platform also demonstrated robust T-cell responses in immunised pigs that was greater than seen in the other vaccine groups (data not shown), which is unsurprising given viral-vectored vaccines are known to induce strong T-cell responses [344]. A licensed vaccine using the ChAdOx1 platform was approved for use against SARS-CoV-2 [90] and further clinical trials using this vaccine platform are underway for other viruses including Middle Eastern Respiratory Syndrome coronavirus (MERS-CoV) [345], Hepatitis B virus [346], Rift Valley fever virus [347], Chikungunya virus [348] and more recently, NiV (NIV001, Eudract number 2023-503872-25), demonstrating its safety and efficacy. Indeed, this vaccine platform is promising for future candidate henipavirus vaccines.

Comparable results were noted in pigs immunised with the NiVmcsF vaccine and the NiVsG vaccine group (**Figure 5.7C**). Further analysis could be conducted to investigate the cross-reactive antibody responses against different henipavirus F proteins, which were not performed here, particularly as the henipavirus F sequences appear to be more conserved than the G proteins, suggesting that this protein is more likely to provide antibody-mediated cross-protection. This is further supported by data obtained using mAbs against the F and G glycoproteins of HeV and NiV where it was observed that the F-specific mAb 5B3 was able to induce both neutralising and cell-fusion inhibitory antibodies against NiVM, NiVB and HeV. The same was not seen for the G-specific m102.4, which produced nAbs against NiVM, NiVB and HeV, but only fusion inhibitory antibodies against HeV (**Figure 5.7F and G**). A humanised mAb 1F5 against the NiV-F protein has been shown to be protective against NiVB infection in hamsters and African green monkeys, with comparable survival data noted in animals between this mAb and m102.4 [173]. However, m102.4 has also been shown to be protective in several animal studies, has been administered to at-risk individuals on compassionate grounds and is currently in clinical trial for approved use in humans [110, 138, 163, 166, 167]. It would therefore also be useful to perform fusion inhibitory assays on the pig sera from this study to understand if inhibition is only seen in animals receiving an F-based vaccine, or also with G-based vaccine group sera, and whether this inhibition extends to other henipaviruses.

The disadvantage of using an F-based vaccine may be that this immunogen does not produce nAb titres as high as G-based vaccines, particularly when expressed in viral-vectors. For example, a study immunising pigs with a bovine-herpesvirus 4 vector expressing either NiVM-F or NiVM-G (BoHV-4-NiVF, BoHV-4-NiVG) revealed ~8-fold lower nAb titres in BoHV-4-NiVF vaccinated animals compared to BoHV-4-NiVG vaccinated animals using both pseudovirus-based and live virus neutralisation assays [195]. A separate study in pigs using a canarypox-based vaccine vector (ALVAC) expressing either NiV-F or

NiV-G yielded similar results, although both vaccines were still able to protect against challenge with NiVM [182]. In the same study, investigators also tested a vaccine expressing both NiV-F and -G, which produced similar nAb responses to those observed in the ALVAC NiV-G vaccine group [182], suggesting a bivalent vaccine approach may be more favourable to enhance the breadth of the antibody-mediated immune response.

Due to the cross-reactivity observed between NiV and HeV in vaccinated pig sera, yet lack of cross-neutralisation with CedV and GHNV, mice were immunised with heterologous and homologous prime-boost-boosts of NiVBsG and GHNVsG, the two most distantly related henipaviruses. In these experiments NiVBsG was used as the immunogen rather than NiVMsG as, since 2001, the only strain of NiV that has been circulating is NiVB, with isolates from India and Bangladesh (98.6-99.6% nucleotide similarity) being associated with outbreaks of NiV almost annually [349]. As with the pig study, similar cross-reactivity was detected between all the henipavirus sGs with all vaccine groups after two doses by ELISA, but nothing specific to the parahenipavirus MojVsG (**Figure 5.8**), further highlighting the divergence between these two virus genera and the differential antibody-binding epitopes they likely possess.

The cross-neutralisation of NiVM, NiVB and HeV pseudoviruses with sera from either homologous or heterologous GHNVsG vaccinated mice (**Figure 5.9**) suggests that the antibody response generated targets differential epitopes that may induce the generation of more diverse affinity-matured antibodies. Flow cytometric analysis on peripheral blood mononuclear cells (PBMCs) for markers of affinity matured memory (e.g., $CD27^{+}$) [333] and long-lived plasma (e.g., $CD27^{-}$, CD39, CD138) [350] in B cells, and expanding our analysis to sera from vaccinated animals by ELISA to investigate the dominant antibody subclasses (i.e., IgM, IgG1, IgG2, IgA) would provide more details on any differences in B cell populations present in vaccinated mice. In addition, isolation of mAbs, particularly from the heterologous vaccine groups could identify antibodies that neutralise a wider range of henipaviruses and structural modelling could predict where these mAbs bind. This information could help us to understand the conserved residues and epitopes between henipaviruses that are important for cross-protective immunity.

Unlike the mouse and pig studies, cross-reactive or cross-neutralising antibodies were not detected against any of the henipaviruses after homologous prime-boost with NiVBsG or GHNVsG in vaccinated golden Syrian hamsters (**Figure 5.11**). Hamsters have been described as suitable challenge models for NiV and HeV [110, 163], but may not be the most appropriate model to assess immunogenicity of subunit vaccines. Although hamsters have previously been used to assess the efficacy of recombinant viral-vectored NiV

vaccines (ChAdOx1 [191], vaccinia virus [181], vesicular stomatitis virus [187, 188, 351], measles virus [183]), virus-like particles [197] and nanoparticles [352]), data on subunit vaccines is limited. More favourable models to assess subunit vaccines have included ferrets [193] and African green monkeys [116], however we did not have the capacity to conduct such animal studies. Furthermore, similar cross-neutralisation analyses against other henipaviruses have not been performed in these ferret and African green monkey studies. Nonetheless, antigen-matched antibody responses were still detected in each vaccine group and 100% protection in hamsters from the NiVBsG vaccinated group after challenge with NiV (**Figure 5.13, Figure 5.14, Figure 5.15**). These data suggest that the antibody repertoire in hamsters is narrower compared to other animal models. The discrepancies in results with the different animal models described should be corroborated using convalescent human sera to understand which model(s) provide a more accurate representation of what would likely been seen in humans.

In general, more research is required to understand the usefulness of the hamster model in immunogenicity studies for henipavirus subunit vaccines. Considerations should be taken for route of administration, amount of protein subunit, adjuvant type, induction of mucosal immunity (intranasal vaccination/infection), multivalent vaccines and dosing intervals. In the mouse study conducted, a 3-dose immunisation was selected, but only 2-doses for the hamster study. Based on the complete absence of antibody response detected after 2 vaccine doses in the GHNVsG immunised group against NiV, and vice versa, it seems unlikely a third vaccination would have been beneficial here. However, there was evidence of reduced pathology and presence of viral RNA in the tissue of GHNVsG vaccinated hamsters compared to adjuvant-only vaccinated animals (**Figure 5.14, Figure 5.15**), suggesting a role of non-neutralising antibodies in mediating some degree of protection against NiVB infection following GHNVsG vaccination. Furthermore, although some antigen-specific IFNγ responses were detected following stimulation of splenocytes from immunised hamsters, the values recorded were relatively low and the assay itself exhibited high background signals (**Figure 5.12**). More research and development is also required for the optimisation of hamster ELIspot assays, for which there is little published data for use in NiV vaccine or challenge studies.

In contrast, the T-cell responses measured in the mouse immunogenicity study revealed a similar pattern of IFNγ responses to those seen for the nAb response, and even exhibited a T-cell specific response when mouse splenocytes were stimulated with CedV-G peptides (**Figure 5.10**). The contrast in nAb response and T-cell response against CedV implies the importance of the cellular response alongside the humoral response in vaccine-derived immunity, but the extent of the role of the cellular response in protection requires further

investigation. This was indicated by the reduced pathology and viral RNA detected in brain, spleen and lung tissue sections in GHNVsG vaccinated hamsters infected with NiVB (**Figure 5.14, Figure 5.15**), despite the absence of cross-neutralising antibodies against NiV in the GHNVsG vaccine group. Although nucleic acid had been isolated from infected hamsters, follow up examination to detect NiV viral RNA in the blood, for example by qPCR has not yet been performed, but would corroborate the pathology results obtained. Flow cytometric analysis of mouse PBMCs would be useful to understand the types of T-cell that are present in the different vaccine pools, particular the proliferation of T follicular helper cells (Tfh) which provide B-cell help for the generation of high affinity antibodies.

Furthermore, in the pig and mouse models described, there were high antibody responses detected that were non-neutralising. Going forward, investigating the role of non-neutralising antibodies in immune protection would be of interest, using FcγR-based assays, such as antibody dependent cell cytotoxicity (ADCC), antibody dependent cellular phagocytosis (ADCP). These assays could also complement research into the possibility of vaccine-derived antibody dependent enhancement (ADE) when administering heterologous henipavirus vaccination. The latter could likely occur if antibodies bind the attachment G protein, but instead of inhibiting receptor function, act in a manner analogous to receptor binding, resulting in triggering of the F protein. These assays were difficult for us to perform using the mouse and hamster PBMCs from vaccinated animals due to low cell numbers but could be considered in the future.

All the neutralisation assays were performed used surrogate viral pseudotypes, and although these have shown good concordance with live virus assays, it would be valuable to validate our data further using more physiologically relevant models such as live virus or the recombinant CedV reverse genetics platform that has been developed. This presents a suitable alternative as CedV is apathogenic due to the absence of V and W non-structural proteins which code for IFN antagonists [140, 353], yet still produces replication competent virus that can be used at BSL-2. Studies have described a recombinant chimeric CedV that expresses NiV or HeV glycoproteins, and showed they were able to enter cells expressing EphrinB2 and EphrinB3 [142, 143]. Amaya et al., also developed this platform further as a quantitative fluorescence reduction neutralisation test (FRNT) through expression of GFP in a rapid assay that detects fluorescence within 36 hours [142].

To summarise, the data presented here investigate the possibility of generating pan-henipavirus vaccines using more distantly related henipavirus glycoproteins as immunogens. This information could lay the experimental groundwork for heterologous vaccination in an outbreak situation whilst a homologously matched vaccine is developed.

It is likely that the breadth of immunity and utility of the vaccines we are currently designing and testing may be constrained to novel viruses that are more closely related to NiV or HeV. However, future vaccine design could incorporate a multimeric approach, including a number of henipavirus F and/or G proteins, utilising a conserved region of the glycoproteins, as has been described for viruses like influenza (HA stalk) to elicit broader antibody responses against more conserved epitopes [354], or using a multivalent approach to express multiple henipavirus glycoproteins [355]. Expanding our analysis and understanding of vaccine-derived immune responses to characterise the significance of non-neutralising antibody responses, mucosal immunity and T-cell immunity in addition to nAbs will also be vital in generating durable and broad-acting vaccines for emerging viruses.

General Discussion & Future Directions

Vaccines have been one of the most successful medical advances in preventative medicine in limiting the spread of deadly infectious diseases and the symptoms and mortality associated with them. The introduction of mass vaccination programmes has successfully seen the eradication of smallpox in humans [7], and rinderpest in cattle [17]. There has also been great progress in lowering the rates of fatal diseases such as polio, measles and malaria, with many regions of the world already being declared polio-free and malaria-free [11]. The World Organisation for Animal Health also aims to eradicate other animal viruses such as African swine fever virus, foot and mouth disease virus and PPRV [356]. There are several roadblocks however, in reaching these goals due to vaccine hesitancy leading to decrease in vaccine updake [357]. This has certainly been the case with the MeV vaccine (e.g., MMR), due to the spread of misinformation regarding safety and disinformation related to off-target effects of the vaccine, which has resulted in a decline in the number of individuals being vaccinated against measles and a surge in infections over the past decade [11].

A similar issue arose in the wake of the COVID-19 pandemic, with the spread of “fake news” on social media outlets leading to reluctance and refusal of many individuals to have COVID-19 vaccines [357]. Much of this hesitancy arose from the speed at which vaccines were developed for COVID-19, but from a scientific perspective, this was seen as a major triumph for public health strategies, where vaccine trials that usually require decades of approvals, pre-clinical studies and clinical trials were accelerated over a short period. This included animal immunogenicity and efficacy studies that were performed in parallel to elucidate vaccine safety and effectiveness.

The success of COVID-19 rapid vaccine developments led to CEPI introducing a “100-day mission” as the 2022-2026 strategy for research into developing safe, effective and easily accessible vaccines for emerging viruses [329]. In this study, I examined the intraspecies (i.e., between different virus strains) and interspecies (i.e., differences at a genus-wide level) variation of SARS-CoV-2 by investigating the cross-protective capacity of COVID-19 vaccines. I was actively involved in examining the nAb response in sera from such vaccine studies for the ChAdOx1-nCoV19 vaccine (Vaxzervria, ADZ1222, Wuhan strain) due to my expertise in viral pseudotyping [218], which provides a rapid, high-throughput, low-biocontainment assay to screen hundreds of sera, an assay which was vital for development of the COVID-19 vaccines. The ADZ1222 vaccine was examined initially in mouse, pig, non-human primate and ferret models, revealing the induction of robust nAb responses, which are essential for the development of long-lasting immunity (**Figure 3.2**)

[240, 241]. An advantage of using a viral-vectored platform such as the ChAdOx1 system is the induction of a strong cell-mediated response in addition to the humoral response without the requirement of an adjuvant, which has been suggested to play a more significant role in immunity than previously thought [344]. The COVID-19 pandemic also saw the approval of the first mRNA-based vaccine technology with the Comirnaty BNT162b2 and mRNA-1273 vaccines, both expressing the Wuhan Spike [96, 258]. These vaccines induced strong antibody (**Figure 3.7**) and T-cell responses in immunised individuals and helped to reduce the disease severity and hospitalisation associated with COVID-19 (**Table 1.1**).

However, as new SARS-CoV-2 variants emerged, the effectiveness of the COVID-19 vaccines reduced, with immune escape being observed in more divergent variants harbouring mutations in the Spike protein (**Figure 3.8**). Subsequently, booster vaccinations were delivered with the same Spike antigen, particularly to clinically vulnerable individuals, including older adults, which appeared to recover some of the lost nAb response (**Figure 3.9A and B**). However, the emergence of the Omicron variants and subvariants revealed an antigenically distant lineage of SARS-CoV-2 variants which have continued to evolve and emerge (**Figure 3.6**). Recently, a study has shown that the emergence of Omicron exhibits distinct phenotypic trajectories of SARS-CoV-2 pre- and post-Omicron, with post-Omicron variants evolving with enhanced immune evasion, altered tissue tropism, a switch in entry mechanisms and a reduction in Spike fusogenicity [358]. This has led to the development of updated COVID-19 vaccines expressing the Spike of clinically relevant Omicron variants, which showed an increase in nAb response against new variants as they emerged (**Figure 3.10**). The immune escape that was observed in vaccinated individuals was largely attributed to mutations in the Spike RBD, with amino acid changes such as E484K/A, K417N and L452R playing a significant role in driving this reduction in nAb response. In addition to the RBD being the main target for nAbs, neutralisation supersites are also present in the NTD of Spike. In particular, deletions in NTD appear to drive immune escape from monoclonal antibodies and polyclonal sera (**Figure 3.12, Figure 3.13, Figure 3.15**). Mutations outside Spike have also been implicated in immune escape, including mutations in the nucleocapsid which have been shown to affect virus replication and pathogenesis [359], but also in non-structural proteins such as NSP12, with mutations in this gene affection transcription and replication [360].

Animal models are not only important for studying vaccine efficacy, but also to better understand virus pathogenesis and disease. One requirement of the animal model is to express the same (proteinaceous) receptor required for viral entry, with disease outcome in that animal model then more likely to closely match the severity observed in humans. Although mouse and ferret models were suitable systems for testing COVID-19 vaccine

immunogenicity, these animals do not mimic all the clinical signs associated with SARS-CoV-2 infection due to restrictions in mouse and ferret ACE2 usage [219], so were not appropriate challenge or pathogenesis models. For mice, this was revealed to be because of amino acids at position 353 in mice ACE2 (histidine, K) compared to humans (lysine, L), leading to sub-optimal replication of SARS-CoV-2 (**Figure 4.6**) [305]. Indeed, C57BL/6, BALB/c and CD1 mice that were intranasally challenged with SARS-CoV-2 developed infection, but they did not display clinical signs and the virus was subsequently cleared 3-days postinfection [361, 362]. However, mice are favourable models in infectious disease research because their immune system is well-characterised and they are relatively cheap. Therefore, various transgenic mouse models were developed that express the hACE2 receptor (e.g., K18-hACE2 mice), which exhibited infectivity and subsequent pathology analogous to that in humans [315]. Similarly, ferret models were initially the prime choice to study SARS-CoV-2 infection and pathogenicity due to their historical use in other respiratory diseases such as SARS-CoV-1. Although ferrets were shown to be permissive to SARS-CoV-2 infection, they were unable to recapitulate the severity of clinical signs and symptoms as that observed in humans and infection led to ACE2 adaptive mutations in Spike [298, 362].

Understanding the permissiveness of animals to SARS-CoV-2 is also prudent for identifying potential animal reservoirs for the virus that could support sustained transmission or reverse zoonosis. It has been demonstrated that SARS-CoV-2 has broad tropism for mammalian ACE2 *in vitro* (**Figure 4.1**) [219] and that this tropism is altered following the emergence of SARS-CoV-2 variants (**Figure 4.4**) [305], particularly with rodent and bat species (**Figure 4.5**). This is largely due to altered binding to ACE2 by SARS-CoV-2, particularly in the RBD, where several mutations arose in SARS-CoV-2 variants. For example, *Rh. pusillus, Rh. cornutus* and *Rh. ferrumequinum* ACE2s restricted entry of wildtype B.1 Spike pseudovirus but demonstrated increased entry with BA.1 Spike pseudovirus (**Figure 4.7 B-D**). Mutagenesis of key residues in the B.1 RBD to make them more BA.1-like revealed that mutations at positions 493 and 501 in Spike were sufficient to overcome the restriction observed with B.1 (**Figure 4.7**). Indeed, these types of mutations in Spike have been shown to be ecologically relevant, e.g. similar mutations increased transmission in mink in the Netherlands, and on Danish mink farms showed evidence of spillback into humans [299]. This mink-derived lineage exhibited 5 mutations in the Spike protein – Δ69/70 (associated with increased infectivity [234]), Y453F, D614G, I692V, M1229I – and showed evidence of immune escape, which ultimately led to the culling of ~17million mink in Denmark [299]. Furthermore, spillover and significant onwards transmission of the Omicron variant was reported from humans into wild white-tailed deer in the USA in late 2021 [363]. These changes in species tropism and spillover/spillback events in mammalian species highlight

the need for continued surveillance in wildlife and livestock species, particularly those in close contact and proximity to humans. The use of deep mutational scanning would allow prediction of mutations likely to be involved in immune escape, as has been demonstrated with BA.2 and XBB.1.5 Spike with hACE2 [364], and could be applied to other mammalian ACE2, particularly to predict whether emerging SARS-CoV-2 variants could acquire mutations that could allow infection of new hosts.

There is also concern that novel sarbecoviruses also possess zoonotic potential, particularly those of bat origin. Several bat sarbecoviruses have been discovered globally that cluster into distinct clades (**Figure 4.8**), some of which show phylogenetic similarity with SARS-CoV-2 and high affinity for hACE2 (**Figure 4.11A**) [66]. These bat sarbecoviruses also showed broad tropism for other bat ACE2s and mammalian ACE2s, namely clade Ia and Ib viruses (**Figure 4.11, Figure 4.12**), suggesting the possibility of these viruses emerging in humans, via an intermediate host. This raises questions about whether current immunity against SARS-CoV-2, acquired through vaccination or natural infection could provide any degree of cross-protection against other bat sarbecoviruses. Although studies in mice immunised with a SARS-CoV-1 vaccine conferred protection against SARS-CoV-2 [104] and sera from SARS-CoV-1 survivors developed strong nAb responses against SARS-CoV-2 variants [105], the opposite was not observed as SARS-CoV-2 immunisation did not induce nAb responses against SARS-CoV-1 [106]. However, COVID-19 vaccine-derived immunity has been shown to induce nAb responses against other bat sarbecoviruses, including RaTG13 and WIV16 [106].

The use of convalescent sera from individuals infected with different SARS-CoV-2 variants also resulted in the presence of cross-reactive and cross-neutralising antibodies against a range of bat sarbecoviruses, with the most potent responses detected against BANAL-20-52, BANAL-20-103 and BANAL-20-236 (clade Ib viruses), modest responses against Rs4231 and WIV-1 (clade Ia viruses), and low but detectable antibody responses against RhGB07 and Rc-o319 (clade III and V viruses, respectively) (**Figure 4.13**). Furthermore, a similar trend was noted using mAbs isolated from SARS-CoV-2 breakthrough infections, whereby the clade Ia, III and V viruses were bound to and neutralised poorly compared to clade Ib viruses (**Figure 4.15. Table 4.2**). Elucidating the RBD epitopes involved in immune escape would help to understand the regions of Spike that could be targeted to produce pan-sarbecovirus therapeutics. Future work would involve interchanging the RBD of a virus that is strongly neutralised by these sera and mAbs (e.g., SARS-CoV-2, BANAL-20-52) with that of a poorly neutralised virus (e.g, Rs4231, RhGB07) and subsequently, introducing individual amino acid mutations within the RBD to assess whether the neutralisation phenotype can be lost/gained for each respective virus. Additionally, these studies have

only used samples from a small panel of convalescent sera, so expanding this analysis to investigate the cross-neutralisation capacity of bat sarbecoviruses by vaccinee sera would provide a clearer understanding of the utility of COVID-19 vaccination against related emerging viruses. Moreover, investigating whether any cross-protection elicited by COVID-19 vaccines also extends to other betacoronaviruses would be of interest, particular against seasonal coronaviruses such as hCoV-HKU1 and hCoV-229E, to understand the breadth of COVID-19 induced immunity.

Applying knowledge from the COVID-19 pandemic regarding vaccine efficacy to other emerging viruses is also of interest. The WHO have listed several priority pathogens for research and development of vaccines and therapeutics, of which NiV and the henipaviruses were included [109]. NiV and HeV are the only paramyxoviruses that exhibit broad host range and are classified as BSL4 pathogens, which also makes research on these viruses difficult. The development of low bio-containment assays for the henipaviruses, such as the use of lentiviral pseudotypes or cell-cell fusion assays provides an alternative approach to characterising the effectiveness of vaccines and therapeutics, rapidly and at a lower cost. These assays have successfully been established for NiVM, NiVB, HeV, CedV and GHNV (**Figure 5.4**), but not for the parahenipaviruses MojV and MeliV (**Figure 5.6**) as the receptor for the parahenpaviruses is yet unknown. More recently, a recombinant CedV system has been established that will allow the study of NiV and HeV transmission and replication using a genetically relevant, non-pathogenic virus [142]. Future studies on the parahenipaviruses would likely require discovery of a functional receptor, which could be carried out using high-throughput receptor screening platforms to determine interactions of human proteins with the parahenipavirus attachment proteins [148].

These established assays were used to determine the nAb responses in various animal models following vaccination with henipavirus vaccines. Pigs receiving homologous prime-boosts of a NiV- or HeV-based vaccines exhibited cross-neutralising antibody responses against both viruses. However, only cross-reactive antibodies were detected against CedV and GHNV, which were strongest in the subunit vaccine groups compared to the ChAdOx1 vaccine group, further highlighting differences between different vaccine platforms (**Figure 5.7**). It is likely that NiV vaccines only provide cross-protection against closely related viruses (i.e., HeV), but are ineffective against more distantly related henipaviruses or parahenipaviruses.

Alternative vaccine approaches may include heterologous prime-boosts using the attachment protein of more distant henipaviruses as immunogens. In mice, this resulted in the development of cross-reactive antibodies against both immunogens – NiVB and GHNV,

but also against HeV and CedV, but not MojV (**Figure 5.8**). Immunisation with 3 doses of a GHNVsG vaccine was also able to induce potent cross-neutralising Ab responses against GHNV, NiVB and NiVM, whereas nAb titres against HeV were lower, and were completely absent against CedV, with a similar trend in T-cell response observed (**Figure 5.9, Figure 5.10**). This immunogenicity however, did not translate to a hamster challenge model, where only immunogen-specific antibody responses were detected, with some low level T-cell responses in splenocytes stimulated with both NiVB-G and GHNV-G peptides in the GHNVsG vaccinated group (**Figure 5.11, Figure 5.12**). Furthermore, only hamsters immunised with a NiVBsG vaccine conferred protection against NiVB infection, but not GHNVsG immunised hamsters. However, histopathology and NiVB RNA quantification in the lung, spleen and brain of infected animals showed reduced pathology in GHNVsG immunised hamsters compared to adjuvant control groups (**Figure 5.13, Figure 5.14, Figure 5.15**).

These data suggest discrepancies in different animal models in testing vaccine efficacy, but also highlight the importance of different immune responses (i.e., cellular and non-neutralising) in mediating protection, e.g. in the absence of a robust humoral response, reduced pathology and clinical disease was still observed in some infected hamsters. This is analogous to what was observed with the COVID-19 pandemic and the emergence of the Omicron variants and subvariants. Although large decreases in nAb responses were observed, generally individuals were protected from serious disease by pre-existing immunity derived from natural infection or repeated vaccination [61, 64, 65, 268]. An alternative approach could be the use of multivalent vaccines to express different viral glycoproteins, for example Li et al., have constructed a tetravalent Fc heterodimer fusion protein expressing the G proteins of NiV, HeV, GHNV and MojV, which has been shown to elicit broad antibody responses against all four henipaviruses in mice [355].

Future research would look to measure the nucleic acid levels in isolated blood samples, which will indicate whether virus dissemination is taking place. Furthermore, an appropriate comparison for the hamster efficacy study would be to investigate whether immunisation with NiVBsG or GHNVsG provides any protection against GHNV infection. However, a viral isolate of GHNV has not been obtained, nevertheless use of the recombinant CedV tool could provide an alternative method. In addition, due to the differences in results obtained in the pig, mouse and hamster models, with regards to antibody responses, analysing human convalescent sera from NiV or HeV survivors in henipavirus pseudovirus neutralisation assays would allow comparison of data obtained from animal studies with responses in humans.

In sum, the data presented within this study indicates that cross-protection against different strains of a virus and closely related viruses at the genus level is possible with pre-existing immunity, but this does not extend to more phylogenetically distant viruses. However, where cross-neutralisation is observed, this is not always bi-directional. For example, SARS-CoV-1 immunity provided cross-protection against SARS-CoV-2, but not vice versa [104, 106]. Likewise, it is well documented that immunisation against HeV induces strong cross-neutralisation against NiV, but NiV immunisation confers poorer antibody responses against HeV (**Figure 5.7E**) [163]. Similar trends have been observed with other viruses, including RPV, where a vaccine against rinderpest induces cross-protection against PPRV, but the converse is not observed; with a lack in neutralisation of RPV when using a PRRV vaccine [16, 17]. Therefore, design of vaccines for emerging viruses in the future should focus on targeting highly neutralising conserved epitopes within a virus family, targeting multiple epitopes (i.e., multiple structural proteins), or using a multivalent approach (i.e., different viral glycoproteins). Virus platforms that are able to also induce non-neutralising antibody responses, cell-mediated immunity and mucosal immunity to maximise the immune response should also be favoured. Furthermore, considerations should be taken to minimise costs, cold-chains, length of vaccine production and vaccine allocation to maximise pandemic preparedness should a novel virus, either known (e.g., a known sarbecovirus or henipavirus) or unknown (e.g., Disease “X”) emerge in the human population. However, the advances made in vaccine design and production, particularly over the course of the COVID-19 pandemic, are promising for the development of novel, pan-family viral vaccines in the future.

Appendix

Appendix 1: pHLSec vector map encoding for a 6xHis tag, used for generating henipavirus and parahenipavirus attachment ectodomain proteins. Inserts were cloned into the region highlighted in red, flanked by the AgeI and KpnI restriction endonucleases.

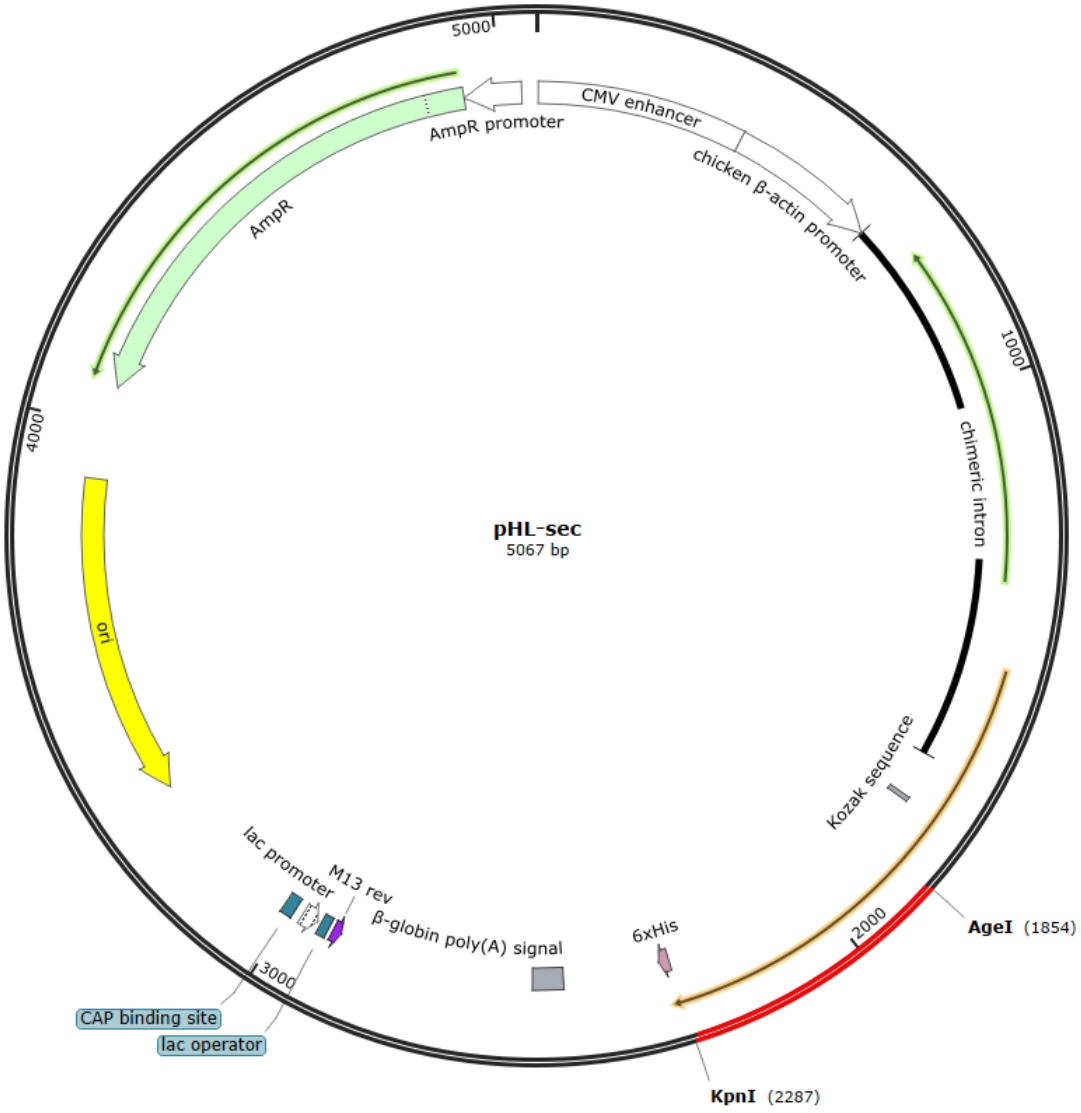

Vector size (bp):	5067
Insert sizes (bp):	
NiVB-G:	1645
HeV-G:	1651
CedV-G:	1636
GHNV-G:	1690
MojV-G:	1729
MeliV-G:	1698

Appendix 2: pOPINNTGneo vector plasmid map encoding for a biotin acceptor peptide and 6xHis tag, used for generating sarbecovirus RBD proteins. Inserts were cloned into the region highlighted in red, flanked by the KpnI and NotI restriction endonucleases.

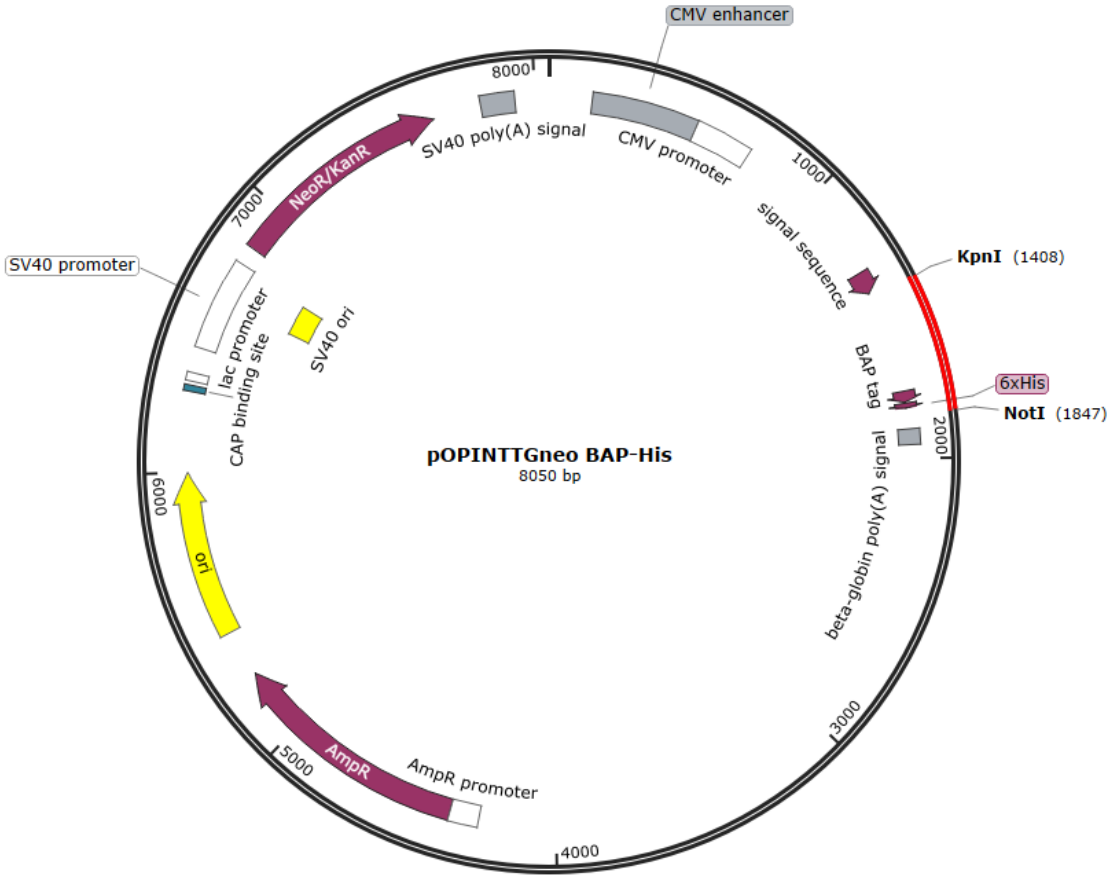

Vector size (bp):	8050
RBD insert sizes (bp):	
SARS-CoV-2:	672
BANAL-20-52:	672
BANAL-20-236:	672
BANAL-20-103:	672
WIV-1:	669
Rs4231:	669
Rc-o319:	645
RacCS203:	615
BA.1:	669

Appendix 3: Primers for cloning henipavirus G proteins and sarbecovirus RBDs into protein expression vectors

Cloning strategy	Forward Primer	Reverse Primer
NiVB-G into pHLSec	gatgggttgcgtagctgaaaccggtCAGAACTACACCAGAAGCACCG	gtgatggtggtgcttggtaccaatGGTGCACTGCTCGGGGAT
HeV-G into pHLSec	gatgggttgcgtagctgaaaccggtCAGAACTACACCAGGACCACCG	gtgatggtggtgcttggtacgtacGGACTCGCTGCACTGGGC
CedV-G into pHLSec	gatgggttgcgtagctgaaaccggtACCAGGCTGAAGGTGCAC	gtgatggtggtgcttggtacgtacGCAGTACTTAGGGATCTTGTAGG
GHNV-G into pHLSec	gatgggttgcgtagctgaaaccggtTACTACCAGAACGATAACATC	gtgatggtggtgcttggtacgtacGTAGTTGTATGTGGACCTC
MojV-G into pHLSec	gatgggttgcgtagctgaaaccggtACCGCCGCCAAGAGTCAG	gtgatggtggtgcttggtacgtacGTACCGCCTAATTGTGATGTTCTTGG
MeliV-G into pHLSec	cagtcagaccggtAACCTGGAGGGCATCAAGCACCAGAATGA	cagtcaggtaccGCGTGTTCGGCGGTTT
SARS-CoV-2 RBD into pOPIN	tctaccagacaagcaactttCGGGTGCAGCCCACCGAA	cctgtcaggccgttaaagttGAAGTTCACGCATTTGTTCTTCACGAGATTGG
BANAL-20-52 RBD into pOPIN	gttgcgtagctgaaaccggtAGGGTCCAGCCTACAGAG	tcaaaaatatcattaagcttAAAGTTCACGCACTTGTTCTTAATC
BANAL-20-103 RBD into pOPIN	gttgcgtagctgaaaccggtAGAGTCCAGCCCACCGATAG	tcaaaaatatcattaagcttGAAGTTCACGCACTTGTTCTTG
BANAL-20-236 RBD into pOPIN	gttgcgtagctgaaaccggtCGGGTGCAGCCCACCGAT	tcaaaaatatcattaagcttAAAGTTCACGCACTTGTTCTTAATGAGGTTTGTG
Rs4231 RBD into pOPIN	gttgcgtagctgaaaccggtAGGGTGGCCCCTAGCAAG	tcaaaaatatcattaagcttGAAGTTCACGCACTGGTTCTTG
WIV-1 RBD into pOPIN	gttgcgtagctgaaaccggtCGGGTGGCCCCCAGCAAG	tcaaaaatatcattaagcttAAAGTTCACGCACTGGTTCTTAATCAGATCGG
Rc-o319 RBD into pOPIN	gttgcgtagctgaaaccggtAGAGTGCAGCCCCAGGATAC	tcaaaaatatcattaagcttGAAGTTCACGCACTTGTTCTTAATCAG
RacCS203 RBD into pOPIN	gttgcgtagctgaaaccggtAGGGTCCTGCCCTCCACC	tcaaaaatatcattaagcttAAAGTTCACGCACCTGTTCTTCACG

Appendix 4: Sera from various SARS-CoV-2 pre-clinical animal studies assessing ChAdOx-1 AZD1222 and AZD2816 vaccines.

Animal model	Vaccination	Study leads	Ref
BALB/c and CD1 mice	Prime-boost i.m. 10^8 i.u. AZD1222 (n=3)	Prof Teresa Lambe and Dr Alexandra Spencer, The University of Oxford	-
BALB/c mice	Prime-boost-boost i.m. 10^8 i.u. ADZ1222 or ADZ2816 (n=6)	Prof Teresa Lambe and Dr Alexandra Spencer, The University of Oxford	[242]
CD1 mice	Prime-boost i.m. 10^8 i.u. B.1, Beta or Delta Spike (n=6)	Cameron Bissett and Prof Teresa Lambe, University of Oxford	
Pig	Prime-only or prime-boost i.m. 10^9 i.u. AZD1222 (n=3)	Prof Simon Graham, The Pirbright Institute	[240]
Pig	Prime-boost i.m. 10^9 i.u. ADZ1222 or ADZ2816 (n=3)	Prof Simon Graham, The Pirbright Institute	-
Non-human primate	Prime-boost i.m. $2.5x10^{10}$ vp ADZ1222 (n=6)	Prof Teresa Lambe and Prof Sarah Gilbert, University of Oxford	[241]
Ferret	Prime-boost i.m. $2.5x10^{10}$ vp ADZ1222 (n=12)	Prof Teresa Lambe and Prof Sarah Gilbert, University of Oxford	[241]
Syrian Hamster	Prime-boost i.m. $2.5x10^8$ vp ADZ1222 or ADZ2186 (n=8)	Dr Neeltje van Doreamlen and Dr Vincent Munster, National Institutes of Health	[243]

i.m = intramuscular immunisation; i.u = infection units; vp = virus particles

Appendix 5: Peptide libraries comprising overlapping sequences (20mers offset by set amino acids) representing NiVB-G, GHNV-G and CedV-G

Peptide	NiVB-G Sequence	GHNV-G Sequence	CedV-G Sequence
1	MPTESKKVRFENTASDKGKN	MPQKTVEFINMNSPLERGVS	MLSQLQKNYLDNSNQQGDKM
2	ENTASDKGKNPSKVIKSYYG	MNSPLERGVSTLSDKKTLNQ	DNSNQQGDKMNNPDKKLSVN
3	PSKVIKSYYGTMDIKKINEG	TLSDKKTLNQSKITKQGYFG	NNPDKKLSVNFNPLELDKGQ
4	TMDIKKINEGLLDSKILSAF	SKITKQGYFGLGSHSERNWK	FNPLELDKGQKDLNKSYYVK
5	LLDSKILSAFNTVIALLGSI	LGSHSERNWKKQKNQNDHYM	KDLNKSYYVKNKNYNVSNLL
6	NTVIALLGSIVIIVMNIMII	KQKNQNDHYMTVSTMILEIL	NKNYNVSNLLNESLHDIKFC
7	VIIVMNIMIIQNYTRSTDNQ	TVSTMILEILVVLGIMFNLI	NESLHDIKFCIYCIFSLLII
8	QNYTRSTDNQAMIKDALQSI	VVLGIMFNLIVLTMVYYQND	IYCIFSLLIIITIINIITIS
9	AMIKDALQSIQQQIKGLADK	VLTMVYYQNDNINQRMAELT	ITIINIITISIVITRLKVHE
10	QQQIKGLADKIGTEIGPKVS	NINQRMAELTSNITVLNLNL	IVITRLKVHEENNGMESPNL
11	IGTEIGPKVSLIDTSSTITI	SNITVLNLNLNQLTNKIQRE	ENNGMESPNLQSIQDSLSSL
12	LIDTSSTITIPANIGLLGSK	NQLTNKIQREIIPRITLIDT	QSIQDSLSSLTNMINTEITP
13	PANIGLLGSKISQSTASINE	IIPRITLIDTATTITIPSAI	TNMINTEITPRIGILVTATS
14	ISQSTASINENVNEKCKFTL	ATTITIPSAITYILATLTTR	RIGILVTATSVTLSSSINYV
15	NVNEKCKFTLPPLKIHECNI	TYILATLTTRISELLPSINQ	VTLSSSINYVGTKTNQLVNE
16	PPLKIHECNISCPNPLPFRE	ISELLPSINQKCEFKTPTLV	GTKTNQLVNELKDYITKSCG
17	SCPNPLPFREYKPQTEGVSN	KCEFKTPTLVLNDCRINCTP	LKDYITKSCGFKVPELKLHE
18	YKPQTEGVSNLVGLPNNICL	LNDCRINCTPPLNPSDGVKM	FKVPELKLHECNISCADPKI
19	LVGLPNNICLQKTSNQILKP	PLNPSDGVKMSSLATNLVAH	CNISCADPKISKSAMYSTNA
20	QKTSNQILKPKLISYTLPVV	SSLATNLVAHGPSPCRNFSS	SKSAMYSTNAYAELAGPPKI
21	KLISYTLPVVGQSGTCITDP	GPSPCRNFSSVPTIYYYRIP	YAELAGPPKIFCKSVSKDPD
22	GQSGTCITDPLLAMDEGYFA	VPTIYYYRIPGLYNRTALDE	FCKSVSKDPDFRLKQIDYVI
23	LLAMDEGYFAYSHLEKIGSC	GLYNRTALDERCILNPRLTI	FRLKQIDYVIPVQQDRSICM
24	YSHLEKIGSCSRGVSKQRII	RCILNPRLTISSTKFAYVHS	PVQQDRSICMNNPLLDISDG
25	SRGVSKQRIIGVGEVLDRGD	SSTKFAYVHSEYDKNCTRGF	NNPLLDISDGFFTYIHYEGI
26	GVGEVLDRGDEVPSLFMTNV	EYDKNCTRGFKYYELMTFGE	FFTYIHYEGINSCKKSDSFK
27	EVPSLFMTNVWTPSNPNTVY	KYYELMTFGEILEGPEKEPR	NSCKKSDSFKVLLSHGEIVD
28	WTPSNPNTVYHCSAVYNNEF	ILEGPEKEPRMFSRSFYSPT	VLLSHGEIVDRGDYRPSLYL
29	HCSAVYNNEFYYVLCAVSVV	MFSRSFYSPTNAVNYHSCTP	RGDYRPSLYLLSSHYHPYSM
30	YYVLCAVSVVGDPILNSTYW	NAVNYHSCTPIVTVNEGYFL	LSSHYHPYSMQVINCVPVTC
31	GDPILNSTYWSGSLMMTRLA	IVTVNEGYFLCLECTSSDPL	QVINCVPVTCNQSSFVFCHI
32	SGSLMMTRLAVKPKNNGESY	CLECTSSDPLYKANLSNSTF	NQSSFVFCHISNNTKTLDNS
33	VKPKNNGESYNQHQFALRNI	YKANLSNSTFHLVILRHNKD	SNNTKTLDNSDYSSDEYYIT

34	NQHQFALRNIEKGKYDKVMP	HLVILRHNKDEKIVSMPSFN	DYSSDEYYITYFNGIDRPKT
35	EKGKYDKVMPYGPSGIKQGD	EKIVSMPSFNLSTDQEYVQI	YFNGIDRPKTKKIPINNMTA
36	YGPSGIKQGDTLYFPAVGFL	LSTDQEYVQIIPAEGGGTAE	KKIPINNMTADNRYIHFTFS
37	TLYFPAVGFLVRTEFTYNDS	IPAEGGGTAESGNLYFPCIG	DNRYIHFTFSGGGGVCLGEE
38	VRTEFTYNDSNCPIAECQYS	SGNLYFPCIGRLLHKRVTHP	GGGGVCLGEEFIIPVTTVIN
39	NCPIAECQYSKPENCRLSMG	RLLHKRVTHPLCKKSNCSRT	FIIPVTTVINTDVFTHDYCE
40	KPENCRLSMGIRPNSHYILR	LCKKSNCSRTDDESCLKSYY	TDVFTHDYCESFNCSVQTGK
41	IRPNSHYILRSGLLKYNLSD	DDESCLKSYYNQGSPQHQVV	SFNCSVQTGKSLKEICSESL
42	SGLLKYNLSDEENSKIVFIE	NQGSPQHQVVNCLIRIRNAQ	SLKEICSESLRSPTNSSRYN
43	EENSKIVFIEISDQRLSIGS	NCLIRIRNAQRDNPTWDVIT	RSPTNSSRYNLNGIMIISQN
44	ISDQRLSIGSPSKIYDSLGQ	RDNPTWDVITVDLTNTYPGS	LNGIMIISQNNMTDFKIQLN
45	PSKIYDSLGQPVFYQASFSW	VDLTNTYPGSRSRIFGSFSK	NMTDFKIQLNGITYNKLSFG
46	PVFYQASFSWDTMIKFGDVQ	RSRIFGSFSKPMLYQSSVSW	GITYNKLSFGSPGRLSKTLG
47	DTMIKFGDVQTVNPLVVNWR	PMLYQSSVSWHTLLQVAEIT	SPGRLSKTLGQVLYYQSSMS
48	TVNPLVVNWRDNTVISRPGQ	HTLLQVAEITDLDKYQLDWL	QVLYYQSSMSWDTYLKAGFV
49	DNTVISRPGQSQCPRFNKCP	DLDKYQLDWLDTPYISRPGG	WDTYLKAGFVEKWKPFTPNW
50	SQCPRFNKCPEVCWEGVYND	DTPYISRPGGSECPFGNYCP	EKWKPFTPNWMNNTVISRPN
51	EVCWEGVYNDAFLIDRINWI	SECPFGNYCPTVCWEGTYND	MNNTVISRPNQGNCPRYHKC
52	AFLIDRINWISAGVFLDSNQ	TVCWEGTYNDVYSLTPNNDL	QGNCPRYHKCPEICYGGTYN
53	SAGVFLDSNQTAENPVFTVF	VYSLTPNNDLFVTVYLKSEQ	PEICYGGTYNDIAPLDLGKD
54	TAENPVFTVFKDNEVLYRAQ	FVTVYLKSEQVAENPYFAIF	DIAPLDLGKDMYVSVILDSD
55	KDNEVLYRAQLASEDTNAQK	VAENPYFAIFSRDQILKEFP	MYVSVILDSDQLAENPEITV
56	LASEDTNAQKTITNCFLLKN	SRDQILKEFPLDAWISSART	QLAENPEITVFNSTTILYKE
57	TITNCFLLKNKIWCISLVEI	LDAWISSARTTTISCFMFNN	FNSTTILYKERVSKDELNTR
58	KIWCISLVEIYDTGDNVIRP	TTISCFMFNNEIWCIAALEI	RVSKDELNTRSTTTSCFLFL
59	YDTGDNVIRPKLFAVKIPEQ	EIWCIAALEITRLNDDIIRP	STTTSCFLFLDEPWCISVLE
60	TGDNVIRPKLFAVKIPEQCT	TRLNDDIIRPIYYSFWLPTD	DEPWCISVLETNRFNGKSIR
61		IYYSFWLPTDCRTPYPHTGK	TNRFNGKSIRPEIYSYKIPK
62		CRTPYPHTGKMTRVPLRSTY	RFNGKSIRPEIYSYKIPKYC
63		TPYPHTGKMTRVPLRSTYNY	

The NiVB-G peptide library was used as three peptides pools (Pool 1: 1-18, pool 2: 19-39, pool 3: 40-60), indicated by a red line. GHNV-G and CedV-G peptides libraries were used as a single pool.

References

1. Chaplin, D.D., *Overview of the immune response.* J Allergy Clin Immunol, 2010. **125**(2 Suppl 2): p. S3-23.
2. Mistry, P., et al., *SARS-CoV-2 Variants, Vaccines, and Host Immunity.* Frontiers in Immunology, 2022. **12**.
3. Pishesha, N., T.J. Harmand, and H.L. Ploegh, *A guide to antigen processing and presentation.* Nature Reviews Immunology, 2022. **22**(12): p. 751-764.
4. Primorac, D., et al., *Adaptive Immune Responses and Immunity to SARS-CoV-2.* Frontiers in Immunology, 2022. **13**.
5. Riedel, S., *Edward Jenner and the history of smallpox and vaccination.* Proc (Bayl Univ Med Cent), 2005. **18**(1): p. 21-5.
6. Roth, G.A. and E. Fee, *Images of health. Smallpox: the first vaccine.* Am J Public Health, 2011. **101**(7): p. 1217.
7. Liu, H., et al., *Global perspectives on smallpox vaccine against monkeypox: a comprehensive meta-analysis and systematic review of effectiveness, protection, safety and cross-immunogenicity.* Emerg Microbes Infect, 2024. **13**(1): p. 2387442.
8. Shchelkunov, S.N., et al., *Human monkeypox and smallpox viruses: genomic comparison.* FEBS Lett, 2001. **509**(1): p. 66-70.
9. Hübschen, J.M., I. Gouandjika-Vasilache, and J. Dina, *Measles.* The Lancet, 2022. **399**(10325): p. 678-690.
10. Griffin, D.E., *Measles Vaccine.* Viral Immunol, 2018. **31**(2): p. 86-95.
11. Moss, W.J. and D.E. Griffin, *Global measles elimination.* Nat Rev Microbiol, 2006. **4**(12): p. 900-8.
12. Lam, E., J.B. Rosen, and J.R. Zucker, *Mumps: an Update on Outbreaks, Vaccine Efficacy, and Genomic Diversity.* Clin Microbiol Rev, 2020. **33**(2).
13. Langedijk, J.P.M., et al., *Universal paramyxovirus vaccine design by stabilizing regions involved in structural transformation of the fusion protein.* Nat Commun, 2024. **15**(1): p. 4629.
14. McLellan, J.S., et al., *Structure-based design of a fusion glycoprotein vaccine for respiratory syncytial virus.* Science, 2013. **342**(6158): p. 592-8.
15. Walsh, E.E., et al., *A Randomized Phase 1/2 Study of a Respiratory Syncytial Virus Prefusion F Vaccine.* J Infect Dis, 2022. **225**(8): p. 1357-1366.
16. Taylor, W.P., *Protection of goats against peste-des-petits-ruminants with attenuated rinderpest virus.* Res Vet Sci, 1979. **27**(3): p. 321-4.
17. Holzer, B., et al., *Protection of Cattle against Rinderpest by Vaccination with Wild-Type but Not Attenuated Strains of Peste des Petits Ruminants Virus.* J Virol, 2016. **90**(10): p. 5152-5162.
18. Wang, W.C., et al., *Progress towards the Development of a Universal Influenza Vaccine.* Viruses, 2022. **14**(8).
19. Xu, L., et al., *Advances in Nucleic Acid Universal Influenza Vaccines.* Vaccines (Basel), 2024. **12**(6).
20. CDC. *Types of Influenza Viruses*. [cited 2025 12/01/2025]; Available from: https://www.cdc.gov/flu/about/viruses-types.html#:~:text=Influenza%20A%20viruses%20are%20divided%20into%20subtypes%20based,%28H1%20through%20H18%20and%20N1%20through%20N11%2C%20respectively%29.

21. Cheng, Z.A.-O., J.A.-O. Ma, and C.A.-O.X. Zhao, *Advantages of Broad-Spectrum Influenza mRNA Vaccines and Their Impact on Pulmonary Influenza*. *LID - 1382*. 2024(2076-393X (Electronic)).
22. Xu, H., et al., *Multiple Vaccines and Strategies for Pandemic Preparedness of Avian Influenza Virus*. Viruses, 2023. **15**(8).
23. He, X., et al., *Novel Influenza Vaccines: From Research and Development (R&D) Challenges to Regulatory Responses*. Vaccines (Basel), 2023. **11**(10).
24. Kim, Y.H., et al., *Influenza vaccines: Past, present, and future*. Rev Med Virol, 2022. **32**(1): p. e2243.
25. Lee, I.T., et al., *Safety and immunogenicity of a phase 1/2 randomized clinical trial of a quadrivalent, mRNA-based seasonal influenza vaccine (mRNA-1010) in healthy adults: interim analysis*. Nat Commun, 2023. **14**(1): p. 3631.
26. Lu, I.N., et al., *Identification of a CD4 T-cell epitope in the hemagglutinin stalk domain of pandemic H1N1 influenza virus and its antigen-driven TCR usage signature in BALB/c mice*. Cell Mol Immunol, 2017. **14**(6): p. 511-520.
27. Vatzia, E., et al., *Aerosol immunization with influenza matrix, nucleoprotein, or both prevents lung disease in pig*. NPJ Vaccines, 2024. **9**(1): p. 188.
28. Li, Y.D., et al., *Coronavirus vaccine development: from SARS and MERS to COVID-19*. J Biomed Sci, 2020. **27**(1): p. 104.
29. Paules, C.I., H.D. Marston, and A.S. Fauci, *Coronavirus Infections—More Than Just the Common Cold*. JAMA, 2020. **323**(8): p. 707-708.
30. Song, Z., et al., *From SARS to MERS, Thrusting Coronaviruses into the Spotlight*. Viruses, 2019. **11**(1).
31. Banerjee, A., et al., *Bats and Coronaviruses*. Viruses, 2019. **11**(1).
32. Si, F., et al., *Towards a Safer Future: Enhancing Vaccine Development to Combat Animal Coronaviruses*. Vaccines (Basel), 2024. **12**(3).
33. Hartenian, E., et al., *The molecular virology of coronaviruses*. J Biol Chem, 2020. **295**(37): p. 12910-12934.
34. Tan, C.W., et al., *Broad-spectrum pan-genus and pan-family virus vaccines*. Cell Host Microbe, 2023. **31**(6): p. 902-916.
35. Everest, H., et al., *Known Cellular and Receptor Interactions of Animal and Human Coronaviruses: A Review*. Viruses, 2022. **14**(2).
36. Costantini, V., et al., *Respiratory and fecal shedding of porcine respiratory coronavirus (PRCV) in sentinel weaned pigs and sequence of the partial S-gene of the PRCV isolates*. Arch Virol, 2004. **149**(5): p. 957-74.
37. Lau, S.K. and J.F. Chan, *Coronaviruses: emerging and re-emerging pathogens in humans and animals*. Virol J, 2015. **12**: p. 209.
38. Lu, R., et al., *Genomic characterisation and epidemiology of 2019 novel coronavirus: implications for virus origins and receptor binding*. The Lancet, 2020. **395**(10224): p. 565-574.
39. Domingo, E., J. Sheldon, and C. Perales, *Viral Quasispecies Evolution*. Microbiology and Molecular Biology Reviews, 2012. **76**(2): p. 159-216.
40. Hodcroft, E. *Overview of Variants in Countries*. 2020-2024 [cited 2024; 0.1.0:[Available from: https://covariants.org/per-country.
41. Challen, R., et al., *Risk of mortality in patients infected with SARS-CoV-2 variant of concern 202012/1: matched cohort study*. Bmj, 2021. **372**: p. n579.
42. Hou, Y.J., et al., *SARS-CoV-2 D614G variant exhibits efficient replication ex vivo and transmission in vivo*. Science, 2020. **370**(6523): p. 1464-1468.

43. Plante, J.A., et al., *Spike mutation D614G alters SARS-CoV-2 fitness*. Nature, 2021. **592**(7852): p. 116-121.
44. Hodcroft, E. *Overview of Variants/Mutants*. 2020-2024 [cited 2024; Available from: https://covariants.org/variants.
45. Konings, F., et al., *SARS-CoV-2 Variants of Interest and Concern naming scheme conducive for global discourse*. Nature Microbiology, 2021. **6**(7): p. 821-823.
46. Winger, A. and T. Caspari, *The Spike of Concern-The Novel Variants of SARS-CoV-2*. Viruses, 2021. **13**(6).
47. Calistri, P., et al., *Infection sustained by lineage B.1.1.7 of SARS-CoV-2 is characterised by longer persistence and higher viral RNA loads in nasopharyngeal swabs*. Int J Infect Dis, 2021. **105**: p. 753-755.
48. Graham, M.S., et al., *Changes in symptomatology, reinfection, and transmissibility associated with the SARS-CoV-2 variant B.1.1.7: an ecological study*. Lancet Public Health, 2021. **6**(5): p. e335-e345.
49. Newman, J., et al., *Neutralizing antibody activity against 21 SARS-CoV-2 variants in older adults vaccinated with BNT162b2*. Nature Microbiology, 2022. **7**(8): p. 1180-1188.
50. Zhou, D., et al., *Evidence of escape of SARS-CoV-2 variant B.1.351 from natural and vaccine-induced sera*. Cell, 2021. **184**(9): p. 2348-2361.e6.
51. Wang, P., et al., *Increased resistance of SARS-CoV-2 variant P.1 to antibody neutralization*. Cell Host Microbe, 2021. **29**(5): p. 747-751.e4.
52. Liu, C., et al., *Reduced neutralization of SARS-CoV-2 B.1.617 by vaccine and convalescent serum*. Cell, 2021. **184**(16): p. 4220-4236.e13.
53. Motozono, C., et al., *SARS-CoV-2 spike L452R variant evades cellular immunity and increases infectivity*. Cell Host Microbe, 2021. **29**(7): p. 1124-1136.e11.
54. Saito, A., et al., *Enhanced fusogenicity and pathogenicity of SARS-CoV-2 Delta P681R mutation*. Nature, 2022. **602**(7896): p. 300-306.
55. Cele, S., et al., *Omicron extensively but incompletely escapes Pfizer BNT162b2 neutralization*. Nature, 2022. **602**(7898): p. 654-656.
56. Dejnirattisai, W., et al., *Reduced neutralisation of SARS-CoV-2 omicron B.1.1.529 variant by post-immunisation serum*. Lancet, 2022. **399**(10321): p. 234-236.
57. Syed, A.M., et al., *Omicron mutations enhance infectivity and reduce antibody neutralization of SARS-CoV-2 virus-like particles*. Proceedings of the National Academy of Sciences, 2022. **119**(31): p. e2200592119.
58. WHO. *Statement on the antigen composition of COVID-19 vaccines*. 2024 26/04/2024 [cited 2025 12/01/2025]; Available from: https://www.who.int/news/item/26-04-2024-statement-on-the-antigen-composition-of-covid-19-vaccines.
59. Burki, T., *COVID vaccine booster doses for omicron variants*. Lancet Respir Med, 2022. **10**(10): p. 936.
60. Garcia-Beltran, W.F., et al., *mRNA-based COVID-19 vaccine boosters induce neutralizing immunity against SARS-CoV-2 Omicron variant*. Cell, 2022. **185**(3): p. 457-466.e4.

61. Shrestha, L.B., et al., *Bivalent Omicron BA.1 vaccine booster increases memory B cell breadth and neutralising antibodies against emerging SARS-CoV-2 variants*. EBioMedicine, 2024. **110**: p. 105461.
62. Kirsebom, F.C.M., et al., *Effectiveness of the Sanofi/GSK (VidPrevtyn Beta) and Pfizer-BioNTech (Comirnaty Original/Omicron BA.4-5) bivalent vaccines against hospitalisation in England*. EClinicalMedicine, 2024. **71**: p. 102587.
63. Patel, N., et al., *XBB.1.5 spike protein COVID-19 vaccine induces broadly neutralizing and cellular immune responses against EG.5.1 and emerging XBB variants*. Scientific Reports, 2023. **13**(1): p. 19176.
64. Chalkias, S., et al., *A Bivalent Omicron-Containing Booster Vaccine against Covid-19*. N Engl J Med, 2022. **387**(14): p. 1279-1291.
65. Scheaffer, S.M., et al., *Bivalent SARS-CoV-2 mRNA vaccines increase breadth of neutralization and protect against the BA.5 Omicron variant in mice*. Nature Medicine, 2023. **29**(1): p. 247-257.
66. Roelle, S.M., et al., *Expanded ACE2 dependencies of diverse SARS-like coronavirus receptor binding domains*. PLoS Biol, 2022. **20**(7): p. e3001738.
67. Seifert, S.N., et al., *An ACE2-dependent Sarbecovirus in Russian bats is resistant to SARS-CoV-2 vaccines*. PLoS Pathog, 2022. **18**(9): p. e1010828.
68. Lee, J., et al., *Broad receptor tropism and immunogenicity of a clade 3 sarbecovirus*. Cell Host & Microbe, 2023. **31**(12): p. 1961-1973.e11.
69. Wells, H.L., et al., *The evolutionary history of ACE2 usage within the coronavirus subgenus Sarbecovirus*. Virus Evol, 2021. **7**(1): p. veab007.
70. Murakami, S., et al., *Isolation of Bat Sarbecoviruses, Japan*. Emerg Infect Dis, 2022. **28**(12): p. 2500-2503.
71. Si, J.-Y., et al., *Sarbecovirus RBD indels and specific residues dictating multi-species ACE2 adaptiveness*. Nature Communications, 2024. **15**(1): p. 8869.
72. Ge, X.Y., et al., *Isolation and characterization of a bat SARS-like coronavirus that uses the ACE2 receptor*. Nature, 2013. **503**(7477): p. 535-8.
73. Yan, H., et al., *ACE2 receptor usage reveals variation in susceptibility to SARS-CoV and SARS-CoV-2 infection among bat species*. Nature Ecology & Evolution, 2021. **5**(5): p. 600-608.
74. Tan, C.C.S., et al., *Genomic screening of 16 UK native bat species through conservationist networks uncovers coronaviruses with zoonotic potential*. Nat Commun, 2023. **14**(1): p. 3322.
75. Guo, H., et al., *Identification of a novel lineage bat SARS-related coronaviruses that use bat ACE2 receptor*. Emerg Microbes Infect, 2021. **10**(1): p. 1507-1514.
76. Yang, H. and Z. Rao, *Structural biology of SARS-CoV-2 and implications for therapeutic development*. Nature Reviews Microbiology, 2021. **19**(11): p. 685-700.
77. Naqvi, A.A.T., et al., *Insights into SARS-CoV-2 genome, structure, evolution, pathogenesis and therapies: Structural genomics approach*. Biochim Biophys Acta Mol Basis Dis, 2020. **1866**(10): p. 165878.
78. Yan, R., et al., *Structural basis for the different states of the spike protein of SARS-CoV-2 in complex with ACE2*. Cell Research, 2021. **31**(6): p. 717-719.
79. Artika, I.M., A.K. Dewantari, and A. Wiyatno, *Molecular biology of coronaviruses: current knowledge*. Heliyon, 2020. **6**(8): p. e04743.

80. Yu, W., et al., *Structure Based Affinity Maturation and Characterizing of SARS-CoV Antibody CR3022 against SARS-CoV-2 by Computational and Experimental Approaches*. Viruses, 2022. **14**(2).
81. Zhao, F., et al., *Broadening a SARS-CoV-1–neutralizing antibody for potent SARS-CoV-2 neutralization through directed evolution*. Science Signaling, 2023. **16**(798): p. eabk3516.
82. Miguez-Rey, E., et al., *Monoclonal antibody therapies in the management of SARS-CoV-2 infection*. Expert Opin Investig Drugs, 2022. **31**(1): p. 41-58.
83. Jones, B.E., et al., *The neutralizing antibody, LY-CoV555, protects against SARS-CoV-2 infection in nonhuman primates*. Sci Transl Med, 2021. **13**(593).
84. Cohen, M.S., et al., *Effect of Bamlanivimab vs Placebo on Incidence of COVID-19 Among Residents and Staff of Skilled Nursing and Assisted Living Facilities: A Randomized Clinical Trial*. Jama, 2021. **326**(1): p. 46-55.
85. Gottlieb, R.L., et al., *Effect of Bamlanivimab as Monotherapy or in Combination With Etesevimab on Viral Load in Patients With Mild to Moderate COVID-19: A Randomized Clinical Trial*. Jama, 2021. **325**(7): p. 632-644.
86. Baum, A., et al., *REGN-COV2 antibodies prevent and treat SARS-CoV-2 infection in rhesus macaques and hamsters*. Science, 2020. **370**(6520): p. 1110-1115.
87. Weinreich, D.M., et al., *REGN-COV2, a Neutralizing Antibody Cocktail, in Outpatients with Covid-19*. N Engl J Med, 2021. **384**(3): p. 238-251.
88. Gupta, A., et al., *Early Treatment for Covid-19 with SARS-CoV-2 Neutralizing Antibody Sotrovimab*. N Engl J Med, 2021. **385**(21): p. 1941-1950.
89. Destras, G., et al., *Sotrovimab drives SARS-CoV-2 omicron variant evolution in immunocompromised patients*. The Lancet Microbe, 2022. **3**(8): p. e559.
90. Folegatti, P.M., et al., *Safety and immunogenicity of the ChAdOx1 nCoV-19 vaccine against SARS-CoV-2: a preliminary report of a phase 1/2, single-blind, randomised controlled trial*. The Lancet, 2020. **396**(10249): p. 467-478.
91. Polack Fernando, P., et al., *Safety and Efficacy of the BNT162b2 mRNA Covid-19 Vaccine*. New England Journal of Medicine, 2020. **383**(27): p. 2603-2615.
92. Sahin, U., et al., *BNT162b2 vaccine induces neutralizing antibodies and poly-specific T cells in humans*. Nature, 2021. **595**(7868): p. 572-577.
93. Sampath, V., et al., *Vaccines and allergic reactions: The past, the current COVID-19 pandemic, and future perspectives*. Allergy, 2021. **76**(6): p. 1640-1660.
94. El Sahly, H.M., et al., *Efficacy of the mRNA-1273 SARS-CoV-2 Vaccine at Completion of Blinded Phase*. N Engl J Med, 2021. **385**(19): p. 1774-1785.
95. Sadoff, J., et al., *Final Analysis of Efficacy and Safety of Single-Dose Ad26.COV2.S*. N Engl J Med, 2022. **386**(9): p. 847-860.
96. Payne, R.P., et al., *Immunogenicity of standard and extended dosing intervals of BNT162b2 mRNA vaccine*. Cell, 2021. **184**(23): p. 5699-5714.e11.
97. Falsey, A.R., et al., *Phase 3 Safety and Efficacy of AZD1222 (ChAdOx1 nCoV-19) Covid-19 Vaccine*. N Engl J Med, 2021. **385**(25): p. 2348-2360.
98. Halperin, S.A., et al., *Final efficacy analysis, interim safety analysis, and immunogenicity of a single dose of recombinant novel coronavirus vaccine (adenovirus type 5 vector) in adults 18 years and older: an international, multicentre, randomised, double-blinded, placebo-controlled phase 3 trial*. Lancet, 2022. **399**(10321): p. 237-248.

99. Ella, R., et al., *Efficacy, safety, and lot-to-lot immunogenicity of an inactivated SARS-CoV-2 vaccine (BBV152): interim results of a randomised, double-blind, controlled, phase 3 trial*. Lancet, 2021. **398**(10317): p. 2173-2184.
100. Al Kaabi, N., et al., *Effect of 2 Inactivated SARS-CoV-2 Vaccines on Symptomatic COVID-19 Infection in Adults: A Randomized Clinical Trial*. Jama, 2021. **326**(1): p. 35-45.
101. Jin, L., et al., *CoronaVac: A review of efficacy, safety, and immunogenicity of the inactivated vaccine against SARS-CoV-2*. Hum Vaccin Immunother, 2022. **18**(6): p. 2096970.
102. Heath, P.T., et al., *Safety and Efficacy of NVX-CoV2373 Covid-19 Vaccine*. N Engl J Med, 2021. **385**(13): p. 1172-1183.
103. Huisman, W., et al., *Vaccine-induced enhancement of viral infections*. Vaccine, 2009. **27**(4): p. 505-12.
104. Dangi, T., et al., *Cross-protective immunity following coronavirus vaccination and coronavirus infection*. J Clin Invest, 2021. **131**(24).
105. Tan, C.W., et al., *Pan-Sarbecovirus Neutralizing Antibodies in BNT162b2-Immunized SARS-CoV-1 Survivors*. N Engl J Med, 2021. **385**(15): p. 1401-1406.
106. Cantoni, D., et al., *Pseudotyped Bat Coronavirus RaTG13 is efficiently neutralised by convalescent sera from SARS-CoV-2 infected patients*. Communications Biology, 2022. **5**(1): p. 409.
107. Stamatatos, L., et al., *A single mRNA immunization boosts cross-variant neutralizing antibodies elicited by SARS-CoV-2 infection*. medRxiv, 2021.
108. Cohen, A.A., et al., *Mosaic RBD nanoparticles protect against challenge by diverse sarbecoviruses in animal models*. Science, 2022. **377**(6606): p. eabq0839.
109. WHO. *R&D Blueprint: Nipah and Henipaviruses*. 2019 10/01/2019 [cited 2025 12/01/2025]; Available from: https://www.who.int/teams/blueprint/nipah-henipaviruses.
110. Thakur, N. and D. Bailey, *Advances in diagnostics, vaccines and therapeutics for Nipah virus*. Microbes Infect, 2019. **21**(7): p. 278-286.
111. Ang, B.S.P., T.C.C. Lim, and L. Wang, *Nipah Virus Infection*. J Clin Microbiol, 2018. **56**(6).
112. Eaton, B.T., et al., *Hendra and Nipah viruses: different and dangerous*. Nat Rev Microbiol, 2006. **4**(1): p. 23-35.
113. Mahalingam, S., et al., *Hendra virus: an emerging paramyxovirus in Australia*. The Lancet Infectious Diseases, 2012. **12**(10): p. 799-807.
114. Wang, J., et al., *A new Hendra virus genotype found in Australian flying foxes*. Virology Journal, 2021. **18**(1): p. 197.
115. Annand, E., et al., *Novel Hendra Virus Variant Detected by Sentinel Surveillance of Horses in Australia*. Emerging Infectious Disease journal, 2022. **28**(3): p. 693.
116. Bossart, K.N., et al., *A Hendra virus G glycoprotein subunit vaccine protects African green monkeys from Nipah virus challenge*. Sci Transl Med, 2012. **4**(146): p. 146ra107.
117. Rodrigue, V., et al., *Current progress towards prevention of Nipah and Hendra disease in humans: A scoping review of vaccine and monoclonal antibody candidates being evaluated in clinical trials*. Trop Med Int Health, 2024. **29**(5): p. 354-364.

118. de Wit, E. and V.J. Munster, *Animal models of disease shed light on Nipah virus pathogenesis and transmission*. J Pathol, 2015. **235**(2): p. 196-205.
119. Halpin, K., et al., *Pteropid bats are confirmed as the reservoir hosts of henipaviruses: a comprehensive experimental study of virus transmission*. Am J Trop Med Hyg, 2011. **85**(5): p. 946-51.
120. Wacharapluesadee, S. and T. Hemachudha, *Duplex nested RT-PCR for detection of Nipah virus RNA from urine specimens of bats*. J Virol Methods, 2007. **141**(1): p. 97-101.
121. Middleton, D.J., et al., *Experimental Nipah virus infection in pteropid bats (Pteropus poliocephalus)*. J Comp Pathol, 2007. **136**(4): p. 266-72.
122. Clayton, B.A., et al., *Transmission routes for nipah virus from Malaysia and Bangladesh*. Emerg Infect Dis, 2012. **18**(12): p. 1983-93.
123. Parashar, U.D., et al., *Case-control study of risk factors for human infection with a new zoonotic paramyxovirus, Nipah virus, during a 1998-1999 outbreak of severe encephalitis in Malaysia*. J Infect Dis, 2000. **181**(5): p. 1755-9.
124. Middleton, D.J., et al., *Experimental Nipah virus infection in pigs and cats*. J Comp Pathol, 2002. **126**(2-3): p. 124-36.
125. Looi, L.M. and K.B. Chua, *Lessons from the Nipah virus outbreak in Malaysia*. Malays J Pathol, 2007. **29**(2): p. 63-7.
126. Uppal, P.K., *Emergence of Nipah virus in Malaysia*. Ann N Y Acad Sci, 2000. **916**: p. 354-7.
127. Reynes, J.M., et al., *Nipah virus in Lyle's flying foxes, Cambodia*. Emerg Infect Dis, 2005. **11**(7): p. 1042-7.
128. Sendow, I., et al., *Henipavirus in Pteropus vampyrus bats, Indonesia*. Emerg Infect Dis, 2006. **12**(4): p. 711-2.
129. Ching, P.K., et al., *Outbreak of henipavirus infection, Philippines, 2014*. Emerg Infect Dis, 2015. **21**(2): p. 328-31.
130. WHO. *Nipah virus infection - Bangladesh*. Disease Outbreak News 2024 27th February 2024 [cited 2025 16/01/2025]; Available from: https://www.who.int/emergencies/disease-outbreak-news/item/2024-DON508.
131. Singh, R.K., et al., *Nipah virus: epidemiology, pathology, immunobiology and advances in diagnosis, vaccine designing and control strategies - a comprehensive review*. Vet Q, 2019. **39**(1): p. 26-55.
132. Satterfield, B.A., B.E. Dawes, and G.N. Milligan, *Status of vaccine research and development of vaccines for Nipah virus*. Vaccine, 2016. **34**(26): p. 2971-2975.
133. Wacharapluesadee, S., et al., *Bat Nipah virus, Thailand*. Emerg Infect Dis, 2005. **11**(12): p. 1949-51.
134. Khan, S., et al., *Twenty-five years of Nipah outbreaks in Southeast Asia: A persistent threat to global health*. IJID Regions, 2024. **13**: p. 100434.
135. Quarleri, J., V. Galvan, and M.V. Delpino, *Henipaviruses: an expanding global public health concern?* Geroscience, 2022. **44**(5): p. 2447-2459.
136. Tan, C.T., et al., *Relapsed and late-onset Nipah encephalitis*. Ann Neurol, 2002. **51**(6): p. 703-8.
137. Sejvar, J.J., et al., *Long-term neurological and functional outcome in Nipah virus infection*. Ann Neurol, 2007. **62**(3): p. 235-42.

138. Mire, C.E., et al., *Pathogenic Differences between Nipah Virus Bangladesh and Malaysia Strains in Primates: Implications for Antibody Therapy.* Sci Rep, 2016. **6**: p. 30916.
139. Clayton, B.A., et al., *The Nature of Exposure Drives Transmission of Nipah Viruses from Malaysia and Bangladesh in Ferrets.* PLoS Negl Trop Dis, 2016. **10**(6): p. e0004775.
140. Marsh, G.A., et al., *Cedar virus: a novel Henipavirus isolated from Australian bats.* PLoS Pathog, 2012. **8**(8): p. e1002836.
141. Schountz, T., et al., *Differential Innate Immune Responses Elicited by Nipah Virus and Cedar Virus Correlate with Disparate In Vivo Pathogenesis in Hamsters.* Viruses, 2019. **11**(3).
142. Amaya, M., et al., *A Recombinant Chimeric Cedar Virus-Based Surrogate Neutralization Assay Platform for Pathogenic Henipaviruses.* Viruses, 2023. **15**(5).
143. Laing, E.D., et al., *Rescue and characterization of recombinant cedar virus, a non-pathogenic Henipavirus species.* Virol J, 2018. **15**(1): p. 56.
144. Drexler, J.F., et al., *Henipavirus RNA in African bats.* PLoS One, 2009. **4**(7): p. e6367.
145. Madera, S., et al., *Discovery and Genomic Characterization of a Novel Henipavirus, Angavokely Virus, from Fruit Bats in Madagascar.* J Virol, 2022. **96**(18): p. e0092122.
146. Pernet, O., et al., *Evidence for henipavirus spillover into human populations in Africa.* Nat Commun, 2014. **5**: p. 5342.
147. Wu, Z., et al., *Novel Henipa-like virus, Mojiang Paramyxovirus, in rats, China, 2012.* Emerg Infect Dis, 2014. **20**(6): p. 1064-6.
148. Zhang, X.A., et al., *A Zoonotic Henipavirus in Febrile Patients in China.* N Engl J Med, 2022. **387**(5): p. 470-472.
149. Lee, S.H., et al., *Discovery and Genetic Characterization of Novel Paramyxoviruses Related to the Genus Henipavirus in Crocidura Species in the Republic of Korea.* Viruses, 2021. **13**(10).
150. Vanmechelen, B., et al., *The characterization of multiple novel paramyxoviruses highlights the diverse nature of the subfamily Orthoparamyxovirinae.* Virus Evol, 2022. **8**(2): p. veac061.
151. Parry, R., et al., *Henipavirus in Northern Short-Tailed Shrew, Alabama, USA.* Emerging Infectious Disease journal, 2025. **31**(2): p. 392.
152. Caruso, S. and S.J. Edwards, *Recently Emerged Novel Henipa-like Viruses: Shining a Spotlight on the Shrew.* Viruses, 2023. **15**(12).
153. Hernández, L.H.A., et al., *First Genomic Evidence of a Henipa-like Virus in Brazil.* Viruses, 2022. **14**(10).
154. Sasaki, M., et al., *Molecular epidemiology of paramyxoviruses in Zambian wild rodents and shrews.* J Gen Virol, 2014. **95**(Pt 2): p. 325-330.
155. Rockx, B., R. Winegar, and A.N. Freiberg, *Recent progress in henipavirus research: Molecular biology, genetic diversity, animal models.* Antiviral Research, 2012. **95**(2): p. 135-149.
156. Mbu'u, C.M., et al., *Henipaviruses at the Interface Between Bats, Livestock and Human Population in Africa.* Vector Borne Zoonotic Dis, 2019. **19**(7): p. 455-465.

157. Spengler Jessica, R., et al., *Henipaviruses: epidemiology, ecology, disease, and the development of vaccines and therapeutics.* Clinical Microbiology Reviews, 2024. **0**(0): p. e00128-23.
158. Bowden, T.A., et al., *Structural basis of Nipah and Hendra virus attachment to their cell-surface receptor ephrin-B2.* Nat Struct Mol Biol, 2008. **15**(6): p. 567-72.
159. Bossart, K.N., et al., *Functional studies of host-specific ephrin-B ligands as Henipavirus receptors.* Virology, 2008. **372**(2): p. 357-371.
160. Xu, K., C.C. Broder, and D.B. Nikolov, *Ephrin-B2 and ephrin-B3 as functional henipavirus receptors.* Seminars in Cell & Developmental Biology, 2012. **23**(1): p. 116-123.
161. Broder, C.C. and K.T. Wong, *Henipaviruses.* Neurotropic Viral Infections, 2016. **9**: p. 45-83.
162. Thakur, N., et al., *Micro-fusion inhibition tests: quantifying antibody neutralization of virus-mediated cell–cell fusion.* Journal of General Virology, 2021. **102**(1).
163. Broder, C.C., et al., *A treatment for and vaccine against the deadly Hendra and Nipah viruses.* Antiviral Res, 2013. **100**(1): p. 8-13.
164. Johnson, K., M. Vu, and A.N. Freiberg, *Recent advances in combating Nipah virus.* Fac Rev, 2021. **10**: p. 74.
165. Zhu, Z., et al., *Exceptionally potent cross-reactive neutralization of Nipah and Hendra viruses by a human monoclonal antibody.* J Infect Dis, 2008. **197**(6): p. 846-53.
166. Bossart, K.N., et al., *A neutralizing human monoclonal antibody protects against lethal disease in a new ferret model of acute nipah virus infection.* PLoS Pathog, 2009. **5**(10): p. e1000642.
167. Geisbert, T.W., et al., *Therapeutic treatment of Nipah virus infection in nonhuman primates with a neutralizing human monoclonal antibody.* Sci Transl Med, 2014. **6**(242): p. 242ra82.
168. Sahay, R.R., et al., *Experiential learnings from the Nipah virus outbreaks in Kerala towards containment of infectious public health emergencies in India.* Epidemiol Infect, 2020. **148**: p. e90.
169. Playford, E.G., et al., *Safety, tolerability, pharmacokinetics, and immunogenicity of a human monoclonal antibody targeting the G glycoprotein of henipaviruses in healthy adults: a first-in-human, randomised, controlled, phase 1 study.* The Lancet Infectious Diseases, 2020. **20**(4): p. 445-454.
170. Dang, H.V., et al., *An antibody against the F glycoprotein inhibits Nipah and Hendra virus infections.* Nat Struct Mol Biol, 2019. **26**(10): p. 980-987.
171. Dang, H.V., et al., *Broadly neutralizing antibody cocktails targeting Nipah virus and Hendra virus fusion glycoproteins.* Nature Structural & Molecular Biology, 2021. **28**(5): p. 426-434.
172. Mire, C.E., et al., *A Cross-Reactive Humanized Monoclonal Antibody Targeting Fusion Glycoprotein Function Protects Ferrets Against Lethal Nipah Virus and Hendra Virus Infection.* J Infect Dis, 2020. **221**(Suppl 4): p. S471-s479.
173. Zeitlin, L., et al., *Therapeutic administration of a cross-reactive mAb targeting the fusion glycoprotein of Nipah virus protects nonhuman primates.* Sci Transl Med, 2024. **16**(741): p. eadl2055.

174. CEPI. *New human trials for novel antibody offer hope for immediate protection against deadly Nipah*. 2024 [cited 2025 5th January 2025]; Available from: https://cepi.net/new-human-trials-novel-antibody-offer-hope-immediate-protection-against-deadly-nipah.
175. McEachern, J.A., et al., *A recombinant subunit vaccine formulation protects against lethal Nipah virus challenge in cats*. Vaccine, 2008. **26**(31): p. 3842-52.
176. Mire, C.E., et al., *A recombinant Hendra virus G glycoprotein subunit vaccine protects nonhuman primates against Hendra virus challenge*. J Virol, 2014. **88**(9): p. 4624-31.
177. Pallister, J., et al., *A recombinant Hendra virus G glycoprotein-based subunit vaccine protects ferrets from lethal Hendra virus challenge*. Vaccine, 2011. **29**(34): p. 5623-30.
178. Pickering, B.S., et al., *Protection against henipaviruses in swine requires both, cell-mediated and humoral immune response*. Vaccine, 2016. **34**(40): p. 4777-86.
179. Mungall, B.A., et al., *Feline model of acute nipah virus infection and protection with a soluble glycoprotein-based subunit vaccine*. J Virol, 2006. **80**(24): p. 12293-302.
180. Findlay-Wilson, S., et al., *Cross-protectivity of henipavirus soluble glycoprotein in an in vivo model of Nipah virus disease*. Frontiers in Immunology, 2025. **16**.
181. Guillaume, V., et al., *Nipah virus: vaccination and passive protection studies in a hamster model*. J Virol, 2004. **78**(2): p. 834-40.
182. Weingartl, H.M., et al., *Recombinant nipah virus vaccines protect pigs against challenge*. J Virol, 2006. **80**(16): p. 7929-38.
183. Yoneda, M., et al., *Recombinant measles virus vaccine expressing the Nipah virus glycoprotein protects against lethal Nipah virus challenge*. PLoS One, 2013. **8**(3): p. e58414.
184. Kong, D., et al., *Newcastle disease virus-vectored Nipah encephalitis vaccines induce B and T cell responses in mice and long-lasting neutralizing antibodies in pigs*. Virology, 2012. **432**(2): p. 327-335.
185. Bossart, K.N., et al., *A neutralizing human monoclonal antibody protects african green monkeys from hendra virus challenge*. Sci Transl Med, 2011. **3**(105): p. 105ra103.
186. Mire, C.E., et al., *Single injection recombinant vesicular stomatitis virus vaccines protect ferrets against lethal Nipah virus disease*. Virol J, 2013. **10**: p. 353.
187. Lo, M.K., et al., *Single-dose replication-defective VSV-based Nipah virus vaccines provide protection from lethal challenge in Syrian hamsters*. Antiviral Res, 2014. **101**: p. 26-9.
188. DeBuysscher, B.L., et al., *Single-dose live-attenuated Nipah virus vaccines confer complete protection by eliciting antibodies directed against surface glycoproteins*. Vaccine, 2014. **32**(22): p. 2637-44.
189. Prescott, J., et al., *Single-dose live-attenuated vesicular stomatitis virus-based vaccine protects African green monkeys from Nipah virus disease*. Vaccine, 2015. **33**(24): p. 2823-9.

190. Ploquin, A., et al., *Protection against henipavirus infection by use of recombinant adeno-associated virus-vector vaccines.* J Infect Dis, 2013. **207**(3): p. 469-78.
191. van Doremalen, N., et al., *A single-dose ChAdOx1-vectored vaccine provides complete protection against Nipah Bangladesh and Malaysia in Syrian golden hamsters.* PLoS Negl Trop Dis, 2019. **13**(6): p. e0007462.
192. van Doremalen, N., et al., *ChAdOx1 NiV vaccination protects against lethal Nipah Bangladesh virus infection in African green monkeys.* npj Vaccines, 2022. **7**(1): p. 171.
193. Pallister, J.A., et al., *Vaccination of ferrets with a recombinant G glycoprotein subunit vaccine provides protection against Nipah virus disease for over 12 months.* Virology Journal, 2013. **10**(1): p. 237.
194. Middleton, D., et al., *Hendra virus vaccine, a one health approach to protecting horse, human, and environmental health.* Emerg Infect Dis, 2014. **20**(3): p. 372-9.
195. Pedrera, M., et al., *Bovine Herpesvirus-4-Vectored Delivery of Nipah Virus Glycoproteins Enhances T Cell Immunogenicity in Pigs.* Vaccines (Basel), 2020. **8**(1).
196. Defang, G.N., et al., *Induction of neutralizing antibodies to Hendra and Nipah glycoproteins using a Venezuelan equine encephalitis virus in vivo expression system.* Vaccine, 2010. **29**(2): p. 212-20.
197. Walpita, P., et al., *A VLP-based vaccine provides complete protection against Nipah virus challenge following multiple-dose or single-dose vaccination schedules in a hamster model.* NPJ Vaccines, 2017. **2**: p. 21.
198. Pedrera, M., et al., *Evaluation of the immunogenicity of an mRNA vectored Nipah virus vaccine candidate in pigs.* Frontiers in Immunology, 2024. **15**.
199. Broder, C.C., D.L. Weir, and P.A. Reid, *Hendra virus and Nipah virus animal vaccines.* Vaccine, 2016. **34**(30): p. 3525-34.
200. Letko, M., et al., *Bat-borne virus diversity, spillover and emergence.* Nature Reviews Microbiology, 2020. **18**(8): p. 461-471.
201. Plowright, R.K., et al., *Urban habituation, ecological connectivity and epidemic dampening: the emergence of Hendra virus from flying foxes (Pteropus spp.).* Proc Biol Sci, 2011. **278**(1725): p. 3703-12.
202. Plowright, R.K., et al., *Transmission or Within-Host Dynamics Driving Pulses of Zoonotic Viruses in Reservoir-Host Populations.* PLoS Negl Trop Dis, 2016. **10**(8): p. e0004796.
203. Irving, A.T., et al., *Lessons from the host defences of bats, a unique viral reservoir.* Nature, 2021. **589**(7842): p. 363-370.
204. Brook, C.E. and A.P. Dobson, *Bats as 'special' reservoirs for emerging zoonotic pathogens.* Trends Microbiol, 2015. **23**(3): p. 172-80.
205. Schuh, A.J., et al., *Egyptian rousette bats maintain long-term protective immunity against Marburg virus infection despite diminished antibody levels.* Sci Rep, 2017. **7**(1): p. 8763.
206. Virtue, E.R., et al., *Interferon production and signaling pathways are antagonized during henipavirus infection of fruit bat cell lines.* PLoS One, 2011. **6**(7): p. e22488.

207. Schuh, A.J., et al., *Antibody-Mediated Virus Neutralization Is Not a Universal Mechanism of Marburg, Ebola, or Sosuga Virus Clearance in Egyptian Rousette Bats*. J Infect Dis, 2019. **219**(11): p. 1716-1721.
208. Luis, A.D., et al., *A comparison of bats and rodents as reservoirs of zoonotic viruses: are bats special?* Proc Biol Sci, 2013. **280**(1756): p. 20122753.
209. Schmaljohn, C. and B. Hjelle, *Hantaviruses: a global disease problem*. Emerg Infect Dis, 1997. **3**(2): p. 95-104.
210. Charrel, R.N. and X. de Lamballerie, *Zoonotic aspects of arenavirus infections*. Vet Microbiol, 2010. **140**(3-4): p. 213-20.
211. Parvate, A., et al., *Diverse Morphology and Structural Features of Old and New World Hantaviruses*. Viruses, 2019. **11**(9).
212. Mackenzie, J.S. and M. Jeggo, *Reservoirs and vectors of emerging viruses*. Curr Opin Virol, 2013. **3**(2): p. 170-9.
213. Cogswell-Hawkinson, A., et al., *Tacaribe virus causes fatal infection of an ostensible reservoir host, the Jamaican fruit bat*. J Virol, 2012. **86**(10): p. 5791-9.
214. Low, D.H.W., et al., *Cencurut virus: A novel Orthonairovirus from Asian house shrews (Suncus murinus) in Singapore*. One Health, 2023. **16**: p. 100529.
215. Plowright, R.K., et al., *Pathways to zoonotic spillover*. Nat Rev Microbiol, 2017. **15**(8): p. 502-510.
216. Temmam, S., et al., *Bat coronaviruses related to SARS-CoV-2 and infectious for human cells*. Nature, 2022. **604**(7905): p. 330-336.
217. Ellwanger, J.H. and J.A.B. Chies, *Zoonotic spillover: Understanding basic aspects for better prevention*. Genet Mol Biol, 2021. **44**(1 Suppl 1): p. e20200355.
218. Thakur, N., et al., *Production of Recombinant Replication-defective Lentiviruses Bearing the SARS-CoV or SARS-CoV-2 Attachment Spike Glycoprotein and Their Application in Receptor Tropism and Neutralisation Assays*. Bio Protoc, 2021. **11**(21): p. e4249.
219. Conceicao, C., et al., *The SARS-CoV-2 Spike protein has a broad tropism for mammalian ACE2 proteins*. PLoS Biol, 2020. **18**(12): p. e3001016.
220. Gallo, G., et al., *Characterising alphacoronavirus phenotypic traits through diversity-driven selection of spike*. bioRxiv, 2024: p. 2024.11.22.624870.
221. Newman, J., et al., *Neutralising antibody activity against SARS-CoV-2 variants, including Omicron, in an elderly cohort vaccinated with BNT162b2*. medRxiv, 2021: p. 2021.12.23.21268293.
222. Berrow, N.S., et al., *A versatile ligation-independent cloning method suitable for high-throughput expression screening applications*. Nucleic Acids Research, 2007. **35**(6): p. e45-e45.
223. Seow, J., et al., *ChAdOx1 nCoV-19 vaccine elicits monoclonal antibodies with cross-neutralizing activity against SARS-CoV-2 viral variants*. Cell Rep, 2022. **39**(5): p. 110757.
224. Seow, J., et al., *Broad and potent neutralizing antibodies are elicited in vaccinated individuals following Delta/BA.1 breakthrough infection*. mBio, 2023. **14**(5): p. e0120623.
225. Amirthalingam, G., et al., *Serological responses and vaccine effectiveness for extended COVID-19 vaccine schedules in England*. Nature Communications, 2021. **12**(1): p. 7217.

226. Akoi Boré, J., et al., *Serological evidence of zoonotic filovirus exposure among bushmeat hunters in Guinea*. Nature Communications, 2024. **15**(1): p. 4171.
227. Roe, M.D., et al., *Performance of an envelope glycoprotein-based multiplex immunoassay for Ebola virus antibody detection in a cohort of Ebola virus disease survivors*. J Virol Methods, 2025. **331**: p. 115057.
228. Isaacs, A., et al., *Combinatorial F-G Immunogens as Nipah and Respiratory Syncytial Virus Vaccine Candidates*. Viruses, 2021. **13**(10).
229. Robson, F., et al., *Coronavirus RNA Proofreading: Molecular Basis and Therapeutic Targeting*. Molecular Cell, 2020. **79**(5): p. 710-727.
230. VanBlargan, L.A., L. Goo, and T.C. Pierson, *Deconstructing the Antiviral Neutralizing-Antibody Response: Implications for Vaccine Development and Immunity*. Microbiol Mol Biol Rev, 2016. **80**(4): p. 989-1010.
231. Hoffmann, M., et al., *SARS-CoV-2 Cell Entry Depends on ACE2 and TMPRSS2 and Is Blocked by a Clinically Proven Protease Inhibitor*. Cell, 2020. **181**(2): p. 271-280.e8.
232. Dejnirattisai, W., et al., *The antigenic anatomy of SARS-CoV-2 receptor binding domain*. Cell, 2021. **184**(8): p. 2183-2200.e22.
233. Greaney, A.J., et al., *Comprehensive mapping of mutations in the SARS-CoV-2 receptor-binding domain that affect recognition by polyclonal human plasma antibodies*. Cell Host & Microbe, 2021. **29**(3): p. 463-476.e6.
234. Meng, B., et al., *Recurrent emergence of SARS-CoV-2 spike deletion H69/V70 and its role in the Alpha variant B.1.1.7*. Cell Rep, 2021. **35**(13): p. 109292.
235. Cerutti, G., et al., *Potent SARS-CoV-2 neutralizing antibodies directed against spike N-terminal domain target a single supersite*. Cell Host & Microbe, 2021. **29**(5): p. 819-833.e7.
236. Wang, P., et al., *Antibody resistance of SARS-CoV-2 variants B.1.351 and B.1.1.7*. Nature, 2021. **593**(7857): p. 130-135.
237. Davies, N.G., et al., *Estimated transmissibility and impact of SARS-CoV-2 lineage B.1.1.7 in England*. Science, 2021. **372**(6538).
238. PublicHealthEngland. *Investigation of novel SARS-CoV-2 variants of concern*. 28th July 2021 [cited 2024 4th November 2024]; Available from: https://www.gov.uk/government/publications/investigation-of-novel-682sars-cov-2-variant-variant-of-concern-20201201.
239. van Doremalen, N., et al., *ChAdOx1 nCoV-19 vaccine prevents SARS-CoV-2 pneumonia in rhesus macaques*. Nature, 2020. **586**(7830): p. 578-582.
240. Graham, S.P., et al., *Evaluation of the immunogenicity of prime-boost vaccination with the replication-deficient viral vectored COVID-19 vaccine candidate ChAdOx1 nCoV-19*. npj Vaccines, 2020. **5**(1): p. 69.
241. Lambe, T., et al., *ChAdOx1 nCoV-19 protection against SARS-CoV-2 in rhesus macaque and ferret challenge models*. Communications Biology, 2021. **4**(1): p. 915.
242. Spencer, A.J., et al., *The ChAdOx1 vectored vaccine, AZD2816, induces strong immunogenicity against SARS-CoV-2 beta (B.1.351) and other variants of concern in preclinical studies*. eBioMedicine, 2022. **77**.
243. van Doremalen, N., et al., *ChAdOx1 nCoV-19 (AZD1222) or nCoV-19-Beta (AZD2816) protect Syrian hamsters against Beta Delta and Omicron variants*. Nature Communications, 2022. **13**(1): p. 4610.

244. Chu, Y.K., et al., *The SARS-CoV ferret model in an infection-challenge study.* Virology, 2008. **374**(1): p. 151-63.
245. Czub, M., et al., *Evaluation of modified vaccinia virus Ankara based recombinant SARS vaccine in ferrets.* Vaccine, 2005. **23**(17-18): p. 2273-9.
246. van den Brand, J.M., et al., *Pathology of experimental SARS coronavirus infection in cats and ferrets.* Vet Pathol, 2008. **45**(4): p. 551-62.
247. Mwenda, M., et al., *Detection of B.1.351 SARS-CoV-2 Variant Strain - Zambia, December 2020.* MMWR Morb Mortal Wkly Rep, 2021. **70**(8): p. 280-282.
248. Tian, D., et al., *The Global Epidemic of the SARS-CoV-2 Delta Variant, Key Spike Mutations and Immune Escape.* Front Immunol, 2021. **12**: p. 751778.
249. Fan, C., et al., *Animal models for COVID-19: advances, gaps and perspectives.* Signal Transduct Target Ther, 2022. **7**(1): p. 220.
250. McCarthy, K.R., et al., *Recurrent deletions in the SARS-CoV-2 spike glycoprotein drive antibody escape.* Science, 2021. **371**(6534): p. 1139-1142.
251. Graham, C., et al., *Neutralization potency of monoclonal antibodies recognizing dominant and subdominant epitopes on SARS-CoV-2 Spike is impacted by the B.1.1.7 variant.* Immunity, 2021. **54**(6): p. 1276-1289.e6.
252. Wang, W.B., et al., *E484K mutation in SARS-CoV-2 RBD enhances binding affinity with hACE2 but reduces interactions with neutralizing antibodies and nanobodies: Binding free energy calculation studies.* J Mol Graph Model, 2021. **109**: p. 108035.
253. Xie, X., et al., *Neutralization of SARS-CoV-2 spike 69/70 deletion, E484K and N501Y variants by BNT162b2 vaccine-elicited sera.* Nat Med, 2021. **27**(4): p. 620-621.
254. Fischer, R.J., et al., *ChAdOx1 nCoV-19 (AZD1222) protects Syrian hamsters against SARS-CoV-2 B.1.351 and B.1.1.7.* Nature Communications, 2021. **12**(1): p. 5868.
255. Tostanoski, L.H., et al., *Immunity elicited by natural infection or Ad26.COV2.S vaccination protects hamsters against SARS-CoV-2 variants of concern.* Science Translational Medicine, 2021. **13**(618): p. eabj3789.
256. Yu, J., et al., *Protective efficacy of Ad26.COV2.S against SARS-CoV-2 B.1.351 in macaques.* Nature, 2021. **596**(7872): p. 423-427.
257. Corbett, K.S., et al., *Evaluation of the mRNA-1273 Vaccine against SARS-CoV-2 in Nonhuman Primates.* New England Journal of Medicine, 2020. **383**(16): p. 1544-1555.
258. Corbett, K.S., et al., *mRNA-1273 protects against SARS-CoV-2 beta infection in nonhuman primates.* Nature Immunology, 2021. **22**(10): p. 1306-1315.
259. Sui, Y., et al., *An intranasally administrated SARS-CoV-2 beta variant subunit booster vaccine prevents beta variant replication in rhesus macaques.* PNAS Nexus, 2022. **1**(3): p. pgac091.
260. Voysey, M., et al., *Single-dose administration and the influence of the timing of the booster dose on immunogenicity and efficacy of ChAdOx1 nCoV-19 (AZD1222) vaccine: a pooled analysis of four randomised trials.* Lancet, 2021. **397**(10277): p. 881-891.
261. Silva-Cayetano, A., et al., *A booster dose enhances immunogenicity of the COVID-19 vaccine candidate ChAdOx1 nCoV-19 in aged mice.* Med, 2021. **2**(3): p. 243-262.e8.

262. Foster, W.S., et al., *Tfh cells and the germinal center are required for memory B cell formation & humoral immunity after ChAdOx1 nCoV-19 vaccination*. Cell Rep Med, 2022. **3**(12): p. 100845.
263. Foster, W.S., et al., *ChAdOx1 nCoV-19 vaccination generates spike-specific CD8(+) T cells in aged mice*. Immunol Cell Biol, 2023. **101**(6): p. 479-488.
264. Noori, M., et al., *Potency of BNT162b2 and mRNA-1273 vaccine-induced neutralizing antibodies against severe acute respiratory syndrome-CoV-2 variants of concern: A systematic review of in vitro studies*. Rev Med Virol, 2022. **32**(2): p. e2277.
265. Bian, L., et al., *Impact of the Delta variant on vaccine efficacy and response strategies*. Expert Rev Vaccines, 2021. **20**(10): p. 1201-1209.
266. Tada, T., et al., *High-titer neutralization of Mu and C.1.2 SARS-CoV-2 variants by vaccine-elicited antibodies of previously infected individuals*. Cell Rep, 2022. **38**(2): p. 110237.
267. Uriu, K., et al., *Neutralization of the SARS-CoV-2 Mu Variant by Convalescent and Vaccine Serum*. N Engl J Med, 2021. **385**(25): p. 2397-2399.
268. Cameroni, E., et al., *Broadly neutralizing antibodies overcome SARS-CoV-2 Omicron antigenic shift*. Nature, 2022. **602**(7898): p. 664-670.
269. Arbel, R., et al., *Effectiveness of a second BNT162b2 booster vaccine against hospitalization and death from COVID-19 in adults aged over 60 years*. Nat Med, 2022. **28**(7): p. 1486-1490.
270. Hyseni, I., et al., *Characterisation of SARS-CoV-2 Lentiviral Pseudotypes and Correlation between Pseudotype-Based Neutralisation Assays and Live Virus-Based Micro Neutralisation Assays*. Viruses, 2020. **12**(9).
271. Syed, A.M., et al., *Rapid assessment of SARS-CoV-2-evolved variants using virus-like particles*. Science, 2021. **374**(6575): p. 1626-1632.
272. Parry, H., et al., *mRNA vaccination in people over 80 years of age induces strong humoral immune responses against SARS-CoV-2 with cross neutralization of P.1 Brazilian variant*. Elife, 2021. **10**.
273. Harvey, W.T., et al., *SARS-CoV-2 variants, spike mutations and immune escape*. Nat Rev Microbiol, 2021. **19**(7): p. 409-424.
274. Cherian, S., et al., *SARS-CoV-2 Spike Mutations, L452R, T478K, E484Q and P681R, in the Second Wave of COVID-19 in Maharashtra, India*. Microorganisms, 2021. **9**(7).
275. Hoffmann, M., et al., *SARS-CoV-2 variant B.1.617 is resistant to bamlanivimab and evades antibodies induced by infection and vaccination*. Cell Rep, 2021. **36**(3): p. 109415.
276. Stankov, M.V., et al., *Humoral and cellular immune responses following BNT162b2 XBB.1.5 vaccination*. Lancet Infect Dis, 2024. **24**(1): p. e1-e3.
277. Wang, L., et al., *Importance of Neutralizing Monoclonal Antibodies Targeting Multiple Antigenic Sites on the Middle East Respiratory Syndrome Coronavirus Spike Glycoprotein To Avoid Neutralization Escape*. J Virol, 2018. **92**(10).
278. Zhou, H., et al., *Structural definition of a neutralization epitope on the N-terminal domain of MERS-CoV spike glycoprotein*. Nat Commun, 2019. **10**(1): p. 3068.
279. Kong, L., et al., *Supersite of immune vulnerability on the glycosylated face of HIV-1 envelope glycoprotein gp120*. Nat Struct Mol Biol, 2013. **20**(7): p. 796-803.

280. Lee, P.S. and I.A. Wilson, *Structural characterization of viral epitopes recognized by broadly cross-reactive antibodies*. Curr Top Microbiol Immunol, 2015. **386**: p. 323-41.
281. Chi, X., et al., *A neutralizing human antibody binds to the N-terminal domain of the Spike protein of SARS-CoV-2*. Science, 2020. **369**(6504): p. 650-655.
282. Chen, Y., et al., *Broadly neutralizing antibodies to SARS-CoV-2 and other human coronaviruses*. Nature Reviews Immunology, 2023. **23**(3): p. 189-199.
283. Li, C.J. and S.C. Chang, *SARS-CoV-2 spike S2-specific neutralizing antibodies*. Emerg Microbes Infect, 2023. **12**(2): p. 2220582.
284. Zhou, P., et al., *A pneumonia outbreak associated with a new coronavirus of probable bat origin*. Nature, 2020. **579**(7798): p. 270-273.
285. Ithete, N.L., et al., *Close relative of human Middle East respiratory syndrome coronavirus in bat, South Africa*. Emerg Infect Dis, 2013. **19**(10): p. 1697-9.
286. Luk, H.K.H., et al., *Molecular epidemiology, evolution and phylogeny of SARS coronavirus*. Infect Genet Evol, 2019. **71**: p. 21-30.
287. Shi, J., et al., *Susceptibility of ferrets, cats, dogs, and other domesticated animals to SARS-coronavirus 2*. Science, 2020. **368**(6494): p. 1016-1020.
288. Kim, Y.I., et al., *Infection and Rapid Transmission of SARS-CoV-2 in Ferrets*. Cell Host Microbe, 2020. **27**(5): p. 704-709.e2.
289. de Vries, R.D., et al., *Animal models of SARS-CoV-2 transmission*. Current Opinion in Virology, 2021. **50**: p. 8-16.
290. Lan, J., et al., *Structure of the SARS-CoV-2 spike receptor-binding domain bound to the ACE2 receptor*. Nature, 2020. **581**(7807): p. 215-220.
291. Letko, M., A. Marzi, and V. Munster, *Functional assessment of cell entry and receptor usage for SARS-CoV-2 and other lineage B betacoronaviruses*. Nat Microbiol, 2020. **5**(4): p. 562-569.
292. Yan, R., et al., *Structural basis for the recognition of SARS-CoV-2 by full-length human ACE2*. Science, 2020. **367**(6485): p. 1444-1448.
293. Wu, K., et al., *Mechanisms of Host Receptor Adaptation by Severe Acute Respiratory Syndrome Coronavirus**. Journal of Biological Chemistry, 2012. **287**(12): p. 8904-8911.
294. Wrobel, A.G., et al., *SARS-CoV-2 and bat RaTG13 spike glycoprotein structures inform on virus evolution and furin-cleavage effects*. Nat Struct Mol Biol, 2020. **27**(8): p. 763-767.
295. Pickering, B., et al., *Divergent SARS-CoV-2 variant emerges in white-tailed deer with deer-to-human transmission*. Nature Microbiology, 2022. **7**(12): p. 2011-2024.
296. Kuchipudi, S.V., et al., *Multiple spillovers from humans and onward transmission of SARS-CoV-2 in white-tailed deer*. Proceedings of the National Academy of Sciences, 2022. **119**(6): p. e2121644119.
297. Hale, V.L., et al., *SARS-CoV-2 infection in free-ranging white-tailed deer*. Nature, 2022. **602**(7897): p. 481-486.
298. Zhou, J., et al., *Mutations that adapt SARS-CoV-2 to mink or ferret do not increase fitness in the human airway*. Cell Rep, 2022. **38**(6): p. 110344.
299. Tan, C.C.S., et al., *Transmission of SARS-CoV-2 from humans to animals and potential host adaptation*. Nature Communications, 2022. **13**(1): p. 2988.

300. Wacharapluesadee, S., et al., *Evidence for SARS-CoV-2 related coronaviruses circulating in bats and pangolins in Southeast Asia*. Nat Commun, 2021. **12**(1): p. 972.
301. Zhou, H., et al., *Identification of novel bat coronaviruses sheds light on the evolutionary origins of SARS-CoV-2 and related viruses*. Cell, 2021. **184**(17): p. 4380-4391.e14.
302. Delaune, D., et al., *A novel SARS-CoV-2 related coronavirus in bats from Cambodia*. Nat Commun, 2021. **12**(1): p. 6563.
303. Hu, B., et al., *Discovery of a rich gene pool of bat SARS-related coronaviruses provides new insights into the origin of SARS coronavirus*. PLoS Pathog, 2017. **13**(11): p. e1006698.
304. Li, W., et al., *Bats are natural reservoirs of SARS-like coronaviruses*. Science, 2005. **310**(5748): p. 676-9.
305. Thakur, N., et al., *SARS-CoV-2 variants of concern alpha, beta, gamma and delta have extended ACE2 receptor host ranges*. Journal of General Virology, 2022. **103**(4).
306. Wu, Z., et al., *A comprehensive survey of bat sarbecoviruses across China in relation to the origins of SARS-CoV and SARS-CoV-2*. Natl Sci Rev, 2023. **10**(6): p. nwac213.
307. Zhang, Y., et al., *Cross-species tropism and antigenic landscapes of circulating SARS-CoV-2 variants*. Cell Rep, 2022. **38**(12): p. 110558.
308. Whelan, S. and N. Goldman, *A general empirical model of protein evolution derived from multiple protein families using a maximum-likelihood approach*. Mol Biol Evol, 2001. **18**(5): p. 691-9.
309. Tamura, K., G. Stecher, and S. Kumar, *MEGA11: Molecular Evolutionary Genetics Analysis Version 11*. Mol Biol Evol, 2021. **38**(7): p. 3022-3027.
310. Seow, J., et al., *Broad and potent neutralizing antibodies are elicited in vaccinated individuals following Delta/BA.1 breakthrough infection*. mBio, 2023. **14**(5): p. e01206-23.
311. Barnes, C.O., et al., *SARS-CoV-2 neutralizing antibody structures inform therapeutic strategies*. Nature, 2020. **588**(7839): p. 682-687.
312. Willett, B.J., et al., *SARS-CoV-2 Omicron is an immune escape variant with an altered cell entry pathway*. Nature Microbiology, 2022. **7**(8): p. 1161-1179.
313. Neerukonda, S.N., et al., *Characterization of Entry Pathways, Species-Specific Angiotensin-Converting Enzyme 2 Residues Determining Entry, and Antibody Neutralization Evasion of Omicron BA.1, BA.1.1, BA.2, and BA.3 Variants*. J Virol, 2022. **96**(17): p. e0114022.
314. Smyth, D.S., et al., *Tracking cryptic SARS-CoV-2 lineages detected in NYC wastewater*. Nature Communications, 2022. **13**(1): p. 635.
315. Horspool, A.M., et al., *SARS-CoV-2 B.1.1.7 and B.1.351 variants of concern induce lethal disease in K18-hACE2 transgenic mice despite convalescent plasma therapy*. bioRxiv, 2021.
316. Huang, H., et al., *SARS-CoV-2 N501Y variants of concern and their potential transmission by mouse*. Cell Death Differ, 2021. **28**(10): p. 2840-2842.
317. Aicher, S.-M., et al., *Species-Specific Molecular Barriers to SARS-CoV-2 Replication in Bat Cells*. Journal of Virology, 2022. **96**(14): p. e00608-22.

318. Wang, Q., et al., *Determinants of species-specific utilization of ACE2 by human and animal coronaviruses*. Communications Biology, 2023. **6**(1): p. 1051.
319. Melin, A.D., et al., *Comparative ACE2 variation and primate COVID-19 risk*. Communications Biology, 2020. **3**(1): p. 641.
320. Kok, K.H., et al., *Co-circulation of two SARS-CoV-2 variant strains within imported pet hamsters in Hong Kong*. Emerg Microbes Infect, 2022. **11**(1): p. 689-698.
321. Kan, B., et al., *Molecular evolution analysis and geographic investigation of severe acute respiratory syndrome coronavirus-like virus in palm civets at an animal market and on farms*. J Virol, 2005. **79**(18): p. 11892-900.
322. Li, P., et al., *The Rhinolophus affinis bat ACE2 and multiple animal orthologs are functional receptors for bat coronavirus RaTG13 and SARS-CoV-2*. Science Bulletin, 2021. **66**(12): p. 1215-1227.
323. Vergara-Alert, J., et al., *Pigs are not susceptible to SARS-CoV-2 infection but are a model for viral immunogenicity studies*. Transboundary and Emerging Diseases, 2021. **68**(4): p. 1721-1725.
324. Sun, B., et al., *Phylogeography, Transmission, and Viral Proteins of Nipah Virus*. Virol Sin, 2018. **33**(5): p. 385-393.
325. Fischer, K., et al., *Indirect ELISA based on Hendra and Nipah virus proteins for the detection of henipavirus specific antibodies in pigs*. PLoS One, 2018. **13**(4): p. e0194385.
326. Le, S.Q. and O. Gascuel, *An improved general amino acid replacement matrix*. Mol Biol Evol, 2008. **25**(7): p. 1307-20.
327. Stone, J.A., et al., *Multiple Strategies Reveal a Bidentate Interaction between the Nipah Virus Attachment and Fusion Glycoproteins*. J Virol, 2016. **90**(23): p. 10762-10773.
328. Aguilar, H.C., et al., *Paramyxovirus Glycoproteins and the Membrane Fusion Process*. Curr Clin Microbiol Rep, 2016. **3**(3): p. 142-154.
329. CEPI. *CEPI 2.0 and the 100 Days Mission*. 2024 [cited 2024 27/12/24]; Available from: https://cepi.net/cepi-20-and-100-days-mission.
330. Aljofan, M., et al., *Characteristics of Nipah virus and Hendra virus replication in different cell lines and their suitability for antiviral screening*. Virus Res, 2009. **142**(1-2): p. 92-9.
331. Sattentau, Q., *Avoiding the void: cell-to-cell spread of human viruses*. Nat Rev Microbiol, 2008. **6**(11): p. 815-26.
332. Kelly, J.T., et al., *BST2/Tetherin Overexpression Modulates Morbillivirus Glycoprotein Production to Inhibit Cell-Cell Fusion*. Viruses, 2019. **11**(8).
333. Weisel, F. and M. Shlomchik, *Memory B Cells of Mice and Humans*. Annu Rev Immunol, 2017. **35**: p. 255-284.
334. Lee, B., et al., *Molecular recognition of human ephrinB2 cell surface receptor by an emergent African henipavirus*. Proc Natl Acad Sci U S A, 2015. **112**(17): p. E2156-65.
335. Laing, E.D., et al., *Structural and functional analyses reveal promiscuous and species specific use of ephrin receptors by Cedar virus*. Proc Natl Acad Sci U S A, 2019. **116**(41): p. 20707-20715.

336. Bowden, T.A., et al., *Crystal structure and carbohydrate analysis of Nipah virus attachment glycoprotein: a template for antiviral and vaccine design*. J Virol, 2008. **82**(23): p. 11628-36.
337. Findlay-Wilson, S., et al., *Establishment of a Nipah Virus Disease Model in Hamsters, including a Comparison of Intranasal and Intraperitoneal Routes of Challenge*. Pathogens, 2023. **12**(8).
338. Rissanen, I., et al., *Idiosyncratic Mòjiāng virus attachment glycoprotein directs a host-cell entry pathway distinct from genetically related henipaviruses*. Nat Commun, 2017. **8**: p. 16060.
339. Millet, J.K., J.A. Jaimes, and G.R. Whittaker, *Molecular diversity of coronavirus host cell entry receptors*. FEMS Microbiol Rev, 2021. **45**(3).
340. Cheliout Da Silva, S., et al., *Functional Analysis of the Fusion and Attachment Glycoproteins of Mojiang Henipavirus*. Viruses, 2021. **13**(3).
341. Voigt, K., et al., *Fusogenicity of the Ghana Virus (Henipavirus: Ghanaian bat henipavirus) Fusion Protein is Controlled by the Cytoplasmic Domain of the Attachment Glycoprotein*. Viruses, 2019. **11**(9).
342. Negrete, O.A., et al., *Single amino acid changes in the Nipah and Hendra virus attachment glycoproteins distinguish ephrinB2 from ephrinB3 usage*. J Virol, 2007. **81**(19): p. 10804-14.
343. Negrete, O.A., et al., *Two key residues in ephrinB3 are critical for its use as an alternative receptor for Nipah virus*. PLoS Pathog, 2006. **2**(2): p. e7.
344. Forbes, E.K., et al., *T cell responses induced by adenoviral vectored vaccines can be adjuvanted by fusion of antigen to the oligomerization domain of C4b-binding protein*. PLoS One, 2012. **7**(9): p. e44943.
345. Bosaeed, M., et al., *Safety and immunogenicity of ChAdOx1 MERS vaccine candidate in healthy Middle Eastern adults (MERS002): an open-label, non-randomised, dose-escalation, phase 1b trial*. Lancet Microbe, 2022. **3**(1): p. e11-e20.
346. Cargill, T., et al., *HBV001: Phase I study evaluating the safety and immunogenicity of the therapeutic vaccine ChAdOx1-HBV*. JHEP Rep, 2023. **5**(11): p. 100885.
347. Jenkin, D., et al., *Safety and immunogenicity of a ChAdOx1 vaccine against Rift Valley fever in UK adults: an open-label, non-randomised, first-in-human phase 1 clinical trial*. Lancet Infect Dis, 2023. **23**(8): p. 956-964.
348. Folegatti, P.M., et al., *A single dose of ChAdOx1 Chik vaccine induces neutralizing antibodies against four chikungunya virus lineages in a phase 1 clinical trial*. Nat Commun, 2021. **12**(1): p. 4636.
349. Rahman, M.Z., et al., *Genetic diversity of Nipah virus in Bangladesh*. Int J Infect Dis, 2021. **102**: p. 144-151.
350. Halliley, J.L., et al., *Long-Lived Plasma Cells Are Contained within the CD19(-)CD38(hi)CD138(+) Subset in Human Bone Marrow*. Immunity, 2015. **43**(1): p. 132-45.
351. Monath, T.P., et al., *Recombinant vesicular stomatitis vaccine against Nipah virus has a favorable safety profile: Model for assessment of live vaccines with neurotropic potential*. PLoS Pathog, 2022. **18**(6): p. e1010658.
352. Chen, S., et al., *Ferritin nanoparticle-based Nipah virus glycoprotein vaccines elicit potent protective immune responses in mice and hamsters*. Virol Sin, 2024.

353. Lieu, K.G., et al., *The non-pathogenic Henipavirus Cedar paramyxovirus phosphoprotein has a compromised ability to target STAT1 and STAT2.* Antiviral Research, 2015. **124**: p. 69-76.
354. De Jong, N.M.C., et al., *Development of broadly reactive influenza vaccines by targeting the conserved regions of the hemagglutinin stem and head domains.* Expert Rev Vaccines, 2020. **19**(6): p. 563-577.
355. Li, Y., et al., *Fc-Based Recombinant Henipavirus Vaccines Elicit Broad Neutralizing Antibody Responses in Mice.* Viruses, 2020. **12**(4).
356. WOAH. *Disease Eradication*. 2024 [cited 2025 08/01/2025]; Available from: https://www.woah.org/en/what-we-do/global-initiatives/disease-eradication/.
357. Pitts, P.J. and G.A. Poland, *Addressing vaccine hesitancy: Learning from the successes and failures of the COVID-19 pandemic.* Vaccine, 2024. **42**(13): p. 3145-3147.
358. Furnon, W., et al., *Phenotypic evolution of SARS-CoV-2 spike during the COVID-19 pandemic.* Nature Microbiology, 2025.
359. Johnson, B.A., et al., *Nucleocapsid mutations in SARS-CoV-2 augment replication and pathogenesis.* PLoS Pathog, 2022. **18**(6): p. e1010627.
360. Cosar, B., et al., *SARS-CoV-2 Mutations and their Viral Variants.* Cytokine Growth Factor Rev, 2022. **63**: p. 10-22.
361. Glass, W.G., et al., *Mechanisms of host defense following severe acute respiratory syndrome-coronavirus (SARS-CoV) pulmonary infection of mice.* J Immunol, 2004. **173**(6): p. 4030-9.
362. Pandey, K., et al., *Animal models for SARS-CoV-2 research: A comprehensive literature review.* Transbound Emerg Dis, 2021. **68**(4): p. 1868-1885.
363. Vandegrift, K.J., et al., *Detection of SARS-CoV-2 Omicron variant (B.1.1.529) infection of white-tailed deer.* bioRxiv, 2022.
364. Dadonaite, B., et al., *Spike deep mutational scanning helps predict success of SARS-CoV-2 clades.* Nature, 2024. **631**(8021): p. 617-626.